Design and development of smart cool materials for the built environment

Konstantinos Gobakis

School of Environmental Engineering

Technical University of Crete

This dissertation is submitted for the degree of

Doctor of Philosophy

February 2018

PhD. Dissertation Committee

- Associate Professor Dionysia Kolokotsa (supervisor), School of Environmental Engineering, Technical University of Crete
- Associate Professor Pagona - Noni Maravelaki, School of Architecture, Technical University of Crete
- Professor Matheos Santamouris, Architectural Science and Technology, The University of New South Wales, Australia
- Professor Mihalis Lazaridis, School of Environmental Engineering, Technical University of Crete
- Professor Theocharis Tsoutsos, School of Environmental Engineering, Technical University of Crete
- Emeritus Professor Vassilis Perdikatsis School of Mineral Resources Engineering, Technical University of Crete
- Assistant Professor Nikolaos Xekoukoulotakis, School of Environmental Engineering, Technical University of Crete

Acknowledgements

Above all I would like to express my deep gratitude to my supervisor, Professor Dionysia Kolokotsa. First of all, I thank her warmly and express my sincere appreciation for her excellent scientific supervision, patience, perseverance and unwavering support over the years. I thank her for the guidance that she always gave me generously, both scientifically and personally. A huge Thanks for everything!

I was very fortunate to have the additional guidance of Professor Pagona-Noni Maravelaki-Kalaitzaki whose invaluable directions and stimulating presence had a great impact on this work. I want to thank her for the many ways in which she supported my research.

I have greatly benefited from many discussions with Professor Mattheos Santamouris and I want to thank him for his support.

I would like to express my special thanks to Emeritus Professor of the School of Mineral Resources Engineering, Prof. Vassileios Perdikatsi and Member of the Examination Committee. I thank him for his excellent cooperation, his scientific contribution, his interest and his important suggestions during the course of my dissertation.

I would like to thank Professor Theocharis Tsoutsos, Professor Mihalis Lazaridis and Assistant Professor Nikolaos Xekoukoulotakis members of the Examination Committee for the time they devoted to my thesis.

I want to thank fellow PhD candidate Katerina Drossou for her useful help during my first steps into chemical synthesis.

I am very grateful to my colleagues of the Energy Management in the Built Environment Laboratory of the Technical University of Crete.

This work has received funding from the Technical University of Crete, Research Committee under Grant Agreement no. 80710, Development of cool materials for energy savings in buildings.

Περίληψη

Τις τελευταίες δεκαετίες έχει σημειωθεί σημαντική αύξηση στον αστικό πληθυσμό του πλανήτη. Ένα από τα σημαντικότερα προβλήματα του αστικού περιβάλλοντος είναι η υπερθέρμανση των πόλεων. Τα κτίρια και τα αστικά δομικά υλικά διαδραματίζουν σημαντικό ρόλο στην υπερθέρμανση των πόλεων. Επιπλέον, τα κτίρια ευθύνονται για το 40% της παγκόσμιας κατανάλωσης πρωτογενούς ενέργειας. Ως εκ τούτου, υπάρχει επείγουσα ανάγκη για τη βελτίωση της ενεργειακής απόδοσης των κτιρίων μέσω προηγμένων υλικών. Το αντικείμενο της παρούσας εργασίας είναι η ανάπτυξη, πειραματική αξιολόγηση και ενσωμάτωση των ψυχρών επιχρισμάτων στο δομημένο περιβάλλον. Η εισαγωγή των ψυχρών επιχρισμάτων οδηγεί σε εξοικονόμηση ενέργειας και καλύτερη ποιότητα περιβάλλοντος τόσο στα κτίρια όσο και στους εξωτερικούς χώρους.

Η παρούσα εργασία διαρθρώνεται σε επτά κεφάλαια. Στο Κεφάλαιο 1 δίνεται μια εισαγωγή στα ψυχρά υλικά. Επιπλέον παρουσιάζεται η στάθμη περιεχομένου, οι ερευνητικοί στόχοι και η μεθοδολογία της διατριβής. Το Κεφάλαιο 2 είναι αφιερωμένο στον πειραματικό εξοπλισμό που χρησιμοποιήθηκε για τον χαρακτηρισμό, την ανάπτυξη και τη μέτρηση των ψυχρών επιχρισμάτων. Στο Κεφάλαιο 3 παρουσιάζεται η ανάπτυξη και η δοκιμή των ανόργανων ψυχρών επιχρισμάτων. Παρέχεται λεπτομερής ανάλυση των πρώτων υλών που χρησιμοποιούνται για τη κατασκευή τους. Είκοσι δύο ψυχρά επιχρίσματα αναπτύσσονται και υποβάλλονται σε πειραματικές μετρήσεις. Οι μετρήσεις περιλαμβάνουν τη μέτρηση της ανακλαστικότητας στην ηλιακή ακτινοβολία και τον συντελεστή εκπομπής υπέρυθρης ακτινοβολίας. Τέλος, τα ψυχρά επιχρίσματα εκτίθενται στο εξωτερικό περιβάλλον και μετριέται η ικανότητά τους να μειώνουν την επιφανειακή θερμοκρασία. Το καλύτερο ψυχρό επίχρισμα παρουσίασε μείωση της επιφανειακής θερμοκρασίας έως και 7K. Στο Κεφάλαιο 4 παρουσιάζεται η ανάπτυξη και δοκιμή των θερμοχρωμικών επιχρισμάτων. Δύο κύριες οικογένειες θερμοχρωμικών επιχρισμάτων αναπτύσσονται και υποβάλλονται σε πειραματικές μετρήσεις: ανόργανες και οργανικές. Παρουσιάζεται η σύνθεση και ο χαρακτηρισμός του ανόργανου θερμοχρωμικού επιχρίσματος. Επιπλέον, τρία εμπορικά διαθέσιμα οργανικά θερμοχρωμικά επιχρίσματα χρησιμοποιούνται. Αξιολογείται η ανακλαστικότητα στην ηλιακή ακτινοβολία και ο συντελεστή εκπομπής υπέρυθρης ακτινοβολίας όλων των θερμοχρωμικών επιχρισμάτων. Επιπλέον, η θερμοκρασία επιφανείας των θερμοχρωμικών επιχρισμάτων μετράται να είναι έως 5K χαμηλότερη, σε

σύγκριση με το συμβατικό επίχρισμα με το ίδιο χρώμα. Στο Κεφάλαιο 5 αναλύεται η επίδραση της περιβαλλοντικής γήρανσης στα ψυχρά επιχρίσματα. Όλα τα επιχρίσματα εκτίθενται στις εξωτερικό περιβάλλον. Η αρχική και τελική ανακλαστικότητα στην ηλιακή ακτινοβολία και ο συντελεστή εκπομπής υπέρυθρης ακτινοβολίας μετριούνται. Τα ανόργανα ψύχρα επιχρίσματα παρουσίασαν μικρή μείωση στην ανακλαστικότητα στην ηλιακή ακτινοβολία και στον συντελεστή εκπομπής υπέρυθρης ακτινοβολίας. Τα θερμοχρωμικα επιχρίσματα παρουσίασαν μικτά αποτελέσματα. Η επίδραση των εξωτερικών συνθηκών στα ανόργανα θερμοχρωμικά είναι αμελητέα. Ενώ παρατηρείται σημαντική αποδόμηση για τα οργανικά θερμοχρωμικά επιχρίσματα. Στο Κεφάλαιο 6 εξετάζονται οι αλλαγές στα κτίρια και στο εξωτερικό περιβάλλον με τη χρήση των αναπτυγμένων ψυχρών επιχρισμάτων. Οι επιδράσεις των αναπτυγμένων επιχρισμάτων σε καλά και μη καλά μονωμένο κτίριο υπολογίζονται χρησιμοποιώντας το ΕΣΠ-ρ. Όλα τα επιχρίσματα συμβάλλουν στην ενεργειακή μείωση τόσο των καλά και μη μονωμένων κτιρίων κατά 5-14% σε ετήσια βάση. Επιπλέον, υπολογίζεται η επίδραση των ψυχρών επιχρισμάτων στο αστικό περιβάλλον. Αναπτύχτηκε μια νέα μέθοδος για την έμμεση σύζευξη του προηγμένου λογισμικού θερμικής μοντελοποίησης κτιρίου και μικροκλιματικής μοντελοποίησης. Αναφέρεται η σημασία της σύζευξης του εξωτερικού και του εσωτερικού περιβάλλοντος. Οι μικροκλιματικές συνθήκες της υπό διερεύνηση περιοχής μπορεί να οδηγήσουν σε ± 10% αλλαγή των αναγκών θέρμανσης/ψύξης. Εάν η ανταλλαγή δεδομένων μεταξύ των δύο πεδίων ορισμού περιλαμβάνει την ανταλλαγή του συντελεστή μεταφοράς θερμότητας με μεταφορά, η διαφορά στις ανάγκες θέρμανσης / ψύξης μπορεί να φτάσει έως και ± 50%.

Abstract

In recent decades, a significant increase in the world's urban population has been recorded. One of the major problems of the cities' environment is the urban overheating. Buildings and urban construction materials play an important role in the urban overheating. Moreover buildings are responsible for 40% of the world's primary energy consumption. Therefore, there is an urgent need to improve the buildings' energy performance through advanced materials.

The scope of the present thesis is to develop, test and integrate cool coatings into the built environment. The introduction of cool coatings leads to energy saving and better living conditions for the people.

The present thesis is structured in seven chapters.

In Chapter 1 an introduction into cool materials is given. Moreover, the state of the art, research objective and methodology of the thesis is presented. Chapter 2 is devoted to the experimental equipment used for the characterization, development and measurement of the cool coatings.

In Chapter 3 the development and testing of the mineral based cool coating is presented. A detailed analysis for the raw materials used for the formulation of the cool coatings using X-ray diffraction is presented. Twenty two cool coatings are developed, characterised and tested. Their characterization includes the measurement of solar reflectance and infrared emittance. Finally, the cool coatings are exposed to the environment and their ability to reduce the surface temperature is measured. The best performing developed cool coating showed reduction of the surface temperature is up to 7.2K.

In Chapter 4 the development and testing of the thermochromic based cool coatings is presented. Two main families of thermochromic coatings are discussed: inorganic and organic. The synthesis and characterization of the inorganic thermochromic coatings is presented. Three commercially available organic thermochromic coatings are developed. The solar reflectance and infrared emittance of all thermochromic coatings is measured. Furthermore, the surface temperature of the coatings is measured to be 5.5K compared to the conventional coating with the same colour.

In Chapter 5 the ageing effect of the environment on the cool coatings is discussed. All coatings are exposed to the outdoor conditions. The initial and aged solar reflectance and infrared emittance are measured. The mineral based cool coating presented small decrease in the solar reflectance and infrared emittance. The thermochromic coatings presented mixed results. The effect on the outdoor conditions on the inorganic thermochromics is negligible. While significant degradation is observed for the organic thermochromic coatings.

In Chapter 6 the changes on buildings and surrounding areas by the use of the developed cool coatings are examined. The effects of the developed coatings on a well and poor insulated building are calculated using advanced thermal modelling software. All coatings contribute to the energy efficiency of both well and poor insulated buildings by 5-14% on annual basis. Moreover, the impact of cool coatings on the urban environment is calculated. A novel method has been developed on indirect coupling of the building advanced thermal modelling and microclimatic modelling software. The importance of coupling the external and internal environment is presented. The microclimatic condition of the under investigation area can lead to difference of $\pm 10\%$ in power for heating/cooling needs when the local microclimatic conditions are introduced to the weather file. If the exchange of data between the 2 domains includes the exchange of the Convective Heat Transfer Coefficient, the difference in heating/cooling needs can be as high as $\pm 50\%$.

Publications

The following publications have been made in the context of this doctoral dissertation.

Publications in scientific journals

Directly related to the PhD thesis field

1. **Gobakis, K.**, Kolokotsa, D. (2017). Coupling building energy simulation software with micro-climatic simulation for the evaluation of the impact of urban outdoor conditions on the energy consumption and indoor environmental quality. Energy and Buildings, 157, pp. 101–115.

2. **Gobakis, K.**, Kolokotsa, D., Maravelaki-Kalaitzaki, N., Perdikatsis, V., Santamouris, M. (2015). Development and analysis of advanced inorganic coatings for buildings and urban structures. Energy and Buildings, 89, pp. 196–205.

3. Kolokotsa, D., Giannariakis, G., **Gobakis, K.**, Giannarakis, G., Synnefa, A., Santamouris, M. (2018). Cool roofs and cool pavements application in Acharnes, Greece. Sustainable Cities and Society, 37, pp. 466–474.

4. Mastrapostoli, E., Santamouris, M., Kolokotsa, D., Vassilis, P., Venieri, D., **Gobakis, K.** (2016). On the ageing of cool roofs: Measure of the optical degradation, chemical and biological analysis and assessment of the energy impact. Energy and Buildings, 114, pp. 191–199.

5. Mastrapostoli, E., Karlessi, T., Pantazaras, A., Kolokotsa, D., **Gobakis, K.**, Santamouris, M. (2014). On the cooling potential of cool roofs in cold climates: Use of cool fluorocarbon coatings to enhance the optical properties and the energy performance of industrial buildings. Energy and Buildings, 69, pp. 417–425.

Extra research activity

1. Kampelis, N., **Gobakis, K.**, Vagias, V., Kolokotsa, D., Standardi, L., Isidori, D., Cristalli, C., Montagnino, F. M., Paredes, F., Muratore, P., Venezia, L., Dracou, K., Montenon, A., Pyrgou, A., Karlessi, T., Santamouris, M. (2017). Evaluation of the performance gap in industrial, residential & tertiary near-Zero energy buildings. Energy and Buildings, 148, pp. 58–73.

2. **Gobakis, K.**, Mavrigiannaki, A., Kalaitzakis, K., Kolokotsa, D. (2017). Design and development of a Web based GIS platform for zero energy settlements monitoring. In Energy Procedia Vol. 134, pp. 48–60.

3. Kampelis, N., Ferrante, A., Kolokotsa, D., **Gobakis, K.**, Standardi, L., Cristalli, C. (2017). Thermal comfort evaluation in HVAC Demand Response control. In Energy Procedia Vol. 134, pp. 675–682.

4. Kolokotsa, D., **Gobakis**, K., Papantoniou, S., Georgatou, C., Kampelis, N., Kalaitzakis, K., Vasilakopoulou K., Santamouris, M. (2016). Development of a web based energy management system for University Campuses: The CAMP-IT platform. Energy and Buildings, 123, pp. 119–135.

Publications in international scientific conferences with full article peer review process

Directly related to the PhD thesis field

1. **Gobakis, K.**, Kolokotsa, D. (2016). External coupling of Building Energy and external CFD software for better calculation of the total energy usage. In Fourth International conference on Countermeasures to Urban Heat Island. Singapore. **Best applied Urban Heat Island research award**

2. **Gobakis, K.**, Kolokotsa, D., Maravelaki-Kalaitzaki, P., Lionakis, S., Perdikatsis, V., Santamouris, M. (2013). Development and analysis of inorganic coating for energy saving for buildings, in. In Joint Conference 34th AIVC- 3rd TightVent- 2nd Cool Roofs' - 1st venticool. Athens.

3. Mastrapostoli, E., Santamouris, M., Kolokotsa, D., Perdikatsis, V., Venieri, D., **Gobakis, K**. (2013). Numerical and experimental analysis of the aging of the cool roofs for buildings in Greece. In Joint Conference 34th AIVC- 3rd TightVent- 2nd Cool Roofs' - 1st venticool. Athens.

Extra research activity

1. Synnefa, A., Stathopoulou, M., Adaktylou, N., Kolokotsa, D., **Gobakis, K.**, Santamouris, M., Chrysoulakis, N. , Cartalis, C. (2013). A case study of sustainable urban planning with the use of a decision support system. In Joint Conference 34th AIVC- 3rd TightVent- 2nd Cool Roofs' - 1st venticool. Athens.

2. **Gobakis, K.**, Kolokotsa, D., Stavrakakis, Lykas, G. (2012). Application of advanced clustering methods in a GIS based forest fire risk assessment tool. In Industrial and Hazardous Waste Management. Chania.

Contents

Περίληψη **vii**

Abstract **ix**

Publications **xi**

List of Figures **xxi**

List of Tables **xxix**

1 Introduction and state of the art **3**

1.1 Introduction 3

1.2 Cool materials 4

1.2.1 The physics behind cool materials 4

1.2.2 Cool materials properties 6

1.3 State of the art for cool materials 10

1.3.1 Development of cool materials 10

1.3.2 Aging and deterioration of cool materials 12

1.3.3 The effect of cool materials on buildings' energy performance and indoor environmental quality 13

1.3.4 The effect of cool materials on the urban spaces 14

1.4 Research objectives and methodology 15

2 Experimental equipment **19**

2.1 Experimental equipment for materials' development and characterization 19
2.1.1 X-ray diffraction 19
2.1.2 Fourier Transform Infrared Spectroscopy 20
2.1.3 Differential Thermal Analysis 22
2.1.4 Laboratory sieving machine 24
2.1.5 Scale 25
2.2 Experimental equipment used for analysis of cool materials' properties 26
2.2.1 Experimental equipment for measuring the thermal emittance 26
2.2.2 Experimental equipment for measuring the spectral reflectance 28
2.2.3 Standards for measurement and characterization of cool materials properties . 30
2.2.4 Surface temperature data loggers 31
2.2.5 Thermal imaging camera 33

3 Development and testing of inorganic based cool coatings 35

3.1 Introduction 35
3.2 Materials and methods 35
3.2.1 Renders 35
3.2.2 Aggregates 36
3.2.2.1 Dolomite marble powder 36
3.2.2.2 Limestone marble powder 37
3.2.2.3 Quartz sand 38
3.2.2.4 Glass beads 39
3.2.3 Lime 40
3.2.4 Binders 40
3.2.4.1 Natural hydraulic lime with pozzolanic additives 41
3.2.4.2 White Portland cement 41
3.3 Development of the coatings' samples 42
3.4 Experimental procedure 43

3.4.1 Experimental procedure of the first phase 44
3.4.1.1 Spectral reflectance and infrared emittance of cool coatings 45
3.4.1.2 Surface temperature of cool coatings 49
3.4.2 Experimental procedure of the second phase 54
3.4.2.1 Spectral reflectance and infrared emittance of cool coatings 55
3.5 Discussion of results 59

4 Development and testing of thermochromic based cool coatings 67

4.1 Introduction 67
4.2 Inorganic thermochromic coatings 68
4.3 Organic thermochromic coatings 71
4.4 Optical filters for the protection of the inorganic and organic thermochromic coatings 71
4.5 Experimental procedure 72
4.5.1 Inorganic thermochromic coatings 72
4.5.1.1 Preparation of inorganic thermochromic coatings 72
4.5.1.2 Spectral reflectance and infrared emittance of inorganic thermochromic coatings 73
4.5.1.3 Surface temperature measurement of the inorganic thermochromic coatings 76
4.5.1.4 Surface thermal imaging of inorganic thermochromic coatings 78
4.5.2 Organic thermochromic coatings 81
4.5.2.1 Preparation of organic thermochromic coatings 81
4.5.2.2 Spectral reflectance and infrared emittance of organic thermochromic coatings 83
4.5.2.3 Surface temperature measurement of the organic thermochromic coatings 92
4.5.2.4 Surface thermal imaging of organic thermochromic coatings 95

5 Analysis of aging effect for the developed cool coatings 101

5.1 Introduction 101

5.2 Aging of inorganic based cool coatings . . . 101
5.3 Aging of thermochromic based cool coatings . . . 117
5.3.1 Aging of the inorganic thermochromic coatings . . . 117
5.3.2 Aging of the organic thermochromic coatings . . . 119

6 Contribution of cool coatings on the energy efficiency in the built environment: tools and calculation methods 129

6.1 Introduction . . . 129
6.2 Contribution of cool coatings on the energy efficiency of buildings . . . 130
6.3 Contribution of cool coatings on the energy efficiency of buildings coupled with microclimatic simulation . . . 137
6.3.1 Building energy - microclimatic simulation coupling methodology . . . 138
6.3.2 Description of the case study . . . 140
6.3.3 Development of the thermal model of the Case Study Building . . . 143
6.3.4 Modeling of microclimatic conditions . . . 143
6.3.5 Convective Heat Transfer Coefficient Calculations . . . 148
6.3.5.1 CHTC Calculations in Building Energy Simulation tools . . . 149
6.3.5.2 CHTC calculations using Computational Fluid Dynamics . . . 150
6.3.5.3 CHTC calculations from full-scale measurements . . . 150
6.3.6 Coupling of indoor-outdoor models . . . 151
6.3.7 Validation of the coupling methodology . . . 153
6.3.7.1 Simulation in four seasons . . . 156
6.3.8 Integration of developed cool coatings to the case study . . . 162

7 Conclusions and further research 169

Bibliography 171

Appendix A Spectral reflectance of mineral based cool coating 183

Appendix B Aging process of thermochromic samples 197

Appendix C Source code of Sketchup-ESP-r plug-in **205**

List of Figures

1.1 The energy balance of a material. 4

1.2 The basic principles of cool materials. 7

1.3 The impact of solar reflectance on roof surface temperature [29]. 8

1.4 Steps for the creation of the cool coating. 16

1.5 Steps for simulation the developed cool coating. 17

1.6 Methodology followed for the research. 18

2.1 X-Ray diffraction [83]. 20

2.2 Bruker D8 Advance Diffractometer. 20

2.3 Schematic sketch of a Fourier transform infrared spectrometer (FTIR) [87]. 21

2.4 FTIR Perkin-Elmer 1000 spectrometer. 22

2.5 Schematic diagram of thermal analyses layout [88]. 23

2.6 Setaram LabSysEvo 1600. 24

2.7 Laboratory sieving machine, Retsch VE 1000. 25

2.8 High accuracy electronic scale. 26

2.9 Device and Services emissometer model AE1. 27

2.10 Transient response of emmissometer [91]. 28

2.11 Carry 5000 with DRA 2500 integrating sphere. 29

2.12 Schematic representation of Cary 5000. 29

2.13 Data logger HH306A. 32

2.14 Data logger from Campbell Scientific. 32

2.15 K-type thermocouples. 33

2.16 Thermal imaging camera: Flir ThermaCAM B2. 34

2.17 Thermal imaging picture. 34

3.1 XRD spectrum of the dolomite marble powder aggregate. 37

3.2 Aggregates used for the development of the samples. 37

3.3 XRD spectrum of the limestone marble powder aggregate. 38

3.4 XRD spectrum of the quartz sand aggregate. 39

3.5 Glass beads. 40

3.6 XRD spectrum of natural hydraulic lime with pozzolanic additives. 41

3.7 XRD spectrum of white Portland cement. 42

3.8 Metal matrix with substrate. 43

3.9 Grain size distribution of LMP-DMP. 45

3.10 Grain size distribution of QAU. 45

3.11 Solar reflectance spectrum of the 1^{st} group and reference samples. 46

3.12 Solar reflectance spectrum of the 2^{nd} group and reference samples. 46

3.13 Solar reflectance spectrum of the 3^{st} group and reference samples. 47

3.14 Samples placed on the roof of the K2 building. 50

3.15 Surface temperature measurement of the $1^{st.}$ group. 51

3.16 Surface temperature measurement of the $2^{rd.}$ group. 52

3.17 Surface temperature measurement of the $3^{rd.}$ group. 53

3.18 Grain size distribution for coarse, medium, fine. 55

3.19 Solar reflectance spectrum of the LMP samples of 4^{st} group. 56

3.20 Solar reflectance spectrum of the DMP samples of 4^{st} group 56

3.21 Solar reflectance spectrum of the 1^{st} group samples. 57

3.22 Average day/night surface temperatures of the samples for June 2017. 60

3.23 Average day/night surface temperatures of the samples for July 2017. 61

3.24 Difference in average day/night surface temperature sample minus reference. 64

4.1 Inorganic colour changing pigment. 68

4.2 XRD spectrum of the inorganic colour changing pigment. 69

4.3 FTIR spectrum of the inorganic colour changing pigment. 70

4.4 Thermal analysis of the synthesized pigment. 70

4.5 Spectral transmittance of substrate, substrate with Eversorb and substrate with Ilam. 72

4.6 Spectral reflectance of sample: plaster of Paris (Pl), plaster of Paris with inorganic thermochromic (ITC) and plaster of Paris with inorganic thermochromic at transition temperature (45°C) (ITC_45°C). 74

4.7 Spectral reflectance of sample: plaster of Paris + Ilam (Pl_V), plaster of Paris with inorganic thermochromic and Ilam (ITC_V) and plaster of Paris with inorganic thermochromic and Ilam at transition temperature (45°C) (ITC_V_45°C). 75

4.8 Average day/night surface temperature of the inorganic thermochromic samples. . . . 77

4.9 Measuring points of the sample with the use of the thermal imaging camera. 78

4.10 Thermal imaging photographs of inorganic thermochromic samples, plaster of Paris with varnish or UV stabilizer. 80

4.11 Spectral reflectance of red thermochromic sample (RTC), red thermochromic sample at transition temperature (33°C) (RTC_33°C) and red conventional sample (RCO). . . . 83

4.12 Spectral reflectance of red thermochromic sample covered with polyurethane varnish (RTC_V), red thermochromic sample covered with polyurethane varnish at transition temperature (33°C) (RTC_V_33°C) and red conventional sample covered with polyurethane varnish (RCO_V). 84

4.13 Spectral reflectance of blue thermochromic sample (BTC), blue thermochromic sample at transition temperature (38°C) (BTC_38°C) and blue conventional sample (BCO). . 85

4.14 Spectral reflectance of blue thermochromic sample covered with polyurethane varnish (BTC_V), blue thermochromic sample covered with polyurethane varnish at transition temperature (38°C) (BTC_V_38°C) and blue conventional sample covered with polyurethane varnish (BCO_V). 86

4.15 Spectral reflectance of brown thermochromic sample (BrTC), brown thermochromic sample at transition temperature (43°C) (BrTC_43°C) and brown conventional sample (BrCO). 87

4.16 Spectral reflectance of brown thermochromic sample covered with polyurethane varnish (BrTC_V), brown thermochromic sample covered with polyurethane varnish at transition temperature (43°C) (BrTC_V_43°C) and brown conventional sample covered with polyurethane varnish (BrCO_V). 88

4.17 Spectral reflectance of commercial white coating and reference sample. 89

4.18 Conventional white paint (a), red thermochromic at room temperature (b), red thermochromic at 33°C (c). 91

4.19 Blue thermochromic at room temperature (a), blue thermochromic at 43°C (b). 91

4.20 Conventional white paint (a), brown thermochromic at room temperature (b), brown thermochromic at 43°C (c). 91

4.21 Average day/night surface temperature of the organic thermochromic sample. 93

4.22 Photographs of red thermochromic, conventional with varnish or UV stabilizer. 97

4.23 Photographs of blue thermochromic, conventional with varnish or UV stabilizer. . . . 98

4.24 Photographs of brown thermochromic, conventional with varnish or UV stabilizer. . . 99

5.1 Initial and aged spectral reflectance of sample: WCM-LMP. 102

5.2 Initial and aged spectral reflectance of sample: WCM-DMP. 102

5.3 Initial and aged spectral reflectance of sample: NHL-DMP. 103

5.4 Initial and aged spectral reflectance of sample: NHL-LMP. 103

5.5 Initial and aged spectral reflectance of sample: WCM-QUA. 104

5.6 Initial and aged spectral reflectance of sample: NHL-QUA. 104

5.7 Initial and aged spectral reflectance of sample: WCM-LMP-GB. 105

5.8 Initial and aged spectral reflectance of sample: WCM-DMP-GB. 105

5.9 Initial and aged spectral reflectance of sample: NHL-LMP-GB. 106

5.10 Initial and aged spectral reflectance of sample: NHL-DMP-GB. 106

5.11 Initial and aged spectral reflectance of sample: LMP-C-N. 107

5.12 Initial and aged spectral reflectance of sample: LMP-C-S. 107

5.13 Initial and aged spectral reflectance of sample: LMP-M-N. 108

5.14 Initial and aged spectral reflectance of sample: LMP-M-S. 108

5.15 Initial and aged spectral reflectance of sample: LMP-F-N. 109

5.16 Initial and aged spectral reflectance of sample: LMP-F-S. 109

5.17 Initial and aged spectral reflectance of sample: DMP-C-N. 110

5.18 Initial and aged spectral reflectance of sample: DMP-C-S. 110

5.19 Initial and aged spectral reflectance of sample: DMP-M-N. 111

5.20 Initial and aged spectral reflectance of sample: DMP-M-S. 111

5.21 Initial and aged spectral reflectance of sample: DMP-F-N. 112

5.22 Initial and aged spectral reflectance of sample: DMP-F-S. 112

5.23 Initial and aged spectral reflectance of sample: Portland Cement. 113

5.24 Initial and aged spectral reflectance of sample: Commercial cool coating. 113

5.25 Initial and aged spectral reflectance of sample: plaster of Paris (Pl), plaster of Paris with inorganic thermochromic (ITC) and plaster of Paris with inorganic thermochromic at 45°C (ITC_45°C). 118

5.26 Initial and aged spectral reflectance of sample: plaster of Paris + Ilam (Pl_V), plaster of Paris with inorganic thermochromic and Ilam (ITC_V) and plaster of Paris with inorganic thermochromic and Ilam at 45°C (ITC_V_45°C). 118

5.27 Initial and aged spectral reflectance of red thermochromic sample (RTC), red thermochromic sample at transition temperature (33°C) (RTC_33°C) and red conventional sample (RCO). 120

5.28 Initial and aged spectral reflectance of red thermochromic sample covered with polyurethane varnish (RTC_V), red thermochromic sample covered with polyurethane varnish at transition temperature (33°C) (RTC_V_33°C) and red conventional sample covered with polyurethane varnish (RCO_V). 120

5.29 Initial and aged spectral reflectance of blue thermochromic sample (BTC), blue thermochromic sample at transition temperature (38°C) (BTC_38°C) and blue conventional sample (BCO). 121

5.30 Initial and aged spectral reflectance of blue thermochromic sample covered with polyurethane varnish (BTC_V), blue thermochromic sample covered with polyurethane varnish at transition temperature (38°C) (BTC_V_38°C) and blue conventional sample covered with polyurethane varnish (BCO_V). 121

5.31 Initial and aged spectral reflectance of brown thermochromic sample (BrTC), brown thermochromic sample at transition temperature (48°C) (BrTC_48°C) and brown conventional sample (BrCO). 122

5.32 Initial and aged spectral reflectance of brown thermochromic sample covered with polyurethane varnish (BrTC_V), brown thermochromic sample covered with polyurethane varnish at transition temperature (48°C) (BrTC_V_48°C) and brown conventional sample covered with polyurethane varnish (BrCO_V). 122

6.1 3D view of the reference building in ESP-r. 131

6.2 The pertinent energy savings of the inorganic samples used on a poor-insulated building. 134

6.3 The pertinent energy savings of the inorganic samples used on a well-insulated building. 134

6.4 Comparison of the energy reduction on well versus poor insulated building. 135

6.5 The coupling methodology. 139

6.6 Building Model using ESP-r. 140

6.7 Aerial photo of campus buildings K1 and K2. 143

6.8 Building and trees/vegetation representation of the TUC campus. 145

6.9 Surfaces of the TUC campus. 146

6.10 The surface temperature of the TUC Campus for summer period at 12:00. 147

6.11 The air temperature around the TUC Campus Buildings for summer period at 12:00. 147

6.12 The wind speed and direction around the TUC Campus Buildings for summer period at 12:00. 148

6.13 Comparison between the 3 difference methods calculating CHTC. 151

6.14 3D representation of building and outdoor environment using Python. 153

6.15 Comparison of the room temperature for room K2.001. 154

6.16 Comparison of the room temperature for room K2.120. 155

6.17 Total energy needed for heating/cooling for all period. 158

6.18 Difference in power needed for heating for difference external CHTC for winter period. 158

6.19 Difference in power needed for cooling for difference external CHTC for spring period. 160

6.20 Difference in power needed for cooling for difference external CHTC for summer period. 160

6.21 Difference in power needed for cooling for difference external CHTC for autumn period. 161

6.22 Point for calculating the temperature change around the building. 164

6.23 Total energy needed for heating/cooling different SR values and all seasons. 165

6.24 Percentage of change in total energy needed for heating/cooling for different SR values and all seasons. 166

A.1 Spectral reflectance of sample: WCM-LMP. 183

A.2 Spectral reflectance of sample: WCM-DMP. 184

A.3 Spectral reflectance of sample: NHL-DMP. 184

A.4 Spectral reflectance of sample: NHL-LMP. 185

A.5 Spectral reflectance of sample: WCM-QUA. 185

A.6 Spectral reflectance of sample: WCM-DMP-GB. 186

A.7 Spectral reflectance of sample: WCM-LMP-GB. 186

A.8 Spectral reflectance of sample: NHL-QUA. 187

A.9 Spectral reflectance of sample: NHL-DMP-GB. 187

A.10 Spectral reflectance of sample: NHL-LMP-GB. 188

A.11 Spectral reflectance of first phase samples. 188

A.12 Spectral reflectance of sample: LMP-C-N. 189

A.13 Spectral reflectance of sample: LMP-C-S. 189

A.14 Spectral reflectance of sample: LMP-M-N. 190

A.15 Spectral reflectance of sample: LMP-M-S. 190

A.16 Spectral reflectance of sample: LMP-F-N. 191

A.17 Spectral reflectance of sample: LMP-F-S. 191

A.18 Spectral reflectance of sample: DMP-C-N. 192

A.19 Spectral reflectance of sample: DMP-C-S. 192

A.20 Spectral reflectance of sample: DMP-M-N. 193

A.21 Spectral reflectance of sample: DMP-M-S. 193

A.22 Spectral reflectance of sample: DMP-F-N. 194

A.23 Spectral reflectance of sample: DMP-F-S. 194

A.24 Spectral reflectance of sample: Portland Cement. 195

A.25 Spectral reflectance of sample: Cool White. 195

List of Tables

1.1 Comparison between common hot and cool roof systems: Solar reflectance and infrared emittance values 9

2.1 Basic technical characteristic of ThermaCAM B2. 33

3.1 Code names, composition of the samples developed in first phase. 44

3.2 Solar reflectance in near infrared, visible and ultraviolet wave-length of the 1^{st}, 2^{nd}, 3^{nd} group samples. 48

3.3 Infrared emittance of the 1^{st}, 2^{nd}, 3^{nd} group samples. 49

3.4 Code names, composition of samples developed in the second phase. 54

3.5 Solar reflectance in near infrared, visible and ultraviolet wave-length of the 4^{rth} group and reference samples. 58

3.6 Infrared emittance of the 4^{rth} group and reference samples. 59

3.7 Meteorological condition of the measurement site during summer 2017. 60

3.8 Daily monthly average/maximum surface temperatures of samples. 62

3.9 Nightly monthly average/maximum surface temperatures of samples. 63

4.1 Chemical composition of organic thermochromic pigments 71

4.2 Composition and codename of inorganic thermochromic coatings. 73

4.3 Solar reflectance in near infrared, visible, ultraviolet wave-length and infrared emittance of plaster of Paris, plaster of Paris + inorganic thermochromic. 75

4.4 Meteorological conditions during thermochromic coatings testing. 76

4.5 Average and maximum surface temperature for inorganic thermochromic samples during day and night. . . . 77
4.6 Thermal imaging measurement of the inorganic thermochromic samples. . . . 79
4.7 Consecration of organic thermochromic coating. . . . 81
4.8 Composition and codename of organic thermochromic coatings. . . . 82
4.9 Solar reflectance in near infrared, visible and ultraviolet wave-length of the organic thermochromic coatings. . . . 90
4.10 Infrared emittance of the organic thermochromic coatings. . . . 92
4.11 Average and maximum surface temperature for organic thermochromic samples during day and night. . . . 94
4.12 Thermal imaging measurement of the organic thermochromic samples. . . . 96

5.1 Initial and the difference in solar reflectance in near infrared, visible and ultraviolet wave-length of the 22 samples. . . . 115
5.2 Initial and the difference in infrared emittance of the 22 samples. . . . 116
5.3 Initial and the difference in solar reflectance in near infrared, visible, ultraviolet wave-length and infrared emittance of the inorganic thermochromic coatings. . . . 119
5.4 Initial and the difference in solar reflectance in near infrared, visible, ultraviolet wave-length and infrared emittance of the organic thermochromic coatings. . . . 123
5.5 Red thermochromic (RTC) side by conventional sample during the measuring period. . 125
5.6 Red Thermochromic coating covered with polyurethane varnish (RTC_V) side by conventional sample during the measuring period. . . . 126
5.7 Red thermochromic sample covered with UV stabiliser (RTC_S) side by conventional sample during the measuring period. . . . 127

6.1 Single room building characteristics. . . . 132
6.2 Solar reflectance of selected samples. . . . 133
6.3 Comparison of peak power on well and poor insulated building. . . . 135
6.4 Comparison of maximum roof temperature on well and poor insulated building. . . . 136
6.5 Main characteristics of the selected building. . . . 142

6.6 TUC campus surface material. 144

6.7 TUC campus plant species. 145

6.8 Initial meteorological condition for ENVI-met simulations. 156

6.9 Comparison of outdoor temperature and power for heating/cooling. 159

6.10 Comparison of difference in power needed for heating/cooling. 162

6.11 Difference in average air temperature around the K2 buildings (°C). 163

6.12 Comparison of difference in power needed for heating/cooling by different SR values and seasons. 168

B.1 Blue thermochromic (BTC) side by conventional sample during the measuring period. 198

B.2 Blue thermochromic tile covered with polyurethane varnish (BTC_V) side by conventional sample during the measuring period. 199

B.3 Blue thermochromic tile covered with UV stabiliser (BTC_S) side by conventional sample during the measuring period. 200

B.4 Brown thermochromic (BrTC) side by conventional sample during the measuring period. 201

B.5 Brown thermochromic tile covered with polyurethane varnish (BrTC_V) side by conventional sample during the measuring period. 202

B.6 Brown thermochromic tile covered with UV stabiliser (BrTC_S) side by conventional sample during the measuring period. 203

Acronyms

BES Building Energy Simulation.

CCW commercial cool coating.

CHTC Convective Heat Transfer Coefficient.

CICPs complex inorganic coloured pigments.

DMP dolomite marble powder.

DTA-TG Differential Thermal Analysis - Simultaneous Thermogravimetric.

FTIR Fourier transform infrared spectroscopy.

GB glass beads.

GIS Geographical Information System.

IE infrared emittance.

ITC bis(diethylammonium)tetrachlorocuprate(II).

LMP limestone marble powder.

MM5 Fifth-Generation Penn State/NCAR Mesoscale Model.

MMO metal oxide.

NHL natural hydraulic lime with pozzolanic additives.

NIR near infrared.

QUA quartz sand.

SR solar reflectance.

TC thermochromic.

UHI Urban Heat Island phenomenon.

UV ultraviolent.

VIS visible.

WCM white Portland cement.

WCO conventional white paint.

XRD X-ray diffraction.

Chapter 1

Introduction and state of the art

1.1 Introduction

In recent decades, a significant increase in the world's urban population has been recorded [1, 2]. One of the major problems of the cities' environment is the urban overheating. Overheating is attributed to the dense urban construction which accumulates heat over time and creates the Urban Heat Island phenomenon (UHI) [3–5]. According to this phenomenon, the air temperature in the urban areas is higher than the air temperature of sub-urban and rural areas. The air temperature difference between the urban and suburban areas is called the UHI intensity and may reach or exceed 10K in large cities [6]. The causes of the UHI are:

1. Accumulation of heat from anthropogenic activities, e.g. air conditioning [7, 8].
2. Lack of green areas leading to reduced evaporative cooling.
3. Re-emission of radiation from the atmosphere to the ground due to atmospheric pollution [9, 10].
4. Urban materials with high heat capacity and low reflectivity (asphalt, brick, tiles, etc.)[11].

Buildings and urban construction materials play an important role in the urban overheating [12]. Moreover buildings are responsible for the 40% of the world's primary energy consumption [13]. Therefore, there is an urgent need to improve buildings' energy performance through advanced materials.

The most important urban climate mitigation techniques aiming to the reduction of urban Heat Island intensity and contribute to the improvement of the urban thermal environment are:

- the use of highly reflective cool materials for the reduction of solar radiation absorption [14–18].
- the increase of green infrastructure within cities [19–21].
- the use of appropriate heat sink technologies [22, 23].

To this end the present thesis is focusing on cool materials' development, evaluation and testing.

1.2 Cool materials

1.2.1 The physics behind cool materials

When a surface is exposed to the sun the following physical processes take place and determine the surface temperature (Figure 1.1, Equations (1.1) and (1.2)).

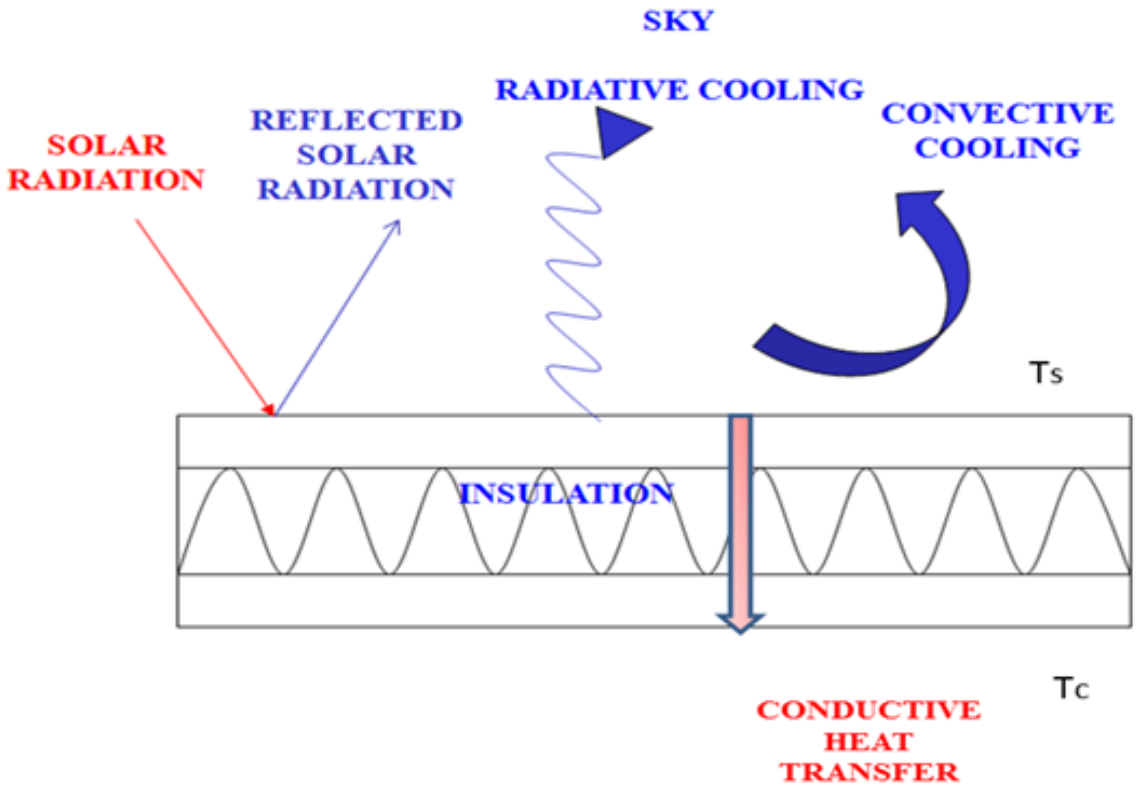

Figure 1.1 The energy balance of a material.

Solar radiation arrives on the surface and part of it is reflected and part absorbed by the material contributing to its heating. Consequently, the surface emits radiation in the far infrared part of the

spectrum as radiation exchange occurs between two surfaces when one is warmer than the other and they "view" each other. In addition, the surface exchanges energy by convection with the adjacent air. Finally, heat is conducted through the layers within the material, Figure 1.1 (insulation etc.) from the warmer side to the cooler side. The conduction induced heat flow through the material - Q_{in}, and hence the energy needed for heating or cooling, depends on the thermal resistance of the material and the difference in temperature between the outer and inner surfaces:

$$Q_{in} = \frac{T_s - T_c}{R} \tag{1.1}$$

where:

R	Overall thermal resistance of the material ($\frac{m^2K}{W}$)
T_s	Temperature of the outer surface of the material (K)
T_c	Temperature of the inner surface of the material (K)

In more detail, the equation describing the thermal balance of a horizontal surface exposed to the sun i.e. a roof [24, 25], is the following:

$$(1 - SR)I = \epsilon\sigma(T_s^4 - T_{sky}^4) + h_c(T_s - T_{sky}) + Q_{in} \tag{1.2}$$

Where:

I	insolation ($\frac{W}{m^2}$)
SR	solar reflectance or albedo of the surface
ϵ	emittance of the surface
σ	the Stefan–Boltzmann constant ($= 5.6685x10^{-8}\frac{W}{m^2}K^4$)
h_c	convection coefficient ($\frac{W}{m^2K}$)
T_{sky}	sky temperature (K)
T_a	air temperature (K)

If we consider that the roof is insulated underneath, the main factors affecting the thermal performance of the surface are the solar reflectance (SR) and the infrared emittance (IE). During the day the dominant factor is solar reflectance and infrared emissivity has a lower effect on the surface temperature. However, during night-time the surface temperature and the infrared emittance are strongly correlated which means that emissivity becomes the most important factor affecting the thermal performance [26, 27].

1.2.2 Cool materials properties

A cool material is characterized by:

a) High solar reflectance (SR), which is a measure of the ability of a surface material to reflect solar radiation. The term solar reflectance designates the total reflectance of a surface, considering the hemispherical reflectance of radiation, integrated over the solar spectrum, including specular and diffuse reflection. It is measured on a scale of 0 to 1 (or 0-100%).

b) High infrared emittance (IE), which is a measure of the ability of a surface to release, absorbed heat. It specifies how well a surface radiates energy away from itself as compared with a black body operating at the same temperature. Infrared emittance is measured on a scale from 0 to 1 (or 0-100%).

These two properties result in affecting the temperature of a surface [26, 28]. If a surface with high SR and IE is exposed to solar radiation it will have a lower surface temperature compared to a similar surface with lower SR. If the cool surface is on the building envelope, this would result in decreasing the heat penetrating into the building and for a surface in the urban environment this would contribute to decrease the temperature of the ambient air as the heat convection intensity from a cooler surface is lower (Figure 1.2).

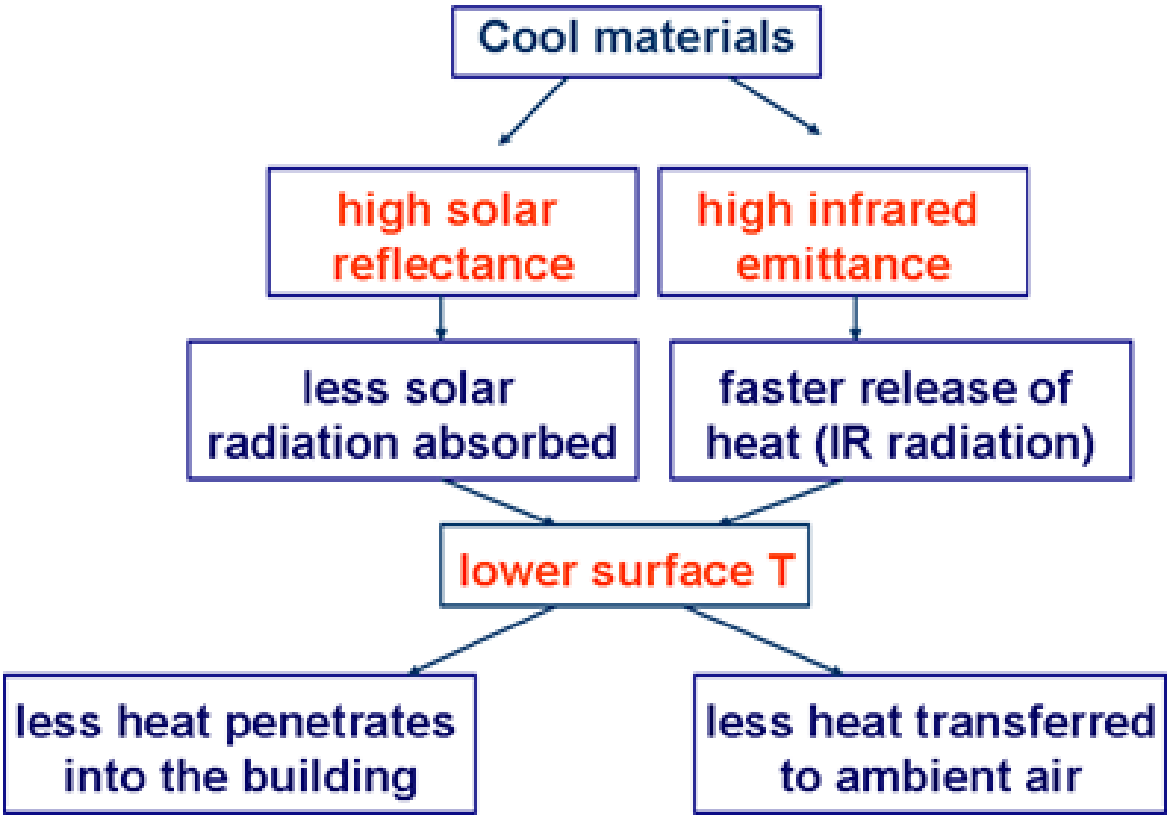

Figure 1.2 The basic principles of cool materials.

In Table 1.1, representative values for SR and IE are given for different conventional building materials and the corresponding available cool option. Figure 1.3 depicts the impact of a cool roof coating on surface temperature. The roof was initially covered by a conventional roof system consisting of asphalt membrane with siliceous aggregates (SR=0.1, IE =0.9). The temperature of the surface under hot summer conditions reached 65°C. On this conventional roof system a cool white elastomeric coating has been applied (SR =0.89, IE=0.9) and the surface temperature under similar weather conditions was reduced to 37°C i.e. a temperature difference of almost 30°C.

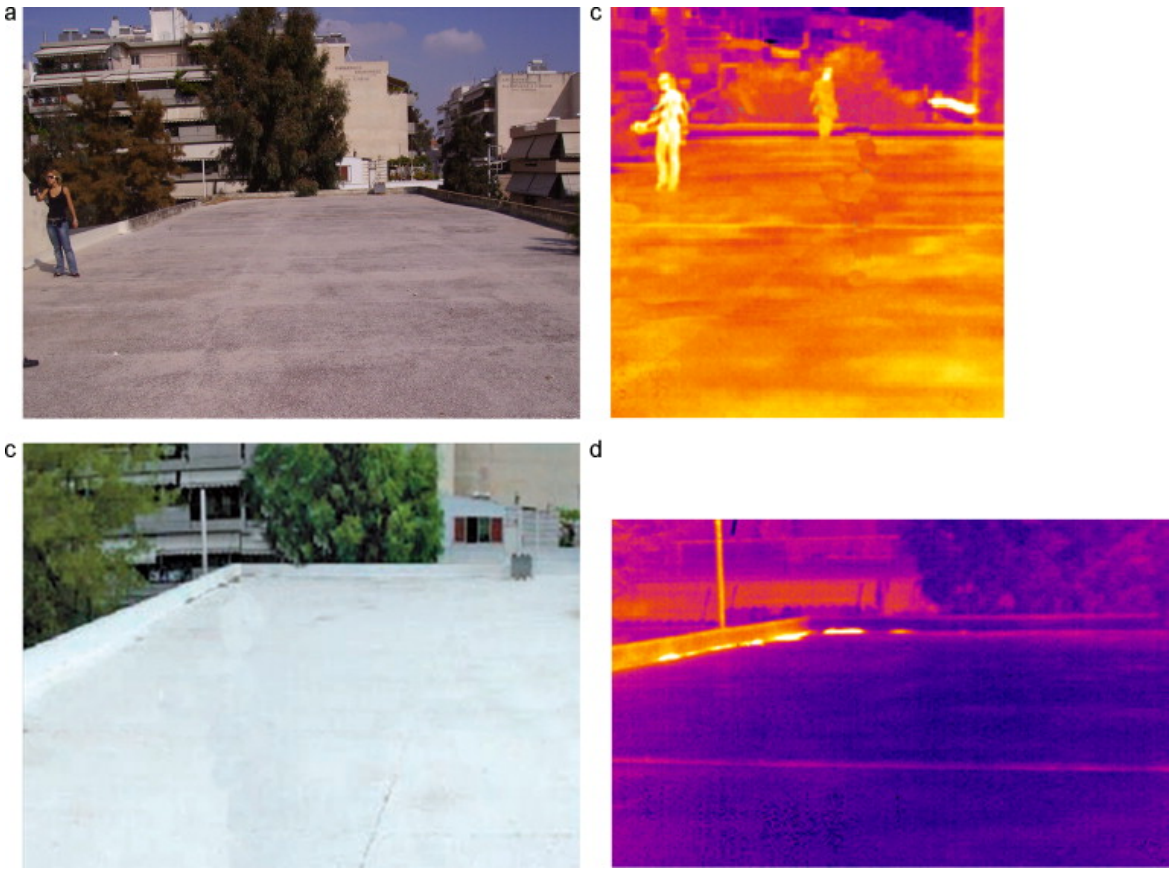

Figure 1.3 The impact of solar reflectance on roof surface temperature [29].

Table 1.1 Comparison between common hot and cool roof systems: Solar reflectance and infrared emittance values

Hot roof systems			Cool roof systems		
Roof Type	Reflectance	Emittance	Roof Type	Reflectance	Emittance
Built-up roof with dark gravel	0.08 – 0.15	0.80 – 0.90	Built-up roof with off-white gravel or cementitious coating	0.50 - 0.70	0.80 – 0.90
Single-ply membrane – Black PVC	0.04 – 0.05	0.80 – 0.90	Single-ply membrane – White PVC	0.70 - 0.78	0.80 – 0.90
Single-ply membrane – Black PVC	0.04 – 0.05	0.80 – 0.90	Single-ply membrane painted with coloured cool coating	0.30 - 0.80	0.80 – 0.90
Modified bitumen with mineral surface capsheet (SBA, APP)	0.10 – 0.20	0.80 – 0.90	Modified bitumen white coating over mineral surface (SBA, APP	0.60 - 0.75	0.80 – 0.90
Concrete tile Dark colour with conventional pigments	0.05 – 0.35	0.80 – 0.90	Cool concrete tile Coloured	0.40 - 0.65	0.80 – 0.90
Metal roof Unpainted, corrugated	0.30 – 0.50	0.05 – 0.30	Metal roof painted with couloured cool coating	0.05 - 0.80	0.80 – 0.90

Another way to assess how “cool” a material is, is to calculate its solar reflectance index (SRI). This is an index that incorporates both SR and IE in a single value. According to ASTM E1980-01 "Standard Practice for Calculating Solar Reflectance Index of Horizontal and Low-Sloped Opaque Surfaces” [30], SRI quantifies how hot a flat surface would get relative to a standard black (SR=0.05, IE=0.9) and a standard white surface (SR=0.8, IE=0.9). The calculation of this index is based on a set of equations (ASTM 1980E-01) that require measured values of SR and IE for specific environmental

conditions. The SRI is a value between zero (for the standard black surface) and 100 (for the standard white surface) and is calculated as follows:

$$SRI = \frac{(T_{\mathrm{B}} - T_{\mathrm{s}})}{T_{\mathrm{B}} - T_{\mathrm{W}}} 100 \tag{1.3}$$

Where T_B, T_W and T_s are the steady state temperatures of the standard black, standard white and the material surface respectively. From the definition of the SRI it is expected that very hot materials can actually have negative values and very cool materials can have values greater than 100.

When an area is needed to be characterised, the term albedo is used. It is defined for the case of diffuse reflection and expresses the ratio of the reflected to incident radiation at all wavelengths of the solar spectrum. It is a measure of the reflectivity of a surface. It is dimensionless in size and does not depend on the direction of the reflected radiation because it is considered as integral to the entire hemisphere of the reflected rays of all directions. Albedo is measured on a scale from zero (corresponding to a black body that absorbs all incident radiation) to one (corresponding to a body that reflects all incident radiation).

1.3 State of the art for cool materials

The state of the art is divided into the following parts:

1. Development of cool materials (Section 1.3.1).
2. Ageing and deterioration of cool materials (Section 1.3.2).
3. Impact of cool materials in buildings (Section 1.3.3).
4. Impact of cool materials in outdoor spaces (Section 1.3.4).

1.3.1 Development of cool materials

Various techniques, materials and methods have been explored for the development of cool materials and coatings, with increased SR and/or IE. Materials that contain transparent polymeric materials (cool paints), such as acrylic, along with white pigment, such as titanium dioxide (rutile), to make them opaque and reflective, have been proposed [27]. Other white pigments used are the anatase form of titanium dioxide, and zinc oxide. These coatings typically reflect 70–85% of the sun's energy. The replacement of conventional inorganic pigments with complex inorganic coloured pigments (CICPs) or metal oxide (MMO) can produce cool colour paints [31–34]. Uemoto *et al.* [34] developed using

CICPs cool white, brown and yellow colours to demonstrate an increase of SR from 20 to 60% and a reduction in air temperature under the roof sheet ranging from 10-30%. Han *et al.* [33] used MMO synthesized coloured coatings with synthesized pigments to get higher SR of 61–75% compared to conventional coating of the same colour and an indoor temperature difference reaching 4.5K.

Special design membranes for the roof can serve a dual purpose. Firstly for waterproofing the roof and secondly to cool it down. By adding specific components, i.e. titanium dioxide (TiO_2) and hollow ceramic microspheres to ordinary white membrane, Pisello *et al.* [35] calculated an improvement of the building's year-round energy efficiency by up to 19.3%. The addition of a mixture of metal oxide pigments i.e. CoAl, FeCr, and NiSbTi was characterized by an increased NIR SR of +0.40 compared to dark traditional membranes [36, 37].

Cool tiles are great in replacing traditional tiles in existing and historical buildings given their improved and architectural aesthetic. The use of ceramic or polymeric cool tiles offers better cool roofing performance, great architectural quality and thermal-energy attributes such as good optical properties and durability [38–40]. Colour composite tiles with relatively high SR, combined with a thin insulating layer made of a silica-gel super-insulating material with an aluminium foil with very low thermal emittance are proposed. The developed tiles provide a significant increase of roof thermal resistance [41].

Another category of cool roofs materials is the natural materials, that can generate important benefits to the buildings' thermal-energy performance given their intrinsic optimal thermal-optical properties. For example, gravel [42–44] is one of the most commonly used natural cool roof material for horizontal applications, especially in the Mediterranean area, as it can be simply applied over the existing bitumen membranes installed on the existing roofs. The specific material is consider sustainable from both an environmental and economic perspective, especially if locally available, due to the naturally light-coloured stones. Levinson *et al.* [42] developed three methods of rating the roofing aggregates' albedo based on pyranometer measurements. Castaldo *et al.* [43] exploited the use of gravel with SR 0.62 to cover the roof of a building and decrease the indoor operative temperature of about 3K in free-floating conditions, with respect to the traditional bitumen membrane. The passive cooling potential of different types of gravels characterized by different grain size was assessed in [45]. It was found that the albedo increases with decreasing grain size. In this same scenario, also light-coloured marble has been designated as a cool natural material due to its intrinsic cool characteristics [46, 47]. Results from experimental testing of the cooling potential of such material showed SR values of up to 79%. Moreover dynamic simulations allowed the calculation of up to 18% in summer cooling energy savings compared to a traditional non-cool concrete envelope.

Aqueous dispersions of organic thermochromic pigments were used to develop thermochromic coatings having a transition temperature of 30°C. The pigmented phase was microencapsulated showing an average particle size of 5μm [48]. Thermochromic cement at normal temperature was proposed by [49, 50] adding reversibly thermochromic microcapsules in white Portland cement. The research showed that the proposed materials could warm buildings' in winter and avoid buildings overheating in summer.

Even though the tested coatings range from cool materials, thermochromic, phase change materials, etc. nevertheless, weathering and corrosion can effectively diminish their performance [51]. This issue underlines the need for further research among the various materials used.

1.3.2 Aging and deterioration of cool materials

The ability of cool materials to maintain their optical properties is an important factor to be taken into consideration in their development. The main environmental factors that effect the aging process of roofing materials are the following [52–54]:

1. Solar radiation and temperature: The exposure of the roofing material to solar radiation ($1\frac{kW}{m^2}$) increases the temperature of the material. Temperature fluctuations damage a material due to the stresses that develop on it due to differential thermal expansion.

2. Wind: High wind speeds can apply high pressure to the roofing material causing structural degradation of the material.

3. Water: The optical characteristics of the roofing material can be altered by rain, hail and snow. Rain can sometimes restore the optical characteristics of the materials by removing dust and other pollutants.

4. Atmospheric gases and pollutants: Various oxides and hydroxides can be formed with the reaction of atmospheric oxygen and water vapour. Furthermore other chemical compounds formulated from combustion (CO_2, CO, SO_x, NO_x) when dissolved into water can produce acid that can cause material degradation. Also, other materials like dust can alter the optical characteristics of the material.

5. Biological growth. The growth of fungus on the materials usually may alter the optical characteristics of the material.

Paolini *et al.*[54] reported that on a four year period the cooling needs of a residential building decreased due to an increase by 26% of the SR. Due to the significance and time-consuming process

of aging the cool material, Sleiman in a series of publications [55–57] developed an accelerated aging method for a wide range of roofing products including cool materials. The developed protocol was evaluated by nine international laboratories and found to be credibly reproduced. According to the protocol, specimens are sprayed with a calibrated mixture of black carbon, salts, dust and organic surrogates. The calibrated mixture is produced using the albedos measured by Cool Roof Rating Council natural exposure program [58].

1.3.3 The effect of cool materials on buildings' energy performance and indoor environmental quality

The broad use of cool materials in the built environment both at the building and city level is beneficiary. The immediate results concerning the buildings, is the reduction of the external surfaces' temperature thus lowering the needed power and peak loads during summer months for air-conditioned buildings. In non air-conditioned buildings the use of cool materials can improve the thermal comfort [59].

The introduction of the cool materials to a building has the following effects:

Decrease of the cooling energy demand: The use of cool material on a building leads to lower surface temperatures. This leads to lower percentage of heat migrating to the interior of the building thus reducing the cooling energy needed for the cooling of the building.

A large amount of experimental measurements has been performed in various types of buildings. The surface temperature of roofs covered with cool materials is measured to be reduced up to 20K [60–63]. Bozonnet at al. [60] reported a reduction of more than 10K in 87 dwellings of a four-storey building in Poitiers, France. Romeo *et al.* [61] demonstrated a roof surface temperature decrease of up to 20K on a 700m^2 roof of a school building in Sicily, Italy. Kolokotroni *et al.* [62] evaluated a reduction of the surface temperature at university office building in London, UK by a maximum of 7.7K and an average of 6K during working hours (7.00–17.00). Pisello *et al.* [63] measured a reduction of approximately 15–18K in summer and by approximately 2–3K during winter in a traditional building in Italy.

The reduction of the external surface temperature has a significant role in lowering the cooling loads. Synnefa *et al.* [18] reported a reduction of the cooling loads by 18–93%. Romeo *et al.* [61] validated a 54% reduction in the cooling energy demand of a office/laboratory building in Sicily, Italy. Rosado *et al.* [64] calculated an annual cooling electricity savings per ceiling area of 2.82 kWh/m^2 (26%) and annual conditioning (heating + cooling) energy cost savings of \$0.886/m^2 (20%) when

compared to the standard home. Stavrakakis *et al.* [65] referred to a minimum 18% reduction of the cooling energy demand and under 12% heating penalty in winter. This leads to a minimum of 1.8% annual energy savings obtained when heat pumps are used for cooling.

Peak power decrease: The use of cool materials results in the reduction of the peak powers. The reduction in peak load in single buildings can be as high as 40% [66, 18, 67]. Miller *et al.* [67] compared dark roofs (SR=0.15) with cool roofs (SR=0.90). They found a peak demand reduction on a hot day ranging from 10% – 40%. Synnefa *et al.* [18] reported a peak cooling demand reduction in air-conditioned buildings by 11 – 27%. Akbari *et al.* [68] estimated that the wide use of cool roofs in USA may have a reduction of the peak load by 7GW (2.5%). The reduction of peak loads leads to cost savings especially in commercial and industrial buildings.

Increase of the thermal comfort: The use of cool material in buildings, contributes to the increase of the thermal comfort. Synnefa *et al.* [18] reported that the thermal comfort conditions were improved by decreasing the hours of discomfort by 9–100% and the maximum temperatures in non air-conditioned residential buildings by 1.2 – 3.3K. Romeo *et al.* [61] demonstrated that the effect of the cool coating in mitigating the thermal conditions resulted to an average operative temperature reduction of 2.3K during the cooling season. Pisello *et al.* [63] reported a decrease in daily average operative temperature in an attic by approximate 2K in June-August. In winter, the temperature decrease was consistently less than 0.5K. Stavrakakis *et al.* [65] measured a reduction of the hourly indoor air temperature below a cool roof by 1 – 2.6K in July. In addition on a warm summer operating day the PMV in the space below the roof was reduced by at least 24% thus increasing the thermal comfort.

1.3.4 The effect of cool materials on the urban spaces

The wide use of cool material in a town/neighbourhood has as an effect the increase of the albedo, improvement of the thermal comfort and the mitigation of the UHI effect during the summer months. The increase of albedo with the use of cool materials, reduces the surface temperature of pavements, roads etc. thus reducing the ambient air temperature [69, 15]. This leads to the increase of the thermal comfort in urban spaces [70]. The wide use of cool materials on the buildings' outer surfaces and on other urban surfaces is followed by a the reduction of the surface temperatures and consequently by a reduction of air temperature near these surfaces. Multi year (1983-2006) observations reported by Campra *et al.* [71], showed an important temperature reduction (0.3K/decade), because of the massive construction of high albedo greenhouses through the Almeria area in Spain.

The reduction in ambient air temperature in peak summer days was calculated to be up to 3K [72–74]. Rosenzweig *et al.* [72] using regional climate model Fifth-Generation Penn State/NCAR Mesoscale Model (MM5) [75] in combination with observed meteorological, satellite, and Geographical Information System (GIS) data determine that average reduction over all hours of the day near-surface air temperature in the New York Metropolitan Region were up to -1.7K with an average reduction at 15:00 as high as 2.9K. Millstein *et al.* [73] exploited a fully coupled regional climate model, Weather Research and Forecasting (WRF) model [76], to investigate feedbacks between surface albedo changes, surface temperature, precipitation and average cloud cover. With the adoption of cool roofs and pavements, domain-wide annual average outgoing radiation increased by 0.16 ± 0.03 W/m^2 and afternoon summertime temperature in urban locations was reduced by 0.11 - 0.53K. Sailor *et al.* [74] developed a regional climate model (MM5) for the city of Philadelphia, USA. By 0.10 increase of urban albedo, they found large regions of depressed air temperatures with average daytime depressions of about 0.3 - 0.5K. Santamouris [77] performed a meta-analysis of meteorological simulations performed in many U.S. cities to demonstrate that each 0.1 rise in urban albedo decreased the average outside air temperature by about 0.3K, and lowered the peak outside air temperature by 0.6–2.3K.

Several studies have been carried out for the effect of cool materials in city neighbourhoods with the use of computational fluid dynamics software [78–82]. Fintikakis *et al.* [81] examined the use of cool materials and other passive cooling techniques in the historical centre of Tirana, Albania. They found a reduction in ambient air temperature and surfaces temperature of 3K and 8K respectively. Dimoudi *et al.* [80] calculated a reduction in surface temperature up to 6.5K by using cool roofs and pavements in a medium size city in Greece.

1.4 Research objectives and methodology

Based on the state of the art previously described, the use of cool materials can contribute to the reduction of the energy consumption and to the increase of the thermal comfort. Several categories of cool materials have been proposed, developed and tested. In this framework, the aim of the present research has two major objectives:

1. Development and testing of a new series of cool materials and coatings using mineral based compounds, inorganic and organic thermochromic coatings. This work shows the ability of natural materials, such as hydraulic lime, etc. that already exist in local level, to formulate a low-cost cool coating alternative for buildings and pavements.

2. Development of an innovative calculation methodology for the evaluation of the cool materials' application in building, neighbourhood and city level. In this thesis a coupling mechanism is

developed that shows the interactions between the indoor and outdoor environment as well as the impact of cool materials in thermal comfort and energy efficiency.

The present thesis is divided into 7 chapters. The experimental equipment used for the characterization and measurements of the raw materials and cool coatings is presented in Chapter 2. The methodology followed for the first objective of the present research is illustrated in Figure 1.4. The work performed is analysed in detail in Chapter 3, 4 and 5. The methodology followed for the second research objective is depicted in Figure 1.5. The work performed is analysed in detail in Chapter 6 while Chapter 7 integrates the conclusions. The methodology and structure of the thesis is presented in Figure 1.6.

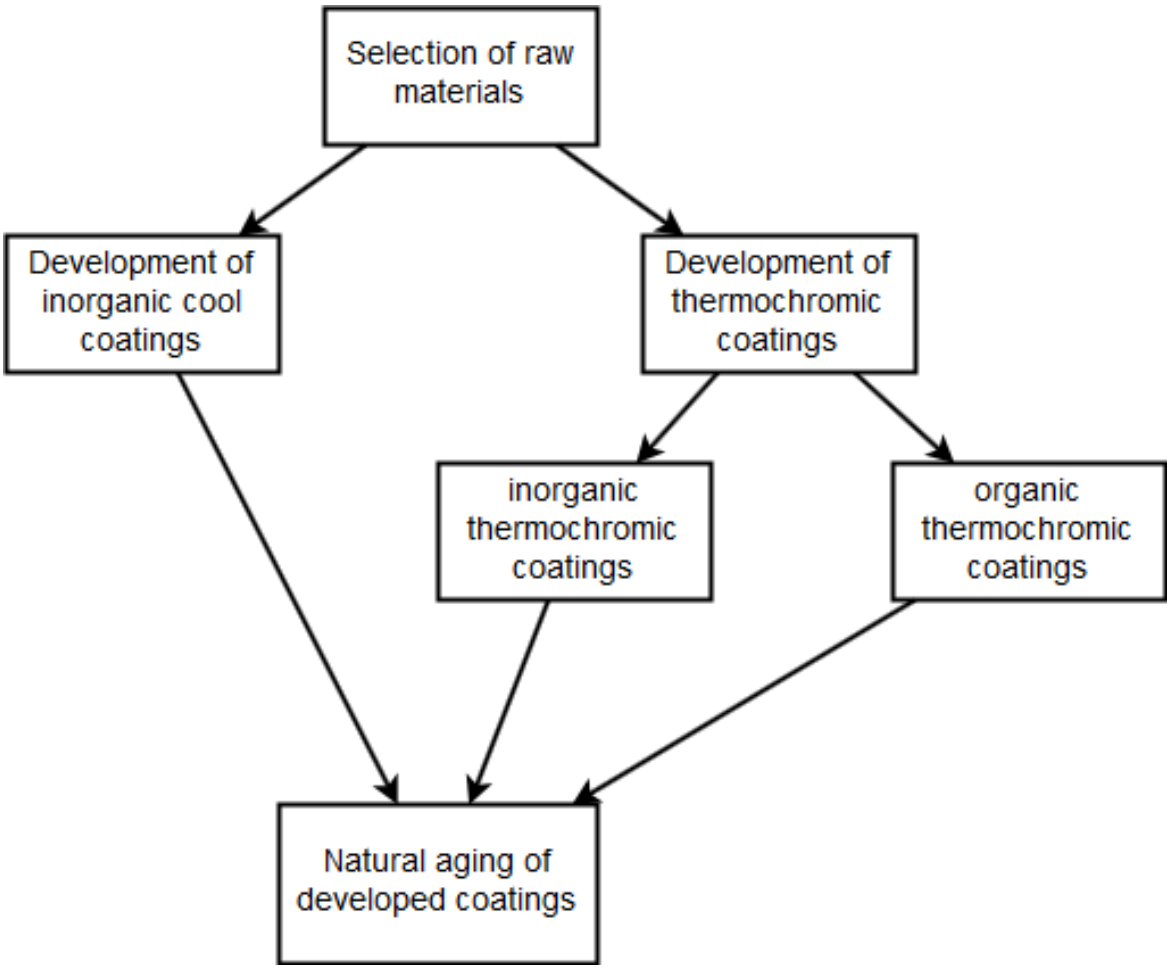

Figure 1.4 Steps for the creation of the cool coating.

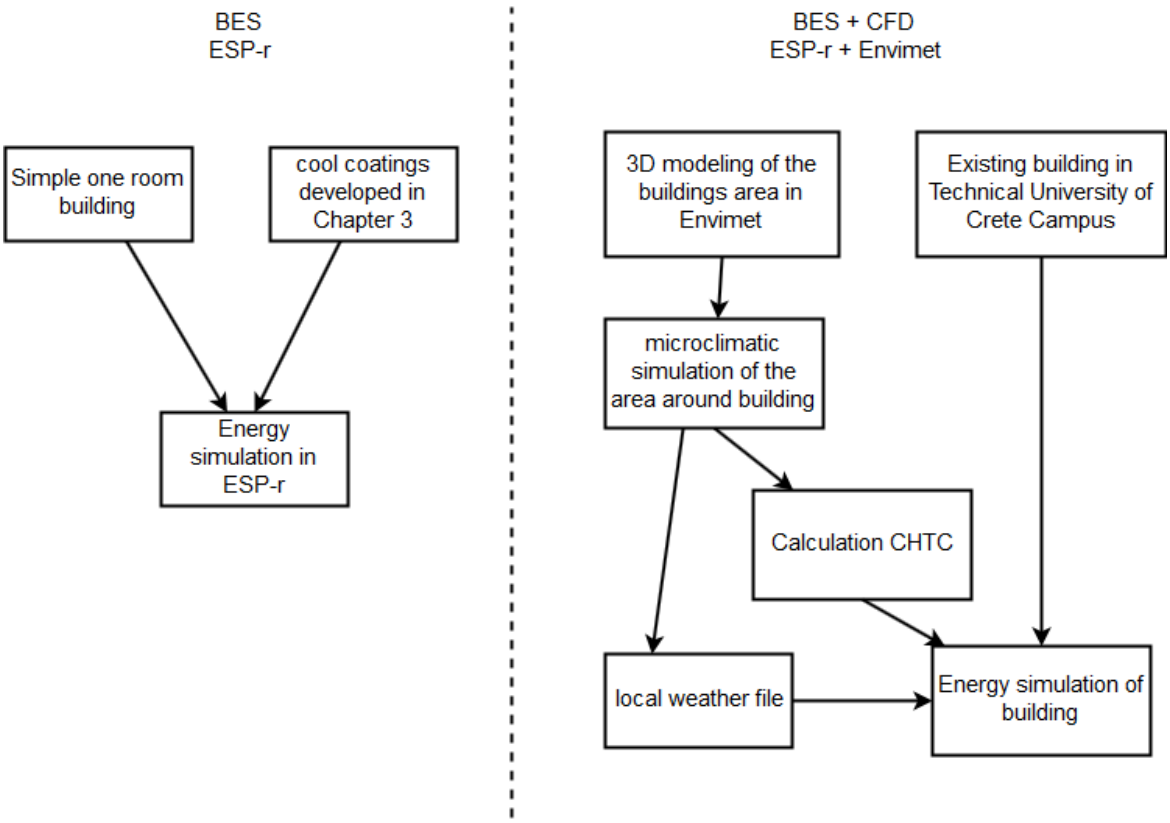

Figure 1.5 Steps for simulation the developed cool coating.

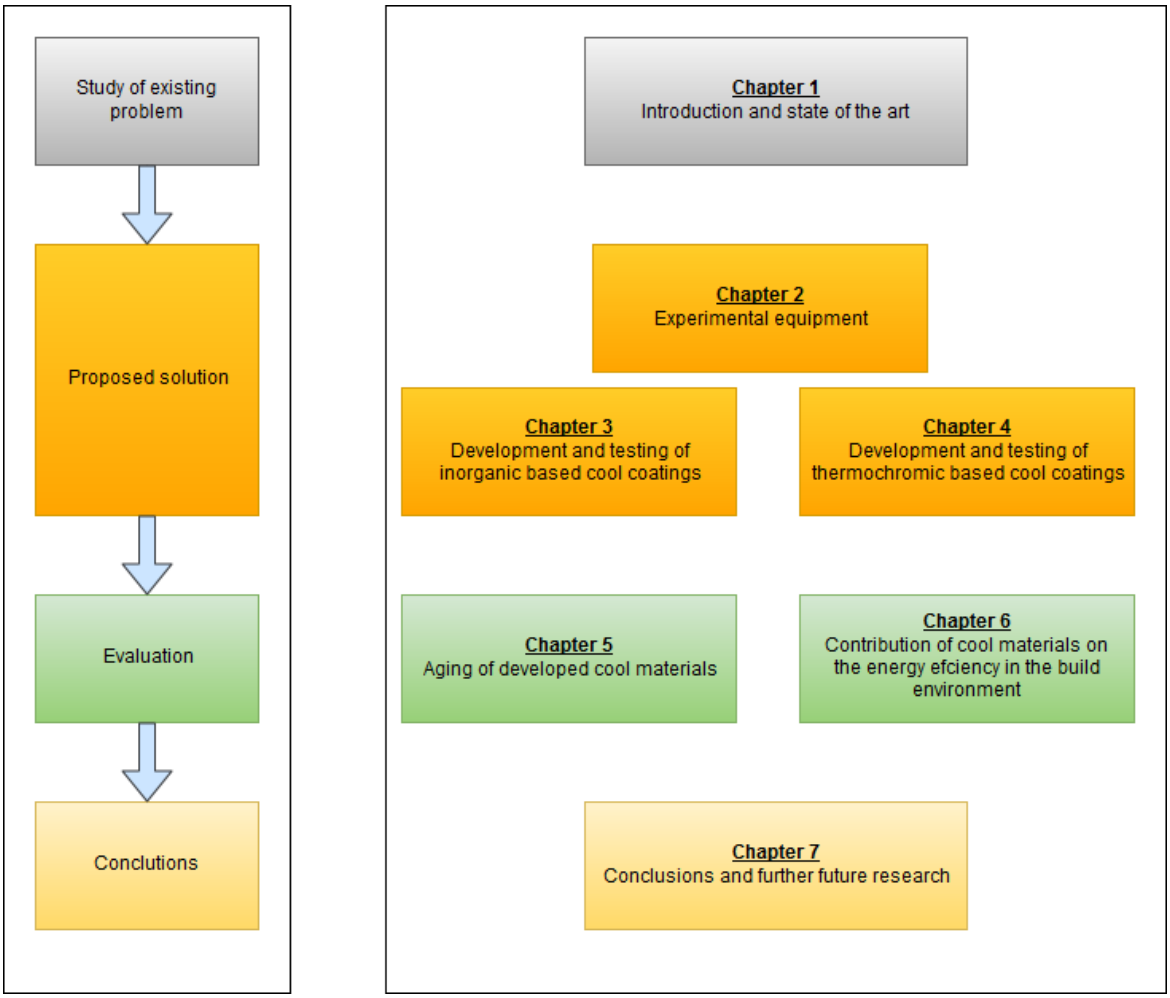

Figure 1.6 Methodology followed for the research.

Chapter 2

Experimental equipment

In the present chapter the characteristics and functionality of the experimental equipment and instruments used throughout the thesis are presented. The chapter in structured into two sections. The first section includes all the instruments used for the characterization of the raw ingredients. The second section is devoted to the instruments used for the analysis of cool material's properties.

2.1 Experimental equipment for materials' development and characterization

2.1.1 X-ray diffraction

X-ray diffraction enables the characterization of the structure and composition of raw ingredients used for the development of the samples. X-rays are electromagnetic radiation with wavelength of 0.01 nm to 10 nm. If an incident X-ray beam encounters a crystal lattice, generally scattering occurs. A regular array of scatterers produces a regular array of spherical waves. The spherical waves interfere either destructively or in a specific direction constructively. This is determined by Bragg's law $2d\sin\theta = n\lambda$ (Figure 2.1). Because each crystalline material has a characteristic atomic structure, it diffracts X-rays in a unique characteristic pattern.

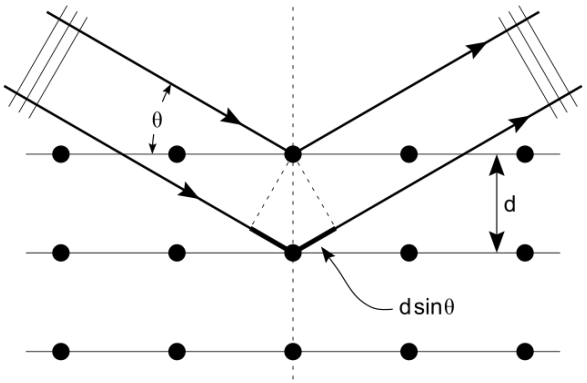

Figure 2.1 X-Ray diffraction [83].

The mineralogical analysis of the aggregates in the present thesis is carried out by X-ray powder diffraction analysis (XRD) on a Bruker D8 Advance Diffractometer (Figure 2.2), using Ni-filtered Cu Ka radiation (35 kV 35mA) and a Bruker Lynx Eye strip silicon detector. The quantitative XRD analysis is performed by the Rietveld method [84] using the software TOPAS from Bruker. A crystal structure Data Base from Bruker is used for the crystalline phases, which are analysed by the Rietveld method.

Figure 2.2 Bruker D8 Advance Diffractometer.

2.1.2 Fourier Transform Infrared Spectroscopy

The interaction between light and a sample can provide useful information about the sample's composition. Processes such as absorption, luminescence, emission and scattering are results of how electromagnetic radiation interacts directly with matter.

Infrared (IR) spectrophotometry is based on the absorption of radiation by matter in the infrared range of the electromagnetic spectrum and is characterized as one of the most important analytical techniques for characterizing the molecular structure and identification of organic and inorganic compounds [85]. Infrared spectroscopy is widely applied in many research and analytical fields.

Infrared radiation due to its low energy (12,800 - 10cm^{-1}), does not cause electron transitions but excitation between different energy levels of vibration and rotation of molecules, while the molecule remains in its fundamental energy state. A molecule is capable of absorbing infrared radiation only if its bipolar torque can be changed during vibration [86]. The absorption bands of the spectrum lead to the identification of the chemical compounds.

The range of infrared spectroscopy has expanded considerably over the past decades due to the development of infrared spectroscopy with Fourier Transform.

Fourier transform is the analysis of a mathematical function or an experimentally obtained curve in the form of a trigonometric series. It is used as a method of determining the harmonic components of a complex periodic wave [86].

In the context of the present thesis the Fourier transform infrared spectroscopy (FTIR) analysis is performed using a FTIR Perkin-Elmer 1000 spectrometer (Figure 2.4).

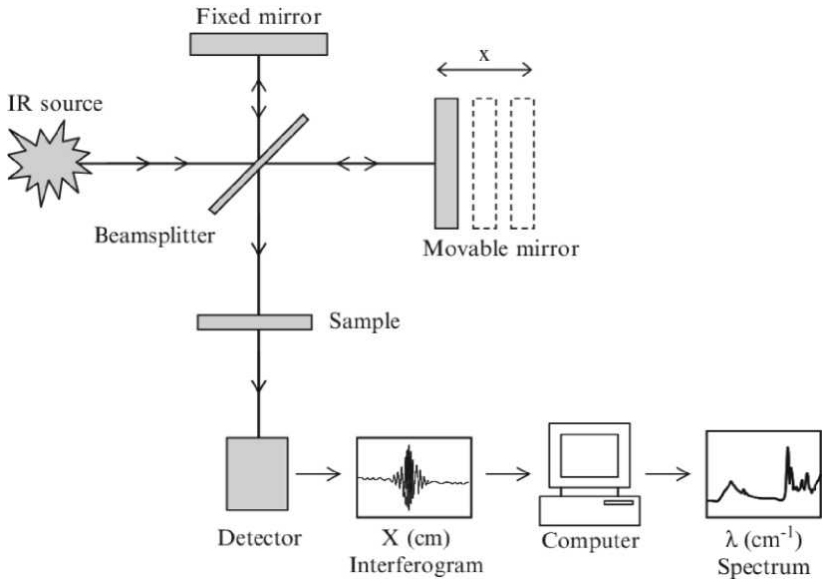

Figure 2.3 Schematic sketch of a Fourier transform infrared spectrometer (FTIR) [87].

Figure 2.4 FTIR Perkin-Elmer 1000 spectrometer.

Following the Figure 2.3 schematics, source emits infrared radiation that impinges on the beam splitter and is divided into two equal bundles (Figure 2.3). One of the two bundles passes the beam splitter and strikes the fixed mirror while the other is reflected to the beam splitter and strikes the mobile mirror. After both bundles reflect on the mirrors, the two beams meet again in the beam splitter and contribute. The merged beam that hits and interacts with the sample ends up to the detector. Then the received signal is transformed via Fourier transformation to produce a typical IR spectra

2.1.3 Differential Thermal Analysis

Thermal Analysis (TA) includes a set of techniques in which a physical property of a substance is recorded as a function of temperature when it changes in a programmed manner. These analytical techniques find application in the research and industrial sector, both for qualitative and quantitative control [86].

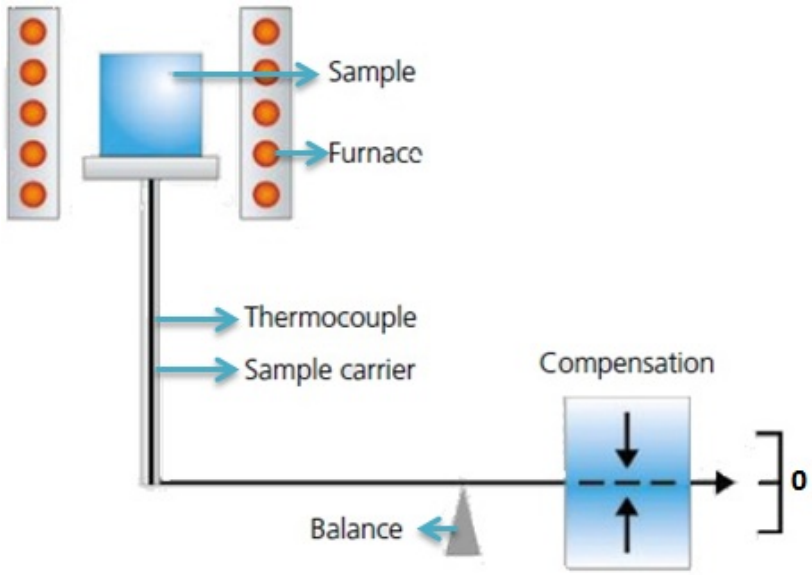

Figure 2.5 Schematic diagram of thermal analyses layout [88].

Thermal analytical techniques include more than 12 individual techniques that differ based on the property being recorded. The most widely used analytical techniques are: Thermogravimetry (TGA), Differential Thermal Analysis (DTA) and Differential Scanning Calorimetry (DSC). TGA analysis is based on the continuous recording of the sample mass as a function of temperature or time and as the temperature increases in a controlled environment. The resulting diagram of the mass change versus time is called thermogram or thermal decomposition curve. The change in the resulting mass relates to both breakdown or oxidation reactions and natural processes such as evaporation, sublimation and desorption [86]. The main parts of a thermal analyser are schematically shown on Figure 2.5.

In the context of the present thesis the Differential Thermal Analysis - Simultaneous Thermogravimetric (DTA-TG) analysis is performed using a Setaram LabSysEvo 1600 (Figure 2.6).

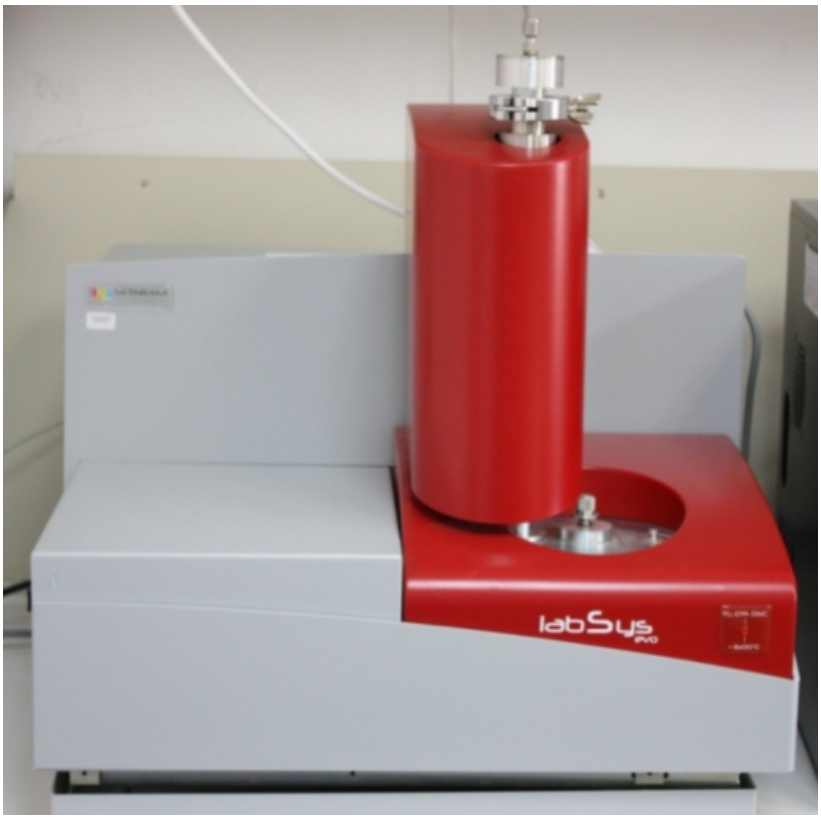

Figure 2.6 Setaram LabSysEvo 1600.

2.1.4 Laboratory sieving machine

For the development of inorganic based cool coatings, a known grading curve is needed for the aggregates. Grading curves of all aggregates are produced by a laboratory sieving machine, Retsch VE 1000 (Figure 2.7). It consists of a series of standard 20cm diameter American Standard Test Sieves (ASTM E11 [89]), having certain mesh sizes. The sieves are placed in a column, reducing the mesh sizes from above downwards. The mesh seize used are: 500 µm, 250 µm, 125 µm and 63 µm. The device can be used in various vibration frequencies and predetermined operating time.

Figure 2.7 Laboratory sieving machine, Retsch VE 1000.

2.1.5 Scale

For the development of cool coatings, the electronic scale Shimadzu TX223L is utilized to weight all the different ingredients (Figure 2.8).

Figure 2.8 High accuracy electronic scale.

2.2 Experimental equipment used for analysis of cool materials' properties

2.2.1 Experimental equipment for measuring the thermal emittance

The thermal emittance of the samples is measured with the aid of the specialized instrument, "Device and Services Emissometer model AE1" shown in Figure 2.9. The device measures the thermal emittance of the sample, relative to two known reference standards. The reference standard with high thermal emittance has a value of 0.88 while the low thermal emittance has a value of 0.06. The detector consists of an array of thermopiles and is heated at a constant temperature of 82°C.

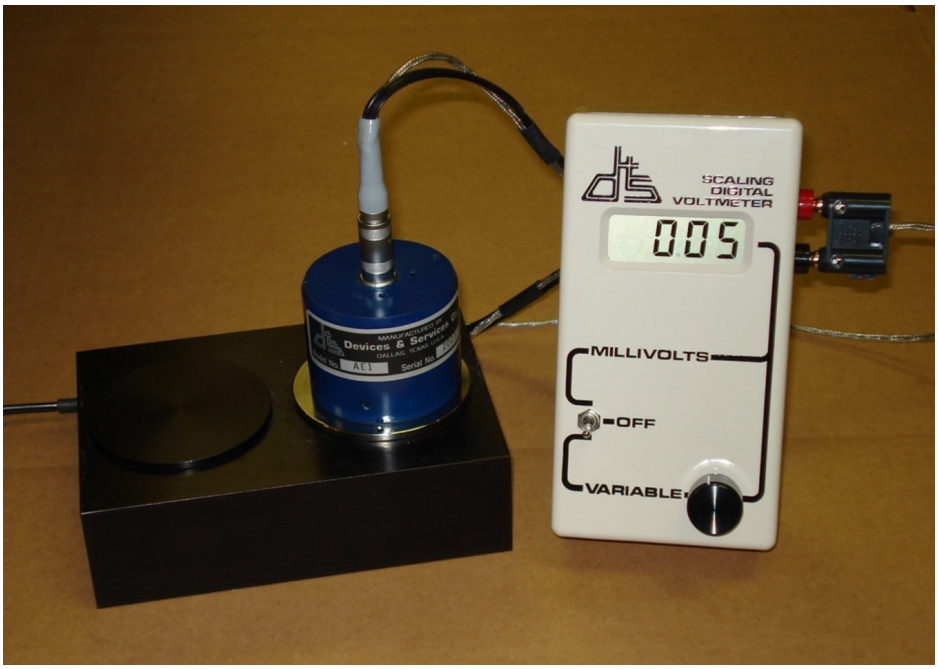

Figure 2.9 Device and Services emissometer model AE1.

Initially the device is calibrated by utilised both high and low reference standards and the calibration procedure is repeated every 20min. Since the samples have low thermal conductivity a special procedure has to be followed as described on the technical note TN 04-1 [90] provided by the manufacturer. The procedure is called "slide Method for high Emittance materials with low thermal conductivity"[91]. Both the samples and the heat sink is covered with the same wide masking tape with known thermal emissivity. A small fan is used to blow air on the surface of both the reference and the sample in order to achieve uniform temperature. A series of nine measurements every 30sec are taken covering the entire surface of the sample. The same procedures is used to measure the heat sink covered with wide masking tape. For both series of measurements, sample's and heat sink the graph of time - emittance is drawn (Figure 2.10). Next the trend line of the linear part of the measurements is drawn and R_o is calculated. The thermal emittance of the sample is calculated from

$$IE_{sample} = \frac{R_o \; for \; sample}{R_o \; for \; wide \; masking \; tape} \times IE_{wide \; masking \; tape} \tag{2.1}$$

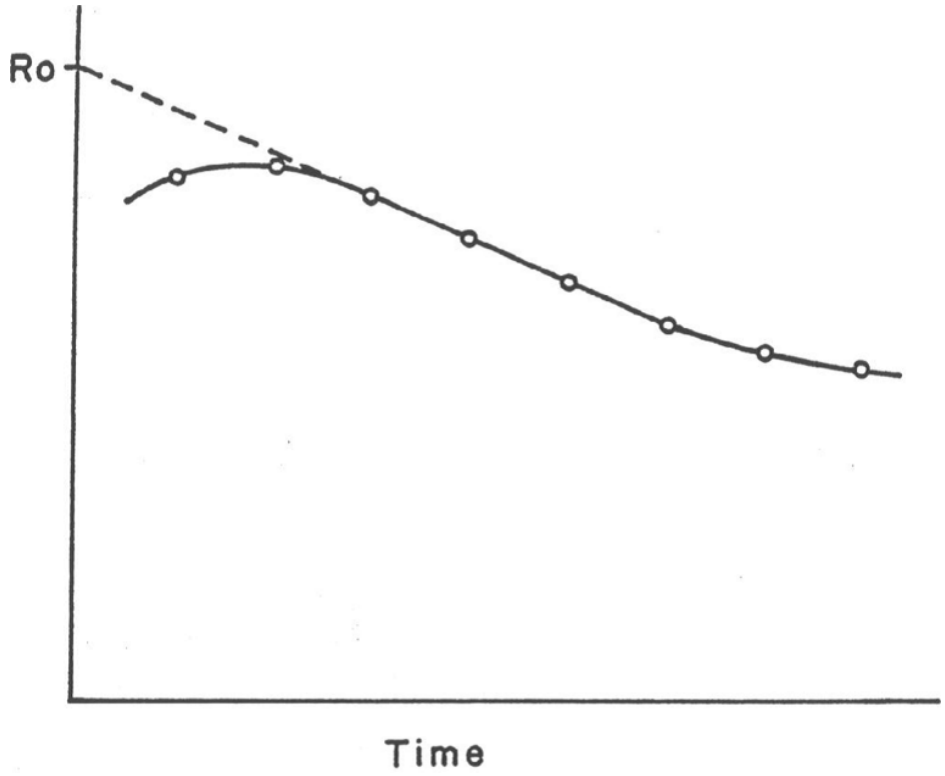

Figure 2.10 Transient response of emmissometer [91].

2.2.2 Experimental equipment for measuring the spectral reflectance

For the measurement of spectral characteristics of the cool materials developed, the ultraviolent (UV)/visible (VIS)/near infrared (NIR) spectrophotometer Carry 5000 by Agilent is used (Figure 2.11). The device measures the light intensity as a function of the light wave length either transmitted or reflected by the sample.

Figure 2.11 Carry 5000 with DRA 2500 integrating sphere.

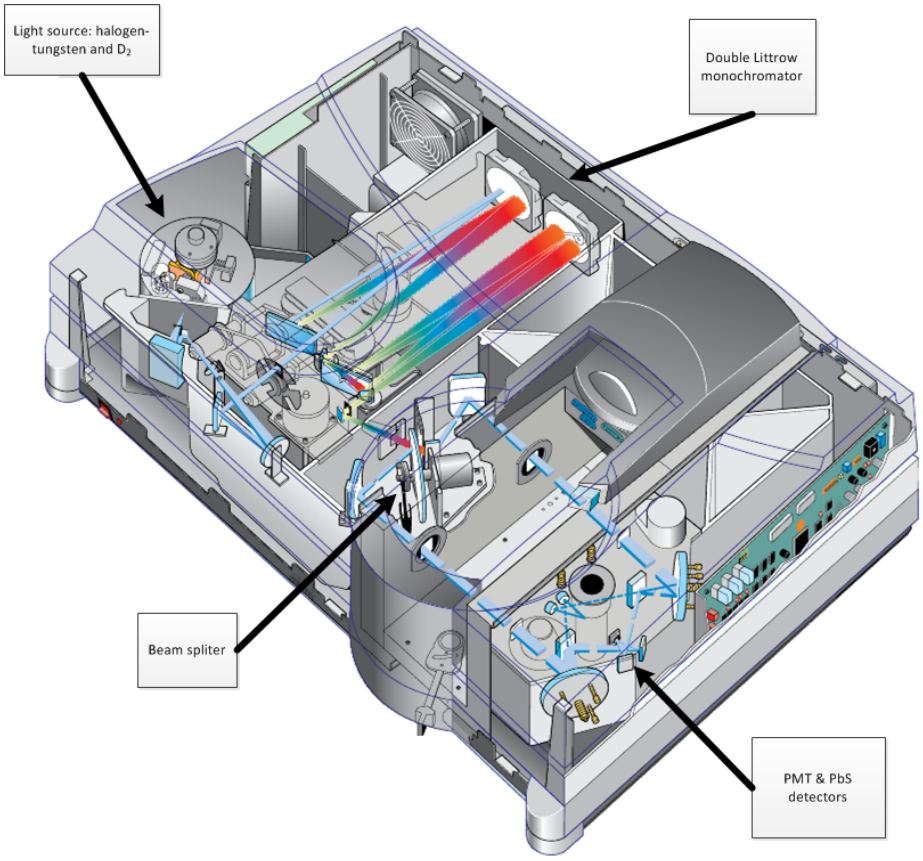

Figure 2.12 Schematic representation of Cary 5000.

Cary 5000 spectrophotometer is equipped with two light sources. The first is a halogen-tungsten lamp to generating light in visible and near infra-red spectrum. The second is a deuterium lamp (D_2) that generates light into ultraviolet spectrum (Figure 2.12). It uses two different light detectors, Photo Multiplier Tube (PMT) for the ultraviolet and visible light (175 nm to 900 nm) and PbS for the near-infra-red light (700 nm to 3000 nm). Depending on the placement of the sample, the measured radiation can be translated either as the reflectance or transmittance of the sample. The optical system of the instrument is equipped with minochromator in order to separate the continuous electromagnetic spectrum of light into a specific narrow band.

For measuring the reflectance of the samples, intergrading sphere with a diameter of 150 µm by Labsphere (DRA 2500) is added to the Cary 5000. The apparatus consists of a sphere with diameter of 150 µm covered with a high reflectance material, in our case Spectralon®[92]. Spectralon is a fluoropolymer produced by Labsphere and is an extremely white material with reflectance of 98% - 99% in the 200 nm to 2500 nm spectrum region. The material has the ability to reflect the incident radiation into a full diffused manner, meaning symmetrical to all directions. In this way, the detector placed at the button of the sphere will receive light regardless of the initial direction of the beam.

One of the main advantages of this instrument is its functionality of double beam measurement. This type of measurement requires a reference standard with known reflectance. The reflected radiation of the reference standard is continuously compared to the sample's reflected radiation. This ensures that any fluctuations or interferences due to the electronics, light source, detector and changes in the sphere are removed from the measurement at each time step.

2.2.3 Standards for measurement and characterization of cool materials properties

Various standards exist for the characterisation of cool materials [93]. Two non-profit organizations the Cool Roof Rating Council (CRRC), in the USA and the European Cool Roofs Council (ECRC) [94], operate to develop accurate and credible methods for evaluating and labelling the solar reflectance and infrared emittance of roofing products. The CRRC and ECRC have published guidelines [95, 96] in order to provide a unified and credible framework for rating and reporting the radiative properties of roofing products. Moreover Energy Star® [97], an government-backed symbol provided by U.S.A Environmental Protection Agency (EPA) has published cool roofs requirements [98]. Specific limits in the initial and aged solar reflectance (SR) for a roofing product to be awarded with Energy star logo are proposed. To measure solar reflectance of roofing materials, pyranometer, portable solar reflectometer and spectrophotometer are used. To measure infrared emittance of roofing materials, portable emissometers are used. The main standards for these measurements are:

1. ASTM E903 [99] in conjunction with ASTM E891 [100] air mass 1.5 beam normal spectrum: Standard Test Method for Solar Absorptance, Reflectance, and Transmittance of Materials Using Integrating Sphere, provides a procedure for measuring near-normal beam-hemispherical spectral reflectance using a spectrophotometer equipped with an integrating sphere. The measurements of spectral near normal-hemispherical reflectance are made over the spectral range from approximately 300 to 2500nm with an integrating sphere spectrophotometer. The solar reflectance is obtained by calculating a weighted average of the reflectance with a standard solar spectral irradiance as the weighting function by direct calculation of suitable convolution integrals.

2. C1549-09 [101] in conjunction with ASTM E891 [100] air mass 1.5 beam normal spectrum: Standard Test Method for Determination of Solar Reflectance Near Ambient Temperature Using a Portable Solar Reflectometer. ASTM C1549-09 describes the process for determining the solar reflectance of flat opaque materials in a laboratory or in the field using a commercial portable solar reflectometer. The portable solar reflectometer is calibrated using specimens of known solar reflectance to determine solar reflectance from measurements at four wavelengths in the solar spectrum: 380nm, 500nm, 650nm, and 1220nm. Software in the instrument combines the outputs of the four detectors in appropriate proportions to approximate the response for incident solar radiation through air mass 1.5.

3. ASTM C1371 [102]: Standard Test Method for Determination of Emittance of Materials Near Room Temperature Using Portable Emissometers, provides a technique for determination of the emittance of typical materials using a portable differential thermopile emissometer. The purpose of the test method is to provide a comparative way of quantifying the emittance of opaque, highly thermally conductive materials, in near room temperature conditions.

2.2.4 Surface temperature data loggers

For the acquisition of surface temperature of the samples, two different types of measuring equipment are used. For the initial measurements, a set of 2 data loggers Omega Engineering HH306A (Figure 2.13) with K-type thermocouples (Figure 2.15a) are utilised. The measurement range of this particular equipment is $-200\,^{\circ}\mathrm{C}$ to $1370\,^{\circ}\mathrm{C}$ $\pm 0.2\%$. With the proposed setup only 12 samples (four thermocouples per data logger) can be measured at the same time. For the remaining of the experiments a CR850 measurement and control datalogger (Figure 2.14a) along with a AM16/32B 32-Channel relay multiplexer (Figure 2.14b) from Campbell Scientific is used. The analogue voltage accuracy is 0.06% of reading at $0\,^{\circ}\mathrm{C}$ to $40\,^{\circ}\mathrm{C}$ and the analogue resolution $0.33\,\mu\mathrm{V}$. The multiplexer has on-board reference junction in order to compensate and accurately calculate the temperature from the voltage

difference of the thermocouple. Custom 10 m K-type thermocouples are constructed (Figure 2.15b). The K-type thermocouples are made from 30 gauge double insulated Kapton thermocouple wire by Omega engineering (product code TT-K-30-500). With the new setup a maximum of 32 simultaneous surface measurements could be achieved. A small 1x1x1 cm white ploysterine block on the top of each sample is placed to ensure transfer of the surface temperature to the thermocouples and eliminate the impact of solar radiation.

Figure 2.13 Data logger HH306A.

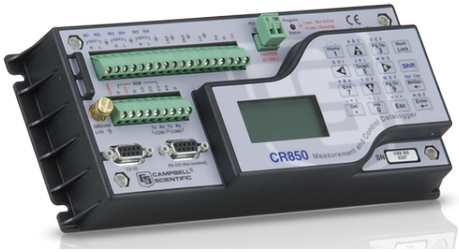

(a) CR850.

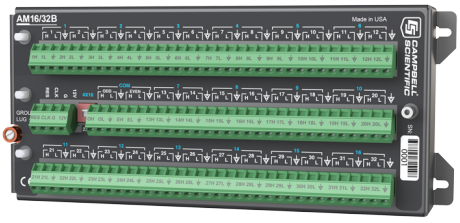

(b) AM16/32B 32-Channel relay multiplexer.

Figure 2.14 Data logger from Campbell Scientific.

(a) K-type thermocouple Model: 5SC-KK-K-30-36.

(b) Custom K-type thermocouple.

Figure 2.15 K-type thermocouples.

2.2.5 Thermal imaging camera

The surface temperature distribution of the developed sample is measured with the thermal imaging camera, ThermaCAM B2 by Flir Systems (Figure 2.16). In the photograph (Figure 2.17) surface temperature is displayed in different colours depending of the temperature scale that exist on the right side of the each thermal imaging picture. The thermal imaging camera measures the temperature using the Stefan-Boltzmann equation (Equation (2.2)).

$$E = \epsilon \sigma T^4 \tag{2.2}$$

where ϵ is the emittance of the material, $\sigma = 5.6703x10^{-8} \frac{W}{m^2 K^4}$ and T the temperature of the material in K.

The technical characteristics of the thermal imaging camera are tabulated in the following Table 2.1:

Table 2.1 Basic technical characteristic of ThermaCAM B2.

Temperature range	−20 °C to 100 °C
Accuracy	±2 °C
Repeatability	±1 °C
Thermal sensitivity	0.1 °C at 30 °C
Field of view/min focus distance	Typical 19°x 14°/0.3 m
Detector type	Focal Plane Array (FPA), uncooled microbolometer 160 x 120 pixels
Spectral range	7.5 µm to 13 µm

Figure 2.16 Thermal imaging camera: Flir ThermaCAM B2.

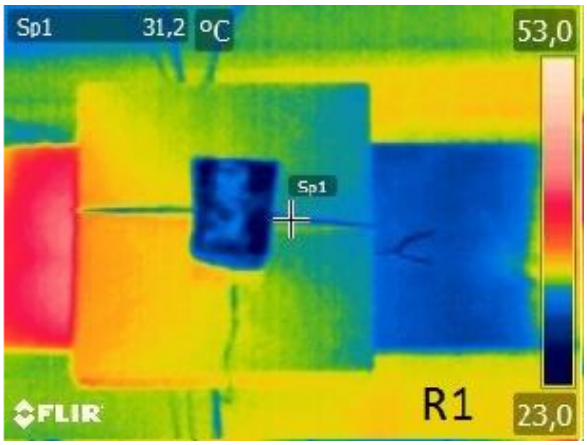

Figure 2.17 Thermal imaging picture.

Chapter 3

Development and testing of inorganic based cool coatings

3.1 Introduction

The aim of the present chapter is to describe the development of inorganic based cool coatings. The development phase of the cool coatings is split into two periods. During the first period ten different coatings are developed using locally sourced raw materials. During the second period two out of the ten different coatings developed in the first period, used to test, different grain sizes of the raw materials along with different surface finishing.

3.2 Materials and methods

3.2.1 Renders

In this section the materials used to create the coatings are explained. First, the render synthesis is described. Render is a mixture of aggregate (usually sand), lime, water and binder. The ration of raw material depends of the render type and use.

Render synthesis and preparation is done in the form of pulp which congeals and hardens under the effect of atmospheric air or water depending on the binder type. In the first step of the synthesis, render in the plastic state, can be formed into any shape and form without affecting its final properties. As time passes (duration depends on the binder type and environmental conditions of temperature

and humidity) the render starts to solidify and to transform into a solid object. The binder is filling the space between aggregate particles, so the ratio of binder/aggregate must be correctly selected. If the mixture has excess amount of binder, the final product will have reduced durability and higher price. If the mixture is poor, the final product is porous and with reduced durability.

Various render types are widely used for coating various surfaces. The aim is to protect, insulate and improve the general aesthetic appearance of the surfaces. These are called "coatings". Coatings are distinguished into two major categories, depending on whether they are used in the inside or outside surfaces of the building. Surface orientation, location and texture dictate the type of render to be used in each application. For hundreds of years external renders are used on the external surface of buildings to increase the resistance to weathering [103–105].

3.2.2 Aggregates

The term "aggregates" generally characterizes all the materials (usually stone and granulates from natural or artificially crushed natural stone) used in conjunction with binders (cement) and welded together to form the render. In this subsection the aggregates used to formulate the cool coatings are described.

3.2.2.1 Dolomite marble powder

Dolomite marble is a carbonate rock that contains up to 10% calcite ($CaCo_3$) and at least 90% mineral dolomite. Dolomite mineral chemical formula is: $CaMg(C0_2)_3$, commonly found in white colour (may also appear as yellow, grey or even black dependently on the impurities) and a Mohs hardness of 3.5 - 4.5.

The dolomite marble powder (DMP) (Figure 3.2a) aggregate used in the experiments according to the results of X-ray diffraction (XRD) (Bruker D8 Advance Diffractometer, Section 2.1.1) analysis contains 92.8% dolomite, chlorite ($Mg_6Si_4O_10(OH)_8$) 3.3%, calcite ($CaCO_3$) 2% and illite ($K(Al_4Si_2O_9(OH)_3$) 1.8%. In Figure 3.1 the XRD pattern of the DMP marble powder is depicted.

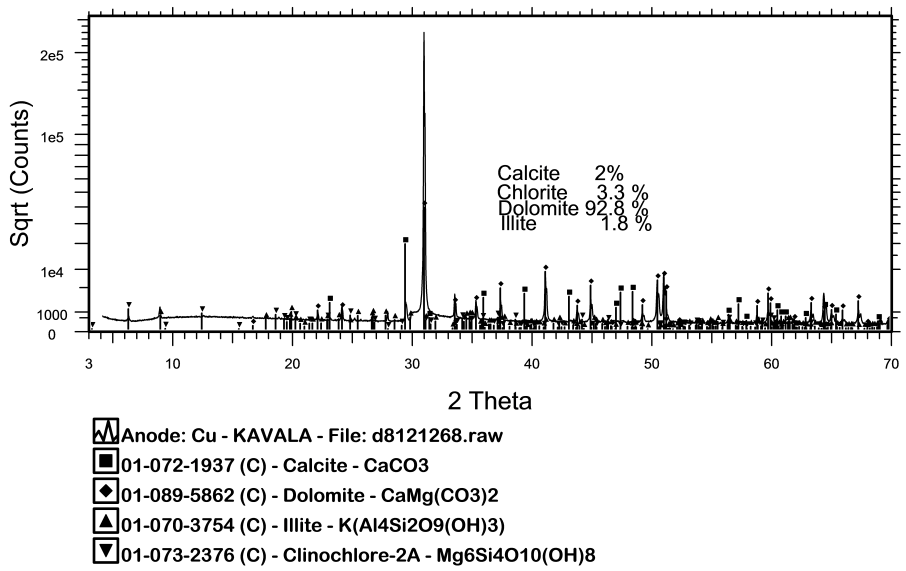

Figure 3.1 XRD spectrum of the dolomite marble powder aggregate.

(a) Dolomite marble powder. (b) Limestone marble powder. (c) Quartz sand.

Figure 3.2 Aggregates used for the development of the samples.

3.2.2.2 Limestone marble powder

Limestone marble is a metamorphic rock composed of recrystallized carbonate minerals, most commonly calcite. Limestone marble is found to be white coloured. The limestone marble powder (LMP) aggregate used in the experiments according to the of XRD (Bruker D8 Advance Diffractometer, Section 2.1.1) analysis shows that the aggregate contains calcite 90%, dolomite 8.9% and quartz (SiO_2) 0.2%.

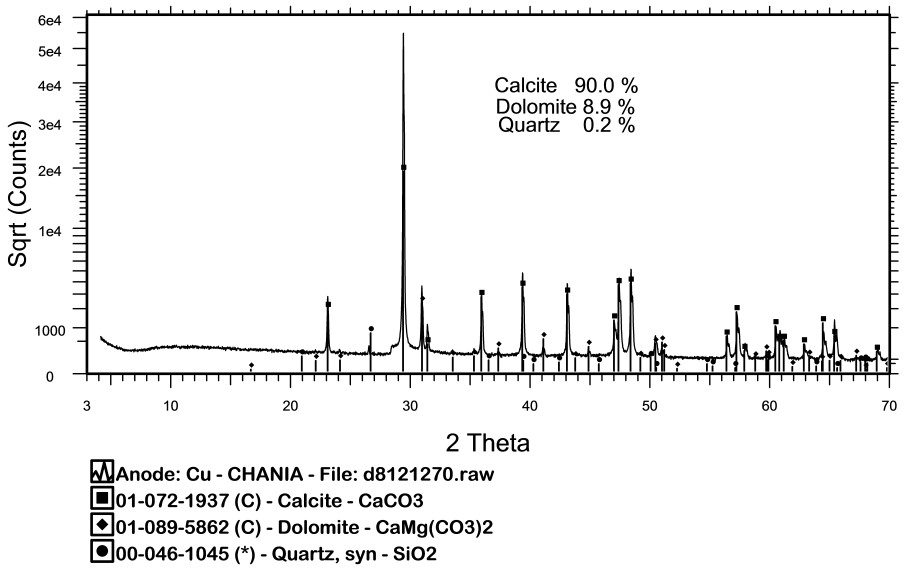

Figure 3.3 XRD spectrum of the limestone marble powder aggregate.

3.2.2.3 Quartz sand

Quartz sand (QUA) (SiO_2) is an important mineral of the lithosphere and participates in the constituents at about 12%. Quartz is the most important sand-forming mineral because it is resistant to both physical and chemical weathering. The QUA aggregate (Figure 3.2c) used in the experiments according to the results of XRD (Bruker D8 Advance Diffractometer, Section 2.1.1) analysis (Figure 3.4), demonstrates that the aggregate contains quartz 96.8%, albite ($NaAlSi_3O_8$) 1.5% , calcite 1.1% and microcline ($KAlSi_3O_8$) 0.6%.

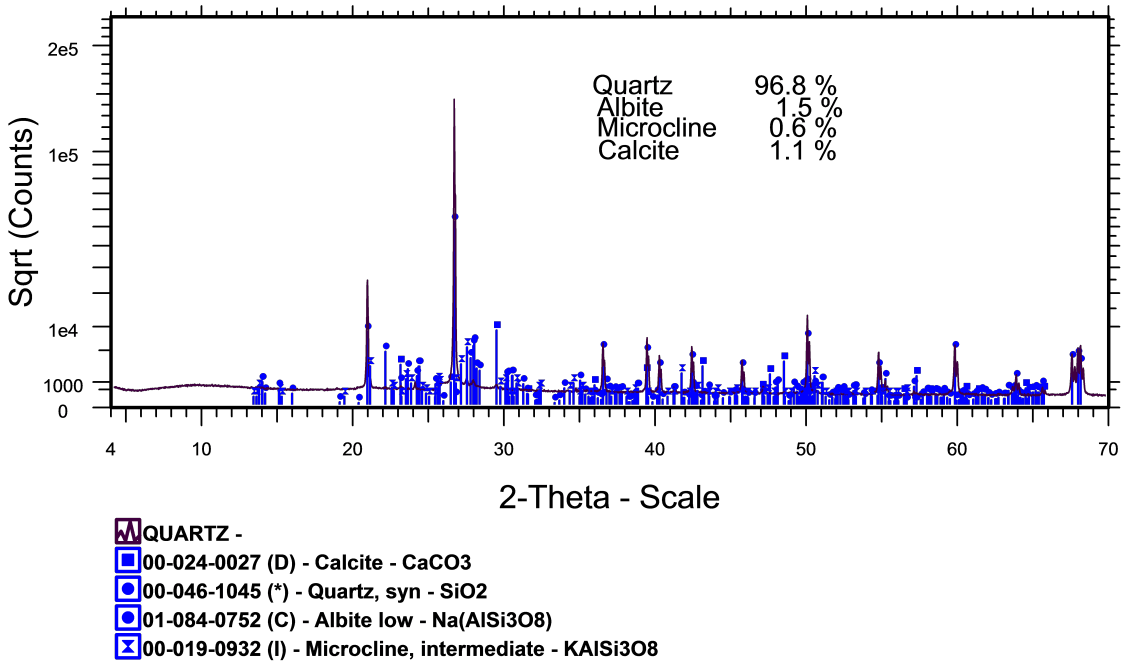

Figure 3.4 XRD spectrum of the quartz sand aggregate.

3.2.2.4 Glass beads

Glass beads (GB) are constructed by the pulverization of new or reclaimed glass into powder. This powder is then poured, sprayed, or sprinkled into a large multi-storey furnace. The individual particles are blown through several flames until they softened and sphere shaped. These spherical droplets are cooled in the top half of the furnace and are then collected and sieved through specially designed grading screens. The glass beads (Figure 3.5) used in the experiment have diameter from 180 nm to 850 nm, with refractive index 1.5 and Mohs hardness 6-7.

Figure 3.5 Glass beads.

3.2.3 Lime

Lime is the conventional name of the white coloured product formed by calcification and further treatment of limestone. It is used to describe both quicklime and the reacted product with water, called slaked lime or hydrated lime. Limes is found in huge spectrum of applications. It is one of the oldest binders used for making mortar. When common limestone is calcined between 800 °C and 1100 °C, calcium carbonate ($CaCO_3$) is decomposed to carbon dioxide gas (CO_2) and the solid calcium oxide or activated calcium (CaO).

$$CaCO_3 \rightarrow CaO + CO_2 \tag{3.1}$$

Calcium oxide reacts rapidly with water, releasing heat and giving hydrated lime, [$Ca(OH)_2$]. The hydration of lime is a reversible reaction described by following equation:

$$CaO + H_2O \rightarrow Ca(OH)_2 \tag{3.2}$$

3.2.4 Binders

The binders used in the present thesis are described in this section.

3.2.4.1 Natural hydraulic lime with pozzolanic additives

Natural hydraulic lime is produced by calcining agillaceous or siliceous limestone at temperatures from 900 °C to 1200 °C [106]. Natural hydraulic lime conforming to EN459 [107] is typically used for repointing/rendering and building works on most masonry types. Pozzolan or pozzolanic materials react with calcium hydroxide and form hydraulic compounds acting as binders, which enhance the strength gain of hydrated, hydraulic and natural hydraulic lime mortars. In particular, pozzolan additions to a lime indicated by the letter Z, following the lime designation e.g. NHL-3.5Z, are also included in this study. Among the specific characteristics of these materials the most important are the high water permeability and the durability to outdoor corrosion [108, 109]. With the help of the XRD (Bruker D8 Advance Diffractometer, Section 2.1.1) the composition of the natural hydraulic lime with pozzolanic additives (NHL) is presented in Figure 3.6.

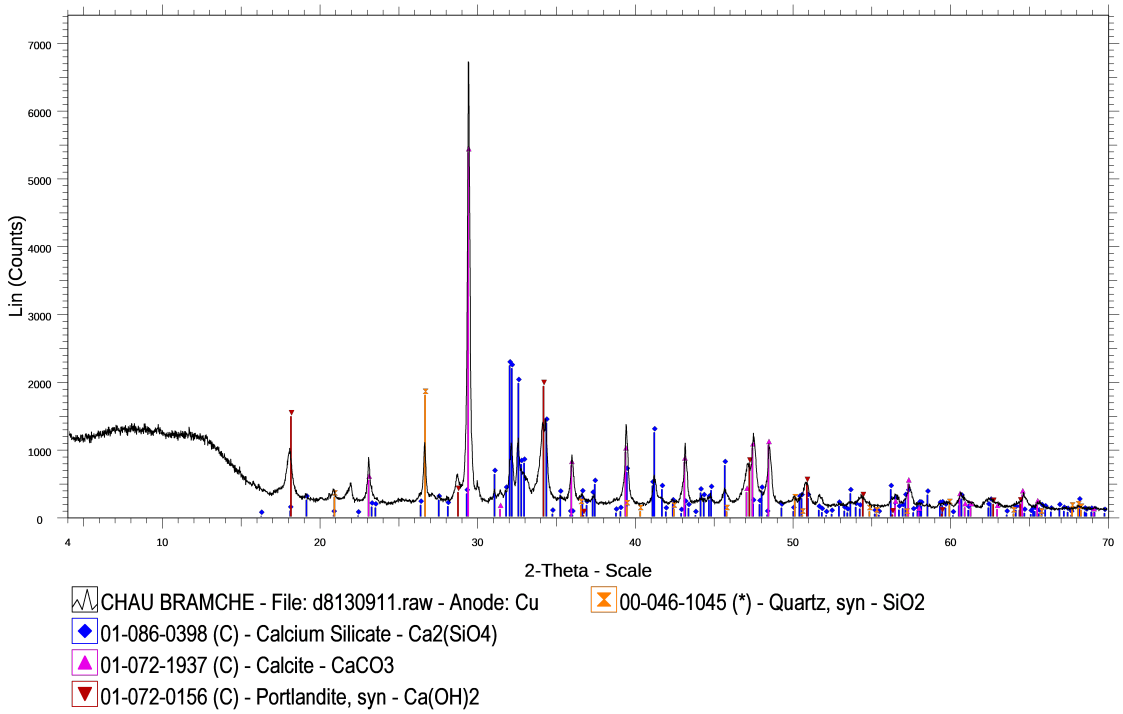

Figure 3.6 XRD spectrum of natural hydraulic lime with pozzolanic additives.

3.2.4.2 White Portland cement

Portland cement is an artificial fine powder which is prepared by fine grinding of the clinker. Clinker internationally is called the product resulting from heating mixture of limestone and aluminosilicate rocks to 1450 °C in a kiln, in a process known as calcination, whereby a molecule of carbon dioxide is liberated from the calcium carbonate to form calcium oxide, or quicklime, which is then blended

with the other materials that have been included in the mix to form calcium silicates and other cementitious compounds. Cement set and hardens when mixed with water at room temperature. The reactions that cause setting and hardening are described as exothermic hydration reactions. It combines large hydraulic capacity and high strength, so it is widely used in construction, as well as in hydraulic engineering.

White Portland cement (WCM) is a special category of Portland cement. The characteristic greenish-gray to brown colour of ordinary Portland cement derives from a number of transition elements in its chemical composition. These are, in descending order of colouring effect, chromium, manganese, iron, copper, vanadium, nickel and titanium. The amount of these in white cement is minimized as far as possible. Cr_2O_3 is kept below 0.003%, Mn_2O_3 is kept below 0.03%, and Fe_2O_3 is kept below 0.35% in the clinker. With the help of the XRD (Bruker D8 Advance Diffractometer, Section 2.1.1) the composition of the WCM is presented in Figure 3.7.

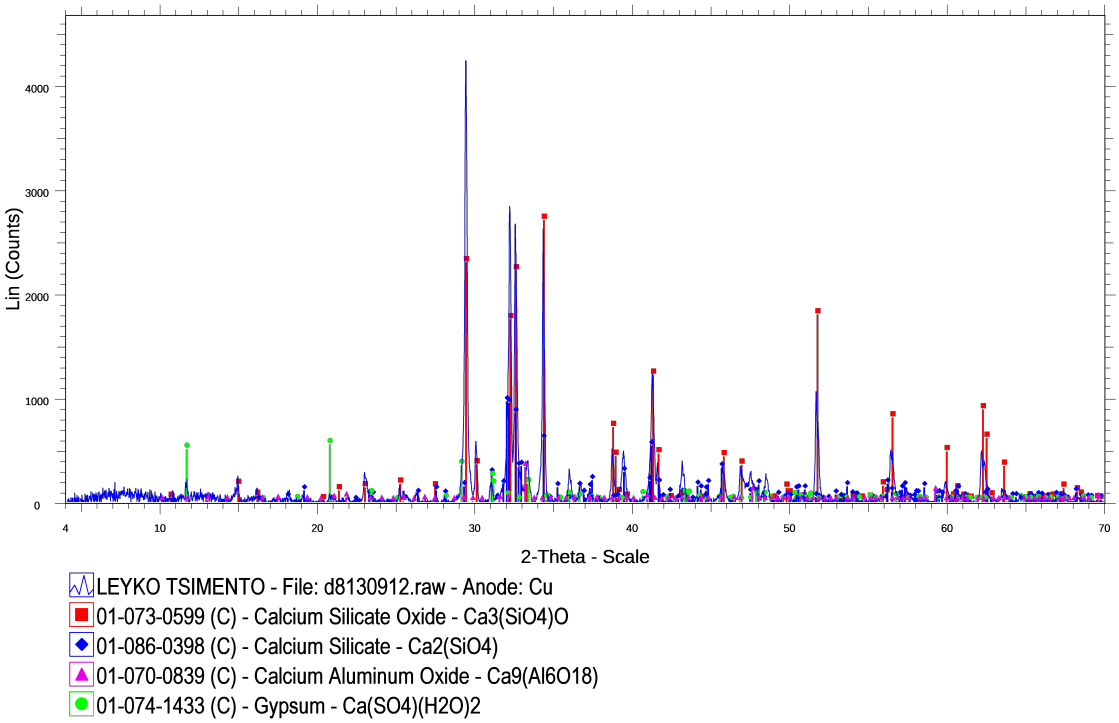

Figure 3.7 XRD spectrum of white Portland cement.

3.3 Development of the coatings' samples

For the development of the samples, a metal matrix (Figure 3.8) ia fabricated. The dimensions of the matrix are 10cm x 10cm x 3cm. These dimensions are selected so that the samples can be fit into the

ultraviolent (UV)/visible (VIS)/near infrared (NIR) spectrophotometer apparatus. The substrate of the coatings' is developed by a mixture of aggregates and normal (black) Portland cement (Figure 3.8) with a ration of 3:1. The substrate provides a base for the coatings', providing mechanical strength and durability that is needed for the transportation and handling of the samples. The substrate occupies 83% (2.5cm) of the metal matrix hight. In an effort to approach as much as possible their behaviour as coatings in building surfaces, the substrates are left to cure for seven days and once per day a small amount of water was purred on the surface in order to prevent cracks during this process.

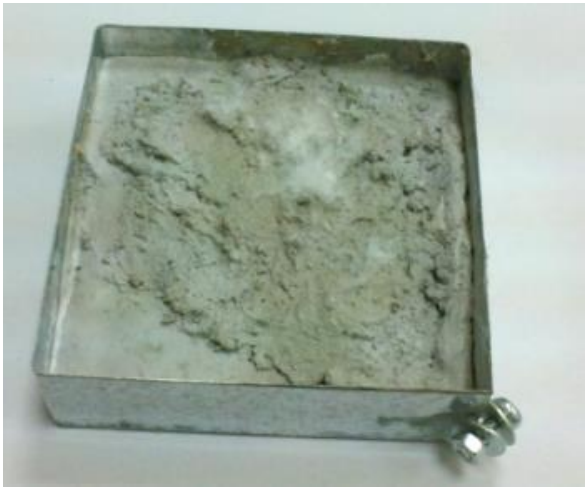

Figure 3.8 Metal matrix with substrate.

The ingredients of the coatings are mixed in small, plastic containers. First the aggregates, lime and binder are weighted, put in the containers and meticulously mixed. Consequently, the required amount of water is added to the mixture. Then all the ingredients are mixed until a uniform pulp is created. A small amount of water is added on the top of the substrate with a help of a paintbrush to ensure good binding with the pulp. The pulp is placed on top of substrate. A smooth and even surface is achieved for all samples by the use of a 15cm spatula. The samples are left to cure for a month in stable humidity and temperature conditions (RH = 50±5% and T = 22±2 °C).

3.4 Experimental procedure

The development of inorganic based cool coatings is performed in two phases:

Phase 1: Using dolomite marble powder (DMP), limestone marble powder (LMP), quartz sand (QUA) with/without glass beads (GB) and binders natural hydraulic lime with pozzolanic additives - NHL or white Portland cement - WCM).

Phase 2: Additional samples using dolomite marble powder (DMP), limestone marble powder (LMP) with three different grain distribution and white Portland cement (WCM) as binder, where half of the samples surfaces are sanded.

At the first phase different materials are chosen based on their availability in the Mediterranean region. The protocol for developing and testing the inorganic cool coatings is developed and verified at this phase. The second phase is based on the results of the first phase. The two parameters that are examined in the second phase, are the grain distribution and surface finishing of the samples. A set of two identical samples are created for this phase. The surface of the first set remains untouched while the surface of the second set is sanded using sand paper.

3.4.1 Experimental procedure of the first phase

Tabulated in Table 3.1 is the composition of the samples created during the first phase. The samples are divided into three groups according to their raw materials. The grain size distribution for the LMP and DMP is presented in Figure 3.9 while for the QUA in Figure 3.10. Moreover a reference sample is created using normal Portland cement.

In the following section the solar reflectance, infrared emittance and surface temperature of the samples are measured and discussed.

Table 3.1 Code names, composition of the samples developed in first phase.

Group	Sample Code	Finishing	Ratio per volume
1	WCM-LMP	WCM/L/LMP	1/1/2
	WCM-DMP	WCM/L/DMP	1/1/2
	NHL -LMP	NHL/L/LMP	1/1/2
	NHL-DMP	NHL/L/DMP	1/1/2
2	WCM-QUA	WCM/L/QUA	1/1/1.8/0.2
	NHL-QUA	NHL/L/QUA	1/1/1.8/0.2
3	WCM-LMP-GB	WCM/L/LMP/GB	1/1/1.8/0.2
	WCM-DMP-GB	WCM/L/DMP/GB	1/1/1.8/0.2
	NHL-LMP-GB	NHL/L/LMP/GB	1/1/1.8/0.2
	NHL -DMP-GB	NHL/L/DMP/GB	1/1/1.8/0.2

NHL: natural hydraulic lime with pozzolanic additives; WCM: white cement Portland; DMP: dolomitic marble; LMP: limestone powered; QUA: quartz sand; GB: glass beads; L: hydrated lime

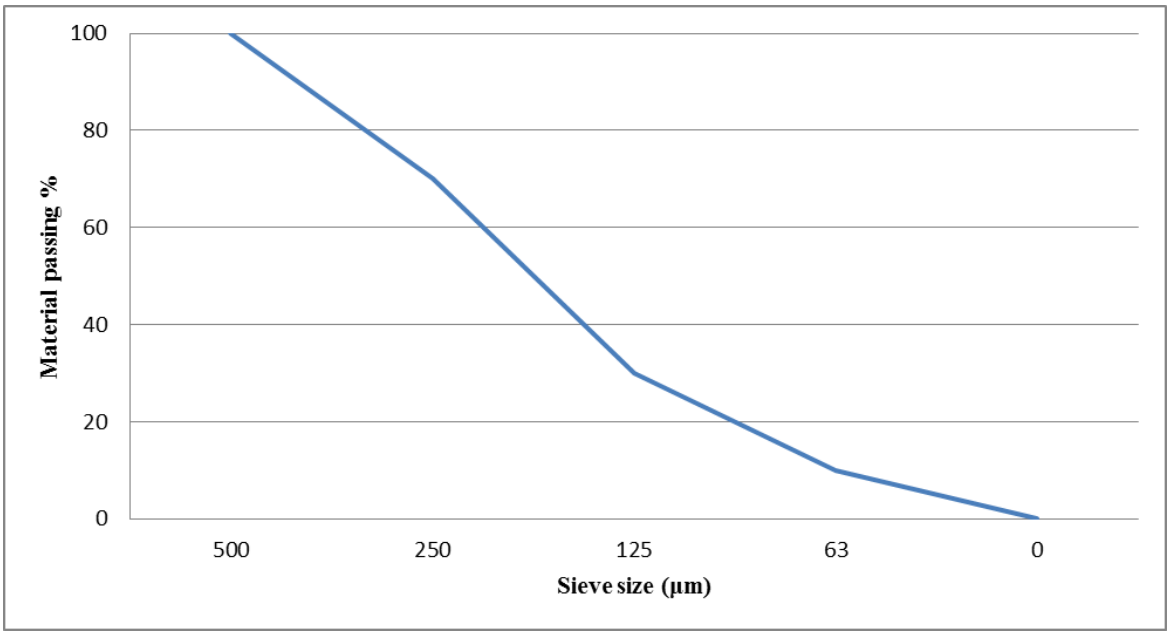

Figure 3.9 Grain size distribution of LMP-DMP.

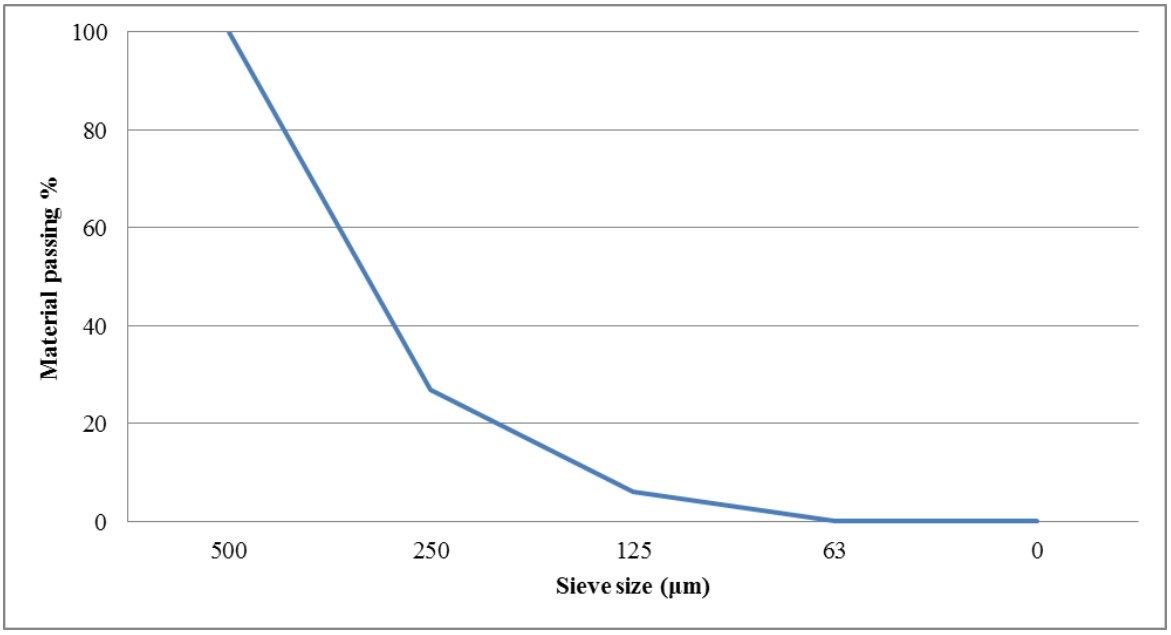

Figure 3.10 Grain size distribution of QAU.

3.4.1.1 Spectral reflectance and infrared emittance of cool coatings

The results of the spectral reflectance measurements of the ten developed coatings as well as the reference sample are presented. Figures 3.11 to 3.13 show the solar reflectance spectrum of the 1st,

2nd and 3nd group respectively. The solar reflectance spectrum of each sample is included in Appendix A (Figures A.1 to A.10). The measurements are conducted using the Carry 5000 with the integrating sphere (Section 2.2.2).

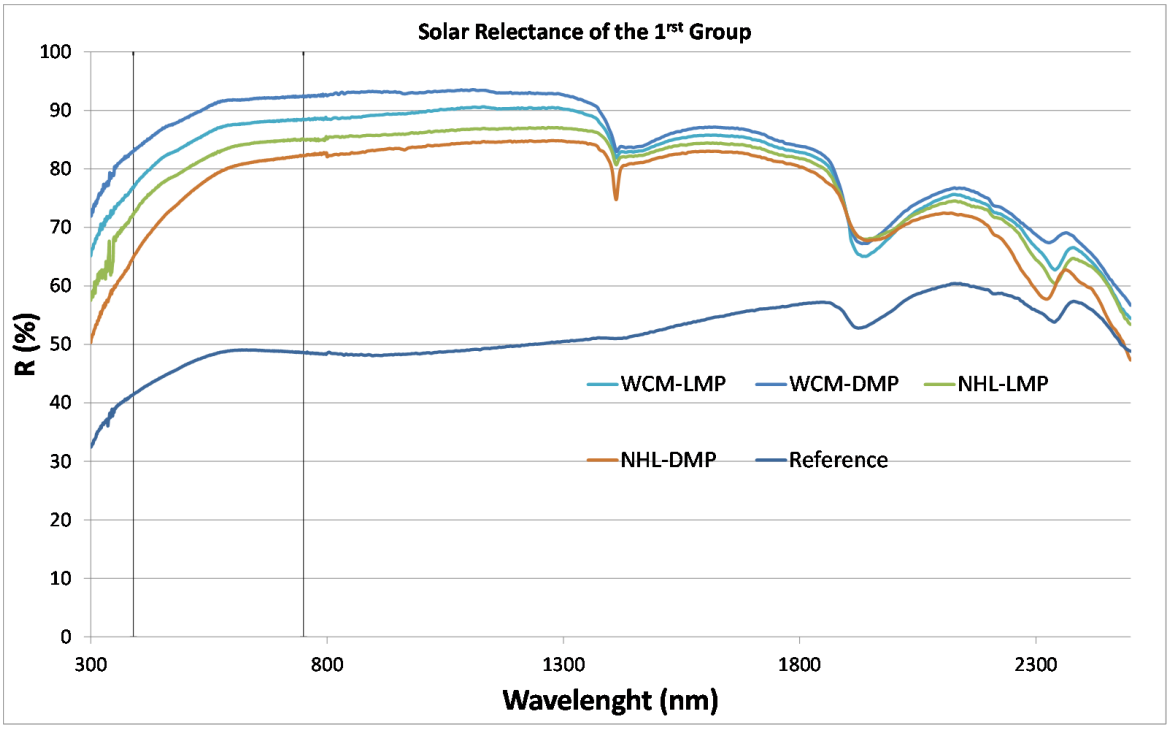

Figure 3.11 Solar reflectance spectrum of the 1st group and reference samples.

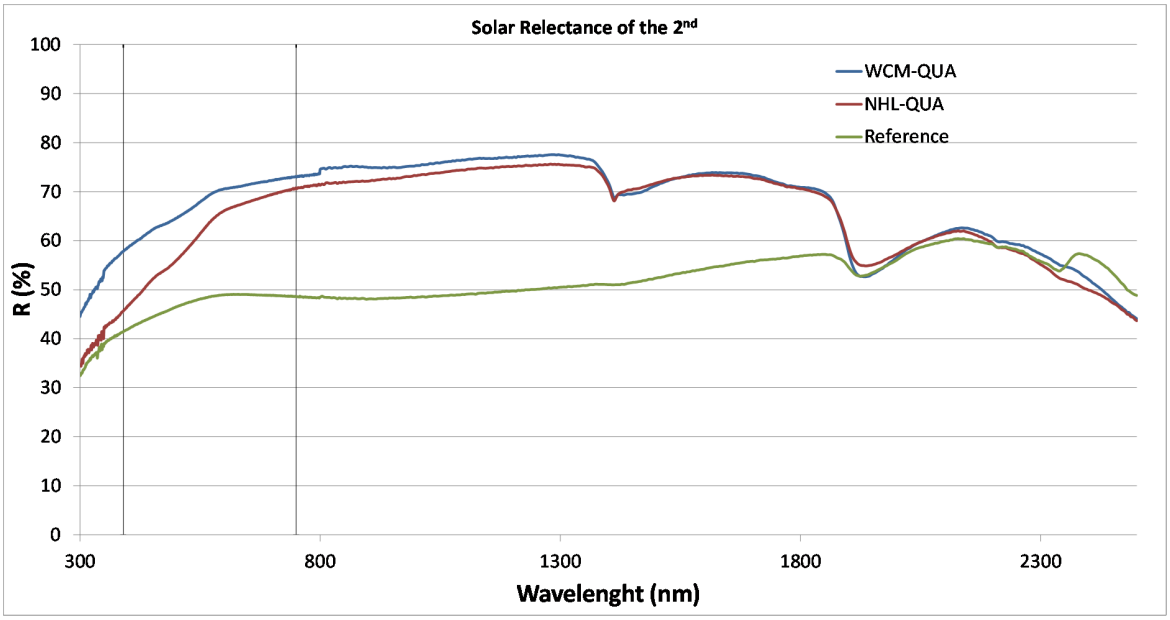

Figure 3.12 Solar reflectance spectrum of the 2nd group and reference samples.

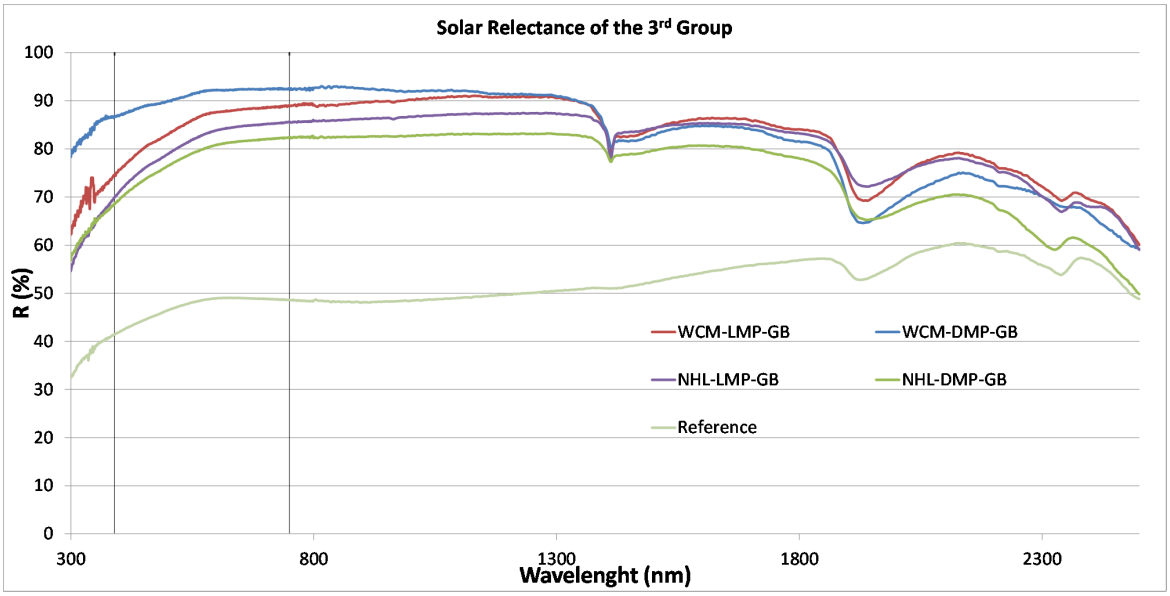

Figure 3.13 Solar reflectance spectrum of the 3st group and reference samples.

All developed samples demonstrate solar reflectance above the reference sample. The samples with WCM as binder have higher solar reflectance values in the whole spectrum comparing with the samples with NHL. Also all samples except the reference have a local minimum around 1410nm.

Based on the measurements of spectral reflectance using the Carry 5000 with the integrating sphere, the solar reflectance (SR) is calculated for each one of the samples using the ASTM E903-12 [99] and ASTM G159-91[110] standards. The total, near infrared (NIR: 300-400nm), visible (VIS: 400-700nm) and ultraviolet (UV: 700-2500nm) SR are tabulated in Table 3.2.

Table 3.2 Solar reflectance in near infrared, visible and ultraviolet wave-length of the 1st, 2nd, 3nd group samples.

Group	No.	Sample Name	SR (%)	SR_{IR} (%)	SR_{VIS} (%)	SR_{UV} (%)
1	1	WCM-LMP	86	86	85	71
	2	WCM-DMP	89	90	88	71
	3	NHL-LMP	82	84	81	64
	4	NHL–DMP	79	81	77	57
2	5	WCM-QUA	70	73	67	51
	6	NHL-QUA	66	71	61	40
3	7	WCM-LMP-GB	87	86	87	76
	8	WCM-DMP-GB	90	91	90	78
	9	NHL-LMP-GB	83	85	81	62
	10	NHL-DMP-GB	79	80	78	63
	11	Portland cement	49	50	47	37

NHL: natural hydraulic lime with pozzolanic additives; WCM: white cement Portland; DMP: dolomitic marble; LMP: limestone powered; QUA: quartz sand; GB: glass beads

Almost all samples present high SR above 0.80. The highest SR is observed for WCM-DMP-GB, WCM-DMP, WCM-LMP. The lowest SR is observed NHL-QUA, WCM-QUA. Quartz sand is used as aggregate giving for those samples a yellowish surface colour. The results for all samples show increased SR_{IR} and SR for all samples comparing to the reference one.

For the 1st group (Figure 3.11) the white Portland cement with either dolomite or limestone marble powder samples as an aggregate have higher solar reflectance than the ones corresponding to the hydraulic lime based samples (NHL-LMP and NHL-DMP). It is worth noting that for the same aggregate, i.e. DMP, a difference of almost 10% in the SR is recorded when using WCM or NHL as a binder. Analogous observations can be made for the 2nd group (Figure 3.12) where the NHL based sample has lower SR compared to the WCM one.

The 3rd group (Figure 3.13) is composed by the 1st group coatings with the addition of an additional component, i.e. the glass beads (GB). In the 3rd group, the addition of glass beads (GB) increase the SR of all samples. Therefore the addition of glass beads improves the optical properties of all samples regardless of the binders and aggregates used.

For the measurement of the infrared emittance (IE) values the "Device and Services Emissometer model AE1" is used (Section 2.2.1). The values of IE are tabulated on Table 3.3. For the 1st group

the hydraulic lime based samples have increased infrared emmitance compared to the white Portland cements ones. The opposite observations can be made for the 2nd group where the NHL based sample has lower infrared emittance compared to the WCM one. A 5%-7% different in infrared emittance is observed comparing the two binders independently the aggregates used.

Increased infrared emittance is measured for samples of the 3rd compared to the 1st group. A considerable increase in the WCM based samples concerning their infrared emittance is observed due to the addition of glass beads. Therefore the addition of the glass beads and quartz in the specific aggregates and binders enhance the cooling effect of the inorganic coatings studied.

Table 3.3 Infrared emittance of the 1st, 2nd, 3nd group samples.

Group	No.	Sample Name	IE
1	1	WCM-LMP	0.81
	2	WCM-DMP	0.83
	3	NHL-LMP	0.88
	4	NHL–DMP	0.88
2	5	WCM-QUA	0.90
	6	NHL-QUA	0.83
3	7	WCM-LMP-GB	0.90
	8	WCM-DMP-GB	0.87
	9	NHL-LMP-GB	0.88
	10	NHL-DMP-GB	0.85
	11	Portland cement	0.78

NHL: natural hydraulic lime with pozzolanic additives; WCM: white cement Portland; DMP: dolomitic marble; LMP: limestone powered; QUA: quartz sand; GB: glass beads

3.4.1.2 Surface temperature of cool coatings

For the first phase, 2 HH306A data loggers (Figure 2.13) are used for measuring the surface temperature of the samples thus a total of 8 samples could be measured at any given time.

Figure 3.14 Samples placed on the roof of the K2 building.

The samples are placed on the roof of K2 building of the School of Environmental Engineering in Technical University of Crete. The placement of the samples on top of a wooden structure is chosen to minimize the effect of the concrete tiles covering the building roof. The data logger is in a close proximity to the samples inside a well-ventilated white box. The meteorological station [111] (Davis Vantage Pro2 wireless fan-aspirated [112]) located 200m North-East of the K2 building is used to measure the air temperature, relative humidity, air speed and solar radiation.

A series of surface measurements are performed using 2 HH306A along with K-type thermocouples. Due to limited number of data loggers the surface temperature measurements took place during different days of May 2013 for each of the three groups. In order to be able to compare the results, the difference between the surface temperature of the samples and a reference sample is examined. The reference sample used is the Portland cement. Thus the greater the difference of the temperatures the cooler the sample under investigation is. The results of the 1st group which contain only the binders and the different aggregates are depicted in Figure 3.15. The specific figure corresponds to two days measurements in July 2013. The average ambient temperature was 25.53°C (max: 31.3°C min: 21.8°C), relative humidity 70% (max: 90%, min:48%) and solar radiation 250 W/m^2 (max: 822W/m^2)

The samples of the 1st group with the lowest temperature difference are NHL-LMP followed by NHL-DMP, WCM-LMP, and WCM-DMP. A difference of 3.2K is observed between the maximum

temperatures of WCM-DMP and NHL-LMP. The highest temperature difference between the inorganic samples and the reference sample is 5.6K for the WCM-DMP. Moreover it is worth noting that the peak difference occurs later during the day for the NHL based samples than the WCM based samples. Therefore the cement based sample with the dolomite aggregate has the highest reduction of the surface temperature. This is in accordance with the optical properties measured in Section 3.4.1.1.

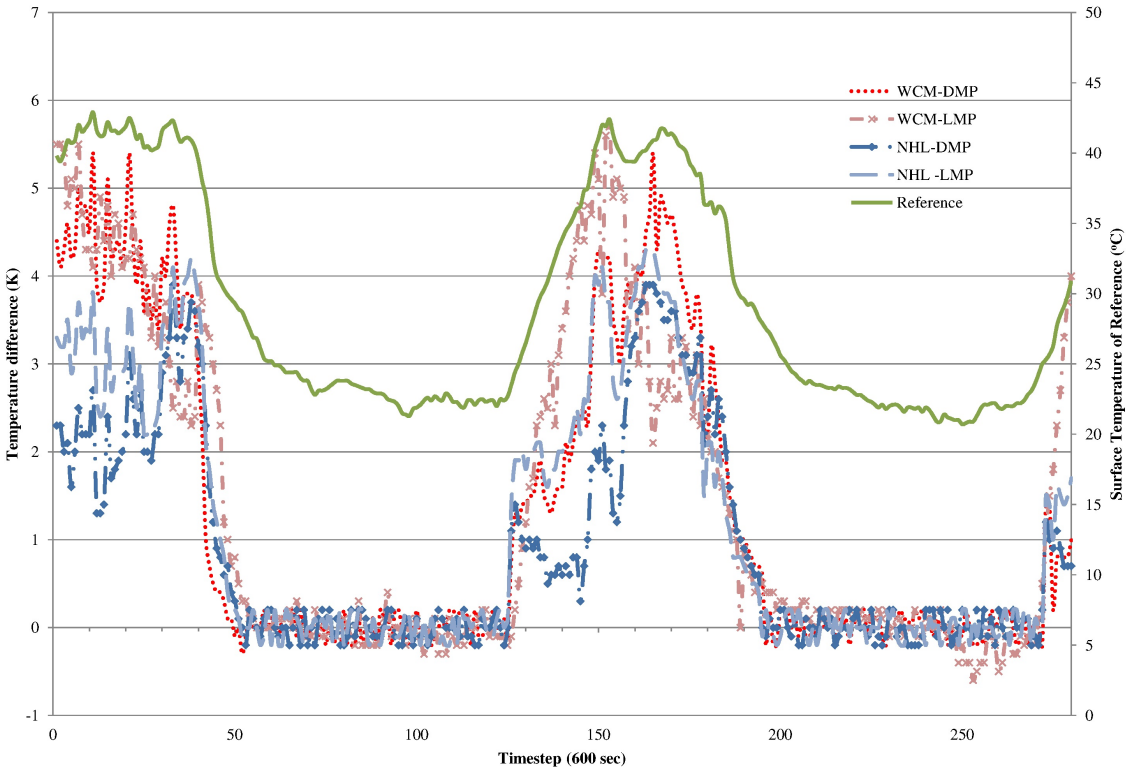

Figure 3.15 Surface temperature measurement of the 1st. group.

The surface measurements results of the 2nd group samples are illustrated in Figure 3.16. The maximum temperature difference of the WCM-QUA and the reference is almost 5.5K. In this figure the peak time of the NHL based sample occurs again later than the peak time of the cement based sample. Moreover the temperature decrease of all samples of the 1st and 2nd group are almost of the same levels although the measurements of the solar reflectance show some significant differences. This can be attributed to the increased levels of the IE as measured and tabulated in Table 3.3. The average temperature difference of the two samples is almost 2K.

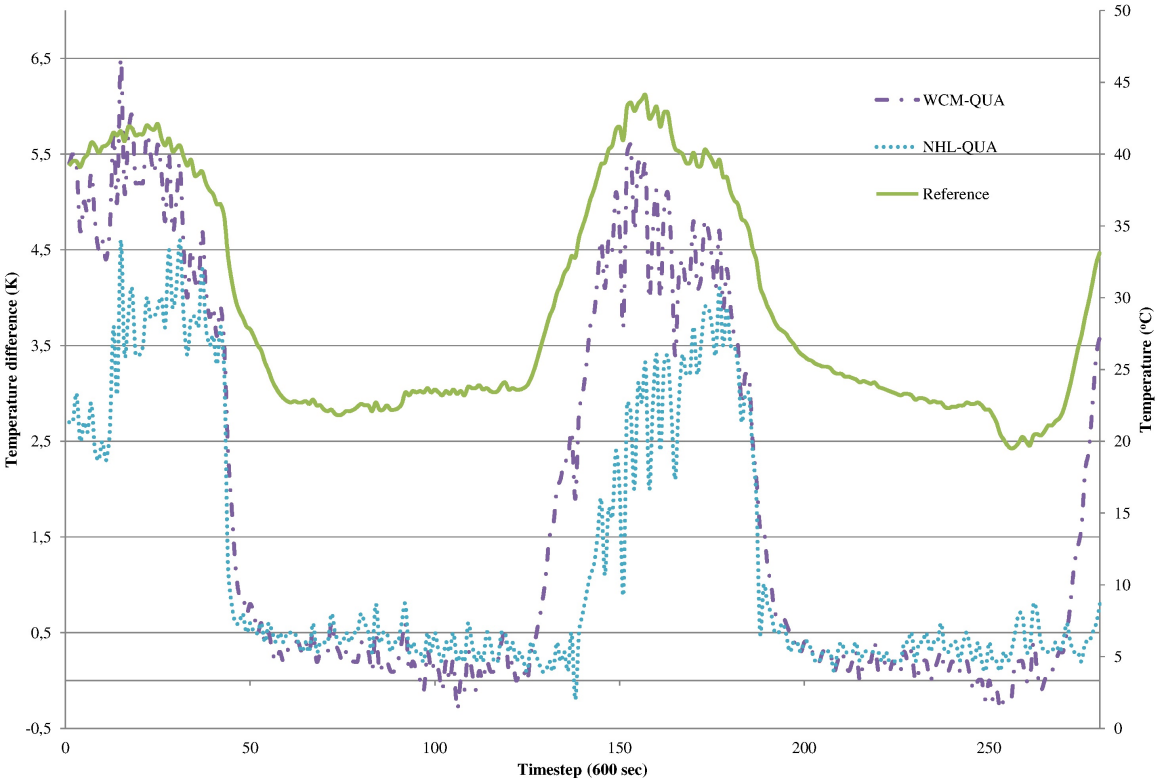

Figure 3.16 Surface temperature measurement of the 2rd. group.

The surface temperature differences for the 3rd group are depicted in Figure 3.17. The inclusion of the glass beads enhances the cooling effect of the samples by almost 3K comparing to the ones depicted in Figure 3.15 while the maximum temperature difference between the 3rd group samples and the reference ones is almost 8.5K. Moreover the results are in accordance with the optical properties measurements.

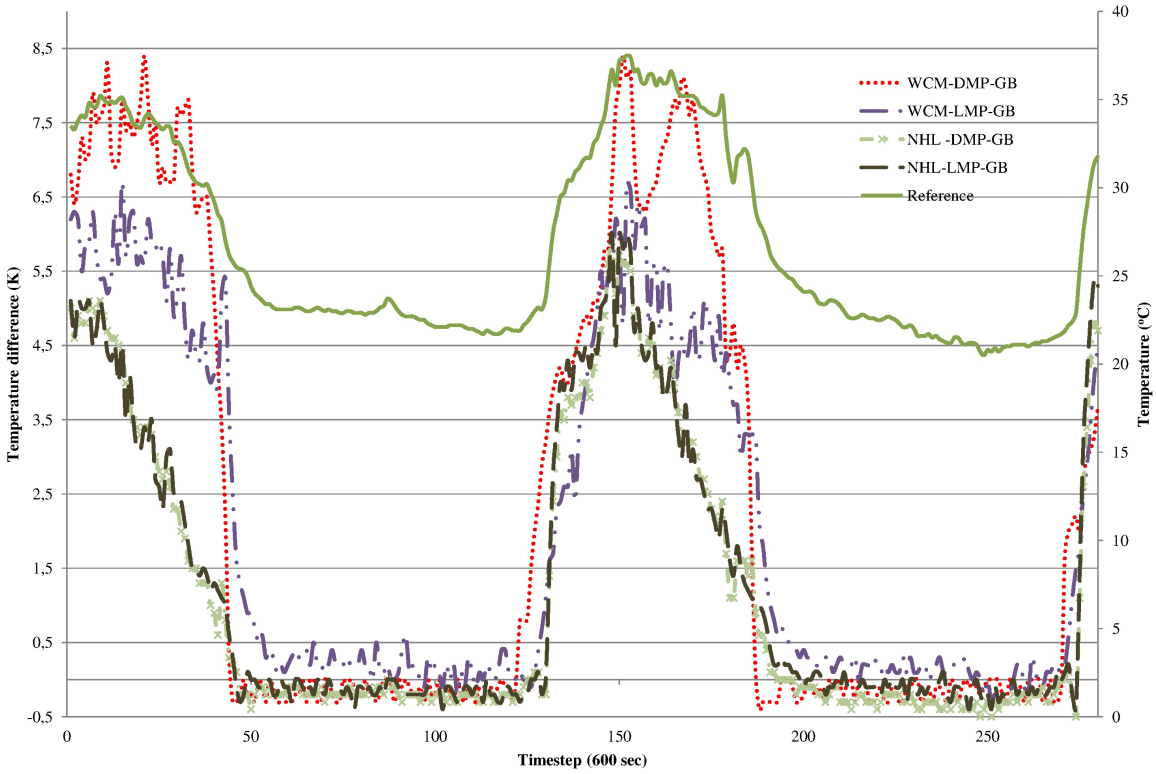

Figure 3.17 Surface temperature measurement of the 3rd. group.

3.4.2 Experimental procedure of the second phase

Spurred by the results presented in Section 3.4.1, an additional set of twelve samples (Table 3.4) are developed to examine the correlation of the different grain sizes and surface finishings. The samples are constructed using three different grain distributions: a) coarse (C), b) medium (M), c) fine (F) (Figure 3.18) and untreated (N) or sanded (S) surfaces. Two different aggregates are used: a) DMP, b) LMP along with WCM as binder that showed the lower surface temperatures during the initial measurements (see Section 3.4.1). A commercial cool coating was purchased from a local store. The application on top of the substrate is performed according to the manufacture recommendation. Moreover the CR850 data logger with AM16/32B (Figure 2.14a) is used so up to 32 samples could be measured.

Table 3.4 Code names, composition of samples developed in the second phase.

Group	Sample Code	Finishing	grain distribution	surface finish
4	LMP-C-N	WCM/L/LMP	coarse	untreated
	LMP-C-S	WCM/L/LMP	coarse	sanded
	LMP-M-N	WCM/L/LMP	medium	untreated
	LMP-M-S	WCM/L/LMP	medium	sanded
	LMP-F-N	WCM/L/LMP	fine	untreated
	LMP-F-S	WCM/L/LMP	fine	sanded
	DMP-C-N	WCM/L/DMP	coarse	untreated
	DMP-C-S	WCM/L/DMP	coarse	sanded
	DMP-M-N	WCM/L/DMP	medium	untreated
	DMP-M-S	WCM/L/DMP	medium	sanded
	DMP-F-N	WCM/L/DMP	fine	untreated
	DMP-F-S	WCM/L/DMP	fine	sanded

WCM: white cement Portland; DMP: dolomitic marble; LMP: limestone powered; L: hydrated lime; C: coarse ; M: medium ; F: fine; S: sanded; N: untreated

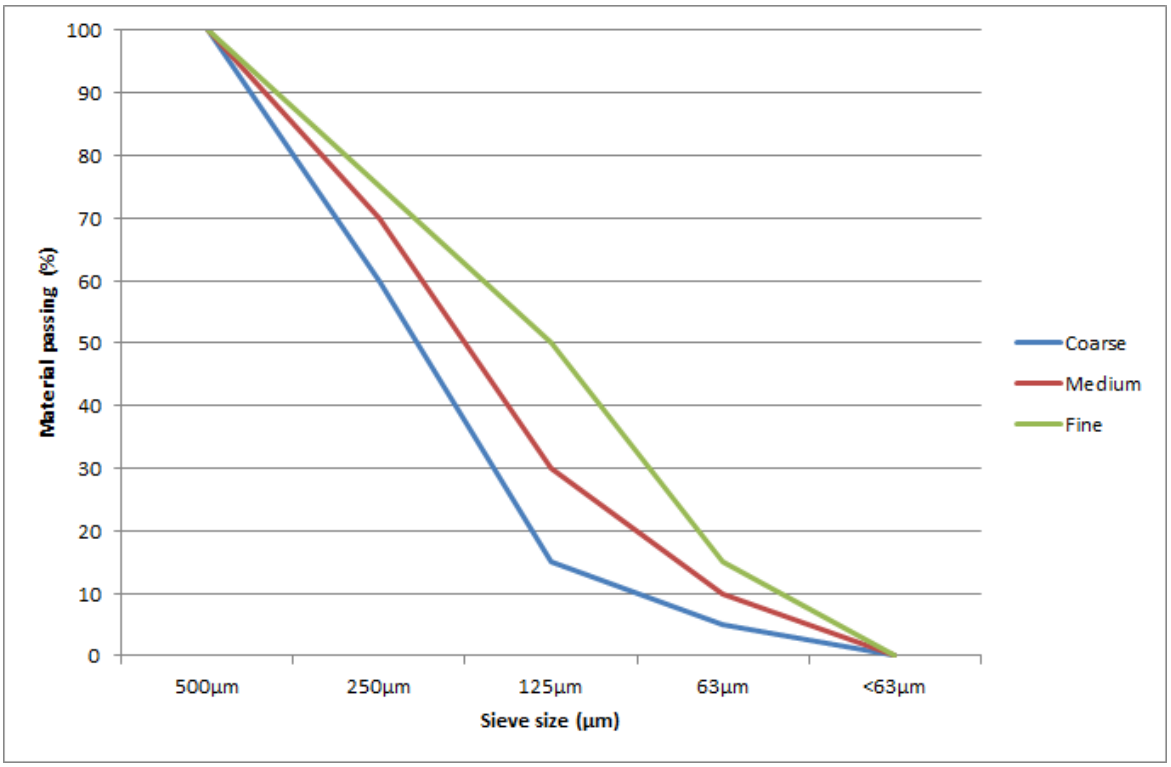

Figure 3.18 Grain size distribution for coarse, medium, fine.

3.4.2.1 Spectral reflectance and infrared emittance of cool coatings

The spectral reflectance of the ten samples, the reference Portland cement and the commercial cool coating (CCW) are performed and discussed in this section. Figures 3.19 to 3.21 shown the solar reflectance spectrum of the 4^{th} group samples with LMP, DMP as aggregate and two reference samples, respectively. Individual solar reflectance spectrums are shown in Appendix A (Figures A.12 to A.24). The measurements are conducted using the Carry 5000 with the integrating sphere.

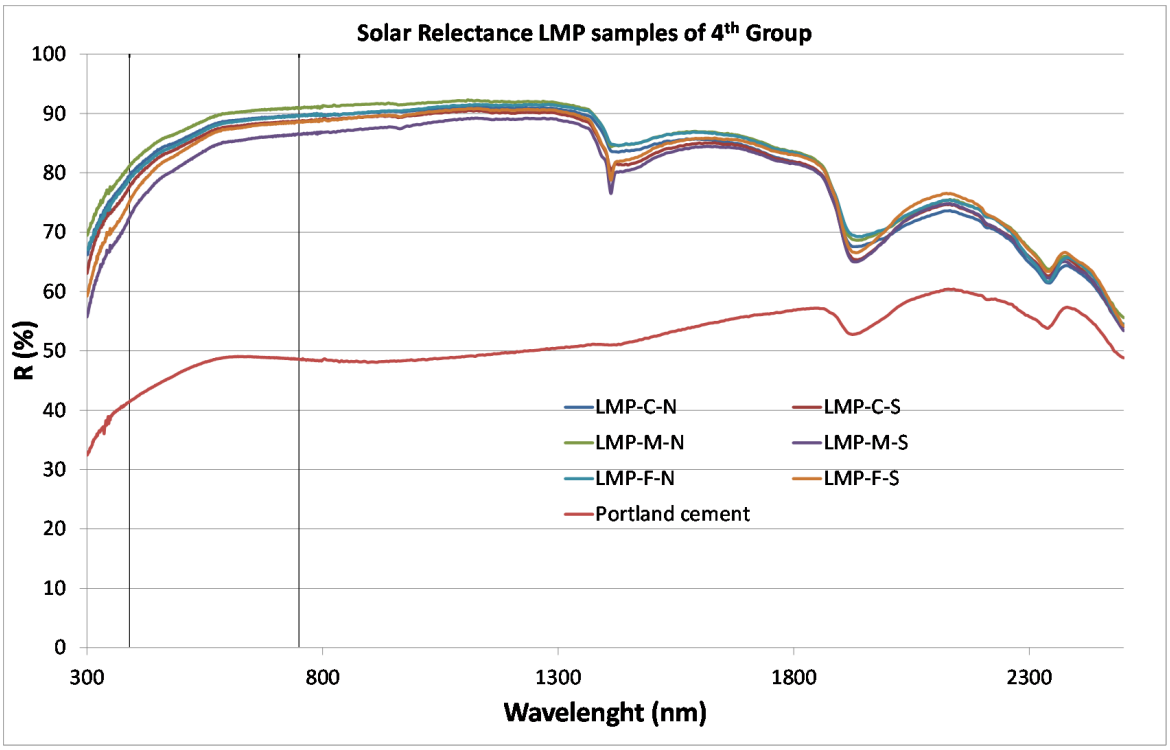

Figure 3.19 Solar reflectance spectrum of the LMP samples of 4st group.

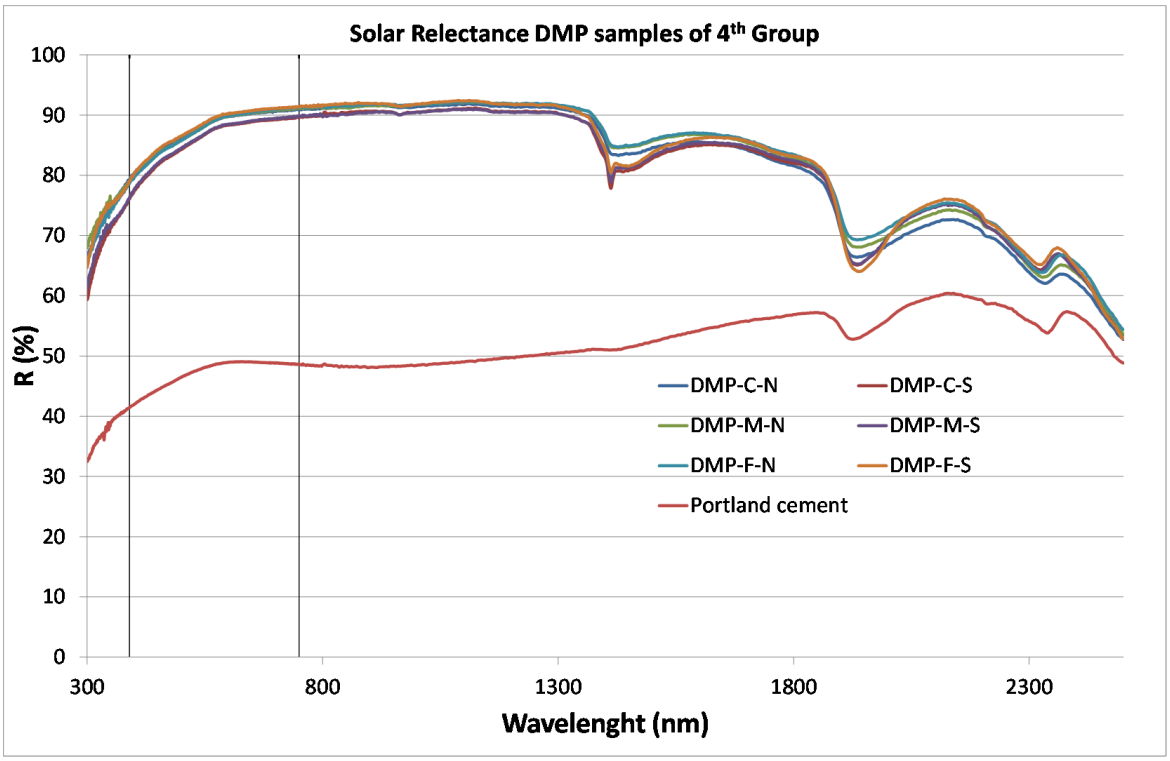

Figure 3.20 Solar reflectance spectrum of the DMP samples of 4st group

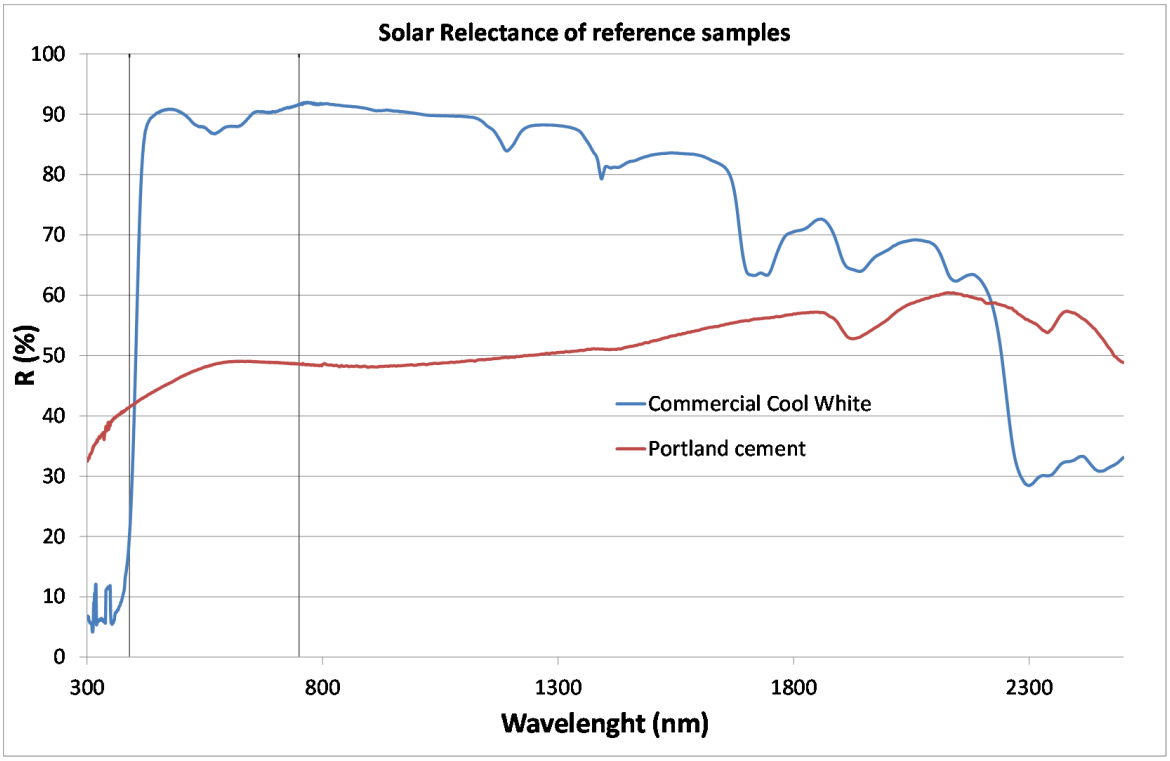

Figure 3.21 Solar reflectance spectrum of the 1st group samples.

All untreated samples (LMP/DMP - C/M/F - **N**) demonstrated higher solar reflectance in the entire spectrum. Moreover a noticeable difference is observed at 1400 - 1450 nm with the absence of the local minimum on the untreated samples.

Based on the measurements of spectral reflectance using the Carry 5000 with the integrating sphere, the SR is calculated for each one of the samples using the ASTM E903-12 [99] and ASTM G159-91[110] standards. The total, near infrared (NIR: 300-400nm), visible (VIS: 400-700nm) and ultraviolet (UV: 700-2500nm) solar reflectance is tabulated in Table 3.5.

The samples of the 4th group have similar SR around 0.88. The results are in line with the corresponding samples (WCM-LMP, WCM-DMP) from the 1st group. The sanded process decrease the SR and SR_{UV} by a small amount in all samples. The different grain distribution does not have any effect on the SR values. The highest SR is observed for LMP-M-N, DMP-F-S, DMP-F-N, DMP-M-N.

For the measurements of the IE the "Device and Services Emissometer model AE1" is used. The values of IE are tabulated in Table 3.6. For the 4th group the DMP untreated samples have significantly higher IE (0.09) compared to the sanded ones. The same phenomenon is not observed for the LMP samples. The DMP untreated sample with coarse grain size have higher IE followed by the medium and fine (DMP-C-N > DMP-M-N > DMP-F-N) and the same order is observed with the sanded

ones (LMP-C-S > LMP-M-S > LMP-F-S). This behaviour is not observed for the LMP samples. The samples with LMP as aggregate have higher IE from the DMP ones by an average of 0.08. The highest IE is measured for the LMP-M-N sample, IE=0.92.

Table 3.5 Solar reflectance in near infrared, visible and ultraviolet wave-length of the 4^{rth} group and reference samples.

Group	No.	Sample Name	SR (%)	SR_{IR} (%)	SR_{VIS} (%)	SR_{UV} (%)
4	1	LMP-C-N	87	87	87	73
	2	LMP-C-S	86	86	86	71
	3	LMP-M-N	88	88	88	75
	4	LMP-M-S	84	85	83	64
	5	LMP-F-N	87	87	86	73
	6	LMP-F-S	86	87	85	67
	7	DMP-C-N	87	88	88	73
	8	DMP-C-S	86	87	86	68
	9	DMP-M-N	88	88	87	73
	10	DMP-M-S	87	88	87	70
	11	DMP-F-N	88	88	87	72
	12	DMP-F-S	88	88	88	72
5	13	Commercial cool coating	84	84	88	8
	14	Portland Cement	49	50	47	37

WCM: white cement Portland; DMP: dolomitic marble; LMP: limestone powered; C: coarse ; M: medium ; F: fine; S: sanded; N: untreated

Table 3.6 Infrared emittance of the 4^{rth} group and reference samples.

Group	No.	Sample Name	IE
4	1	LMP-C-N	0.87
	2	LMP-C-S	0.87
	3	LMP-M-N	0.92
	4	LMP-M-S	0.88
	5	LMP-F-N	0.87
	6	LMP-F-S	0.90
	7	DMP-C-N	0.90
	8	DMP-C-S	0.83
	9	DMP-M-N	0.89
	10	DMP-M-S	0.80
	11	DMP-F-N	0.90
	12	DMP-F-S	0.80
5	13	Commercial cool coating	0.89
	14	Portland Cement	0.78

WCM: white cement Portland; DMP: dolomitic marble; LMP: limestone powered; C: coarse ; M: medium ; F: fine; S: sanded; N: untreated

3.5 Discussion of results

A total of 22 coatings, developed during the first and second phase is measured using the CR850 datalogger with the AM16/32B. The measurements' period, June July 2017, is split into two groups: day (7:00-20:00) and night (22:00-5:00) in order to determine the performance of the samples during day and night. The average and maximum surface temperature of the entire measuring period is tabulated in Table 3.7. The average day/night surface temperatures of the samples for each month are presented in Figures 3.22 and 3.23 using box-plots.

During the course of the measurements the weather can be characterized by clear sky except 2 days that was raining in June 2017. The meteorological conditions of the measurement site are tabulated in Table 3.7.

Table 3.7 Meteorological condition of the measurement site during summer 2017.

		Air temperature (°C)		Relative humidity (%)	Solar radiation (W/m^2)
		Day	Night		
June	Average	27.7	21.9	62	293
	Maximum	40.2	30.7	95	1076
	Minimum	19.9	17.1	22	0
July	Average	30.1	24.7	55	295
	Maximum	40.2	33.2	95	1015
	Minimum	22.8	20.8	15	0

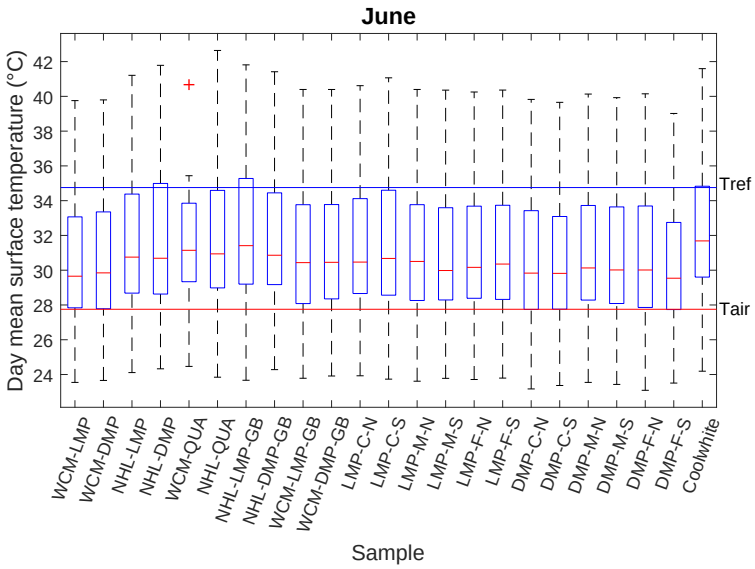

(a) Day.

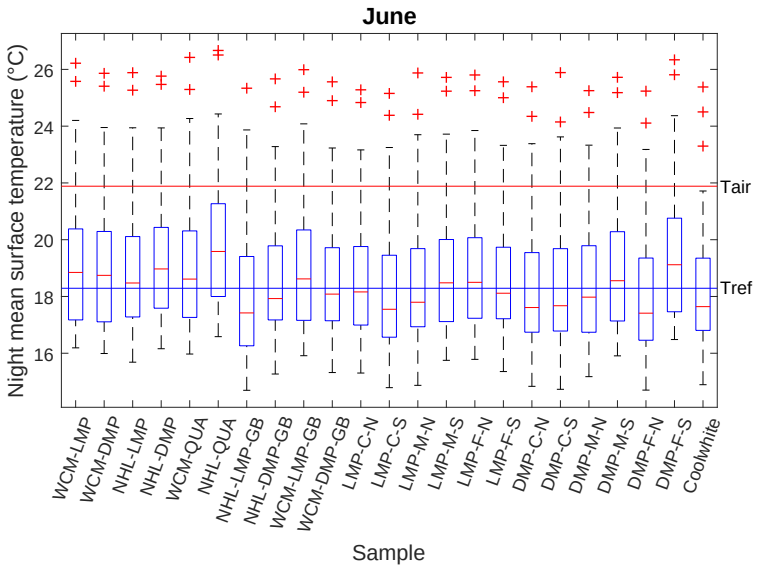

(b) Night.

Figure 3.22 Average day/night surface temperatures of the samples for June 2017.

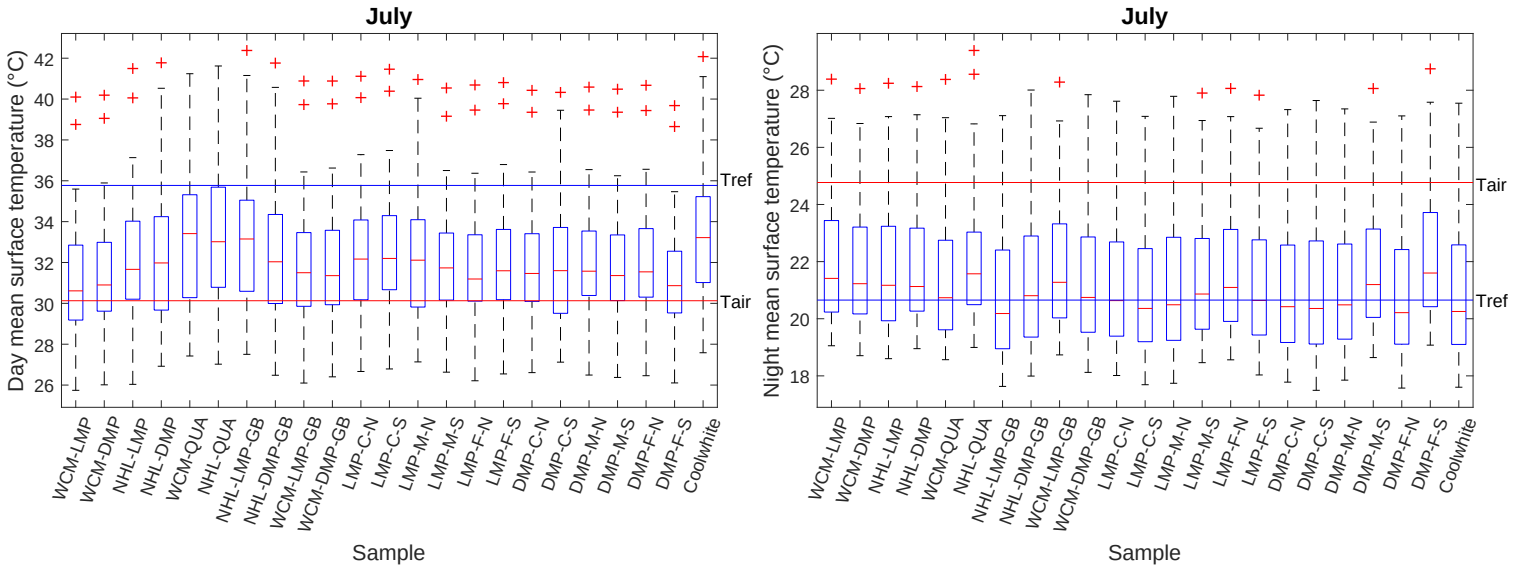

(a) Day. (b) Night.

Figure 3.23 Average day/night surface temperatures of the samples for July 2017.

Box plots break the data into quartiles. On the middle of the box is the average value of the dataset. The upper and lower parts of the box represent the data with values up to 25% greater and smaller respectively to the average value. The whisker (dotted line) represents the maximum and minimum value found on the dataset. Outliers are represented as red crosses.

On Figures 3.22 and 3.23 the average day/night values of the ambient air (T_{air}) with a red horizontal line as well as the reference sample's (T_{ref}) temperature with a blue horizontal line are represented. The reference sample is ordinary Portland cement.

Table 3.8 Daily monthly average/maximum surface temperatures of samples.

		Average surface temperature (°C)		Maximum surface temperature (°C)	
Group	Sample	June	July	June	July
1	WCM-LMP	30.10	31.32	43.53	43.51
	WCM-DMP	30.28	31.65	42.72	43.22
	NHL-LMP	31.19	32.32	45.28	45.69
	NHL-DMP	31.48	32.45	44.87	45.05
2	WCM-QUA	31.20	33.18	46.40	46.93
	NHL-QUA	31.91	33.72	49.91	48.66
3	NHL-LMP-GB	31.86	33.52	46.25	47.54
	NHL-DMP-GB	31.48	32.62	46.46	46.72
	WCM-LMP-GB	30.68	32.03	44.49	44.83
	WCM-DMP-GB	30.84	32.07	44.57	44.99
4	LMP-C-N	31.06	32.57	44.05	45.15
	LMP-C-S	31.32	32.82	45.02	46.20
	LMP-M-N	30.91	32.52	44.41	45.23
	LMP-M-S	30.58	32.08	43.80	44.55
	LMP-F-N	30.66	31.95	44.03	44.00
	LMP-F-S	30.76	32.19	44.08	44.73
	DMP-C-N	30.34	32.06	43.61	44.51
	DMP-C-S	30.32	32.13	44.69	44.74
	DMP-M-N	30.62	32.19	43.94	44.80
	DMP-M-S	30.45	32.06	43.43	44.28
	DMP-F-N	30.51	32.18	44.23	45.19
	DMP-F-S	29.93	31.00	42.74	42.68
5	Commercial cool coating	32.04	33.65	45.41	46.44
	Portland cement	34.75	35.77	52.80	53.91

NHL: natural hydraulic lime with pozzolanic additives; WCM: white cement Portland; DMP: dolomitic marble; LMP: limestone powered; QUA: quartz sand; GB: glass beads; C: coarse ; M: medium ; F: fine; S: sanded; N: untreated

Table 3.9 Nightly monthly average/maximum surface temperatures of samples.

		Average surface temperature (°C)		Maximum surface temperature (°C)	
Group	Sample	June	July	June	July
1	WCM-LMP	19.43	22.12	28.42	31.69
	WCM-DMP	19.23	21.93	27.96	30.94
	NHL-LMP	19.18	21.87	27.81	30.98
	NHL-DMP	19.43	21.92	28.13	30.49
2	WCM-QUA	19.31	21.54	28.20	32.18
	NHL-QUA	19.93	22.49	29.52	31.59
3	NHL-LMP-GB	18.34	20.96	27.01	30.23
	NHL-DMP-GB	18.87	21.29	27.64	30.68
	WCM-LMP-GB	19.29	21.97	27.66	31.41
	WCM-DMP-GB	18.86	21.33	27.53	30.57
4	LMP-C-N	18.80	21.24	27.48	29.97
	LMP-C-S	18.46	21.07	27.02	29.92
	LMP-M-N	18.73	21.27	27.44	31.07
	LMP-M-S	19.05	21.57	27.72	30.64
	LMP-F-N	19.14	21.79	27.73	30.78
	LMP-F-S	18.91	21.35	27.74	30.70
	DMP-C-N	18.53	21.16	26.92	30.29
	DMP-C-S	18.64	21.09	27.55	31.12
	DMP-M-N	18.62	21.22	27.02	30.12
	DMP-M-S	19.19	21.90	27.76	30.71
	DMP-F-N	18.34	21.00	26.68	30.19
	DMP-F-S	19.72	22.32	28.57	31.74
5	Commercial cool coating	18.54	21.00	26.97	30.35
	Portland cement	18.29	20.65	27.44	30.34

NHL: natural hydraulic lime with pozzolanic additives; WCM: white cement Portland; DMP: dolomitic marble; LMP: limestone powered; QUA: quartz sand; GB: glass beads; C: coarse ; M: medium ; F: fine; S: sanded; N: untreated

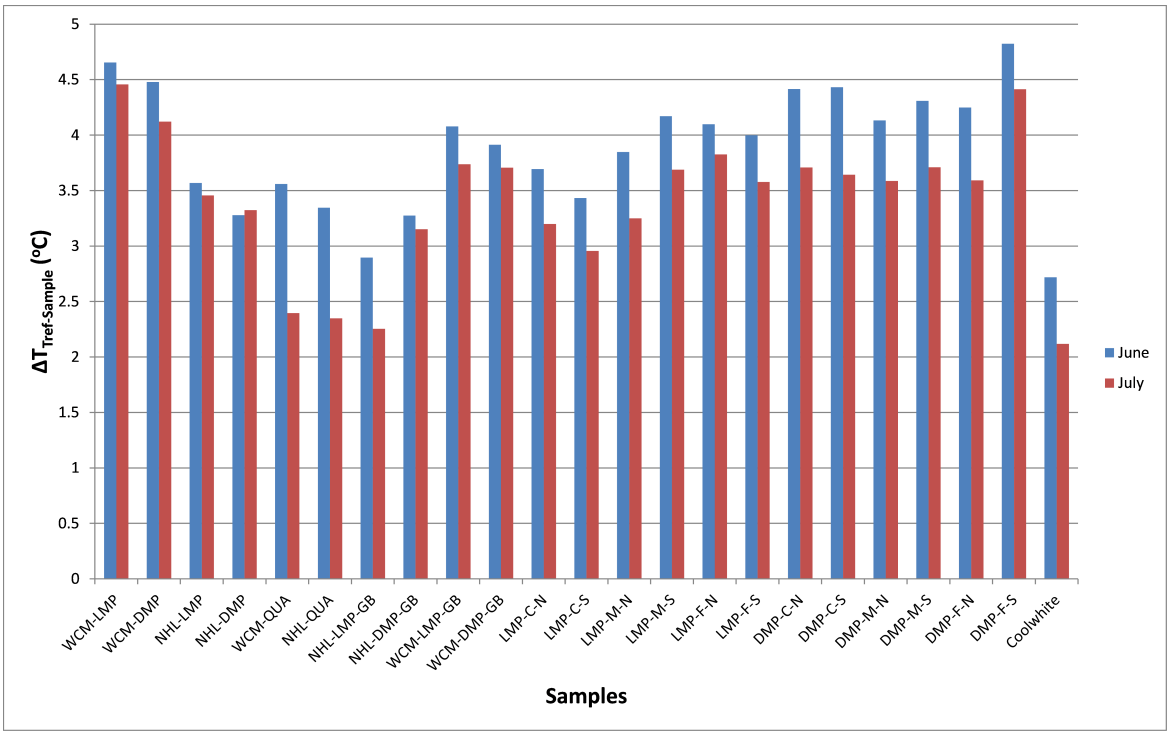

(a) Day.

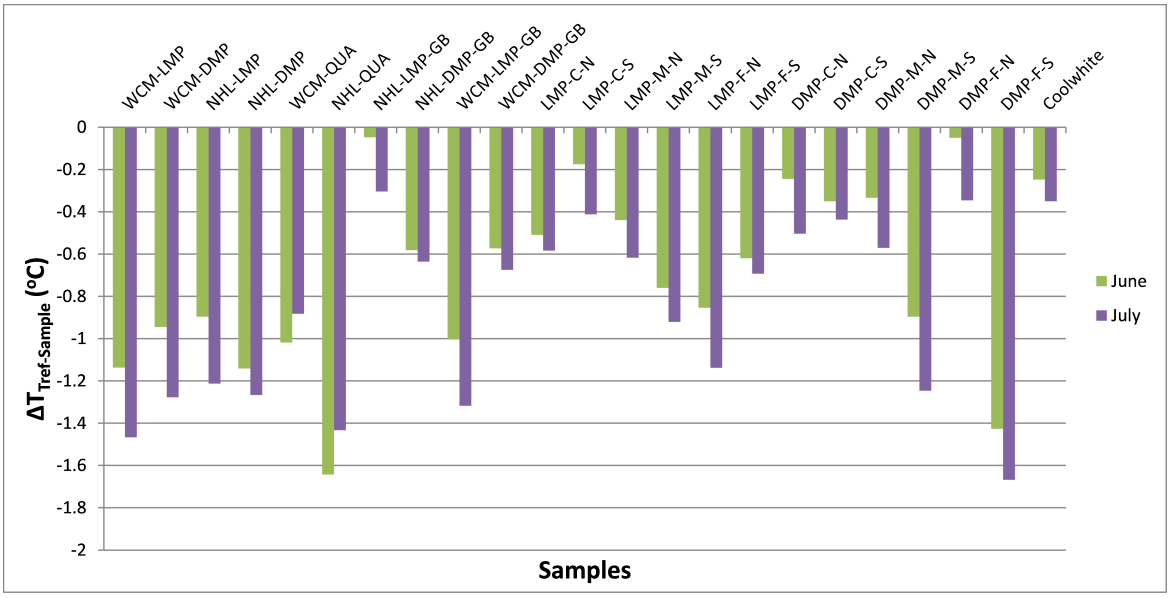

(b) Night.

Figure 3.24 Difference in average day/night surface temperature sample minus reference.

The average and maximum surface temperatures for each day and each night are tabulated in Tables 3.8 and 3.9. The day average surface temperature is from 29.93°C (DMP-F-S) to 31.86°C (NHL-LMP-GB) and 31.32 °C (WCM-LMP) to 33.52°C (NHL-LMP-GB) for June and July respectively. The

day maximum surface temperature for June is from 42.72°C (WCM-DMP) to 49.91°C (NHL-QUA) and 42.68 (DMP-F-S) to 48.66°C (NHL-QUA) for July. The day maximum difference in average surface temperature of 4.8K is observed for DMP-F-S and lowest at 2.9K NHL-LMP-GB for June and 4.5K (WCM-LMP) and 2.3K (NHL-LMP-GB) for July. A maximum deference of -1.6K is observed for NHL-QUA and 0.0K for NHL-LMP-GB, -1.7K DMP-F-S and -0.3K NHL-LMP-GB during night measurements for June and July.

The night average temperature for June is from 18.34 (NHL-LMP-GB) to 19.93°C (NHL-QUA) and 20.96°C (NHL-LMP-GB) to 22.49°C (NHL-QUA). The night maximum surface temperature for June is from 26.68 (DMP-F-N) to 29.52°C (NHL-QUA) and 29.92 (DMP-C-N) to 32.18°C (NHL-QUA) for July respectively. The difference in maximum to minimum average surface temperature for June is 1.6K, 1.5K for July and the equivalent when maximum surface temperatures are considered 2.6K and 2.2K respectively.

The average surface temperature of all samples during the night is lower than the ambient air (Table 3.9) for both months. This phenomenon is expected because during the night the main factor that affects the change in surface temperature is the infrared emittance, if the assumption is made that the heat transfer coefficient for all sample is the same (the sample are places close together so thy exposed to the same air flow and over 75% of their mass is the same, Portland cement). The night average surface temperature WCM-QUA, IE=0.90 is 19.31°C and 21.54°C versus 19.93°C and 22.09°C for NHL-QUA, IE=0.83 for June and July respectively. The same pattern is observed for the DMP samples of the 4^{th} group, DMP-F-N, IE=0.90 18.34°C and 21.00°C versus 19.72°C and 22.32°C for DMP-F-S, IE=0.80 for June and July respectively. The same results are obtained from the night maximum surface temperature. The results from the 1^{st}, 3^{rd} and sample with LMP from 4^{th} are inconclusive due to small difference in IE and average surface temperature.

The second phase of measurements confirmed some of the results from the first phase of measurements. In the 1^{st} phase of measurements, the lower surface temperature (Table 3.8) is observed for sample WCM-LMP followed by WCM-DMP, NHL-LMP and NHL-DMP. Compared to the initial measurements, an agreement is found on the binder with WCM producing lower surface temperatures. On the other hand, LMP performs better than DMP for both months. A lower maximum surface temperature is measured with DMP as aggregate for both binders and measuring periods. For the 2^{nd} group an agreement between the two measuring periods is observed. For the 3^{rd} group no enhancement on the reduction of the surface temperature is observed with the addition of the glass beads.

The analysis of the samples shows the following:

- The DMP-F-S (Table 3.4) has the lower average and maximum surface temperature from all samples.

- Lower average surface temperatures are linked to the samples with DMP as aggregates.
- For LMP the sanded surfaces have lower average and maximum temperature for fine (F) (0.2K, 0.5K) and coarse (C) (0.3K, 1K) grain distribution but higher for medium (M) (0.4K, 0.7K).
- For DMP the sanded surfaces have lower average (0.4K) and maximum surface (1.3K) temperature except for the course grain distribution that have higher maximum surface temperature by 0.7K.

In this chapter the development and testing of 22 inorganic cool coatings was realized. The main results demonstrate that a coating with high solar reflectance can significantly reduce the surface temperature during the day. The higher the SR the higher the reduction of the surface temperature that can reach up to 7.2K.

The use of white Portland cement as binder results in samples with higher SR and eventually lower surface temperature. Dolomite marble powder provides a higher SR than limestone marble powder and quartz sand. The addition of glass beads improves the optical properties of all samples regardless of the binders and aggregates used. The different grain distribution used (Figure 3.18) did not effect solar reflectance but had demonstrated minor fluctuation in the surface temperature of the samples. The best performing sample was white Portland cement, fine grain distribution with sanded surface.

Chapter 4

Development and testing of thermochromic based cool coatings

4.1 Introduction

Colour changing coatings have been introduced by various researchers [113, 48]. Their ability to contribute to the reduction of the buildings' energy demand for cooling as well as to mitigate the urban heat island has been tested [15].

In the framework of the present chapter two main categories of thermochromic (TC) colours are examined: a) inorganic and b) organic. The inorganic colour changing coating used is the bis(diethylammonium)tetrachlorocuprate(II), $[(CH_3CH_2)_2 - NH_2]_2CuCl_4$ with transition temperature of 43-45 °C and transition colours from green to yellow. This coating is synthesised in Technical University of Crete laboratories (Figure 4.1). Three organic thermochromic pigments are examined chosen by New Color Chemical Co. Limited. The three pigments have different colours and transition temperatures. The examined pigments are:

- Vermilion (red) with transition temperature at 33°C
- Turkish-blue with transition temperature at 38°C
- Brown with transition temperature at 43°C

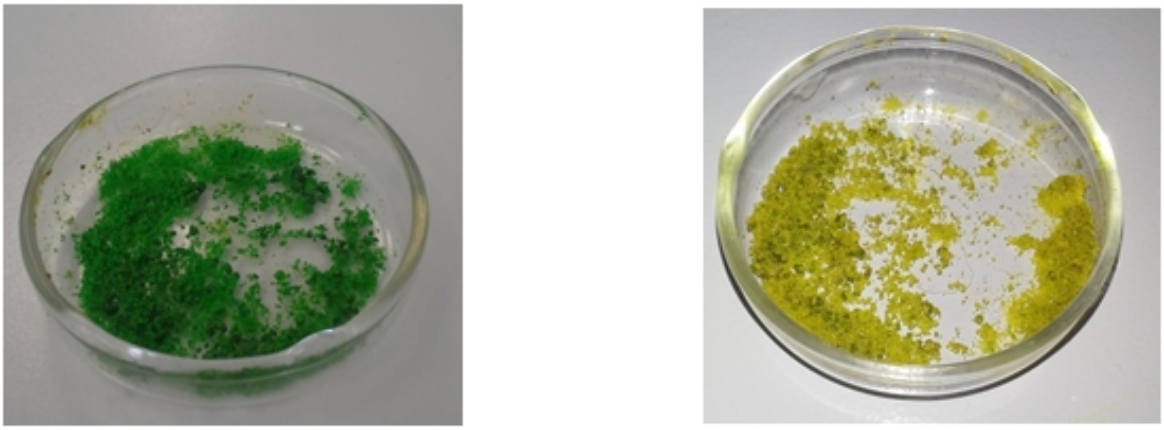

(a) At room temperature. (b) After phase change temperature.

Figure 4.1 Inorganic colour changing pigment.

4.2 Inorganic thermochromic coatings

In the framework of the present research various inorganic thermochromic compounds are examined. Those are:

1. HgI_2 with transition temperature 130°C
2. Tl_2HgI_4 with transition temperature 250°C
3. $AgHgI_4$ with transition temperature 47 - 130°C
4. $[Et_2NH_2]_2CuCl_4$ with transition temperature 45°C
5. Cu_2HgI_4 with transition temperature 70°C

The compounds No 1, 2 and 3 are excluded due to the high transition temperature which is unsuitable for building materials' applications. The compounds 3 and 5 also contain Hg which is considered hazardous material. As a result the $[Et_2NH_2]_2CuCl_4$ (bis(diethylammonium)tetrachlorocuprate(II)) is selected to be tested as a inorganic thermochromic coating for the present research. The formulation of the coating is achieved using the following chemical reaction:

$$CuCl_2 + 2(Et_2NH_2)Cl \rightarrow [Et_2NH_2]_2CuCl_4 \tag{4.1}$$

The raw materials are purchased from Sigma-Aldrich. The colour change is attributed to the tetrachlorocuprate (II) anion ($CuCl_4^{2-}$) due to its coordination geometry change from distorted square-planar to distorted tetrahedral while it is heated [114].

The colour changing pigment's composition, verified by X-ray diffraction (XRD) is illustrated in Figure 4.2. The XRD analysis is performed using a Bruker D8 Advance Diffractometer (Section 2.1.1). For diethylammonium tetrachloridocuprate(II) simulated powder diffraction patterns are calculated, based on single crystal structure data [115]. The Fourier transform infrared spectroscopy (FTIR) analysis is performed using a Perkin-Elmer 1000 spectrometer (Section 2.1.2) with 4 cm^{-1} resolution in the spectral range of 400-4000 cm^{-1}. Prior to the FTIR analysis, the samples are homogenized with KBr and pressed to obtain a pellet with the aid of a vacuum hydraulic press. The FTIR analysis (Figure 4.3) of the specific pigment identified absorptions attributed to N–H stretching, such as 3524 and 3080 cm^{-1}. Further evidence for the ammonium group is provided by the NH_2 deformation bands found at 2461 and 1560 cm^{-1}. Typical absorptions of the ethyl group, such as the C–H stretching occurs at 2988, 2811 cm^{-1}, CH_2 bending modes at 1455 cm^{-1}, CH_3 bending absorption at 1390 cm^{-1}; while the absorptions at 1198 cm^{-1} (CH–NH–C), 1158 cm^{-1}(C–N–C), 1041 cm^{-1}(C–N) and 767 (–CH2 –) confirmed the presence of ethyl and ammonium groups in the pigment (see Figure 4.3)

The thermal decomposition of the synthesized pigment is assessed by means of Differential Thermal Analysis - Simultaneous Thermogravimetric (DTA-TG) with a Setaram LabSysEvo 1600 (Section 2.1.3); the DTA-TG analysis is performed under air atmosphere at a heating rate of 10 °C/min from 27 °C to 1000 °C. The thermal analysis of the synthesized pigment illustrated in Figure 4.4, shows the transition during which the coating turns from green to yellow (45 °C); this peak is very sharp [114]. The second peak at 77 °C is the melting peak, while the peak at 350 °C corresponds to the decomposition of the ethyl groups.

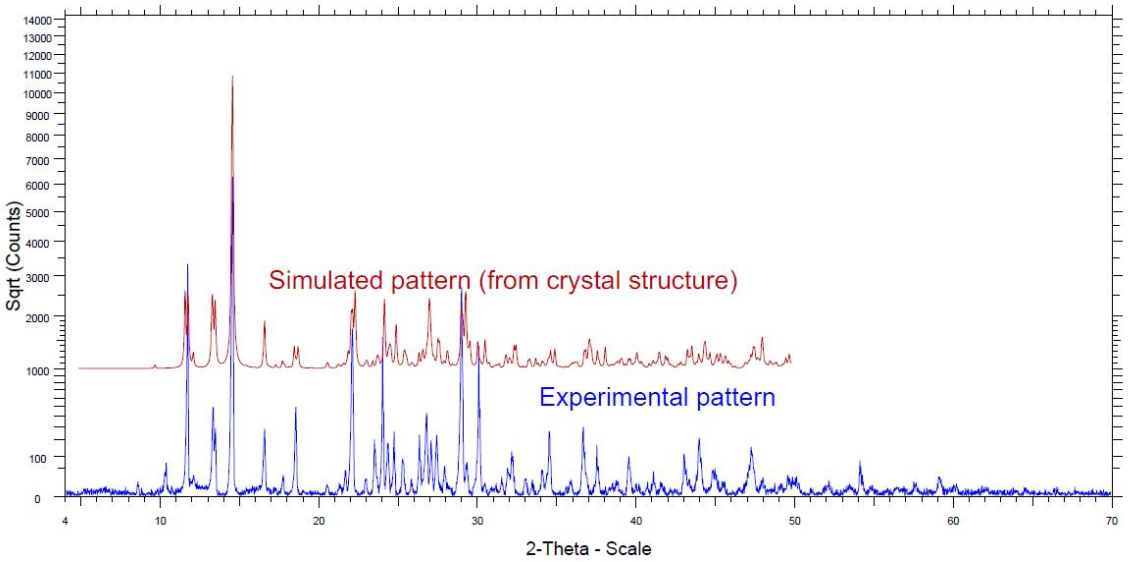

Figure 4.2 XRD spectrum of the inorganic colour changing pigment.

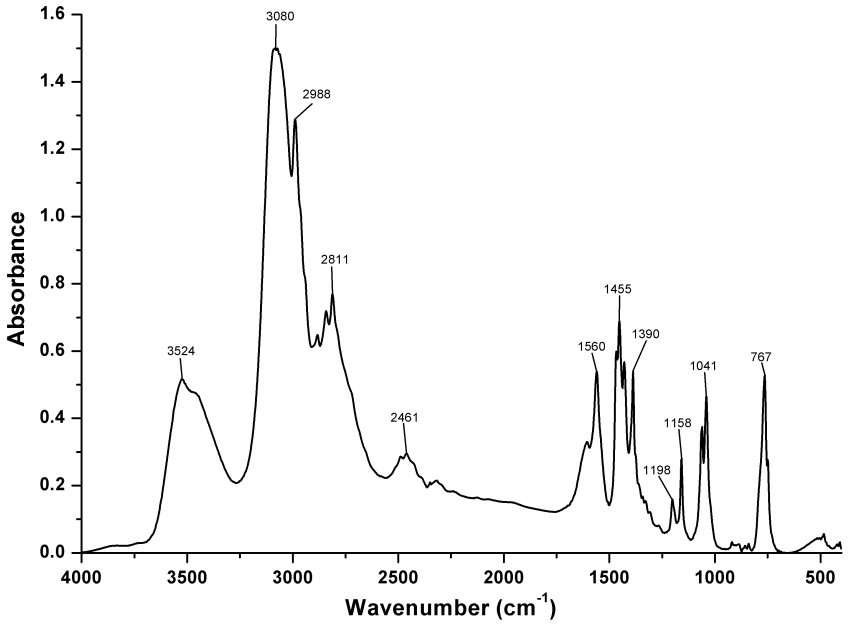

Figure 4.3 FTIR spectrum of the inorganic colour changing pigment.

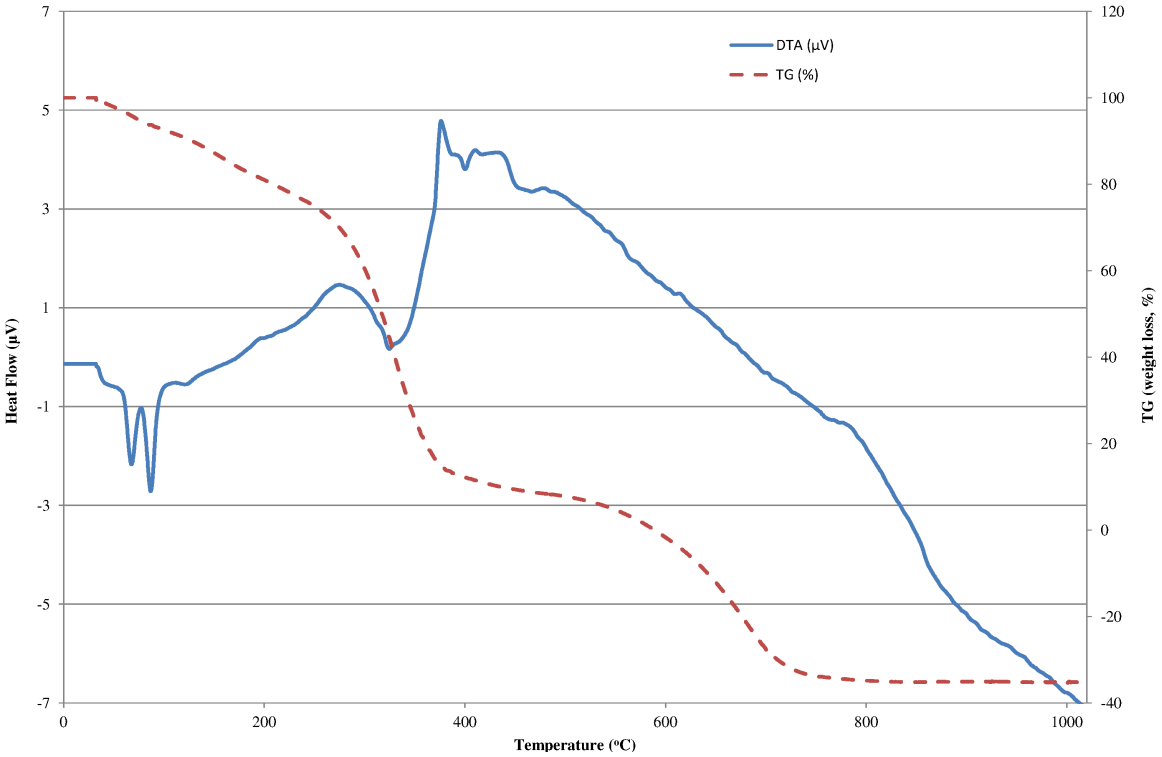

Figure 4.4 Thermal analysis of the synthesized pigment.

4.3 Organic thermochromic coatings

A set of three organic thermochromic pigments are chosen by New Color Chemical Co. Limited. Tabulated in Table 4.8 is presented the composition of the three organic thermochromic pigments. The data are obtained by the manufacturer's Material Safety Data Sheet.

Table 4.1 Chemical composition of organic thermochromic pigments

Pigment	Chemical compunt	Weight (%)	CAS No.
Red	Melamine Formaldehyde Resin	1~5	68002-20-0
	3-Dibuthylamino-6-methyl-7-bromo-fluoran	2~10	117342-26-4
	Bisphenol A	5~15	80-05-7
	Methyl stearate	50~80	112-61-8
Blue	Melamine Formaldehyde Resin	1~5	68002-20-0
	6'-(ethyl(4-methylphenyl)amino)-2'-(methylphenylamino)	2~10	42530-35-8
	Bisphenol A	5~15	80-05-7
	Methyl stearate	50~80	112-61-8
Brown	Melamine Formaldehyde Resin	1~5	68002-20-0
	Spiro(isobenzofuran-1(3H),9'-(9H)xanthen)-3-one	1~4	21934-68-9
	Bisphenol A	5~15	80-05-7
	3-Diethylamino-6-methyl-7-(2,4-xylidino)fluoran	2~10	36431-22-8
	Methyl stearate	50~80	112-61-8

4.4 Optical filters for the protection of the inorganic and organic thermochromic coatings

A major issue with the organic thermochromic coatings is their degradation when they are exposed to solar radiation and especially to the ultraviolent (UV) part of the solar radiation [116–118]. Two commercially available UV protection products (UV stabiliser: Eversorb and polyurethane varnish: Ilam) are applied on top of the thermochromic coating. Using the Carry 5000 with the integrating sphere their transmission spectrum is measured (Figure 4.5). Clear plastic film is used as substrate and on top a thin film of the UV varnish is applied. Eversorb has a very steep descent at 434nm (at the edge of the VIS region) with zero transmittance after 394nm. Ilam has a descent starting at 423nm and ending at 312nm, after which the transmittance is zero.

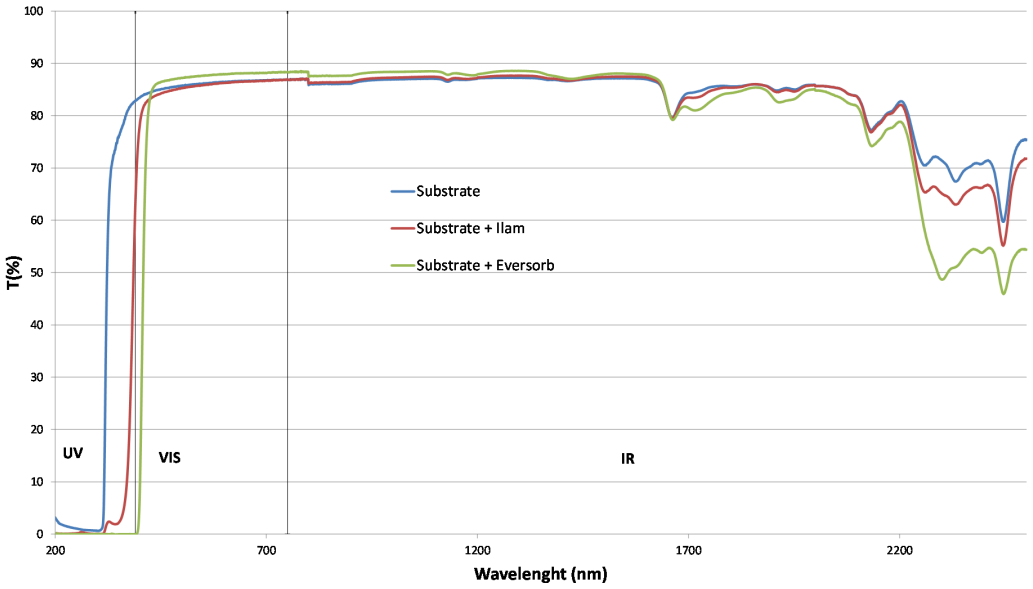

Figure 4.5 Spectral transmittance of substrate, substrate with Eversorb and substrate with Ilam.

4.5 Experimental procedure

4.5.1 Inorganic thermochromic coatings

4.5.1.1 Preparation of inorganic thermochromic coatings

Several experiments are made in order to incorporate the bis(diethylammonium)tetrachlorocuprate(II) (ITC) into a matrix either using water based or solvent based white paints but were unsuccessful. The solution is found to dissolve the compound into purified water and painting it over a plaster of Paris (Pl) covered sample holder. A set of six samples are prepared with black Portland cement as substrate (10cm x 10cm x 2.5cm) and covered with plaster of Paris (thickness: 0.5cm), Table 4.2. For painting the ITC on the plaster of Paris samples, 0.3g of ITC are dissolved into 5g of purified water and then evenly spread over the whole area of the sample. To cover the samples with the UV varnished, the samples are left into a dark chamber at atmospheric conditions in order for the purified water to evaporate.

Table 4.2 Composition and codename of inorganic thermochromic coatings.

No	Code	Type	Type of UV varnish
1	ITC	inorganic thermochromic title	-
2	ITC_V	Inorganic thermochromic sample covered with polyurethane varnish	Ilma
3	ITC_S	Inorganic thermochromic sample covered with UV stabiliser	Eversorb
4	Pl	plaster of Paris	-
5	Pl_V	plaster of Paris covered with polyurethane varnish	Ilma
6	Pl_S	plaster of Paris covered with UV stabiliser	Eversorb

4.5.1.2 Spectral reflectance and infrared emittance of inorganic thermochromic coatings

The results of spectral reflectance measurements for the inorganic thermochromic coating before and after the transition temperature (Table 4.2) is shown at Figures 4.11 to 4.16. The measurements are conducted using the Carry 5000 with integrating sphere (Section 2.2.2). The coatings are raised to their transition temperature using the laboratory furnace. The UV varnish, Eversorb was not cured (a sticky surface was created) after 5 days in room temperature and it was not possible to be measured with the Cary 5000 without removing the varnish from the surface of the samples.

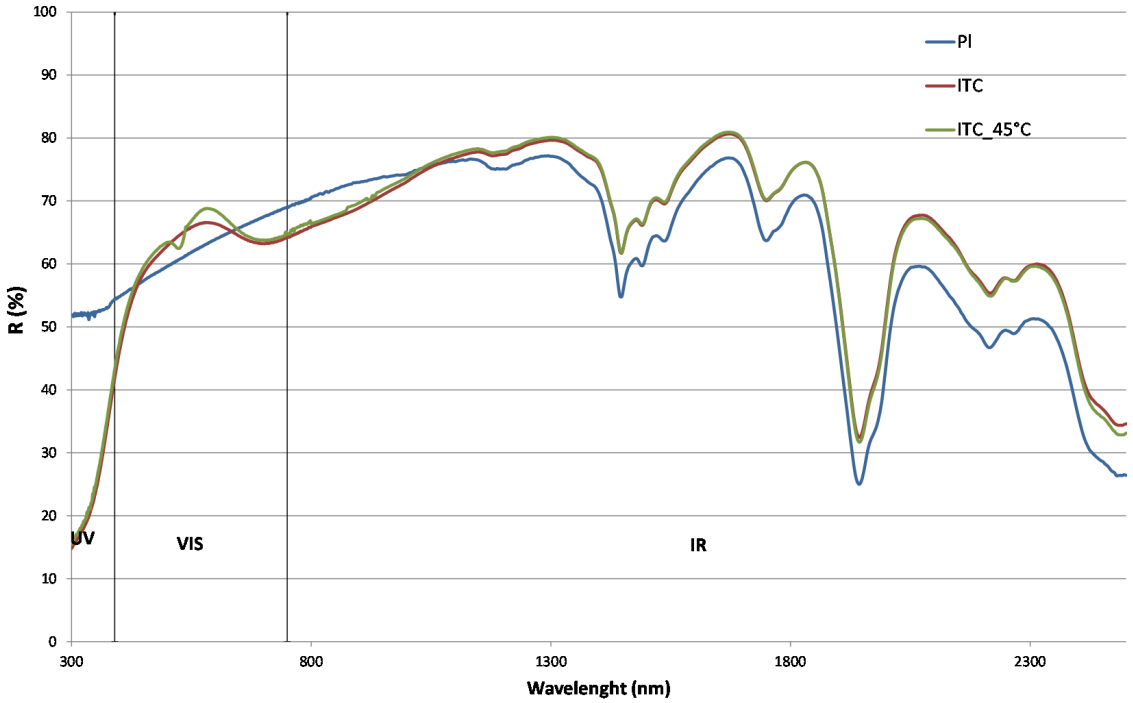

Figure 4.6 Spectral reflectance of sample: plaster of Paris (Pl), plaster of Paris with inorganic thermochromic (ITC) and plaster of Paris with inorganic thermochromic at transition temperature (45°C) (ITC_45°C).

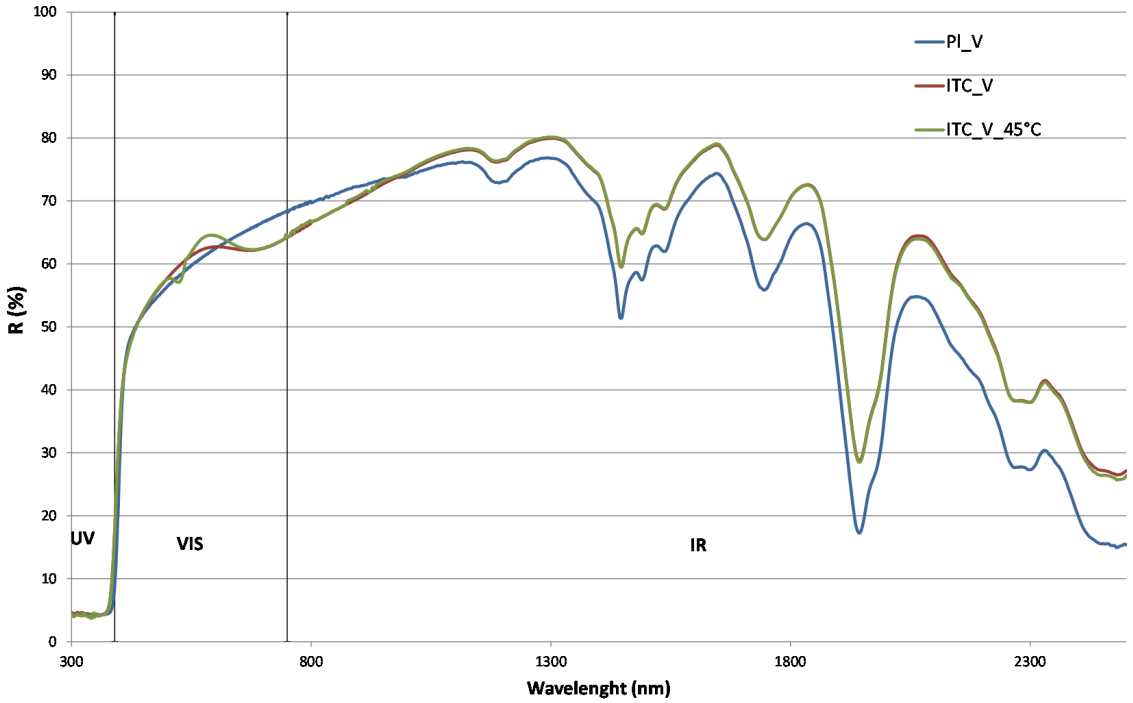

Figure 4.7 Spectral reflectance of sample: plaster of Paris + Ilam (Pl_V), plaster of Paris with inorganic thermochromic and Ilam (ITC_V) and plaster of Paris with inorganic thermochromic and Ilam at transition temperature (45°C) (ITC_V_45°C).

With the addition of the inorganic thermochromic compound, the solar reflectance (SR) is increased in 1000 - 2500nm wavelengths. When the samples are heated to 45°C, an increase is observed at 580nm (light yellow colour) and decrease at 530nm (light green colour) of the solar reflectance values. With the addition of the UV polyurethane varnish a steep decline in the solar reflectance is recorded from 400 - 300nm (Figure 4.7). This result perfectly agrees with the previous findings in Figure 4.5. The same results are anticipated for the UV varnish, Eversorb (_S in the samples codes) according to the Figure 4.5.

Table 4.3 Solar reflectance in near infrared, visible, ultraviolet wave-length and infrared emittance of plaster of Paris, plaster of Paris + inorganic thermochromic.

No.	Sample Name	SR (%)	SR_{IR} (%)	SR_{VIS} (%)	SR_{UV} (%)	IE
1	Pl	66	70	62	52	0.85
2	ITC	67	70	65	36	0.87
3	ITC (45°C)	67	69	66	37	-
4	Pl_V	62	67	59	4	0.86
5	ITC_V	63	69	59	4	0.88
6	ITC_V (45°C)	63	69	59	4	-

In Table 4.3 the SR in near infrared, visible, ultraviolet wave-length and infrared emittance (IE) of plaster of Paris, plaster of Paris + ITC at room and transition temperature are shown. Moreover. the samples covered with UV varnish Ilam are included in Figure 4.7. For the measurement of the IE the "Device and Services Emissometer model AE1" is used. With the addition of the ITC, a small increase is observed in the overall SR and SR_{VIS} but significant decrease in SR_{UV}. A small change is observed in the SR spectrum of the ITC at change temperature only in the visible part of the spectrum. Also the IE of the sample with the ITC is increased. With the introduction of the UV varnish a significant reduction of the SR_{UV} for all samples is observed as expected form the previous results (Figure 4.5). A smaller decrease is recorded for the total SR, SR_{IR}, SR_{VIS}. A small increase is observed for the IE of the samples.

4.5.1.3 Surface temperature measurement of the inorganic thermochromic coatings

A nineteen days measurement period is conducted during September 2017 to investigate the thermal performance of the inorganic thermochromic coatings. Also a reference sample made with Portland cement is measured. The samples are placed on top of a wooden structure at the roof of K2 building at the Technical University of Crete campus. The CR850 datalogger along with the AM16/32B are utilised for the measurements of the surface temperature. The measurements are split into two groups: day (7:00-20:00) and night (22:00-5:00) in order to determine the performance of the samples during day and night.

During the course of the measurements the weather is characterized by clear sky. Tabulated in Table 4.4 are the meteorological conditions of the measuring period.

Table 4.4 Meteorological conditions during thermochromic coatings testing.

		Air temperature (°C)		Relative humidity (%)	Solar radiation (W/m^2)
		Day	Night		
September	Average	28.4	20.4	67	236
	Maximum	36.1	28.3	89	913
	Minimum	19.2	14.9	32	0

The surface temperature of the samples is presented in Figure 4.8 using box plot. The ambient air temperature (T_{air}) is represented using a red horizontal line. The surface temperature of the reference sample is denoted by a blue line. Table 4.5 includes the average and maximum surface temperatures of the samples.

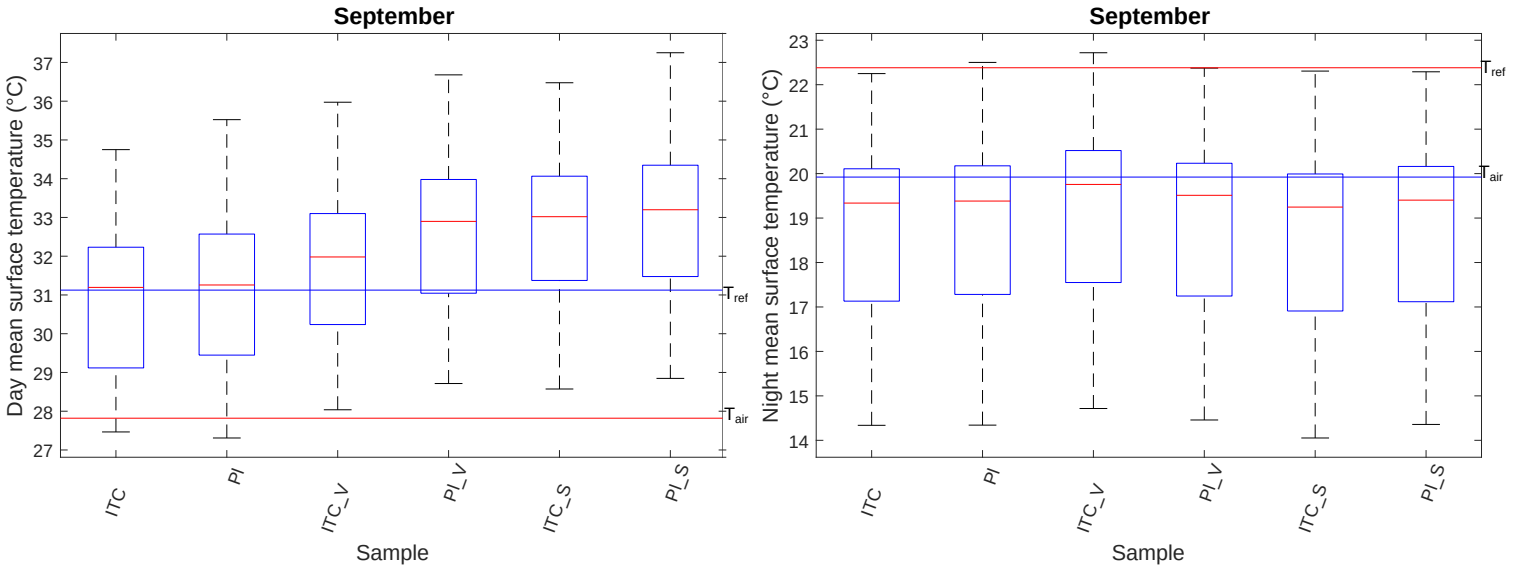

(a) Day. (b) Night.

Figure 4.8 Average day/night surface temperature of the inorganic thermochromic samples.

Table 4.5 Average and maximum surface temperature for inorganic thermochromic samples during day and night.

Group	Sample	Day		Night	
		Average surface temperature (°C)	Maximum surface temperature (°C)	Average surface temperature (°C)	Maximum surface temperature (°C)
Inorganic	ITC	30.59	42.44	18.90	27.23
	Pl	30.98	43.62	19.03	27.44
	ITC_V	31.51	44.41	19.26	27.83
	Pl_V	32.29	45.89	18.98	27.40
	ITC_S	32.47	45.62	18.75	27.18
	Pl_S	32.73	46.51	18.92	27.32
Reference	Portland cement	31.10	46.28	19.96	28.74

All inorganic thermochromic samples have lower average surface temperature ranging from 0.78K for Pl_V to 0.25K Pl_S from the samples covered with plaster (Pl). The addition of the polyurethane varnish (_V) has raised the average surface temperature by 1.12K and 1.82K for the UV stabiliser. A reduction of the maximum surface temperature is observed from 1.48K for Pl_V to 0.89K Pl_S when

compared with sample covered with Pl. Also the increase of the maximum surface temperature is ranging from 2.12K to 3.04K for the samples covered with the polyurethane varnish and UV stabilizer respectively.

4.5.1.4 Surface thermal imaging of inorganic thermochromic coatings

At the present stage of the experiment, the samples' surface temperature is measured using a thermal imaging camera, ThermaCAM B2 (Section 2.2.5). This procedure is repeated twice during the measuring period to ensure reliability of the results. In particular, measurements are taken on the 4^{th} and 8^{th} day, three times per day. Table 4.6 shows the average surface temperatures of the samples based on the measurements of the thermal imaging camera. To obtain the average surface temperature, four measurements are taken, one at each corner of the sample (Figure 4.9), using the software FLIR Tools Software by FLIR® Systems, Inc[119]. All the thermal images are taken with the same emissivity, IE = 0.80 and then were changed into the correct values, using the software tabulated in Table 4.3. For the samples covered with Eversorb the same emissivity as measured for the samples covers with Ilam UV varnish is used.

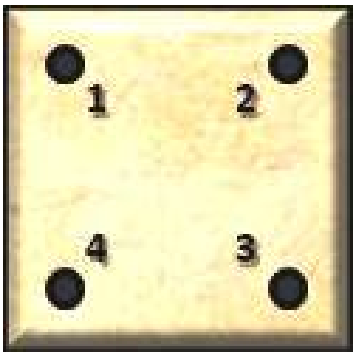

Figure 4.9 Measuring points of the sample with the use of the thermal imaging camera.

The data from the thermal imaging measurements (Table 4.6) are in line with the conclusions obtained from surface temperature measurements with thermocouples (Table 4.5). The thermochromic samples have lower surface temperatures than the samples covered with plaster of Paris (Pl).

Table 4.6 Thermal imaging measurement of the inorganic thermochromic samples.

Day of measurement	4			8		
Sample \ Time	10:30	12:30	13:30	11:30	13:30	15:30
ITC	32.5	37.6	35.8	35.0	31.3	30.7
Pl	34.2	38.8	34.9	35.5	32.9	31.2
ITC_V	33.6	39.2	34.6	35.6	31.8	29.8
Pl_V	35.0	39.7	35.5	36.5	32.6	30.8
ITC_S	33.7	38.1	34.6	34.8	31.9	30.6
Pl_S	35.1	37.8	35.0	35.4	31.4	29.8
Conventional white paint	32.9	36.5	34.5	34.4	31.3	30.0
Portland cement	40.5	-	38.3	43.5	37.0	31.8

In order to compare the surface temperature (Figure 4.10) of the developed coatings a set of thermal imaging photographs are taken on the forth day of the measuring period at 13:30. The scale for all the photographs is set to 23°C - 53°C in order to enable the comparison.

For the inorganic thermochromic samples, (Figure 4.10) it is observed that the sample covered with thermochromics has lower temperature than the samples covered only with plaster of Paris. The addition of polyurethane varnish and UV stabiliser raises the surface temperature of the samples.

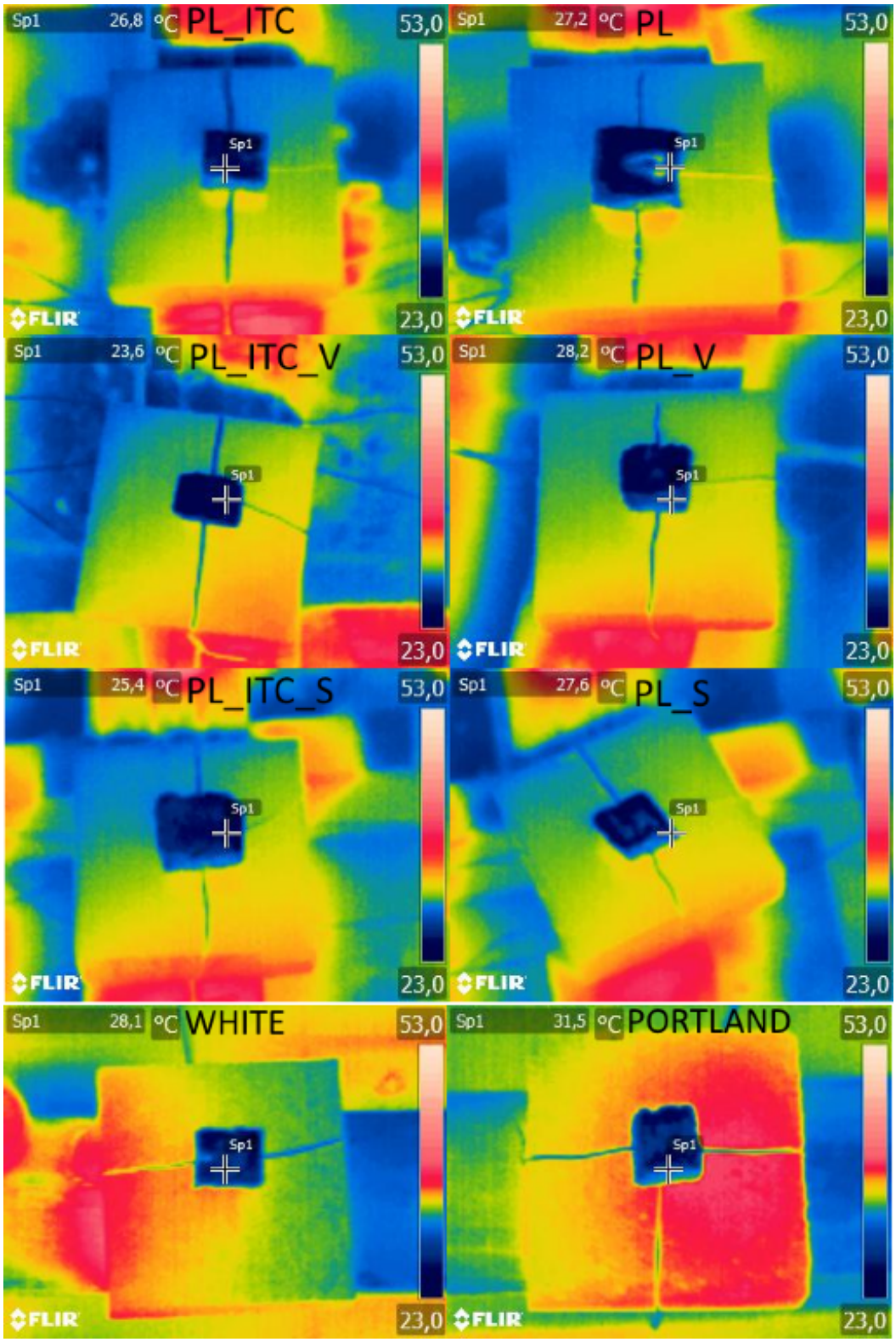

Figure 4.10 Thermal imaging photographs of inorganic thermochromic samples, plaster of Paris with varnish or UV stabilizer.

4.5.2 Organic thermochromic coatings

4.5.2.1 Preparation of organic thermochromic coatings

According to the manufacturer's recommendation a white alkyd (polyester modified by the addition of fatty acids and other components) based enamel paint is used as a base. A number of tests are performed in order to select the pigments' mass content with the white enamel paint in order to select the final colour. A 15% concentration by weight is selected as seen on Table 4.7. A set of matching conventional colour coatings are developed in order to examine the effectiveness of the organic thermochromic coatings. Sample name along with their composition are tabulated on Table 4.8. The white base colour is poured into a single use plastic container, then the pigment is added and thoroughly mixed. All coatings are applied on top of 10cm x 10cm x 3cm white pavement tiles.

Table 4.7 Consecration of organic thermochromic coating.

	Red samples	Blue samples	Brown samples
White enamel paint	11.47g	11.55g	11.39g
Thermochromic pigment	1.74g	1.73g	1.71g
Concentration	15%	15%	15%

Table 4.8 Composition and codename of organic thermochromic coatings.

No	Code	Type	Type of UV varnish	Colour
1	RTC	Thermochromic sample	-	Red
2	RTC_V	Thermochromic sample covered with polyurethane varnish	Ilma	
3	RTC_S	Thermochromic sample covered with UV stabiliser	Eversorb	
4	RCO	Conventional paint	-	
5	RCO_V	Conventional paint covered with polyurethane varnish	Ilma	
6	RCO_S	Conventional paint covered with UV stabiliser	Eversorb	
7	BTC	Thermochromic sample	-	Blue
8	BTC_V	Thermochromic sample covered with polyurethane varnish	Ilma	
9	BTC_S	Thermochromic sample covered with UV stabiliser	Eversorb	
10	BCO	Conventional paint	-	
11	BCO_V	Conventional paint covered with polyurethane varnish	Ilma	
12	BCO_S	Conventional paint covered with UV stabiliser	Eversorb	
13	BrTC	Thermochromic sample	-	Brown
14	BrTC_V	Thermochromic sample covered with polyurethane varnish	Ilma	
15	BrTC_S	Thermochromic sample covered with UV stabiliser	Eversorb	
16	BrCO	Conventional paint	-	
17	BrCO_V	Conventional paint covered with polyurethane varnish	Ilma	
18	BrCO_S	Conventional paint covered with UV stabiliser	Eversorb	

4.5.2.2 Spectral reflectance and infrared emittance of organic thermochromic coatings

The results of the spectral reflectance for the thermochromic coating samples, after the transition temperature (Table 4.1), conventional white paint (WCO) and reference sample (Portland cement) is shown at Figures 4.11 to 4.17. The measurements are conducted using the Carry 5000 with integrating sphere. The samples are raised to the transition temperature using the laboratory furnace.

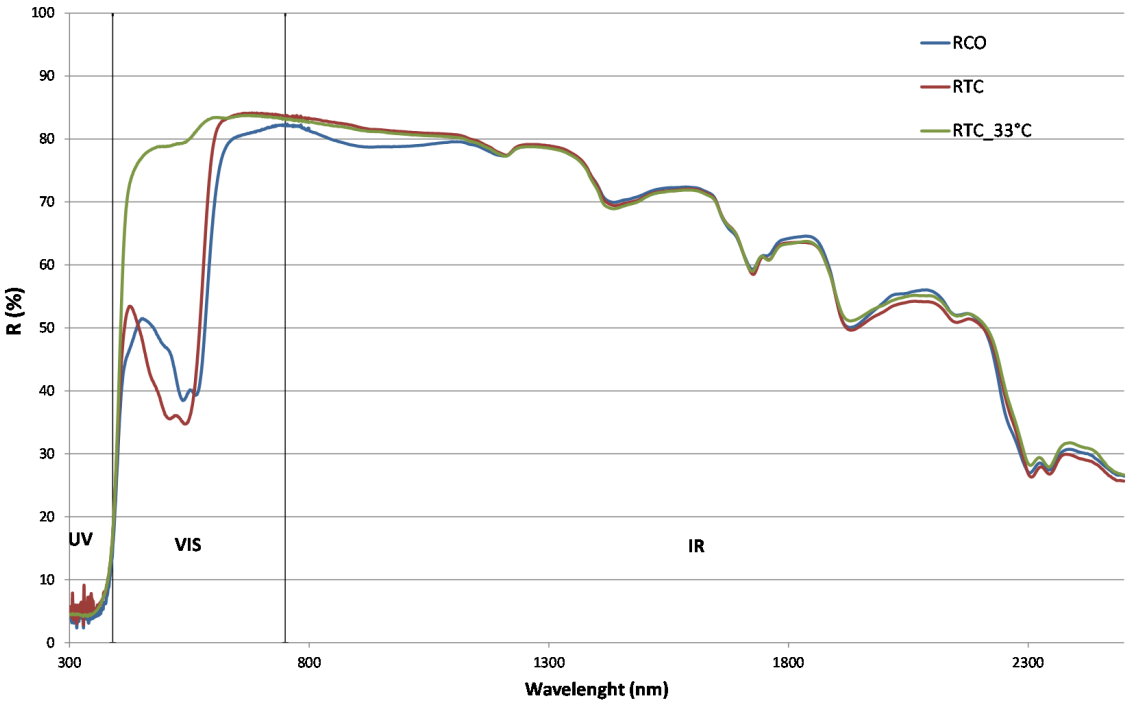

Figure 4.11 Spectral reflectance of red thermochromic sample (RTC), red thermochromic sample at transition temperature (33°C) (RTC_33°C) and red conventional sample (RCO).

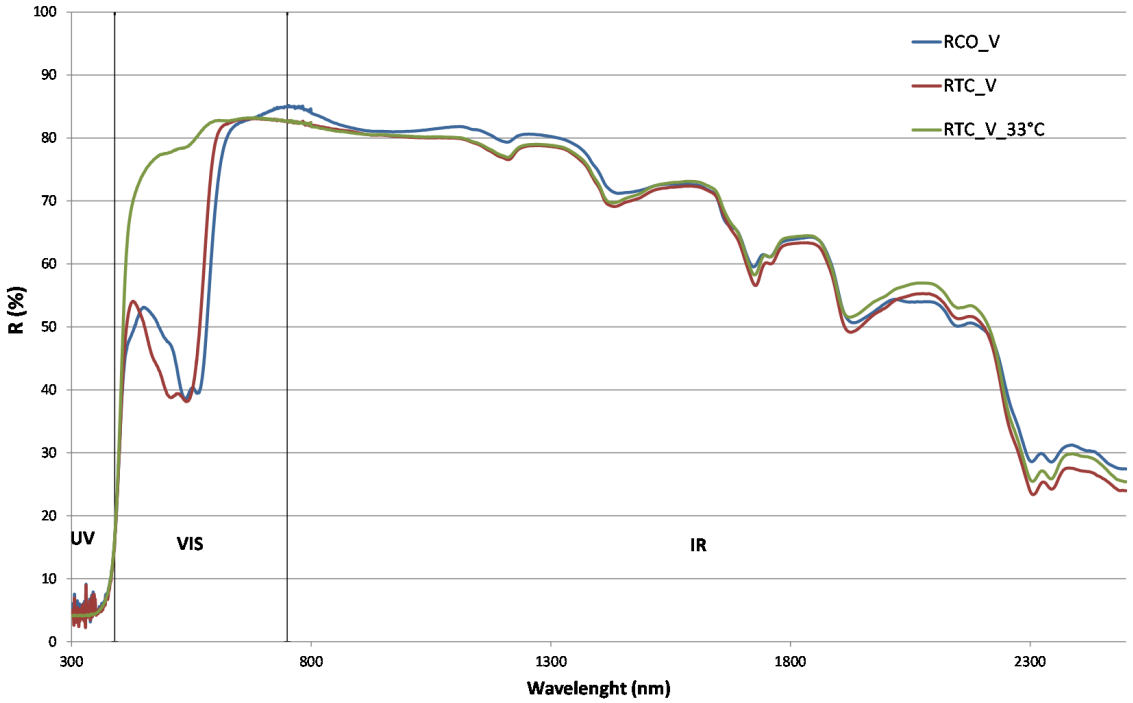

Figure 4.12 Spectral reflectance of red thermochromic sample covered with polyurethane varnish (RTC_V), red thermochromic sample covered with polyurethane varnish at transition temperature (33°C) (RTC_V_33°C) and red conventional sample covered with polyurethane varnish (RCO_V).

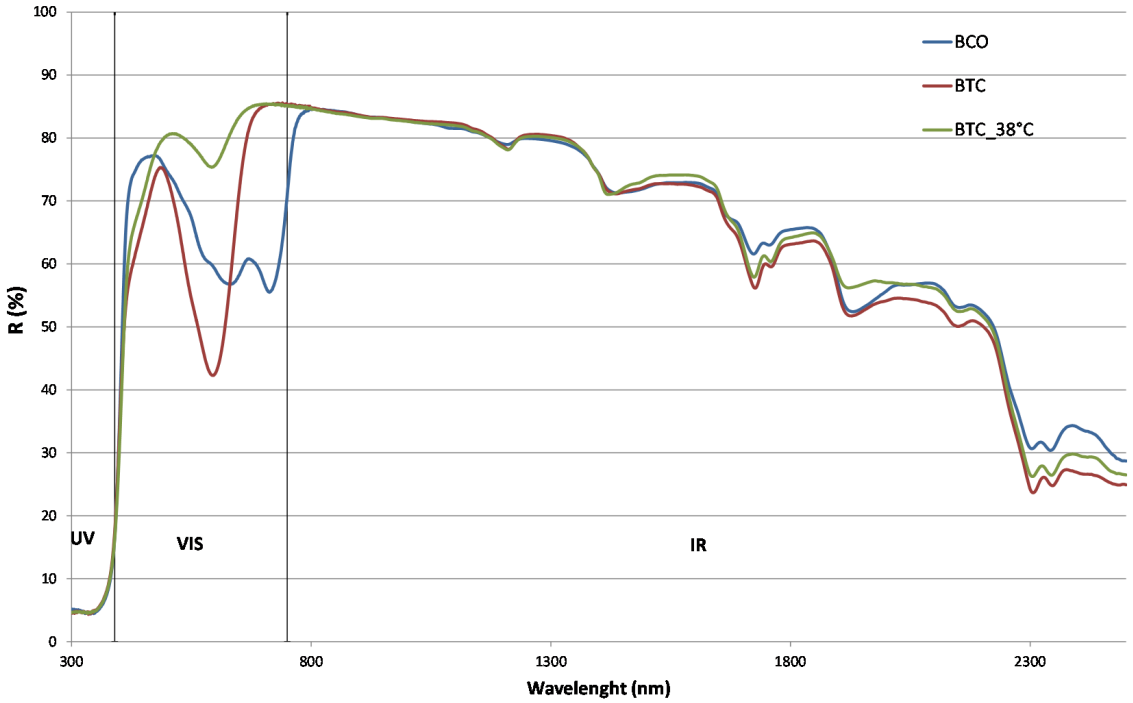

Figure 4.13 Spectral reflectance of blue thermochromic sample (BTC), blue thermochromic sample at transition temperature (38°C) (BTC_38°C) and blue conventional sample (BCO).

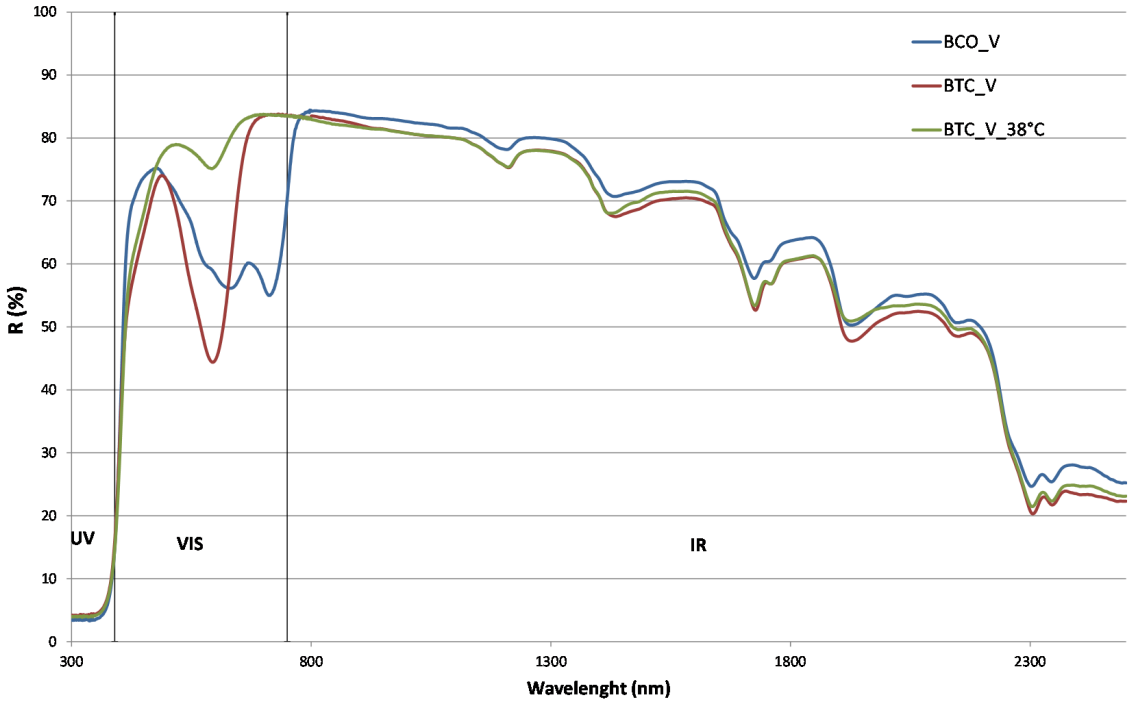

Figure 4.14 Spectral reflectance of blue thermochromic sample covered with polyurethane varnish (BTC_V), blue thermochromic sample covered with polyurethane varnish at transition temperature (38°C) (BTC_V_38°C) and blue conventional sample covered with polyurethane varnish (BCO_V).

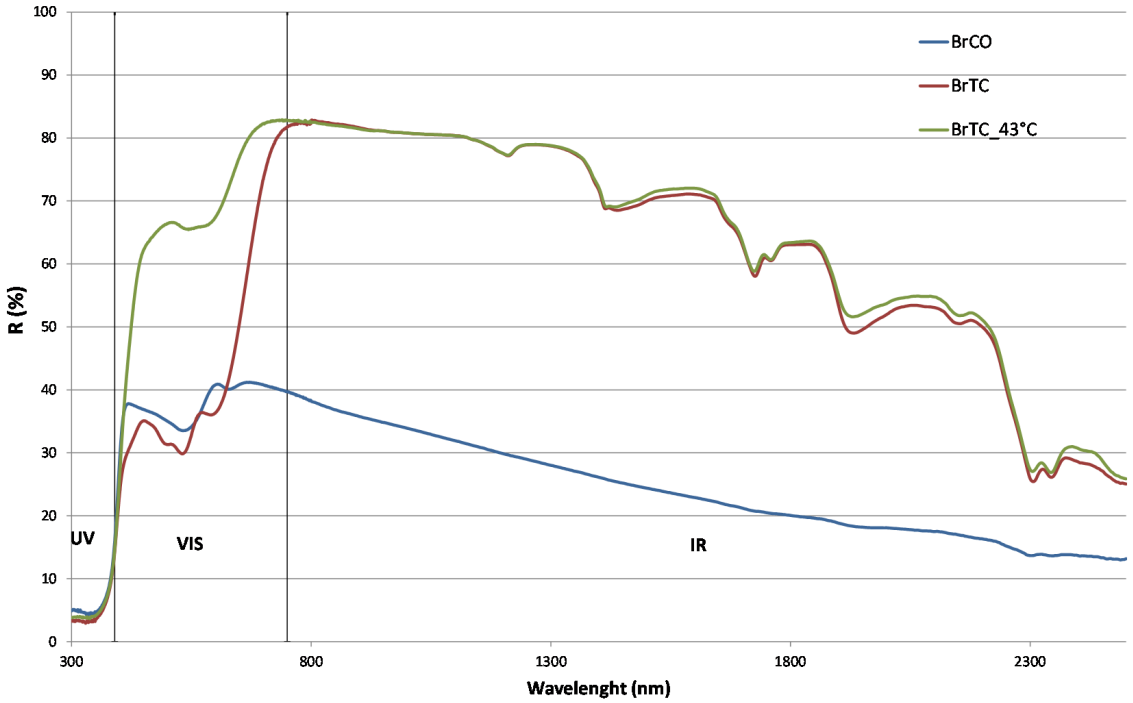

Figure 4.15 Spectral reflectance of brown thermochromic sample (BrTC), brown thermochromic sample at transition temperature (43°C) (BrTC_43°C) and brown conventional sample (BrCO).

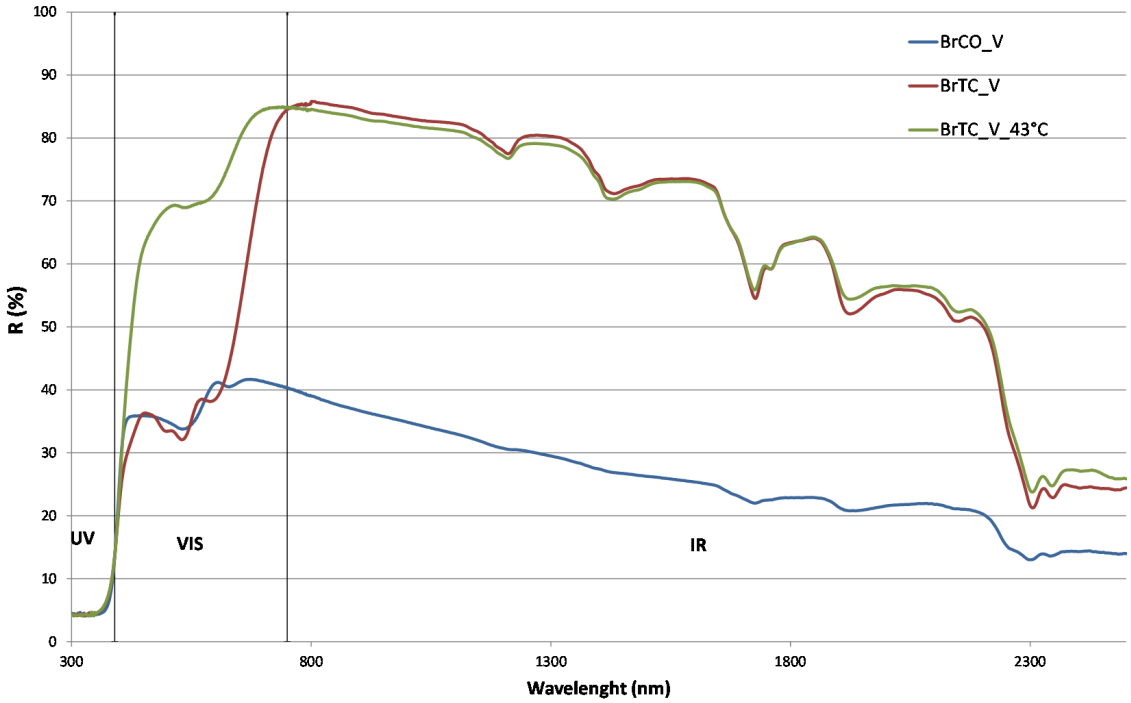

Figure 4.16 Spectral reflectance of brown thermochromic sample covered with polyurethane varnish (BrTC_V), brown thermochromic sample covered with polyurethane varnish at transition temperature (43°C) (BrTC_V_43°C) and brown conventional sample covered with polyurethane varnish (BrCO_V).

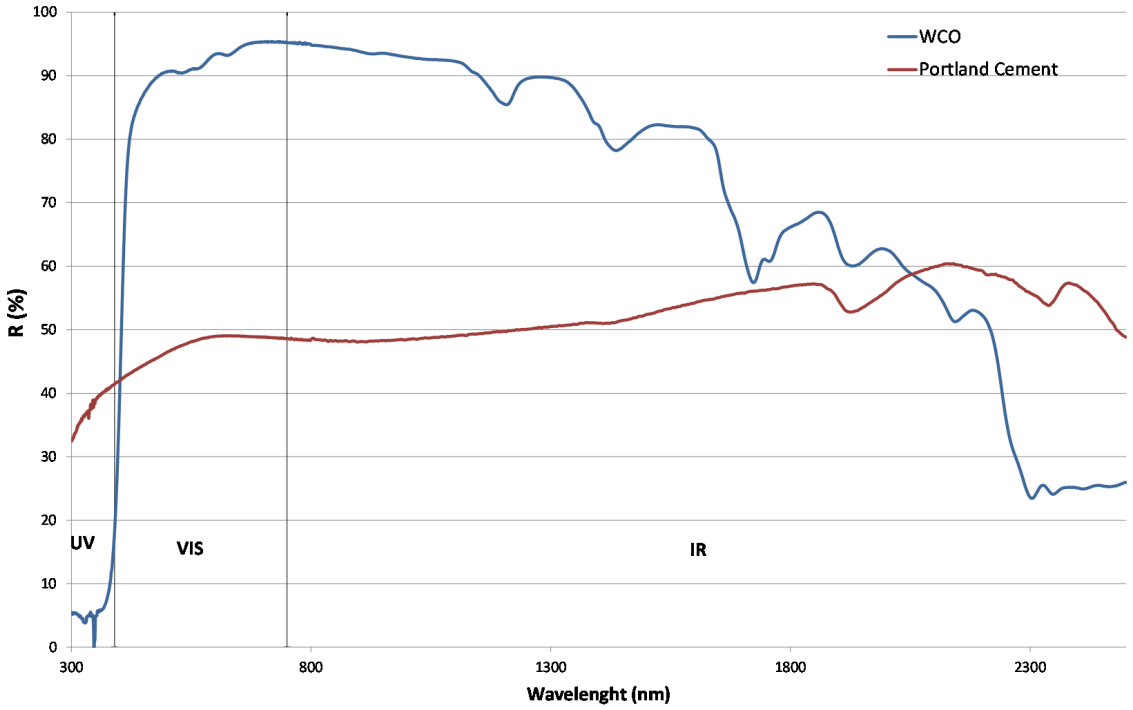

Figure 4.17 Spectral reflectance of commercial white coating and reference sample.

The solar reflectance of organic thermochromic samples display a significant increase in the VIS part of spectrum when they are heated at their transition temperature. For the red and blue thermochromics the solar reflectance is almost the same for the IR and UV part of the spectrum with the conventional one. A significant difference in observed of the solar reflectance for the brown colour between the thermochromic and the conventional. The addition of the UV varnish (Ilma) does not change significantly the solar reflectance in th UV part of the spectrum for either the thermochromic or the conventional samples.

Based on the measurements of spectral reflectance using the Carry 5000 with the integrating sphere, the SR is calculated for each one of the samples using the ASTM E903-12 and ASTM G159-91 standards. The total, near infrared (NIR: 300-400nm), visible (VIS: 400-700nm) and ultraviolet (UV: 700-2500nm) SR are tabulated in Table 4.9.

Table 4.9 Solar reflectance in near infrared, visible and ultraviolet wave-length of the organic thermochromic coatings.

No.	Sample Name	SR (%)	SR_{IR} (%)	SR_{VIS} (%)	SR_{UV} (%)
1	RTC	67	76	58	6
2	RTC_33°C	75	76	79	5
3	RCO	66	75	57	5
4	RTC_V	67	75	60	5
5	RTC_V_33°C	74	75	78	5
6	RCO_V	68	76	59	6
7	BTC	69	77	63	6
8	BTC_38°C	75	77	77	5
9	BCO	69	74	66	5
10	BTC_V	68	75	63	5
11	BTC_V_38°C	73	75	75	5
12	BCO_V	68	74	64	4
13	BrTC	59	75	39	4
14	BrTC_43°C	70	75	67	5
15	BrCO	33	31	38	5
16	BrTC_V	61	77	41	5
17	BrTC_V_43°C	72	76	69	5
18	BrCO_V	34	33	37	5
19	Conventional white paint	85	85	90	6
20	Reference	49	50	47	37

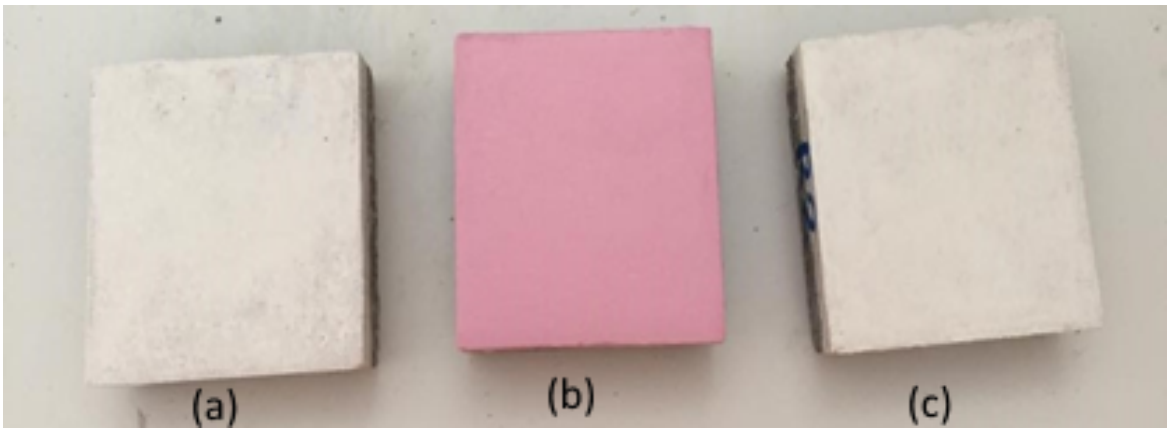

Figure 4.18 Conventional white paint (a), red thermochromic at room temperature (b), red thermochromic at 33°C (c).

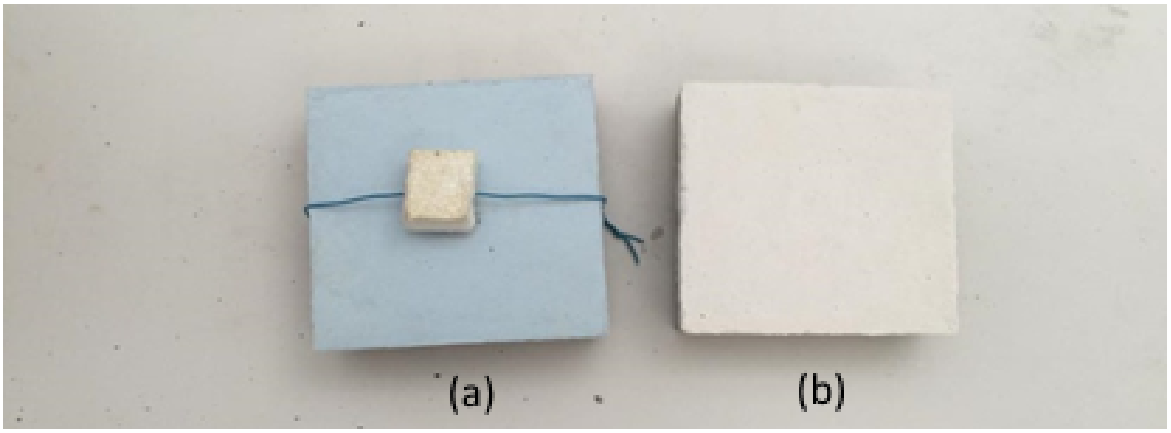

Figure 4.19 Blue thermochromic at room temperature (a), blue thermochromic at 43°C (b).

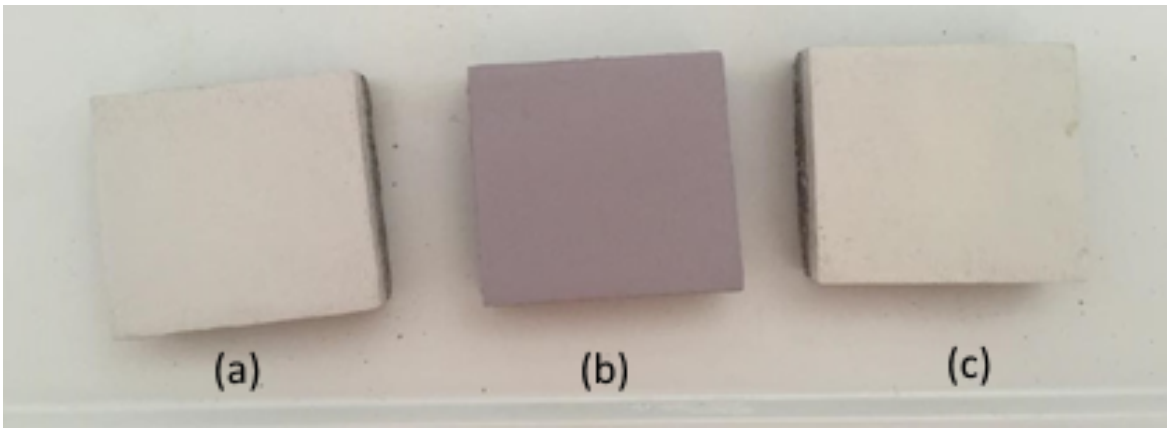

Figure 4.20 Conventional white paint (a), brown thermochromic at room temperature (b), brown thermochromic at 43°C (c).

As shown in Table 4.9 the red and blue thermochromics and conventional coatings have similar values for SR, SR_{IR}, SR_{VIS}, SR_{UV}. While SR, SR_{IR}, SR_{VIS}, SR_{UV} for the conventional brown coatings is almost half than the thermochromic one. A reduction from 8% (blue) to 19% (brown) in the SR values and 23% for blue (Figure 4.19), 36% for red (Figure 4.18) and 71% for brown (Figure 4.20) in the SR_{VIS} values is observed when the thermochromics reach their transition temperature and become white. The addition of the varnish slightly reduces the SR of both the thermochromic and conventional coatings.

Table 4.10 Infrared emittance of the organic thermochromic coatings.

Sample Name	RTC	RCO	RTC_V	RCO_V	BTC	BCO
IE	0.92	0.87	0.93	0.93	0.91	0.87

Sample Name	BTC_V	BCO_V	BrTC	BrCO	BrTC_V	BrCO_V
IE	0.92	0.92	0.91	0.87	0.92	0.92

The values of IE are given in Table 4.10. For the measurement of the infrared emittance values the "Device and Services Emissometer model AE1" is used. In all cases the conventional paint has lower IE from the thermochromic ones. With the addition of the UV varnish, Ilma a small increase in observed in the IE of the thermochromic samples. A small increase in the IE is measured for the conventional samples with the additional of the UV varnish. Also all samples with the UV varnish have almost the same IE values.

4.5.2.3 Surface temperature measurement of the organic thermochromic coatings

The same measurements setup are used for the measurement of the surface temperature of organic thermochromic coatings as described in Section 4.5.1.3.

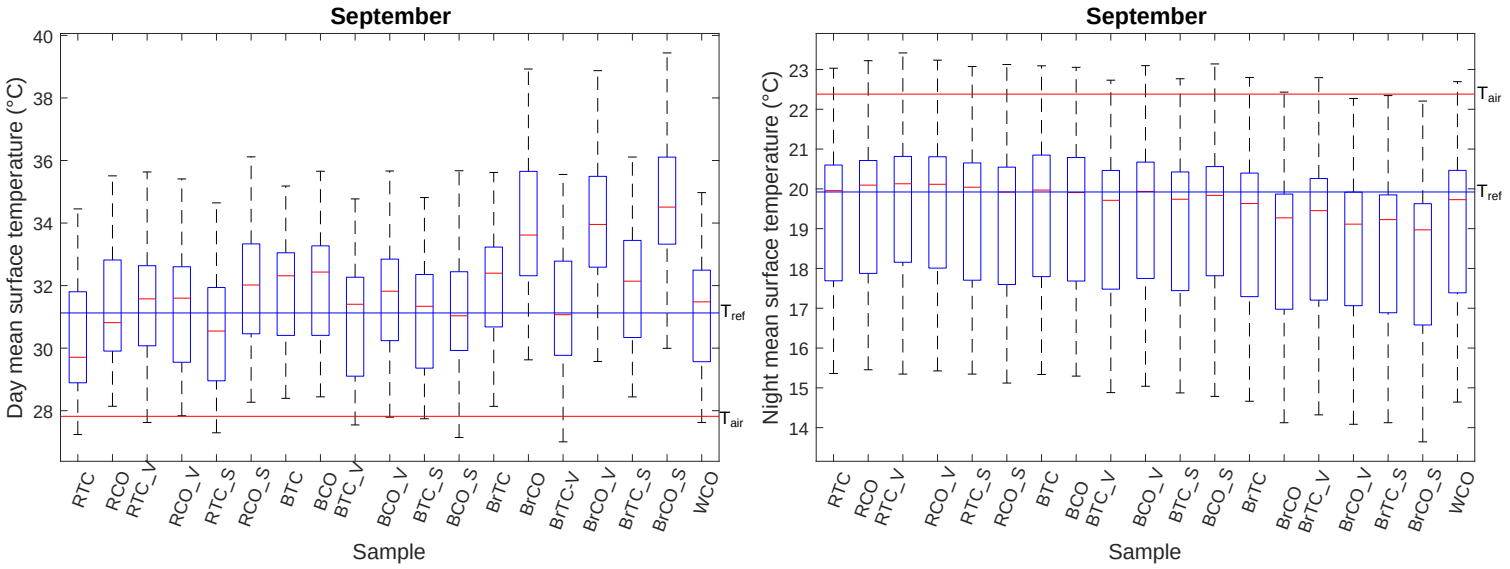

(a) Day.

(b) Night.

Figure 4.21 Average day/night surface temperature of the organic thermochromic sample.

The surface temperature of the samples is presented in Figure 4.21 using box plot. The ambient air temperature (T_{air}) is represented using a red horizontal line. The surface temperature of the reference sample is denoted by a blue line. Table 4.11 includes the average and maximum surface temperatures of the samples.

Table 4.11 Average and maximum surface temperature for organic thermochromic samples during day and night.

Group	Sample	Day		Night	
		Average surface temperature (°C)	Maximum surface temperature (°C)	Average surface temperature (°C)	Maximum surface temperature (°C)
Organic	RTC	30.31	40.98	19.50	27.23
	RCO	31.22	42.84	19.66	27.53
	RTC_V	31.28	44.50	19.79	28.19
	RCO_V	31.02	42.78	19.70	27.89
	RTC_S	30.50	41.78	19.53	27.23
	RCO_S	31.77	44.06	19.45	27.20
	BTC	31.54	43.87	19.54	27.47
	BCO	31.67	44.22	19.49	27.32
	BTC_V	30.73	42.13	19.26	27.23
	BCO_V	31.40	43.53	19.50	27.71
	BTC_S	30.80	42.32	19.26	27.23
	BCO_S	31.13	43.96	19.50	28.17
	BrTC	31.79	43.58	19.15	27.17
	BrCO	33.89	48.91	18.78	26.86
	BrTC_V	31.13	44.19	19.12	28.16
	BrCO_V	33.97	49.17	18.79	27.26
	BrTC_S	31.91	44.77	18.74	26.84
	BrCO_S	34.54	50.36	18.47	26.56
Reference	Conventional white paint	30.93	43.01	19.18	27.60
	Reference	31.10	46.28	19.96	28.74

During the day, all organic thermochromic samples have lower average surface temperatures from the conventional samples. The surface temperature reduction ranges from 0.13K (blue) to 2.10K (brown). Higher maximum surface temperature of 0.35K to 5.33K is observed for blue and brown thermochromics respectively. The application of the varnishes on the organic thermochromics has mixed results in the average and maximum surface temperature comparing to the conventional ones:

- Average surface temperature:

  - A decrease from 0.96K (red) to an increase of 0.81K (brown) is observed for the thermochromic samples covered with polyurethane varnish and a decrease from 0.19K (red) to an increase of 0.73K (blue) for the thermochromic samples covered with UV stabiliser.
  - A decrease from 0.07K (brown) to an increase of 0.27K (blue) is measured for conventional samples covered with polyurethane varnish and a decrease from 0.96K (brown) to an increase of 0.55K (red) for the conventional samples covered with UV stabiliser.

- Maximum surface temperature
  - A decrease from 3.52K (red) to an increase of 1.74K (blue) is observed in the thermochromic samples covered with polyurethane varnish and a decrease from 1.19K (brown) to an increase of 1.55K (blue) for the thermochromic samples covered with UV stabiliser.
  - A decrease from 0.26K (brown) to an increase of 0.70K (blue) is measured for the conventional samples covered with polyurethane varnish and a decrease from 1.45K (brown) to an increase of 0.26K (blue) for the conventional samples covered with UV stabiliser.

The red thermochromic samples have lower average surface temperature when compared to the WCO sample of 0.62K. Blue and brown thermochromics have higher average surface temperature of 0.60K and 0.86K respectively. All the conventional samples have higher average surface temperatures from 0.29K (red) to 2.96K (brown) compared to the WCO sample. For the maximum surface temperatures, the reverse situation is recorded i.e. the thermochromics have higher surface temperature from 0K (red) to 2.7K (blue) and conventional from 10K (blue) to -2.6K (brown) from the WCO sample.

Approximately 84 hours during the measuring period (19 days), the red thermochromic has changed colour from red to white. The blue thermochromic and brown thermochromic have changed to white in approximately 17.5 hours and 1.6 hours, respectively. The colour change does not occurs instantly when the sample reach its transition temperature but gradually and completely change when it reaches the transition temperature.

The average surface temperature of all samples during the night is lower than the ambient air (Figure 4.21). This phenomenon is expected because during the night the main factor that affects the change in surface temperature is the IE. We consider that the heat transfer coefficients for all samples are the same.

4.5.2.4 Surface thermal imaging of organic thermochromic coatings

The same measurement's setup is followed for the measurement of the surface temperature of organic thermochromic coatings using the thermal imaging camera as described in Section 4.5.1.4.

The data from the thermal imaging measurements (Table 4.12) confirm the conclusions obtained from measurements with the thermocouples (Table 4.11). The thermochromic samples have lower temperatures than conventional ones. The red thermochromic has a slightly lower temperature than the white, while the sample with blue and brown thermochromics coatings have a slightly higher temperature than the white sample.

Table 4.12 Thermal imaging measurement of the organic thermochromic samples.

Day of measurement	4			8		
Sample \ Time	10:30	12:30	13:30	11:30	13:30	15:30
RTC	32.7	36.8	33.9	33.4	31.4	30.7
RCO	33.2	38.8	34.2	35.2	31.4	29.4
RTC_V	33.4	37.2	34.6	35.0	31.7	30.3
RCO_V	33.5	38.7	35.3	35.5	31.7	29.6
RTC_S	33.9	37.0	34.1	34.3	31.2	29.5
RCO_S	35.4	40.0	35.6	37.7	33.6	30.7
BTC	33.3	37.7	34.2	34.4	31.5	30.2
BCO	34.7	37.4	34.6	35.0	31.0	29.4
BTC_V	34.2	37.8	35.1	35.6	32.0	30.5
BCO_V	34.2	38.0	35.3	36.0	31.9	30.0
BTC_S	32.1	37.2	35.4	34.6	30.9	30.3
BCO_S	33.8	38.4	34.5	35.1	32.5	30.8
BrTC	33.7	39.1	34.7	34.7	32.6	31.2
BrCO	38.4	44.1	38.9	41.5	36.1	32.0
BrTC_V	33.9	38.9	35.9	35.3	32.2	30.7
BrCO_V	37.8	41.7	37.1	41.2	34.3	31.3
BrTC_S	34.6	39.3	35.1	-	32.2	30.4
BrCO_S	40.3	-	37.2	40.8	35.6	31.2
Conventional white paint	32.9	36.5	34.5	34.4	31.3	30.0
Reference	40.5	-	38.3	43.5	37.0	31.8

In order to compare the surface temperature of the developed coatings a set of thermal imaging photographs are taken on the forth day of the measuring period at 13:30. The scale for all the photographs is set to 23°C - 53°C in order to enable the comparison.

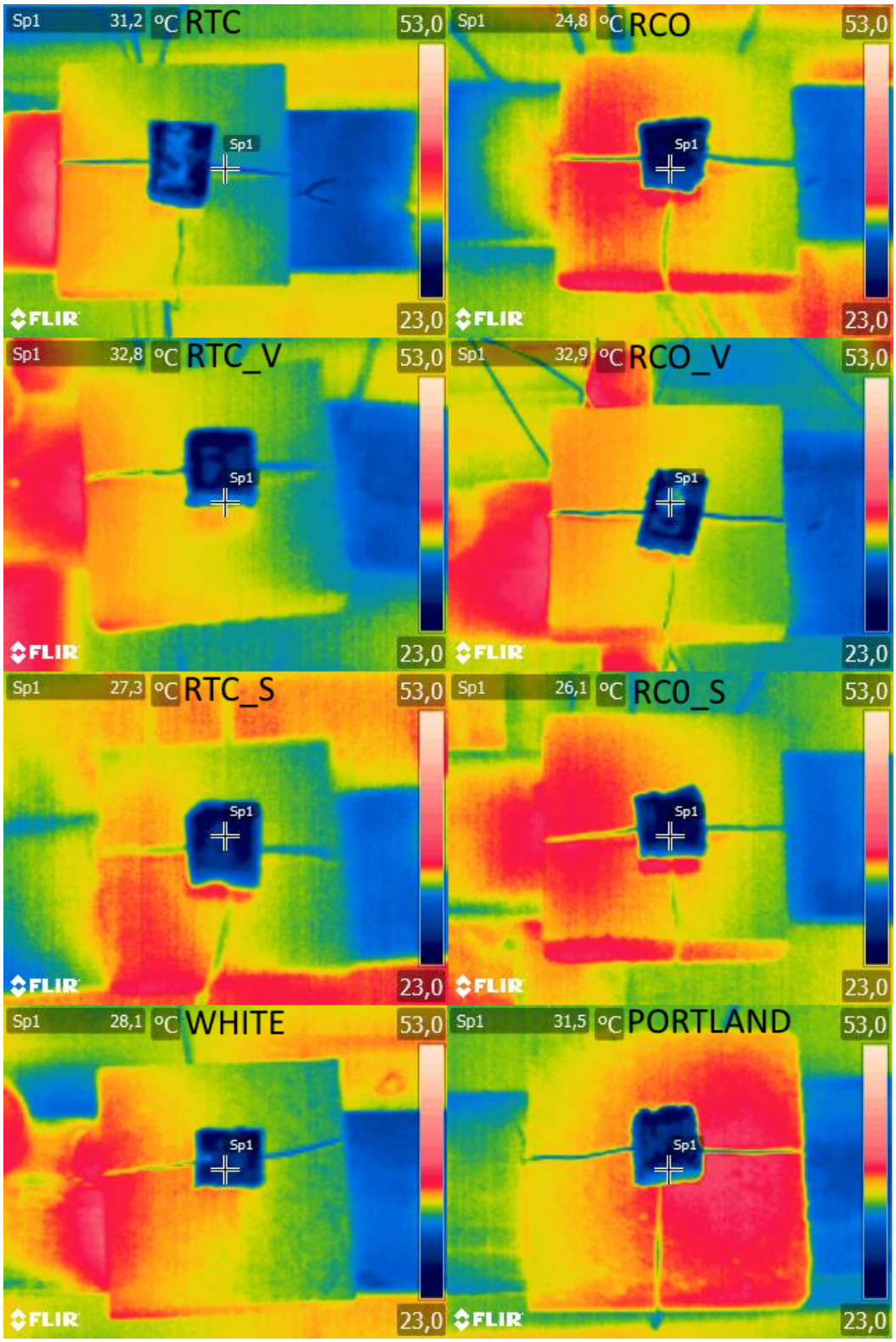

Figure 4.22 Photographs of red thermochromic, conventional with varnish or UV stabilizer.

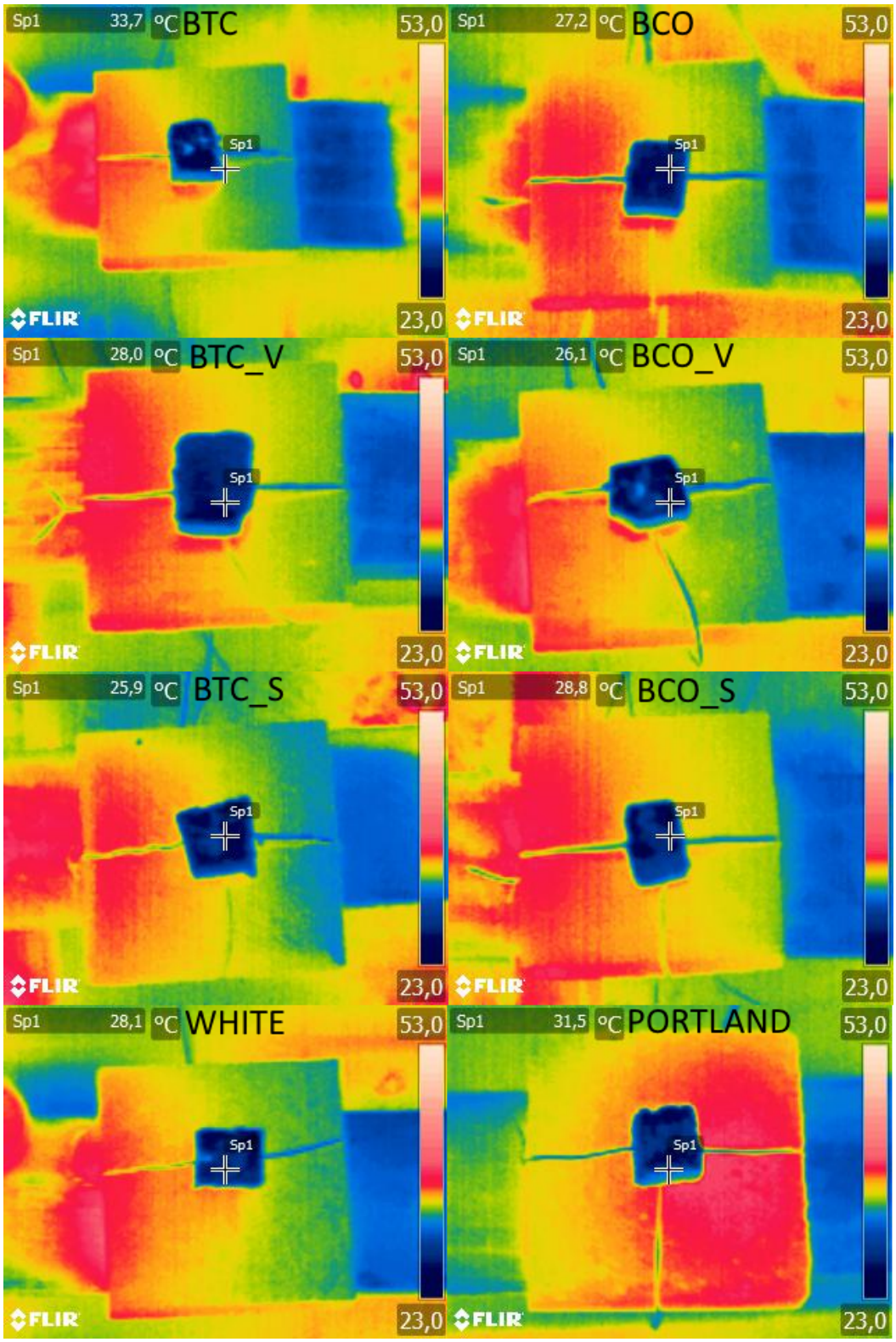

Figure 4.23 Photographs of blue thermochromic, conventional with varnish or UV stabilizer.

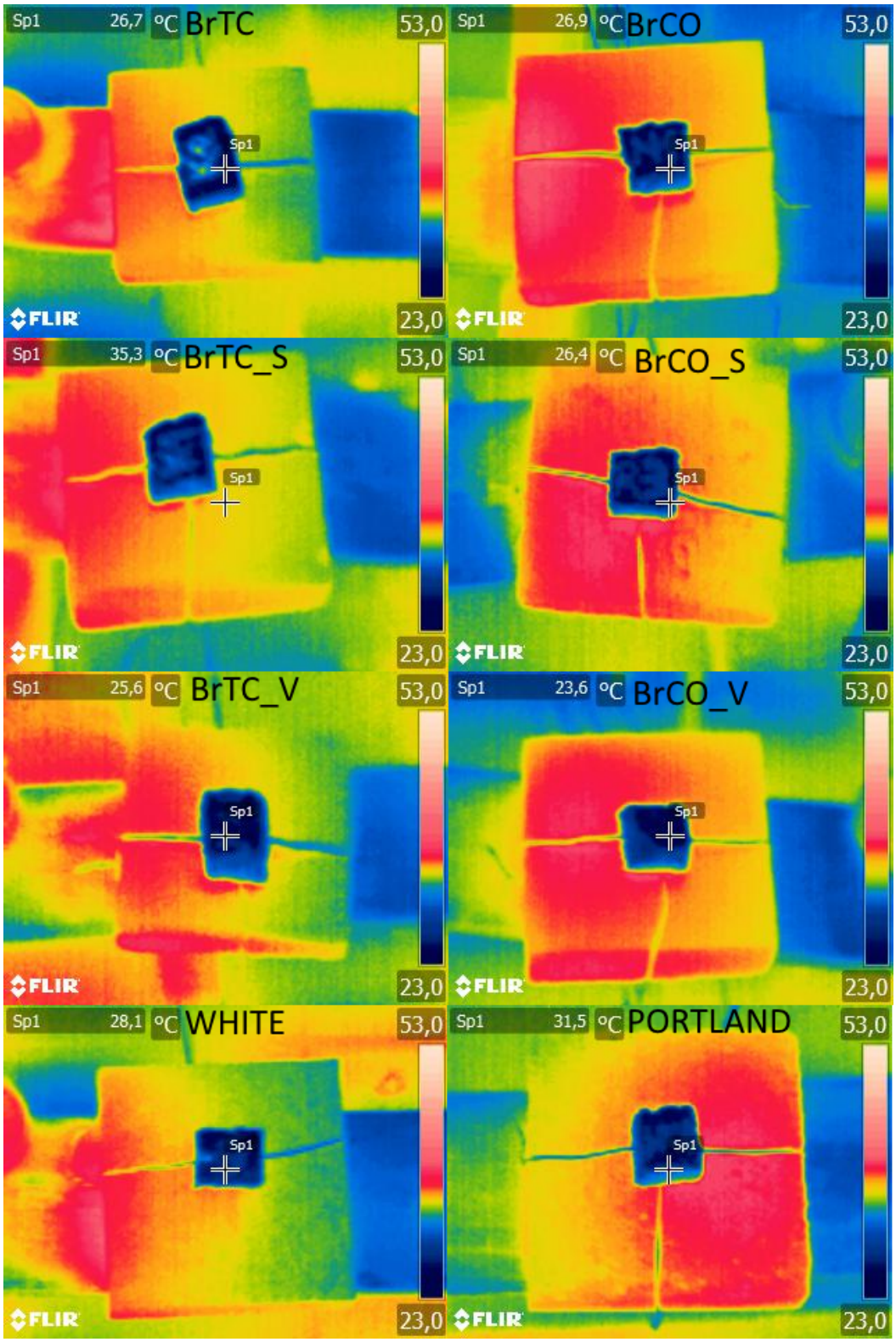

Figure 4.24 Photographs of brown thermochromic, conventional with varnish or UV stabilizer.

For the red coloured samples, (Figure 4.22) it is observed that the sample covered with thermochromic has lower temperature than all the other samples, including the WCO sample. The sample with the conventional red colour has higher temperature than the sample with the WCO and lower temperature than the reference sample (Portland cement). The addition of polyurethane varnish and UV stabiliser raises the surface temperature of the samples but it is still lower than the temperature of the conventional ones.

For the blue coloured samples, (Figure 4.23) it is observed that the sample with the thermochromic has higher temperature than the WCO sample and lower than the rest of the samples. The sample with the conventional colour has higher temperature than the WCO sample but lower temperature than the reference sample. The blue thermochromic sample with the UV stabiliser has higher surface temperature than the sample with the polyurethane varnish but in both cases the conventional blue samples have higher surface temperatures.

For the brown coloured samples, Figure 4.23 it is observed that the thermochromic sample has higher surface temperature than the WCO sample and less than all the other samples. While the conventional brown sample has higher surface temperature than all samples including the reference sample. The addition of either polyurethane varnish or UV stabiliser on the conventional samples kept the surface temperature higher compared to that of reference sample.

Chapter 5

Analysis of aging effect for the developed cool coatings

5.1 Introduction

The aim of the present chapter is to describe the procedure and measurements for the aging of the coatings developed in Chapter 3 and 4 in the outdoor environment.

5.2 Aging of inorganic based cool coatings

The solar reflectance (SR) and infrared emittance (IE) of a surface exposed to outdoor environment can change over time due to aging, soil and dust deposition, etc [120, 54]. In the context of the study of the characteristics and the thermal behaviour of the coatings, it is necessary to take into account not only the initial values of the solar reflectance and infrared emittance but also their respective values after they are exposed to the external environment. For this reason, the 22 samples that are developed and described in Chapter 3 are placed on a horizontal surface and remained exposed to the outdoor conditions for a period of two months in order to study the change in their optical properties. At the end of this time, their SR and IE are measured. After the exposure of the sample to the outdoor conditions for 2 months a new set of SR is taken. The measurements are depicted in Figures 5.1 to 5.24.

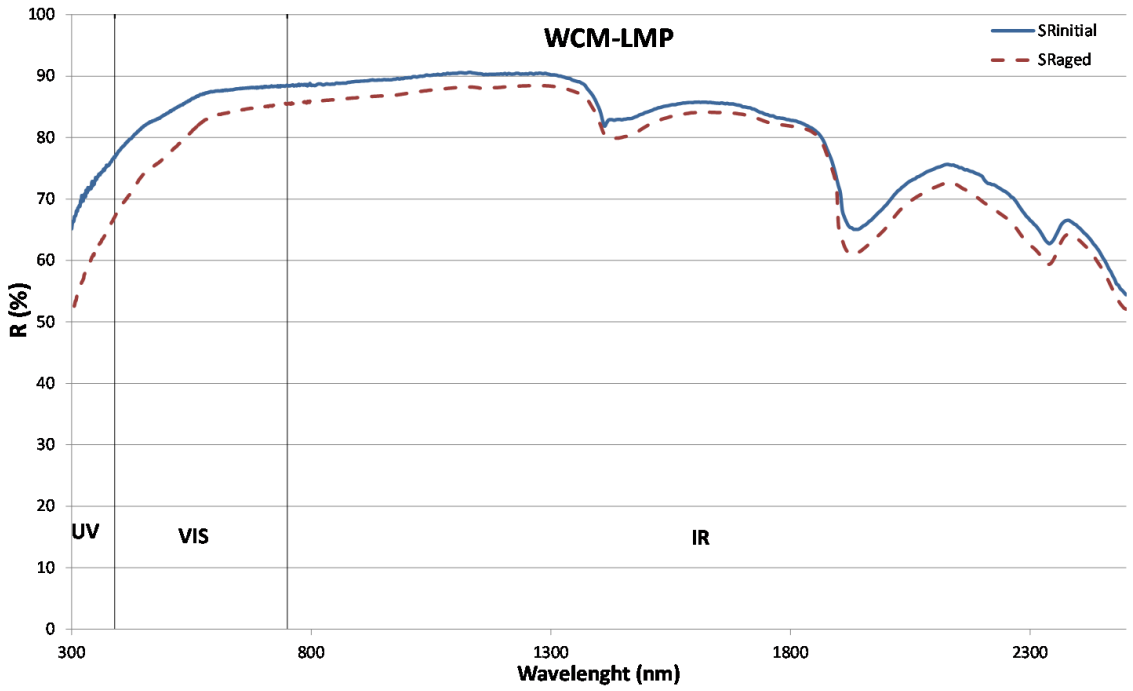

Figure 5.1 Initial and aged spectral reflectance of sample: WCM-LMP.

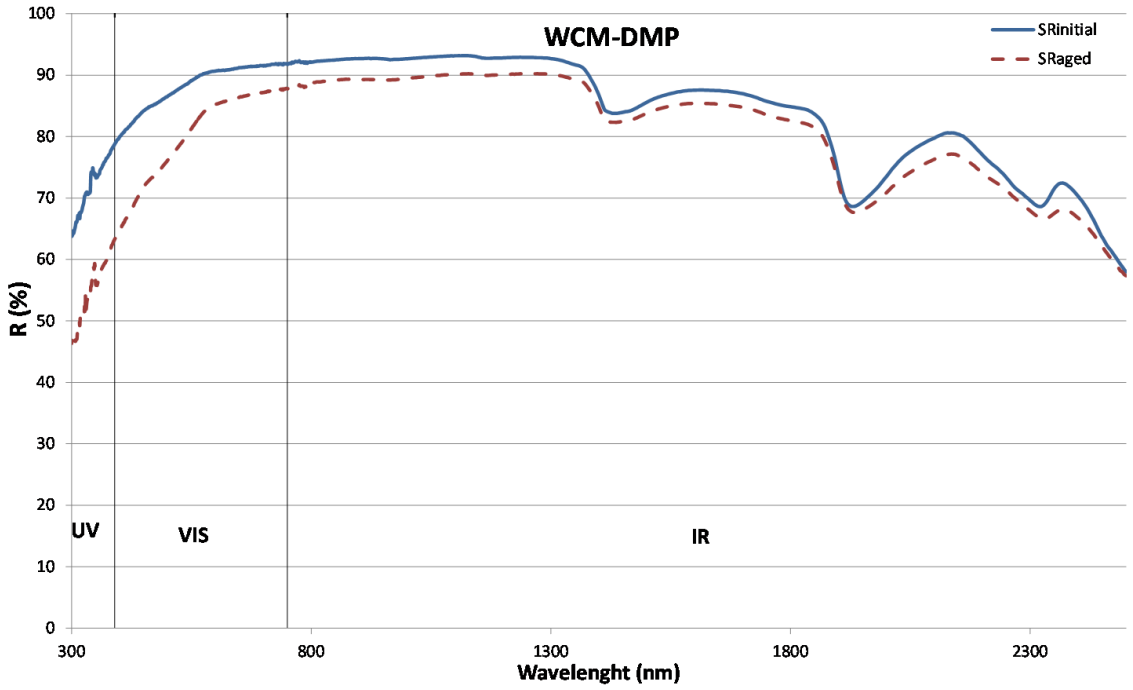

Figure 5.2 Initial and aged spectral reflectance of sample: WCM-DMP.

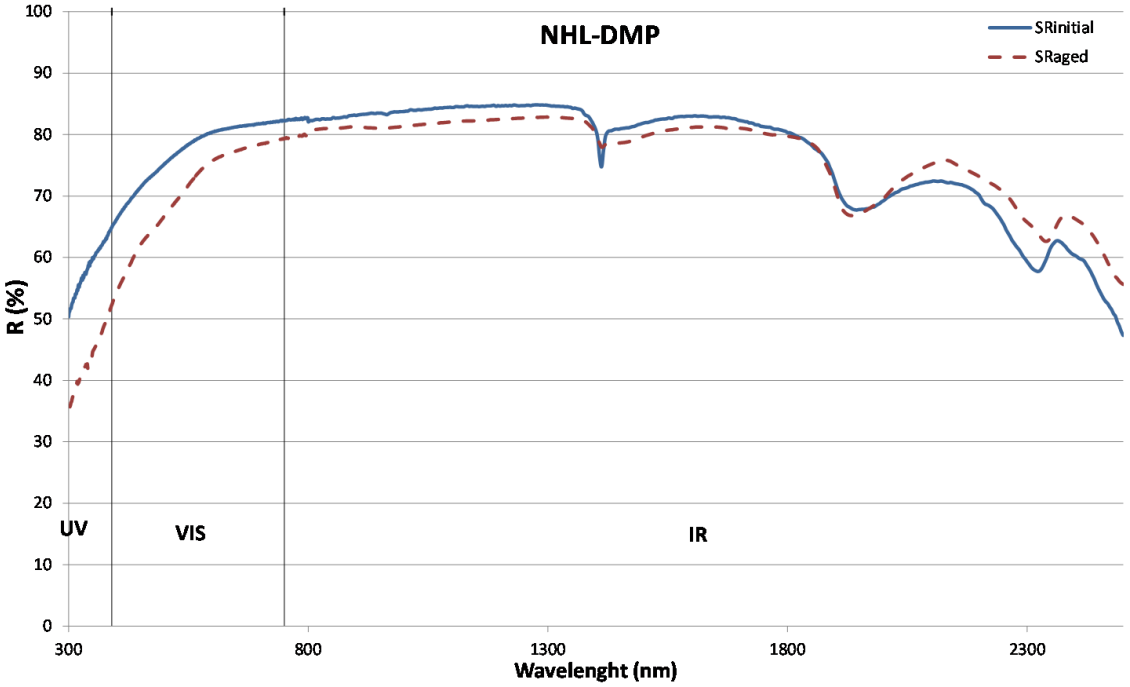

Figure 5.3 Initial and aged spectral reflectance of sample: NHL-DMP.

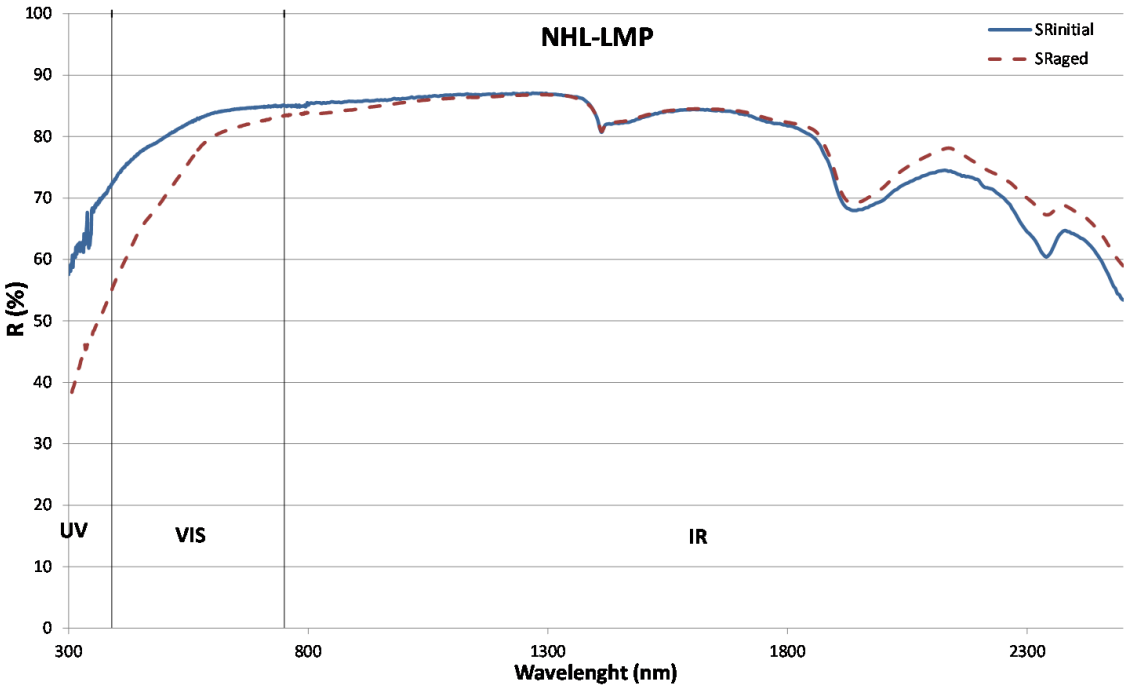

Figure 5.4 Initial and aged spectral reflectance of sample: NHL-LMP.

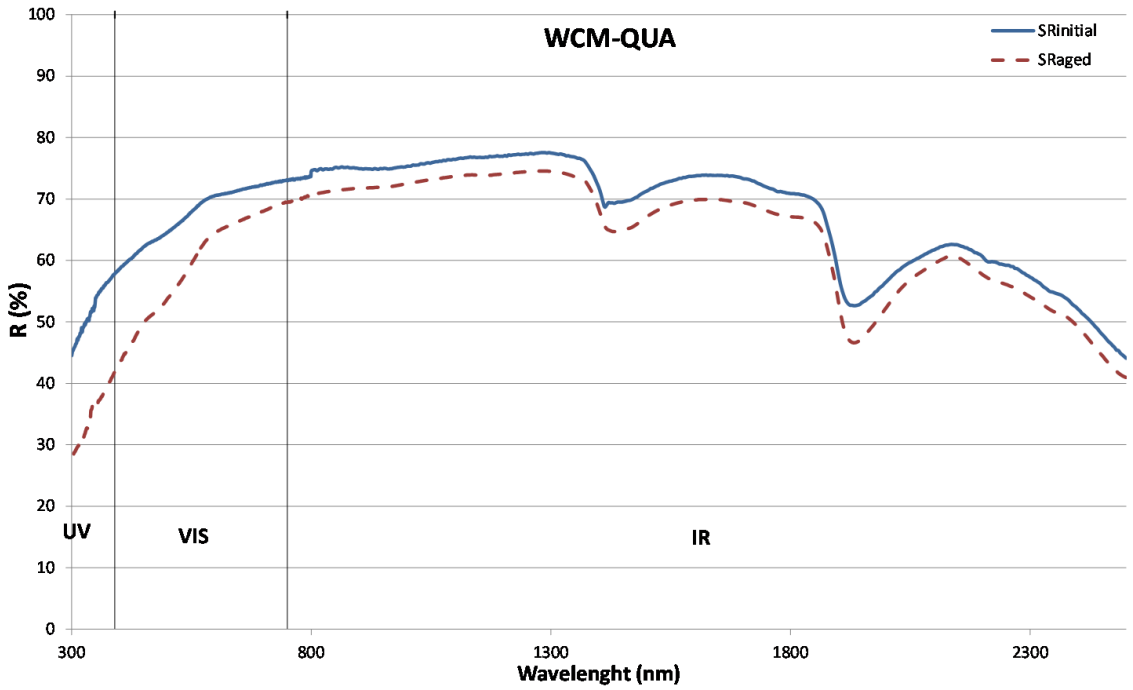

Figure 5.5 Initial and aged spectral reflectance of sample: WCM-QUA.

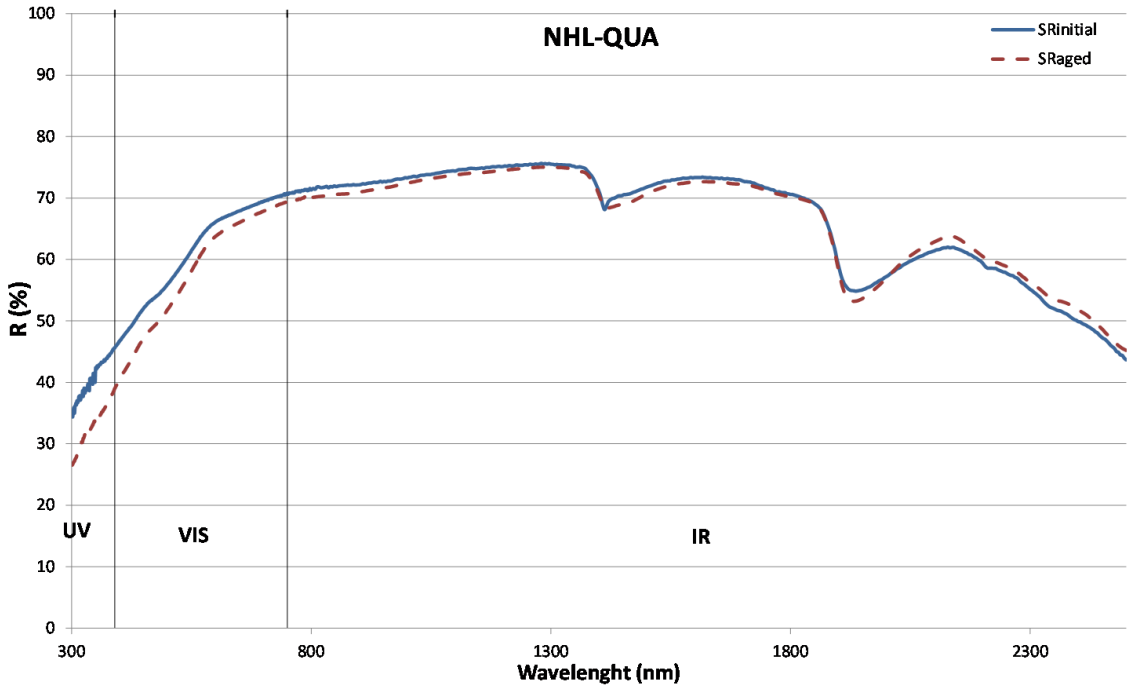

Figure 5.6 Initial and aged spectral reflectance of sample: NHL-QUA.

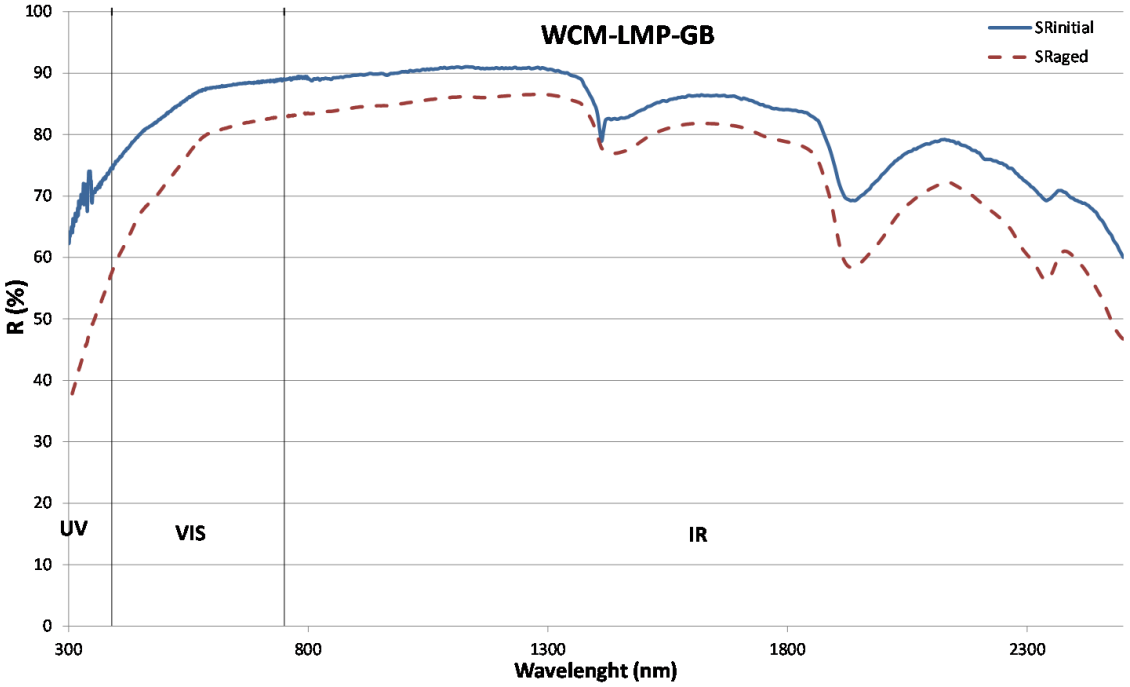

Figure 5.7 Initial and aged spectral reflectance of sample: WCM-LMP-GB.

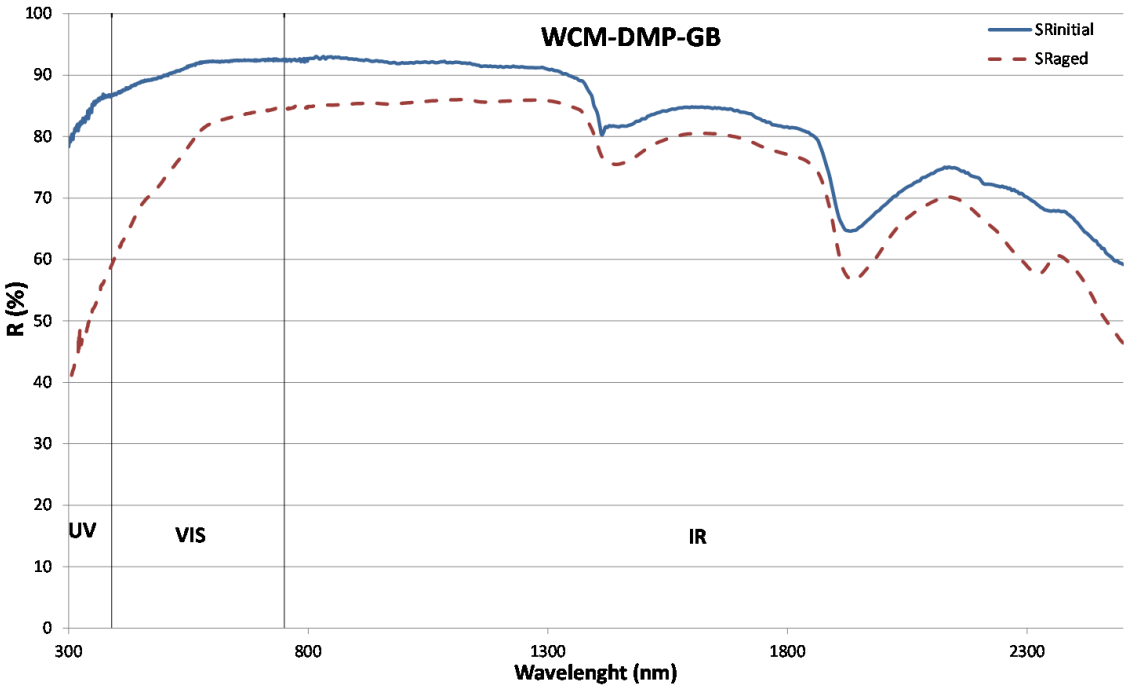

Figure 5.8 Initial and aged spectral reflectance of sample: WCM-DMP-GB.

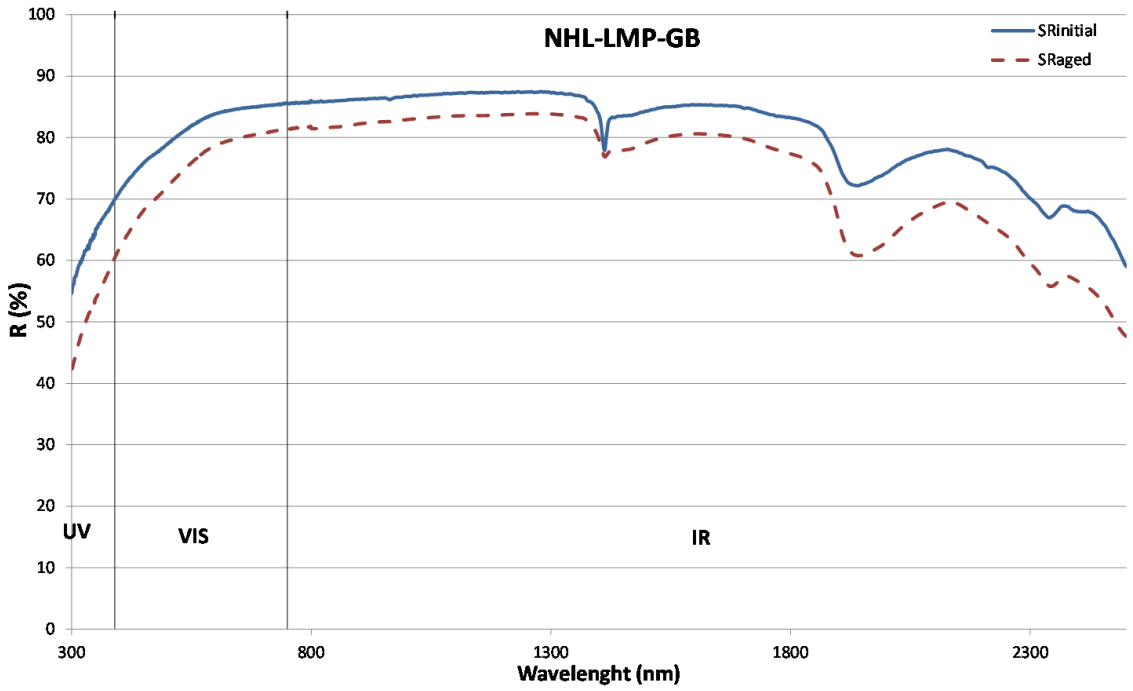

Figure 5.9 Initial and aged spectral reflectance of sample: NHL-LMP-GB.

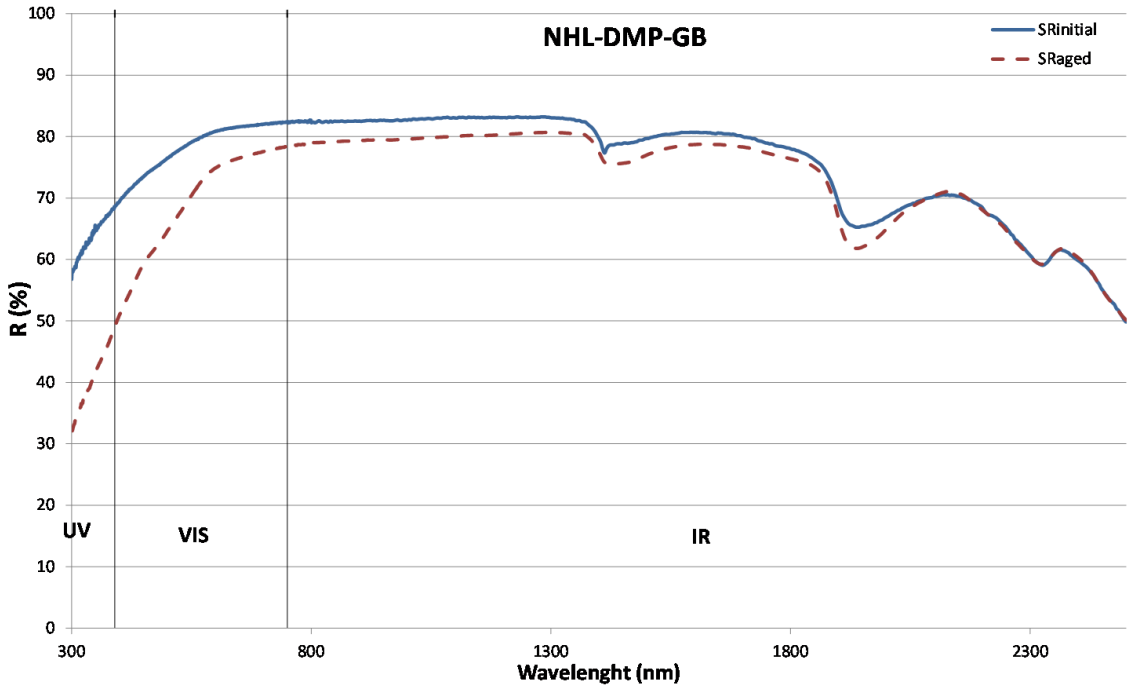

Figure 5.10 Initial and aged spectral reflectance of sample: NHL-DMP-GB.

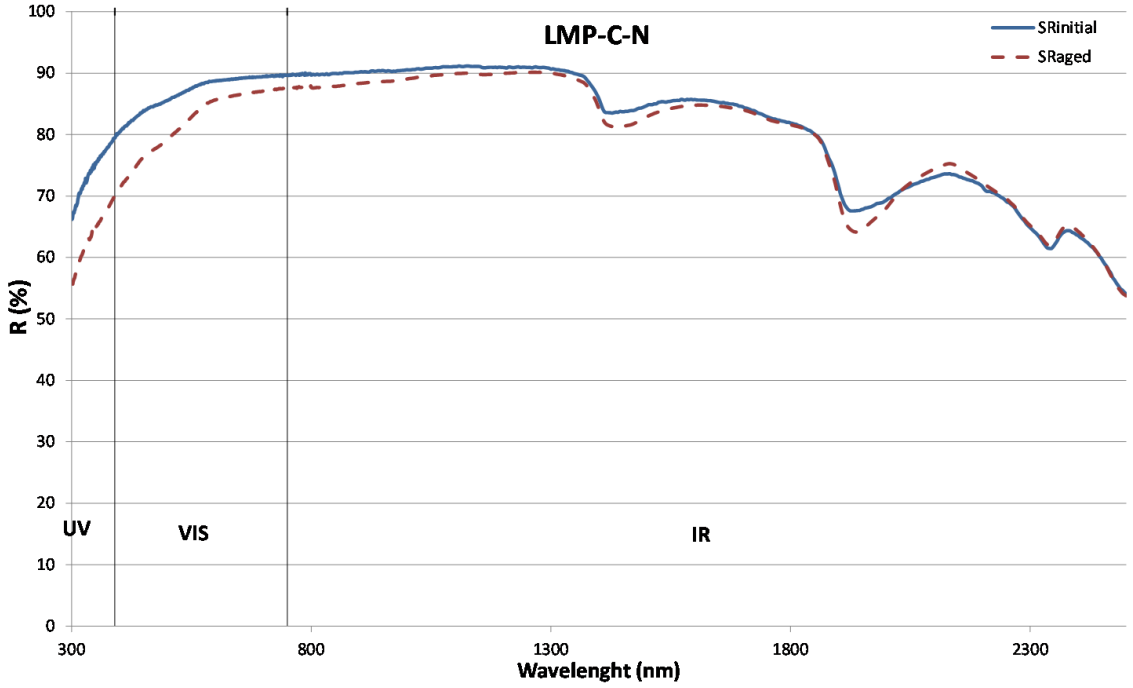

Figure 5.11 Initial and aged spectral reflectance of sample: LMP-C-N.

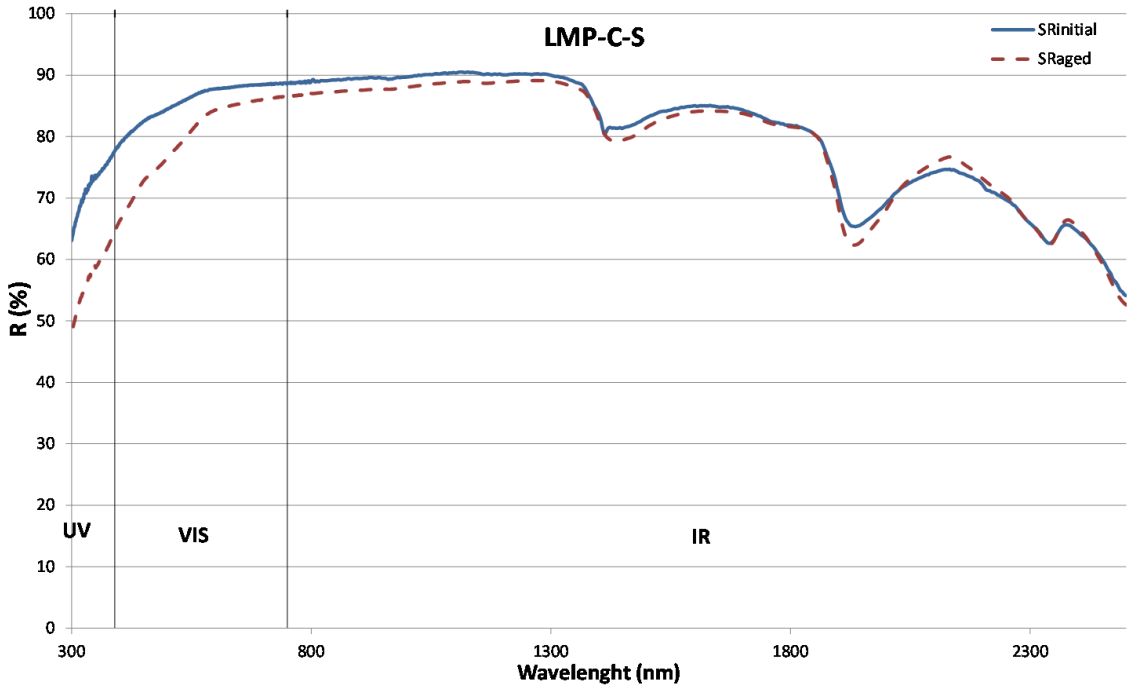

Figure 5.12 Initial and aged spectral reflectance of sample: LMP-C-S.

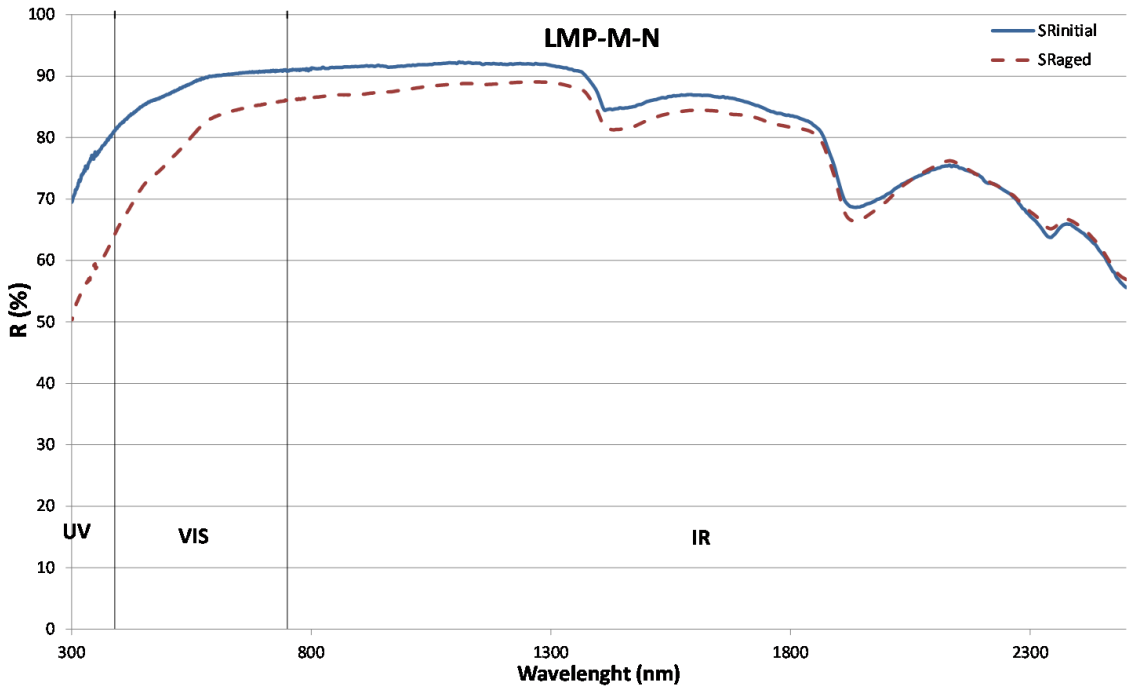

Figure 5.13 Initial and aged spectral reflectance of sample: LMP-M-N.

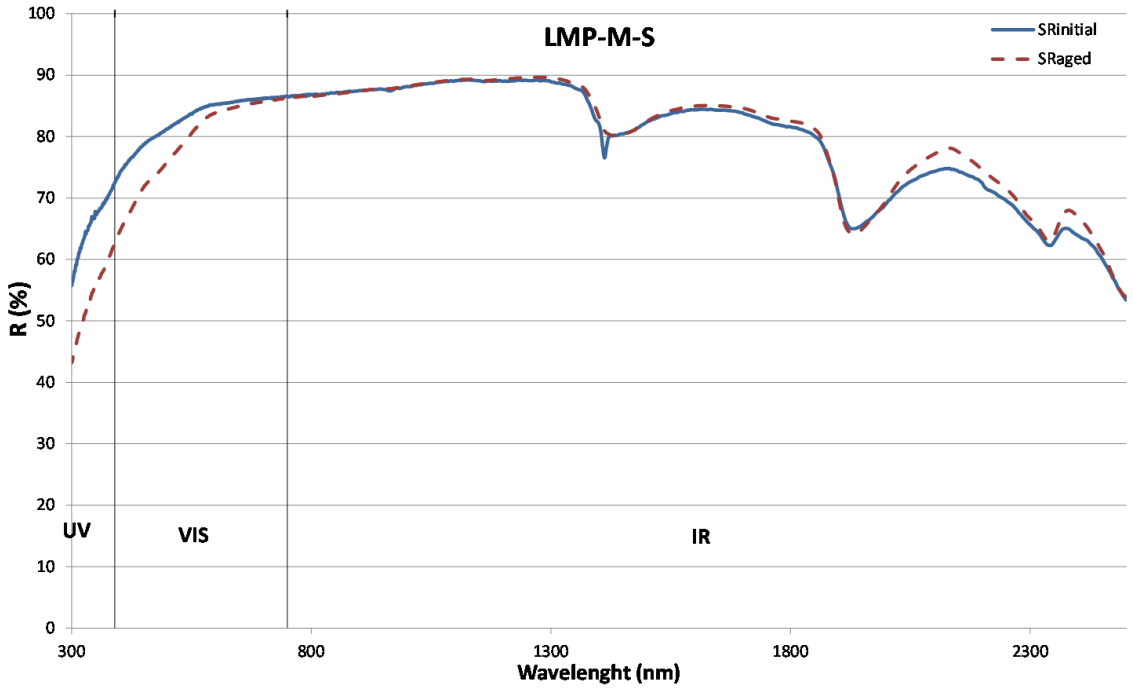

Figure 5.14 Initial and aged spectral reflectance of sample: LMP-M-S.

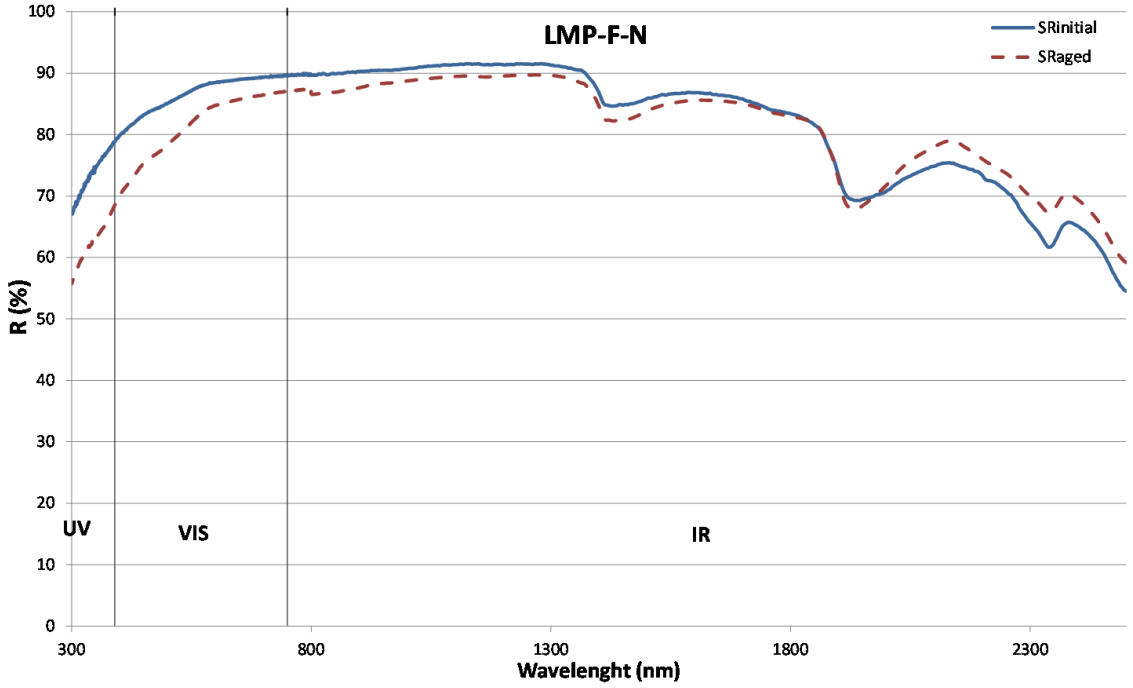

Figure 5.15 Initial and aged spectral reflectance of sample: LMP-F-N.

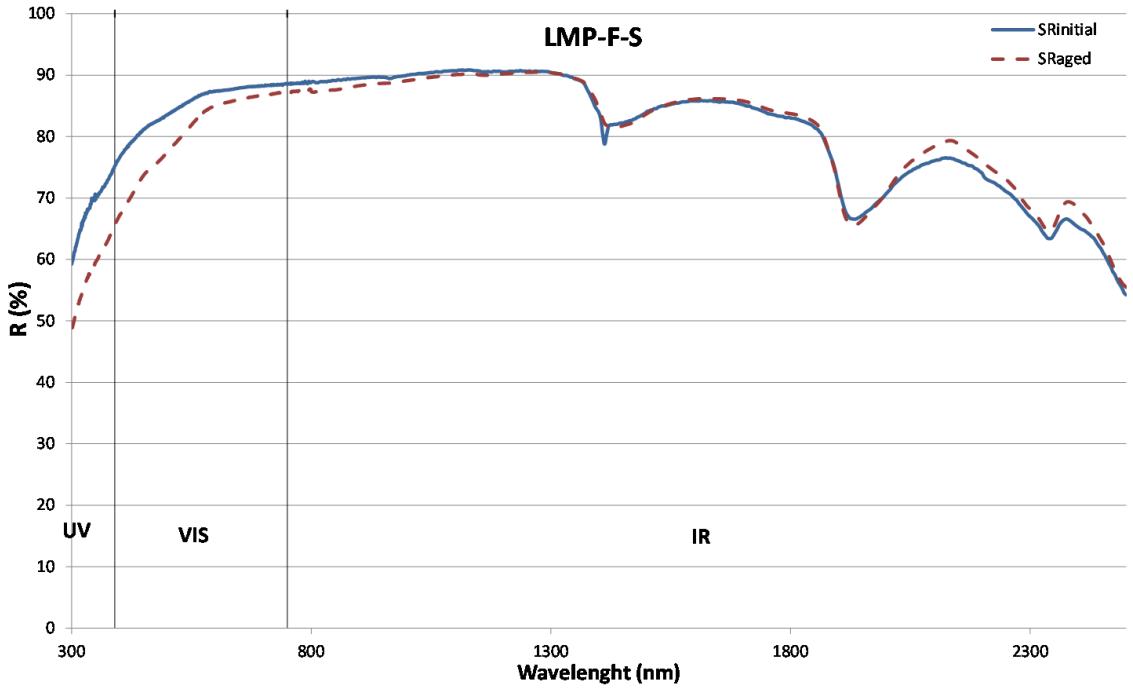

Figure 5.16 Initial and aged spectral reflectance of sample: LMP-F-S.

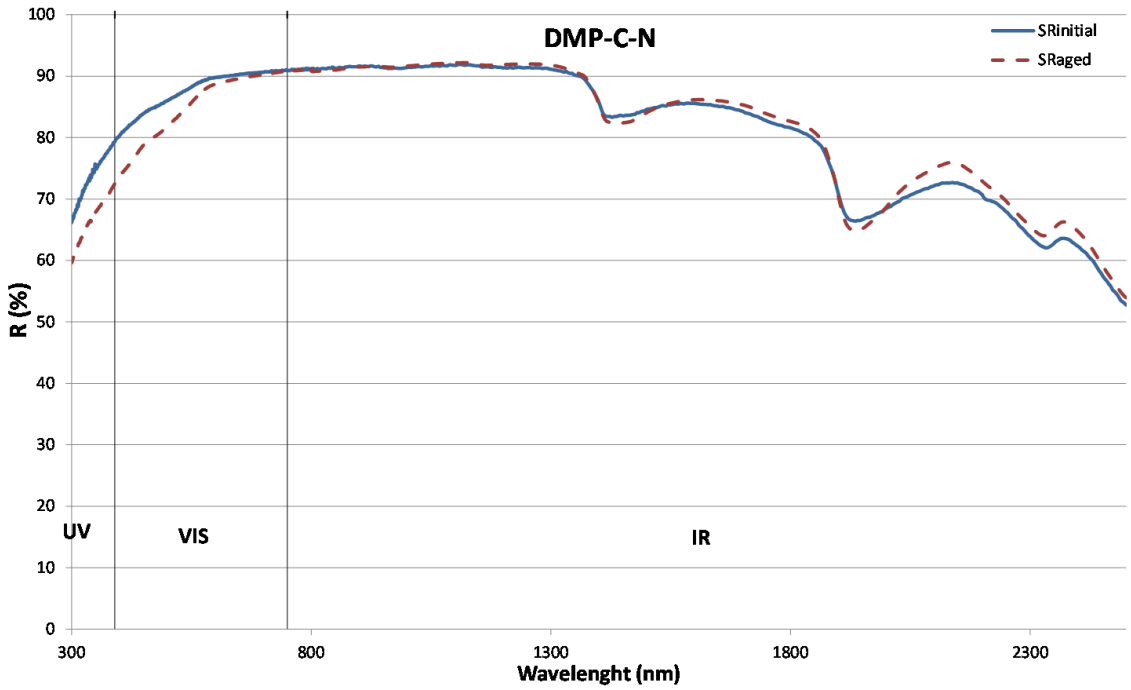

Figure 5.17 Initial and aged spectral reflectance of sample: DMP-C-N.

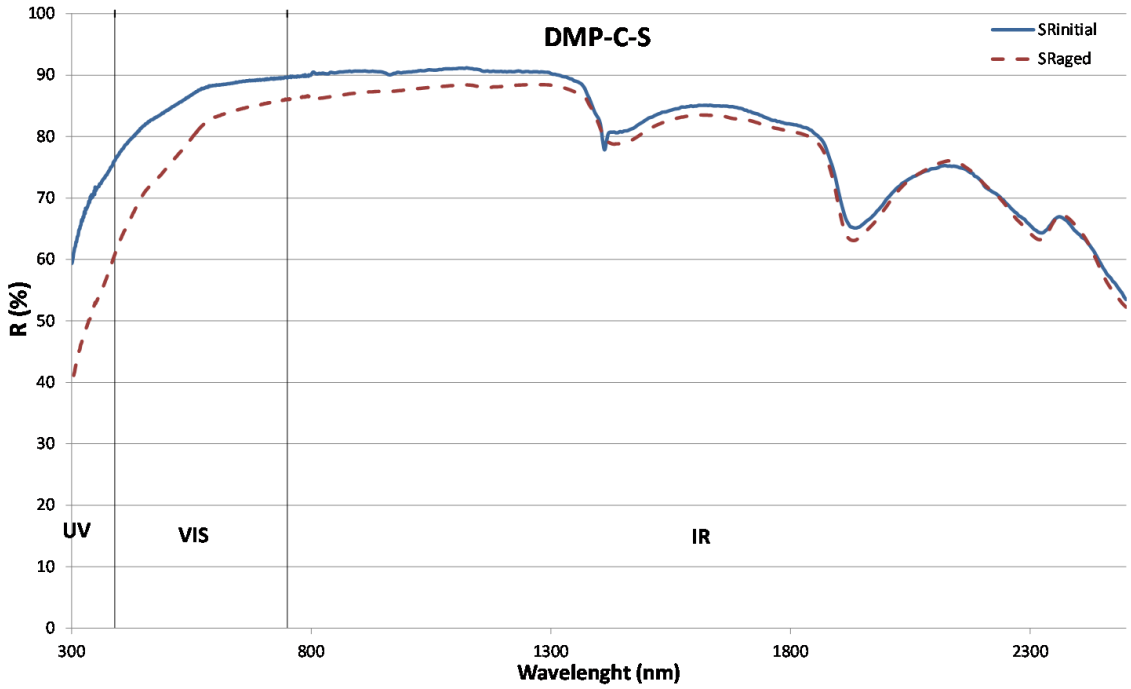

Figure 5.18 Initial and aged spectral reflectance of sample: DMP-C-S.

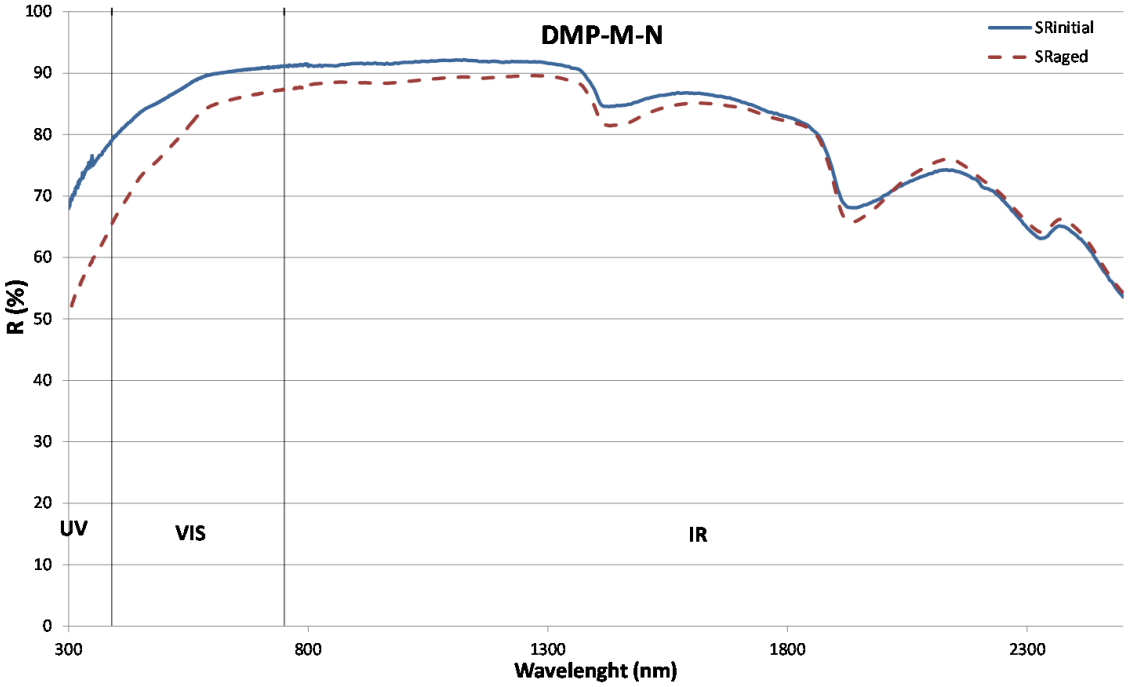

Figure 5.19 Initial and aged spectral reflectance of sample: DMP-M-N.

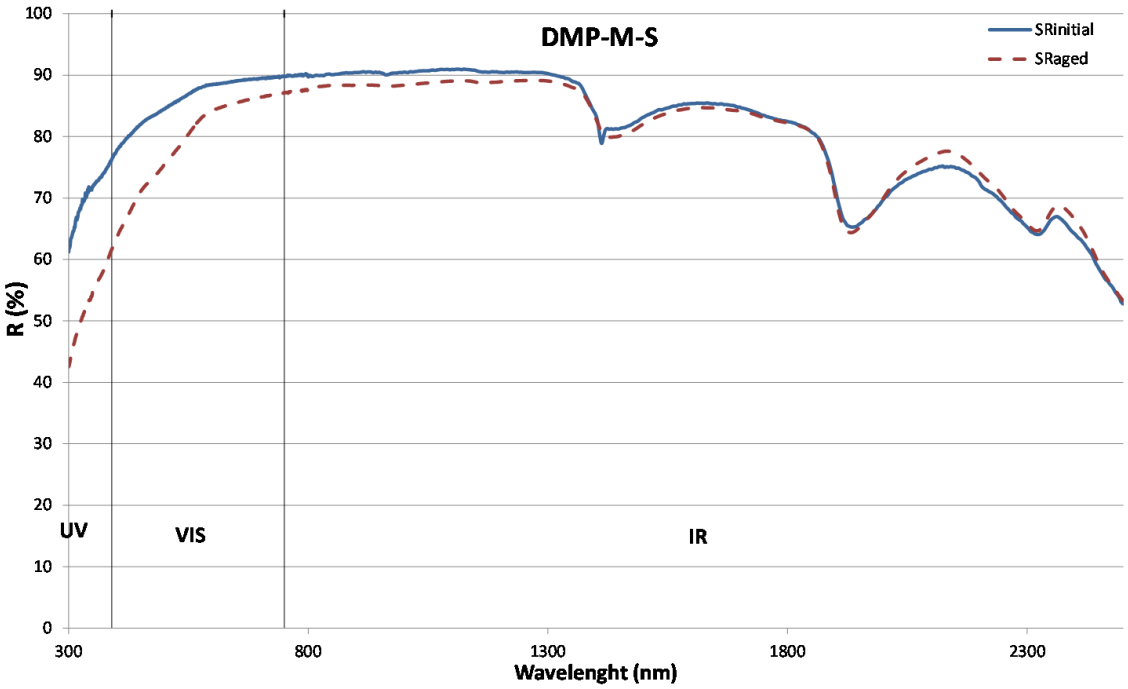

Figure 5.20 Initial and aged spectral reflectance of sample: DMP-M-S.

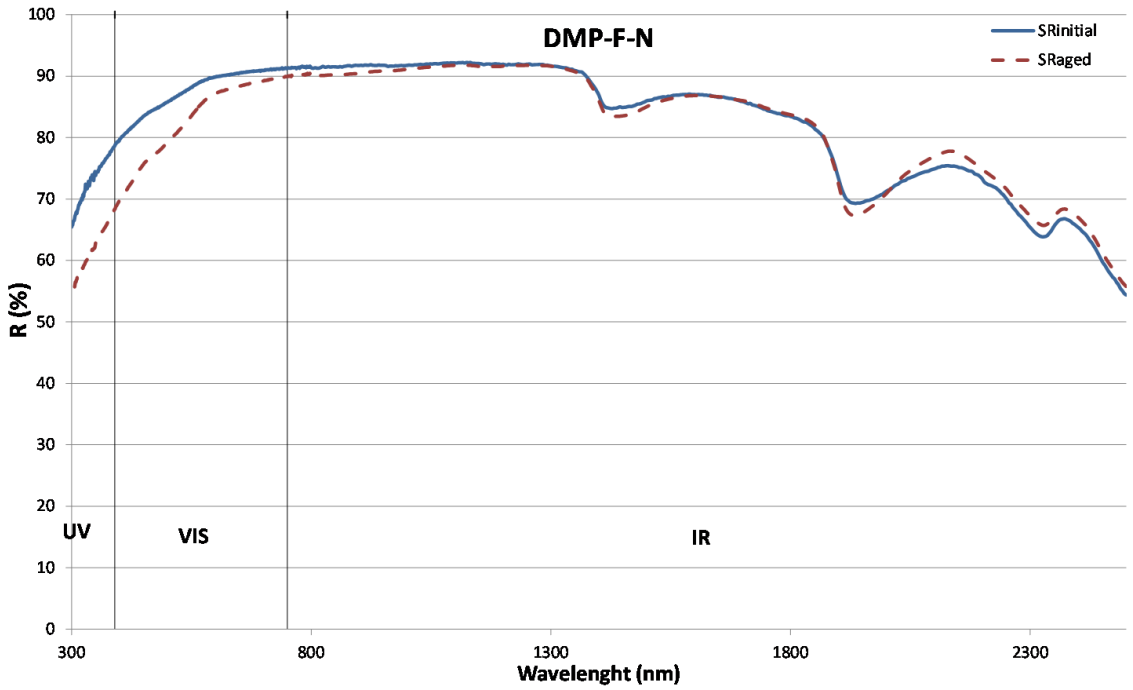

Figure 5.21 Initial and aged spectral reflectance of sample: DMP-F-N.

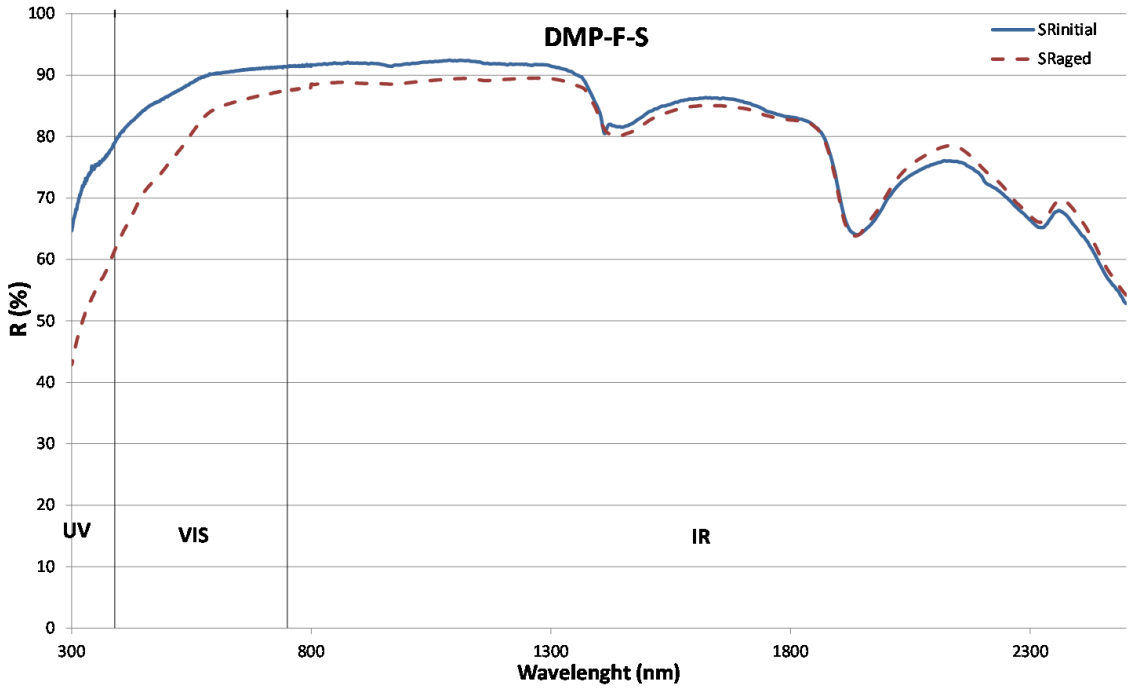

Figure 5.22 Initial and aged spectral reflectance of sample: DMP-F-S.

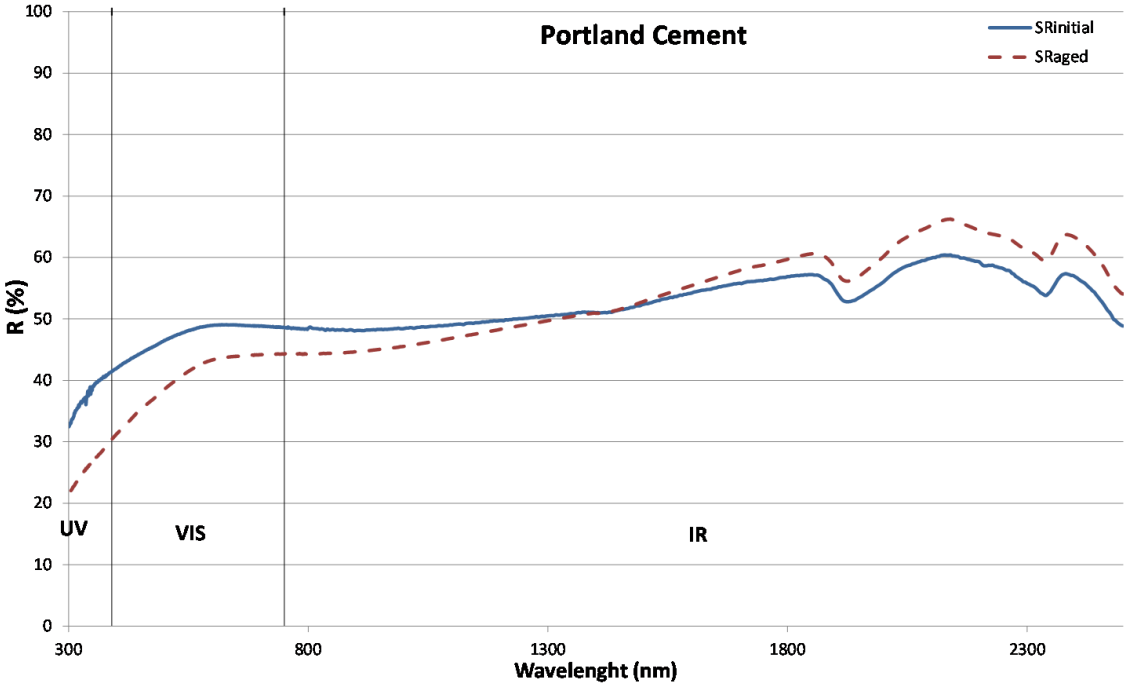

Figure 5.23 Initial and aged spectral reflectance of sample: Portland Cement.

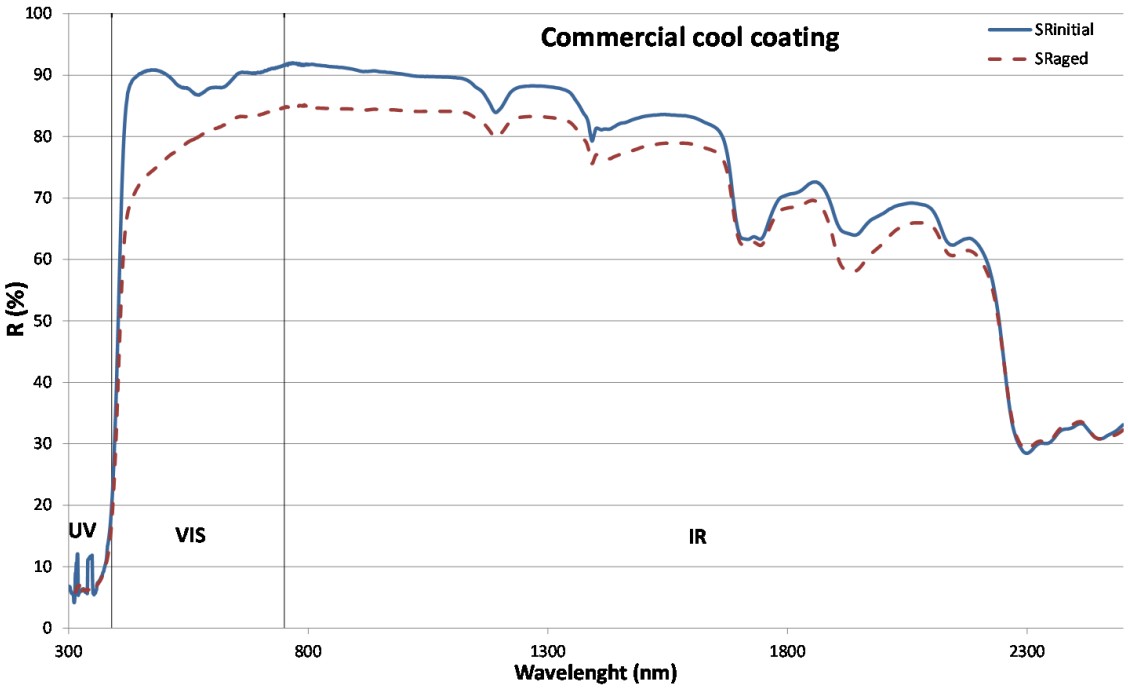

Figure 5.24 Initial and aged spectral reflectance of sample: Commercial cool coating.

In all samples, a small decrease in the solar reflectance is measured. In the following samples that have natural hydraulic lime with pozzolanic additives (NHL) as binder, NHL-LMP, NHL–DMP and NHL-QUA an increase in the solar reflectance is measured at 1850 - 2500nm and decrease in the rest of the spectrum.

Based on the measurements of the spectral reflectance using the Carry 5000 with the integrating sphere, the solar reflectance(SR) is calculated for each one of the samples using the ASTM E903-12 [99] and ASTM G159-90.7 [110] standards. The total, near infrared (NIR: 300-400nm), visible (VIS: 400-700nm) and ultraviolet (UV: 700-2500nm) SR are tabulated in Table 5.1.

Table 5.1 Initial and the difference in solar reflectance in near infrared, visible and ultraviolet wave-length of the 22 samples.

Group	No.	Sample Name	Initial values				Difference			
			SR (%)	SR_{IR} (%)	SR_{VIS} (%)	SR_{UV} (%)	SR (%)	SR_{IR} (%)	SR_{VIS} (%)	SR_{UV} (%)
1	1	WCM-LMP	86	86	85	71	4	2	5	12
	2	WCM-DMP	89	90	88	71	5	3	8	17
	3	NHL-LMP	82	84	81	64	3	1	7	19
	4	NHL–DMP	79	81	77	57	4	1	6	15
2	5	WCM-QUA	70	73	67	51	6	4	8	17
	6	NHL-QUA	66	71	61	40	2	1	4	8
3	7	WCM-LMP-GB	87	86	87	76	9	4	12	31
	8	WCM-DMP-GB	90	91	90	78	11	9	13	29
	9	NHL-LMP-GB	83	85	81	62	6	5	6	11
	10	NHL-DMP-GB	79	80	78	63	6	3	9	24
4	11	LMP-C-N	87	87	87	73	3	1	5	11
	12	LMP-C-S	86	86	86	71	4	1	6	15
	13	LMP-M-N	88	88	88	75	6	3	9	19
	14	LMP-M-S	84	85	83	64	2	0	4	12
	15	LMP-F-N	87	87	86	73	3	2	5	11
	16	LMP-F-S	86	87	85	67	2	1	4	11
	17	DMP-C-N	87	88	88	73	1	0	3	7
	18	DMP-C-S	86	87	86	68	5	3	7	19
	19	DMP-M-N	88	88	87	73	5	3	7	16
	20	DMP-M-S	87	88	87	70	5	3	8	18
	21	DMP-F-N	88	88	87	72	3	1	5	11
	22	DMP-F-S	88	88	88	72	5	2	9	21
	23	Portland Cement	49	50	47	37	4	1	7	12
	24	Commercial cool coating	84	84	88	8	7	5	10	1

NHL: natural hydraulic lime with pozzolanic additives; white Portland cement (WCM): white cement Portland; DMP: dolomitic marble; LMP: limestone powered; QUA: quartz sand; GB: glass beads; C: coarse ; M: medium ; F: fine; S: sanded; N: untreated

Table 5.2 Initial and the difference in infrared emittance of the 22 samples.

Group	No.	Sample Name	IE	δ IE	Group	No.	Sample Name	IE	δ IE
1	1	WCM-LMP	0.81	0.00	4	11	LMP-C-N	0.87	0.03
	2	WCM-DMP	0.83	0.01		12	LMP-C-S	0.87	0.03
	3	NHL-LMP	0.88	0.00		13	LMP-M-N	0.92	0.01
	4	NHL–DMP	0.88	0.01		14	LMP-M-S	0.88	0.01
2	5	WCM-QUA	0.90	0.02		15	LMP-F-N	0.87	0.01
	6	NHL-QUA	0.83	0.02		16	LMP-F-S	0.90	0.01
3	7	WCM-LMP-GB	0.90	0.01		17	DMP-C-N	0.90	0.03
	8	WCM-DMP-GB	0.87	0.01		18	DMP-C-S	0.83	0.03
	9	NHL-LMP-GB	0.88	0.01		19	DMP-M-N	0.89	0.02
	10	NHL-DMP-GB	0.85	0.01		20	DMP-M-S	0.80	0.01
						21	DMP-F-N	0.90	0.00
						22	DMP-F-S	0.80	0.00
						23	Portland Cement	0.78	0.02
						24	Commercial cool coating	0.89	0.03

NHL: natural hydraulic lime with pozzolanic additives; WCM: white cement Portland; DMP: dolomitic marble; LMP: limestone powered; QUA: quartz sand; GB: glass beads; C: coarse ; M: medium ; F: fine; S: sanded; N: untreated

Decrease in solar reflectance is observed in all samples after the 2 months exposure to the environment. The samples with the highest decrease is WCM-DMP-GB (12%), WCM-LMP-GB (10%) and the commercial cool coating (9%). The samples with the smaller decrease in SR is LMP-M-S (2%), DMP-C-N (0.7%). The samples from the 4^{th} group have the higher reduction in SR due to the fact that a portion of the initial SR is attributed to the glass beads. Overall the samples with the WCM reported higher decrease in SR than the samples with NHL as a binder. A very important factor for cool coatings is not the percentage of change in SR but the final values. The final value for all samples are greater then the SR of Portland cement and in most case's greater than the commercial cool white.

Furthermore, it is clear from the graphs that the change in SR due to the exposure of the samples to the external environment is not constant with the wavelength but exhibits spectral selectivity. In all samples the reduction of the SR of the UV portion of the spectrum (300-400nm) is greater than in the IR or VIS part of the spectrum.

The infrared emittance (Table 5.2), is found not to change significantly (on average $\Delta\ IE = 0.01$) during the exposure time.

5.3 Aging of thermochromic based cool coatings

The main problem of the thermochromic based cool coating is photo-degradation when exposed to the outdoor environment. Photodegradation leads to altering of the chemical and mechanical properties as well as loss of the reversible thermochromic effect due to the breaking and/or cross linking of the polymer chains [121].

In order to minimize the effects of photodegradation, two commercial available UV varnishes (Eversorb and Ilam) are applied on top of the thermochromic coating as well as on the conventional paints (Section 4.4). To test the effectiveness of these two methods of protection, a set of samples are created and placed to the external environment for 19 consecutive days. The meteorological conditions of this period are tabulated in Table 4.4.

5.3.1 Aging of the inorganic thermochromic coatings

After exposure to the natural environment, the solar reflectance of the samples are measured (Figures 5.25 and 5.26). The measurements are conducted using the Carry 5000 with integrating sphere. The samples are raised to their transition temperature using the laboratory furnace.

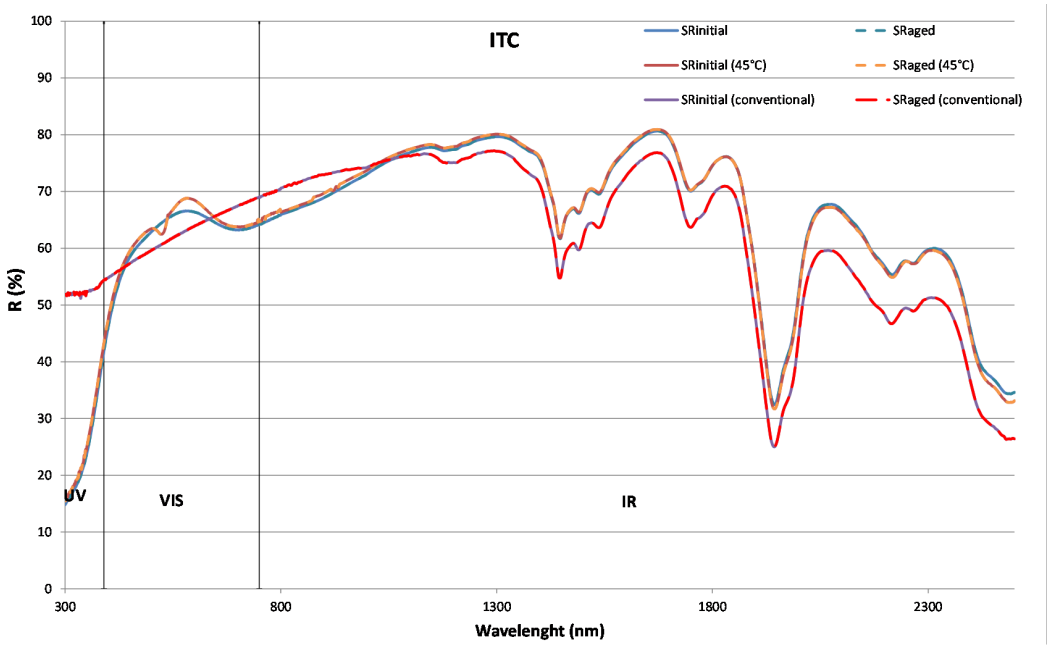

Figure 5.25 Initial and aged spectral reflectance of sample: plaster of Paris (Pl), plaster of Paris with inorganic thermochromic (ITC) and plaster of Paris with inorganic thermochromic at 45°C (ITC_45°C).

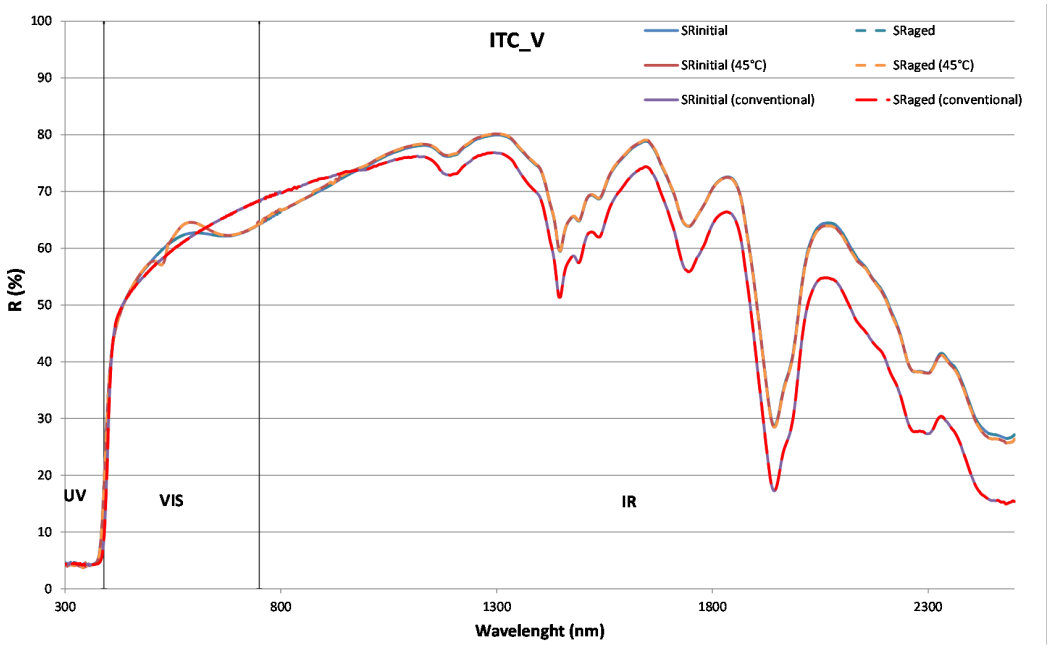

Figure 5.26 Initial and aged spectral reflectance of sample: plaster of Paris + Ilam (Pl_V), plaster of Paris with inorganic thermochromic and Ilam (ITC_V) and plaster of Paris with inorganic thermochromic and Ilam at 45°C (ITC_V_45°C).

The solar reflectance spectrum does not change during the exposure either for the inorganic thermochromic nor for the inorganic thermochromic with the UV varnish (Ilam).

Based on the measurements of the spectral reflectance using the Carry 5000 with the integrating sphere, the SR is calculated for each one of the samples using the ASTM E903-12 [99] and ASTM G159-90.7 [110] standards. The total, near infrared (NIR: 300-400nm), visible (VIS: 400-700nm) and ultraviolet (UV: 700-2500nm) SR are tabulated in Table 5.3.

Table 5.3 Initial and the difference in solar reflectance in near infrared, visible, ultraviolet wave-length and infrared emittance of the inorganic thermochromic coatings.

Group	Sample Name	Initial values				Difference				IE	δIE
		SR (%)	SR_{IR} (%)	SR_{VIS} (%)	SR_{UV} (%)	SR (%)	SR_{IR} (%)	SR_{VIS} (%)	SR_{UV} (%)		
Inorganic	ITC	67	70	65	36	1	1	2	14	0.87	0.01
	ITC_45°C	67	69	66	37	1	0	2	14	-	-
	ITC_V	63	69	59	4	0	0	0	0	0.88	0.00
	ITC_V_45°C	63	69	59	4	0	0	0	0	-	-
	Pl	66	70	62	52	0	0	0	0	0.85	0.00
	Pl_V	62	67	59	4	0	0	0	0	0.86	0.00

The inorganic thermochromic samples are not strongly affected by the weather conditions. A small decrease of the SR of UV part of the spectrum is observed and only for the sample with no protective coating.

5.3.2 Aging of the organic thermochromic coatings

After exposure to the natural environment, the solar reflectance of the samples are measured (Figures 5.27 to 5.32). The measurements are conducted using the Carry 5000 with integrating sphere. The samples are raised to the transition temperature using the laboratory furnace.

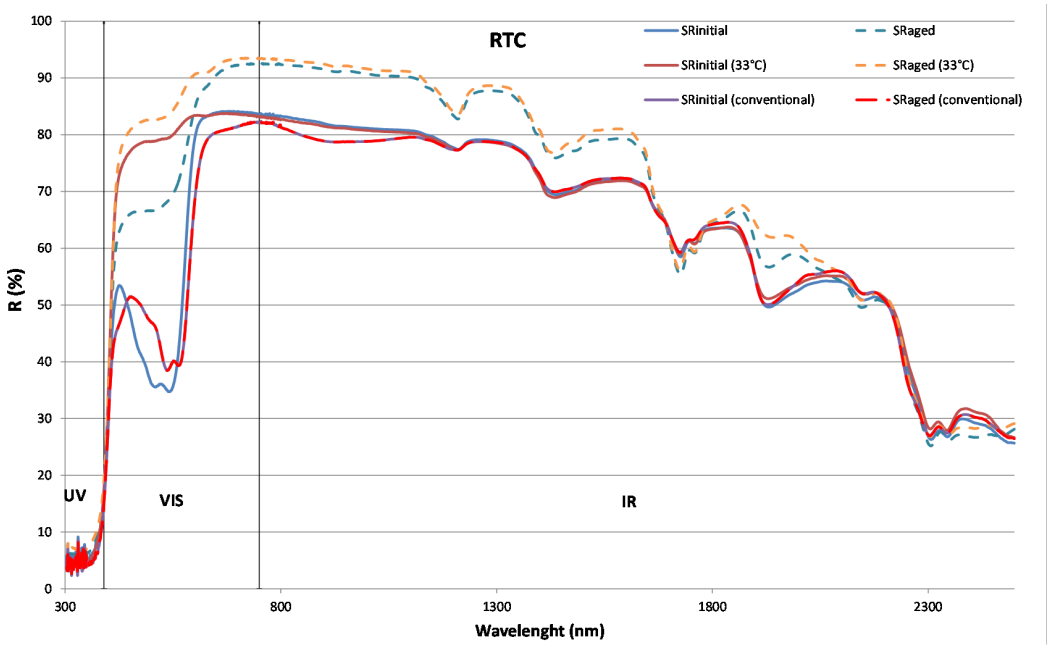

Figure 5.27 Initial and aged spectral reflectance of red thermochromic sample (RTC), red thermochromic sample at transition temperature (33°C) (RTC_33°C) and red conventional sample (RCO).

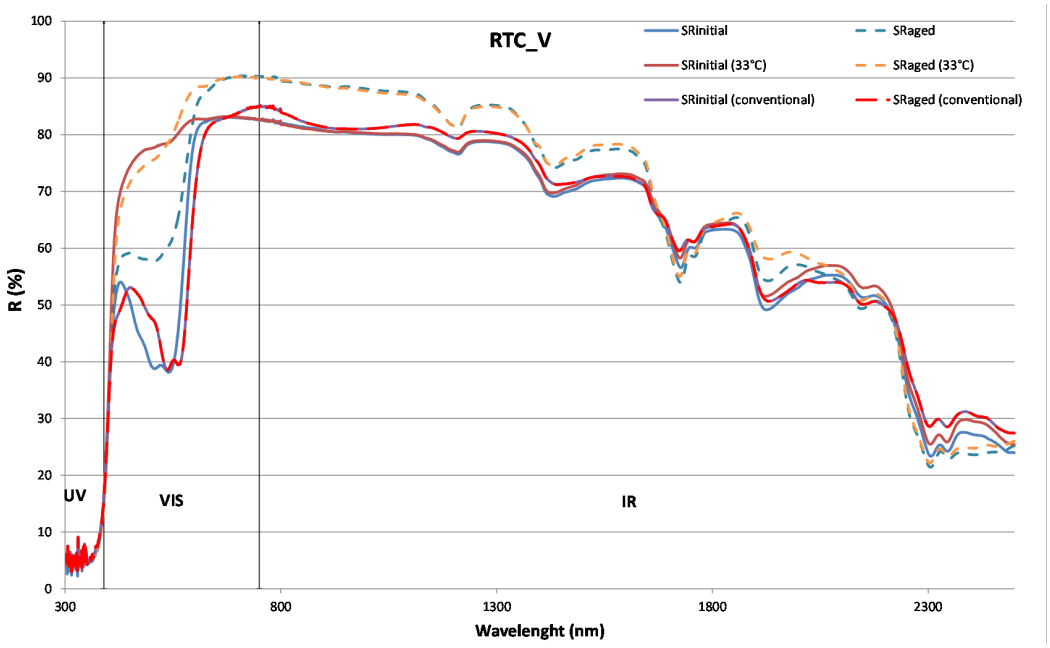

Figure 5.28 Initial and aged spectral reflectance of red thermochromic sample covered with polyurethane varnish (RTC_V), red thermochromic sample covered with polyurethane varnish at transition temperature (33°C) (RTC_V_33°C) and red conventional sample covered with polyurethane varnish (RCO_V).

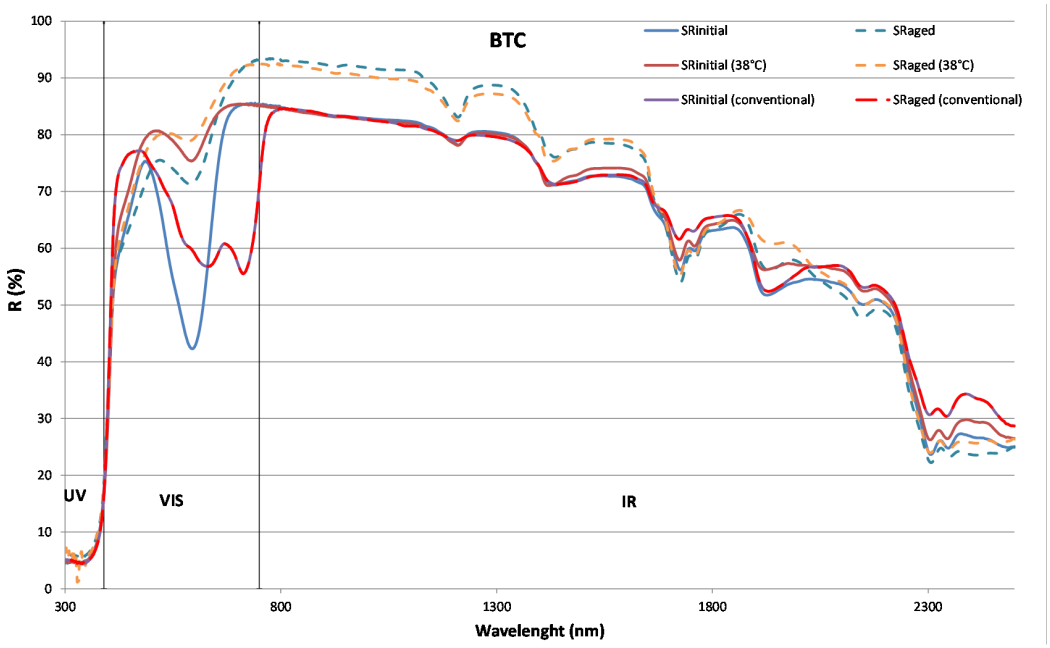

Figure 5.29 Initial and aged spectral reflectance of blue thermochromic sample (BTC), blue thermochromic sample at transition temperature (38°C) (BTC_38°C) and blue conventional sample (BCO).

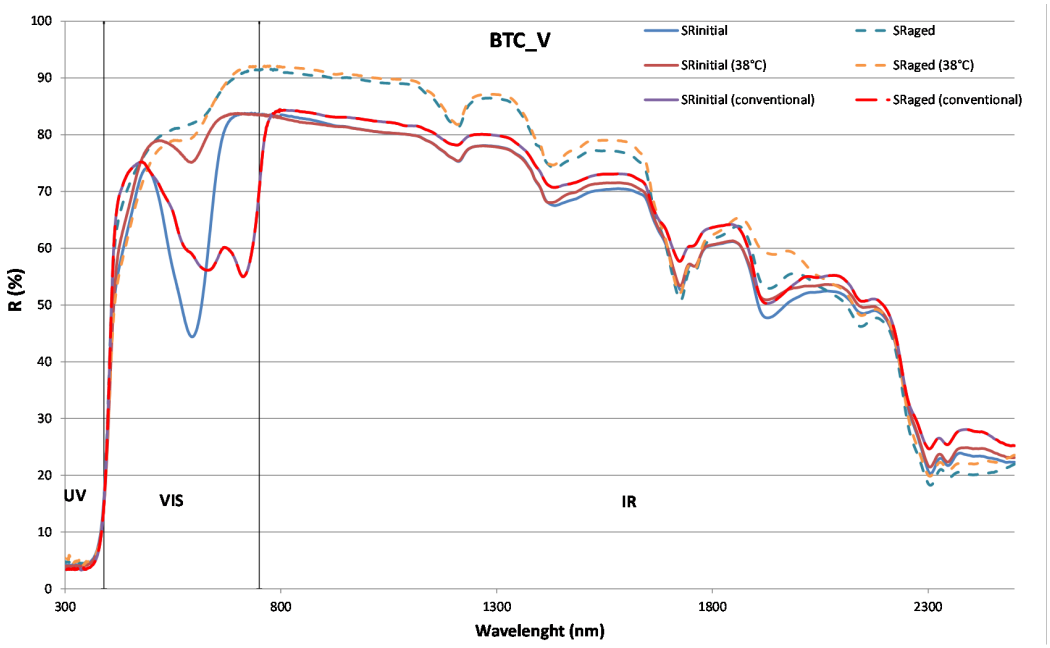

Figure 5.30 Initial and aged spectral reflectance of blue thermochromic sample covered with polyurethane varnish (BTC_V), blue thermochromic sample covered with polyurethane varnish at transition temperature (38°C) (BTC_V_38°C) and blue conventional sample covered with polyurethane varnish (BCO_V).

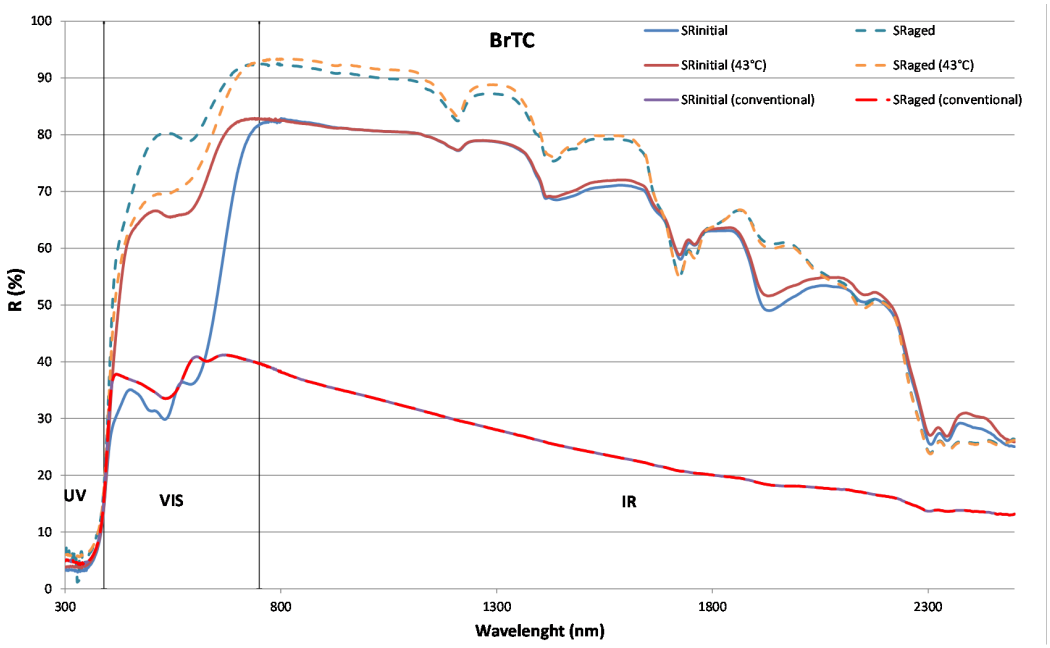

Figure 5.31 Initial and aged spectral reflectance of brown thermochromic sample (BrTC), brown thermochromic sample at transition temperature (48°C) (BrTC_48°C) and brown conventional sample (BrCO).

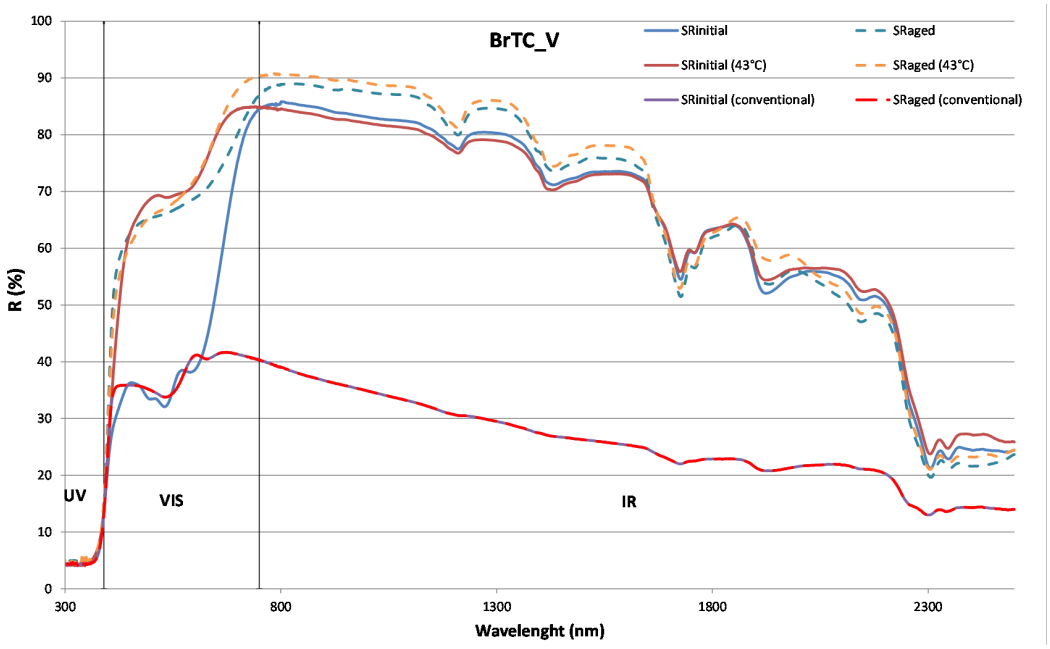

Figure 5.32 Initial and aged spectral reflectance of brown thermochromic sample covered with polyurethane varnish (BrTC_V), brown thermochromic sample covered with polyurethane varnish at transition temperature (48°C) (BrTC_V_48°C) and brown conventional sample covered with polyurethane varnish (BrCO_V).

In all organic thermochromic samples, an increase of the solar reflectance is observed in the entire spectrum, in both phases of the thermochromic coatings. Furthermore, the gap in the solar reflectance between the two phases is reduced.

Based on the measurements of spectral reflectance using the Carry 5000 with the integrating sphere, the SR is calculated for each one of the samples using the ASTM E903-12 [99] and ASTM G159-90.7 [110]. The total, near infrared (NIR: 300-400nm), visible (VIS: 400-700nm) and ultraviolet (UV: 700-2500nm) SR are tabulated in Table 5.4.

Table 5.4 Initial and the difference in solar reflectance in near infrared, visible, ultraviolet wave-length and infrared emittance of the organic thermochromic coatings.

Group	Sample Name	Initial values				Difference				IE	δIE
		SR (%)	SR_{IR} (%)	SR_{VIS} (%)	SR_{UV} (%)	SR (%)	SR_{IR} (%)	SR_{VIS} (%)	SR_{UV} (%)		
Organic	RTC	67	76	58	6	-11	-8	-17	-1	0.92	0.02
	RTC_48°C	75	76	79	5	-7	-9	-6	-3	-	-
	RCO	66	74	57	5	0	0	0	0	0.87	0.00
	RTC_V	67	75	60	5	-8	-6	-11	0	0.93	0.01
	RTC_V_38°C	74	75	78	5	-4	-6	-2	-1	-	-
	RCO_V	68	76	59	6	0	0	0	0	0.93	0.00
	BTC	69	77	63	5	-8	-7	-11	-1	0.91	0.01
	BTC_73°C	75	77	77	5	-4	-6	-1	-1	-	-
	BCO	69	74	66	5	0	0	0	0	0.87	0.00
	BTC_V	68	75	63	5	-10	-7	-16	0	0.92	0.00
	BTC_V_63°C	73	75	75	4	-5	-8	-1	-1	-	-
	BCO_V	68	74	64	4	0	0	0	0	0.92	0.00
	BrTC	59	75	39	4	-20	-8	-39	-2	0.91	0.00
	BrTC_48°C	70	75	67	4	-7	-8	-4	-2	-	-
	BrCO	33	31	38	5	0	0	0	0	0.87	0.00
	BrTC_V	61	77	41	5	-12	-3	-26	0	0.92	0.00
	BrTC_V_48°C	72	76	69	5	-3	-5	0	-1	-	-
	BrCO_S	34	33	37	4	0	0	0	0	0.92	0.10
Reference	WCO	85	85	91	7	0	0	0	0	0.9	0.00
	WCO_V	85	85	90	5	0	0	0	0	0.92	0.00

A series of photographs are taken during the measuring period, three times per day at 9:00, 15:00 and 19:00. Each photograph includes, on the left side the thermochromic samples and on the right the conventional one. Due to a damaged memory card, some photographs are lost. All photographs are tabulated in Table 5.5, Table 5.6, Table 5.7 for RTC, RTC_V and RTC_S respectively. The surface temperatures of the samples, at the time the photographs are taken, is also mentioned in the tables. The remaining samples' photographs are listed in Appendix B (Tables B.1 to B.6).

Table 5.5 Red thermochromic (RTC) side by conventional sample during the measuring period.

Day	Hour of Day: 09:00 Surface Temperature (°C)		15:00 Surface Temperature (°C)		19:00 Surface Temperature (°C)	
	Thermochromic	Conventional	Thermochromic	Conventional	Thermochromic	Conventional
1			31.63	33.1	25.01	25.19
2	24.75	25.11	30.97	32.8	24.56	25.99
3	25.98	25.73	31.57	33.4	25.17	26.72
4	27.38	27.08	34.18	35.6	27.41	29.08
6	26.97	26.44	31.45	35.2	26.73	27.74
7	26.16	26.07			25.16	26.03
8	24.5	24.27				
9	24.35	24.44				
10	25.46	25.44	32.37	35.2		
13	28	28.18	32	34	21.72	21.99
14	30.55	30.65				

Table 5.6 Red Thermochromic coating covered with polyurethane varnish (RTC_V) side by conventional sample during the measuring period.

	Hour of Day								
	09:00			15:00			19:00		
	Surface Temperature (°C)			Surface Temperature (°C)			Surface Temperature (°C)		
Day	Thermochromic		Conventional	Thermochromic		Conventional	Thermochromic		Conventional
1				33.6	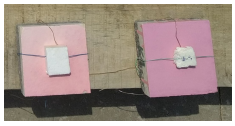	32.5	25.19	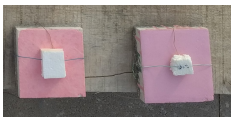	25.04
2	23.93		24.52	33.95	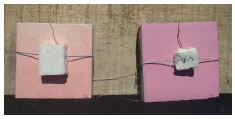	32.2	27.91	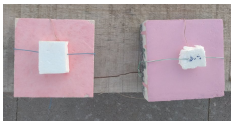	26.98
3	24.32		25.43	34.95	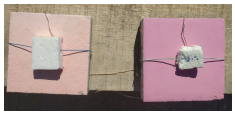	33	28.06		27.24
4	25.86		26.87	35.57	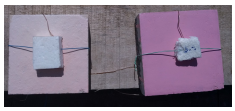	35.1	30.85		30.01
6	25.62	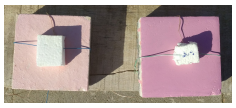	26.61	39.37	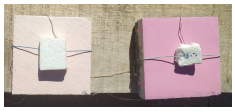	40.2	28.14	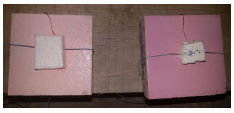	28.04
7	25.01	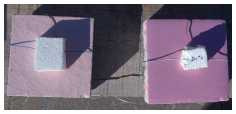	26.09				27.05		26.83
8	23.77	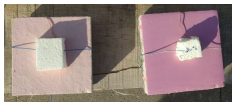	24.1						
9	23.37	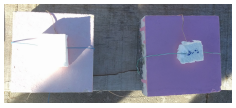	24.26						
10	24.4		25.53	42.13	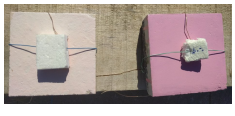	41			
13	26.71	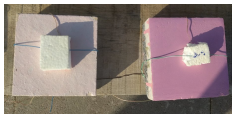	27.95	35.45		33.4	21.37		21.7
14	29.29	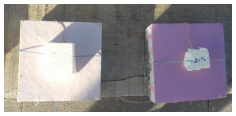	30.5						

Table 5.7 Red thermochromic sample covered with UV stabiliser (RTC_S) side by conventional sample during the measuring period.

	Hour of Day								
	09:00			15:00			19:00		
	Surface Temperature (°C)			Surface Temperature (°C)			Surface Temperature (°C)		
Day	Thermochromic		Conventional	Thermochromic		Conventional	Thermochromic		Conventional
1				31.89	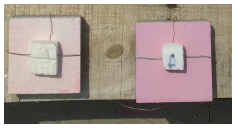	33.8	24.97	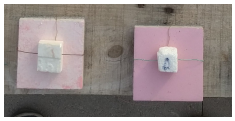	25.4
2	24.18		24.8	31.33		33.5	25.11		26.33
3	25.29		25.73	31.92		34.3	25.83	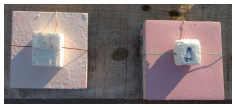	27.03
4	26.73		27.04	34.53		36.7	28.08		29.48
6	26.44		26.6	36.13	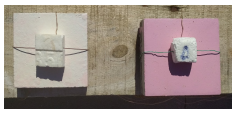	38.9	26.96		27.78
7	25.64		26.21				25.54		26.13
8	24.26	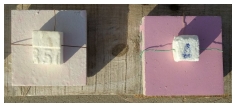	24.53						
9	23.98		24.43						
10	24.88		25.5	35.85		40.3			
13	27.67	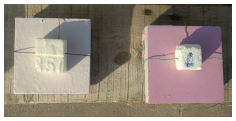	28.44	32.69	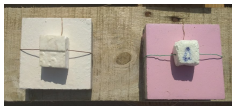	34.7	21.49	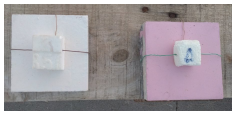	21.87
14	29.97		31.05						

As shown in Table 5.4, the conventional samples are not affected by the exposure to the weather conditions. The degradation of all organic thermochromic samples due to solar radiation is significant. The degradation changed the colour of the blue and brown thermochromic samples, permanently to white. The red thermochromic has retained some of its thermochromic properties. The largest increase, by 20% of the SR, was found for the brown thermochromic sample and the smallest increase, by 8% for the blue thermochromic. Smaller increase of the SR_{UV} is observed in all samples, followed by an increase of almost 40% for the SR_{NIR} and SR_{VIS} for the brown thermochromic. A general remark is that the degradation of the colour and SR is more intense for the initial than the transition phase of the thermochromic samples.

Chapter 6

Contribution of cool coatings on the energy efficiency in the built environment: tools and calculation methods

6.1 Introduction

The residential sector accounts for more than 20% of final energy consumption in the EU and over 36% of CO_2 emissions, with an decreasing trend[122]. According to recent surveys, in residential buildings the energy consumption for space heating accounts for 57%, while for hot water 25% of the total energy is consumed. Simplified methods such as steady-state and steady-cyclic calculations are not sufficient to faithfully represent the complex flowpaths that occur in real buildings. Simulation is a more accurate tool to reflect dynamic systems, as it is an attempt to emulate the reality. It allows users to understand the interrelation between design and performance parameters and to identify potential problem areas. With the use of Building Energy Simulation (BES) users can alter the design and materials of the building and receive a reliable estimation of the consequent energy performance impact.

With the use of BES the building is isolated from the interaction with its surrounding environment. For the investigation of the environment mesoscale or microscale, depending on the area under

investigation, simulation software packages are used. With the use of mesoscale or microscale software the microclimatic variations of the area can be calculated, visualised and exploited.

The aim of present chapter is to investigate the performance changes of a simple building with the use of the coatings developed and presented in Chapter 3. Also a novel technique of coupling the BES with microclimatic simulation of the surrounding environment is presented.

6.2 Contribution of cool coatings on the energy efficiency of buildings

The present section is dedicated to the necessary quantitative analysis on the energy efficiency that can be achieved by the application of the cool coatings developed in the framework of the present thesis examined in the building envelope. A small building placed in the Technical University of Crete, Greece Campus is simulated.

ESP-r [123–125] energy modelling tool is employed for the thermal simulation. ESP-r can simulate complicated elements of the building envelope and electrical/mechanical equipment available. Thermal simulation in ESP-r is based on control-volume heat-balanced approach using numerical discretisation and simultaneous solution[125]. Specifically, ESP-r simulates the thermal state of the building by applying a finite-difference formulation based on a control-volume heat-balance to represent all relevant energy flows.The computational subroutines exchange information (interaction between the parameters of the various thermal zones) in order to accurately calculate the interactions between the systems of the building. One of the most important characteristics of ESP-r is that it co-operates with other simulation tools to provide a wider range of very accurate results.

The input data that ESP-r needs to effective simulate the thermal characteristics of a building are:

1. Geographical location (longitude/latitude) of the building.
2. Weather file of the area. The weather file is a statistical generated file that represent the local weather conditions. The following meteorological data are included:
   (a) Ambient air temperature (°C)
   (b) Relative humidity (%)
   (c) Wind speed (m/s)
   (d) Wind direction (°)
   (e) Direct solar radiation (W/m^2)

(f) Diffused solar radiation (W/m^2)

3. Design and construction characteristics of the building i.e. dimensions and orientation of building surfaces, thermal characteristics of the building materials, thickness as well as how they are layered to constitute constructions.

4. Internal thermal gains and occupancy.

5. Set-points for heating/cooling.

The base case building is a single room building with a flat roof of $20m^2$ and a North facing window of $4.5m^2$. Two variations of the same building are modeled in order to examine the effect of the developed cool coatings on a recently built well insulated and an old poor insulated building. The building's characteristics are included in Table 6.1. The outer (third) layer of the roof and outer (forth) layer of all walls is replaced by the inorganic cool coatings.

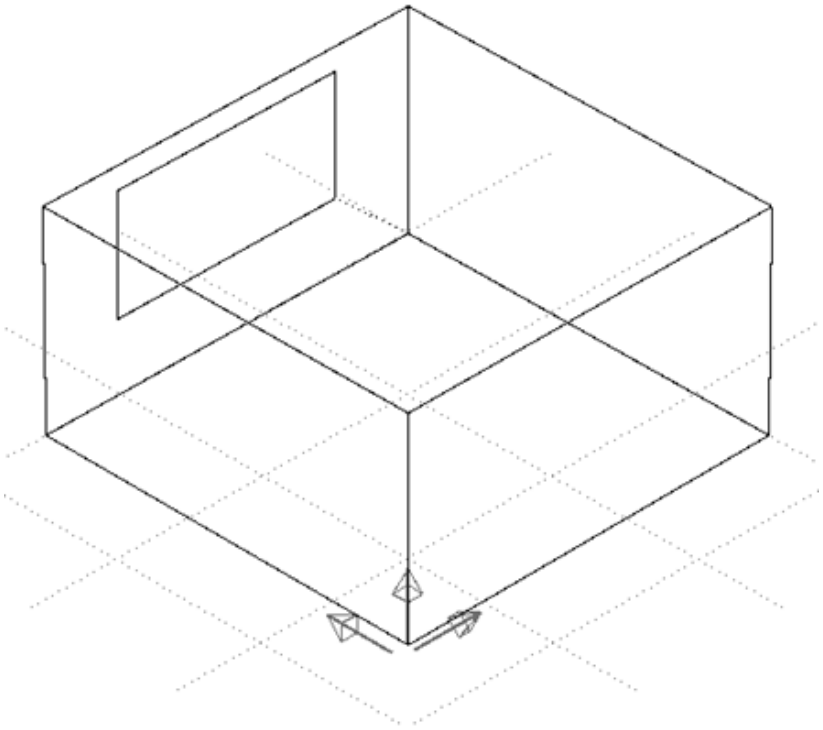

Figure 6.1 3D view of the reference building in ESP-r.

Table 6.1 Single room building characteristics.

General Information		
Surface area	79 m^2, 54 m^2 vertical	
Location	35°32' N, 24°05' E (Chania, Crete, Greece)	
Building Envelope		
	Well insulated building	Low insulated building
Walls	Four-layer (lime cement plaster, brick, insulation, brick) outer walls of total U: 0.513 W/m^2 K	Four-layer (lime cement plaster, brick, air gap, brick) outer walls of total U: 2.178 W/m^2 K
Roof	Tree-layer (plaster, concrete, insulation) ceiling of total U: 0.813 W/m^2 K	Two-layer (plaster, concrete) ceiling of total U: 3.074 W/m^2 K
Windows	North facing (33.33% coverage) double glazing windows with: U = 2.81 W/m^2 K	North facing (33.33% coverage) single glazing windows with: U = 5.570 W/m^2 K
Floor	Two layer (insulation, concrete) floor with U = 0.505 W/m^2 K	One layer (concrete) floor with U = 3.196 W/m^2 K
Building services		
Heating system	Ideal Load 3kW (set point : 20°C) From 8:00 – 16:00	
Cooling system	Ideal Load 3kW (set point : 26°C) From 8:00 – 16:00	
Casual Gain		
Occupancy		
Time	Sensible (W)	Latent (W)
0:00 – 8:00	0	0
8:00 – 12:00	225	165
12:00 – 14:00	150	110
14:00 – 16:00	225	165
16:00 – 24:00	0	0
Small power	8:00 – 16:00 : 258 W (Sensible)	
Lights	10:00 – 14:00 : 288 W (Sensible) from November 1rst – April 30rd	
Air changes per hour	0.3 ACH	

Due to the large number of different developed coatings and similar solar reflectance (SR), a set of ten SR values are chosen to conduct the simulations. The ten coatings used are tabulated in Table 6.2. The cooling and heating loads are calculated for the reference Portland cement (SR=49) and the selected cool coatings (Table 6.2). The contribution of samples on the overall energy efficiency is depicted in Figures 6.2 and 6.3. The energy efficiency achieved is in accordance with the thermal characteristics and optical properties' analysis performed in the previous chapters. The highest energy efficiency is achieved by the samples with SR of 89, with 1.54 kWh/m^2 and 1.49 kWh/m^2 annual reduction for poor and well insulated building respectively. A detailed comparison of the energy reduction on a well versus a poor insulated building can be found in Figure 6.4. On a well-insulated building the heating penalty is higher by 5% while the reduction of the cooling load is almost 4%. Concerning the overall annual energy efficiency, the overall performance of the well-insulated building is higher by 3.5% compared to the poor insulated building. Therefore the inorganic coatings examined can contribute to the reduction of the buildings' energy requirements especially during summer.

Table 6.2 Solar reflectance of selected samples.

No	Solar reflectance	Sample name
1	66	NHL-QUA
2	70	WCM-QUA
3	79	NHL–DMP / NHL-DMP-GB
4	82	NHL-LMP
5	83	NHL-LMP-GB
6	84	LMP-M-S
7	86	LMP-F-S / LMP-F-S / DMP-C-S
8	87	LMP-F-N / LMP-F-N /WCM-LMP-GB / DMP-M-S / DMP-C-N
9	88	DMP-M-N / DMP-F-N / DMP-F-S / LMP-M-N
10	89	WCM-DMP

NHL: natural hydraulic lime with pozzolanic additives; WCM: white cement Portland; DMP: dolomitic marble; LMP: limestone powered; QUA: quartz sand; GB: glass beads; C: coarse ; M: medium ; F: fine; S: sanded; N: untreated

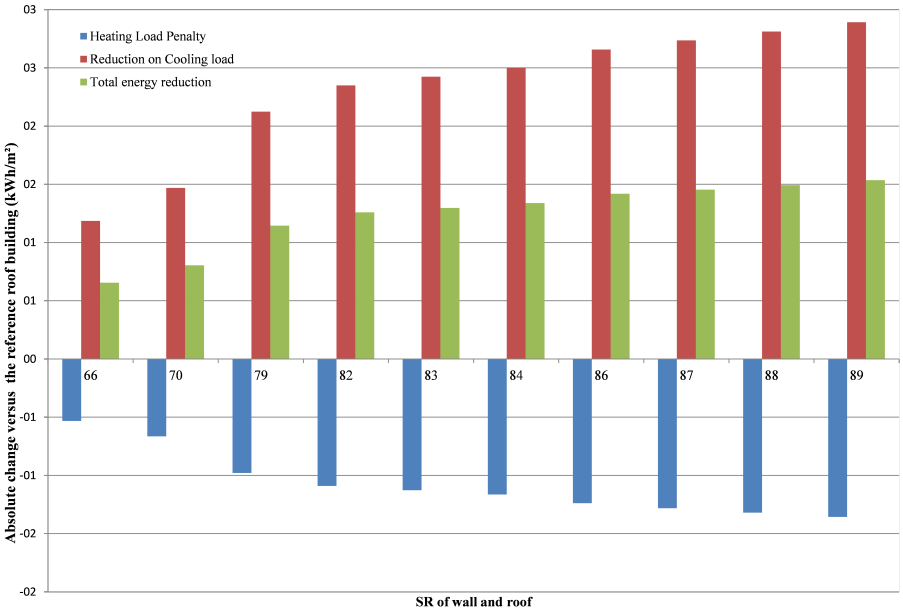

Figure 6.2 The pertinent energy savings of the inorganic samples used on a poor-insulated building.

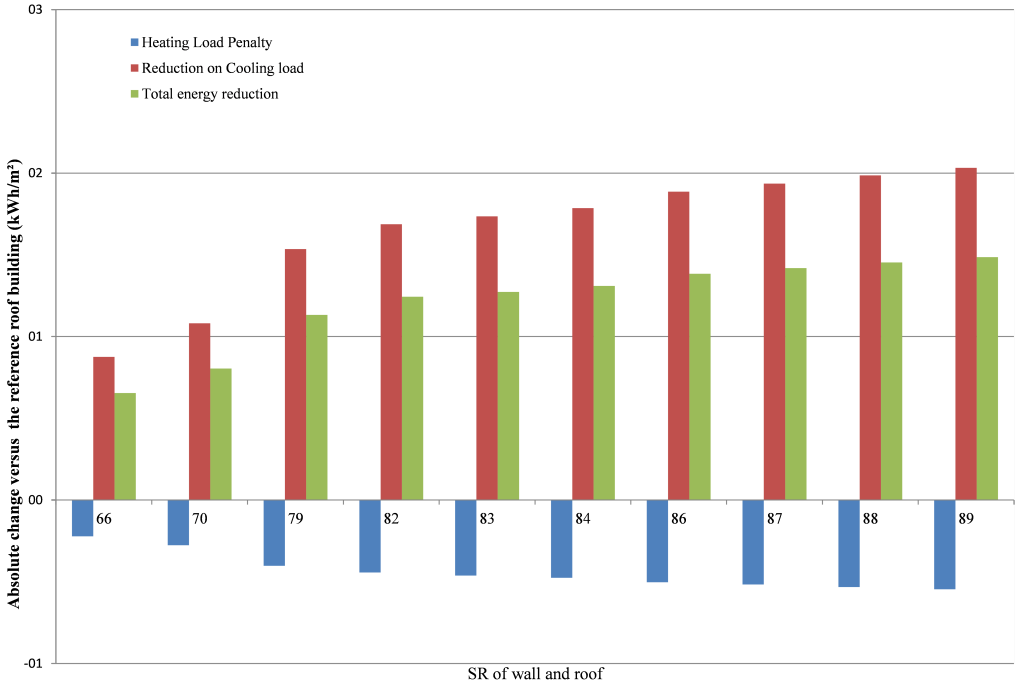

Figure 6.3 The pertinent energy savings of the inorganic samples used on a well-insulated building.

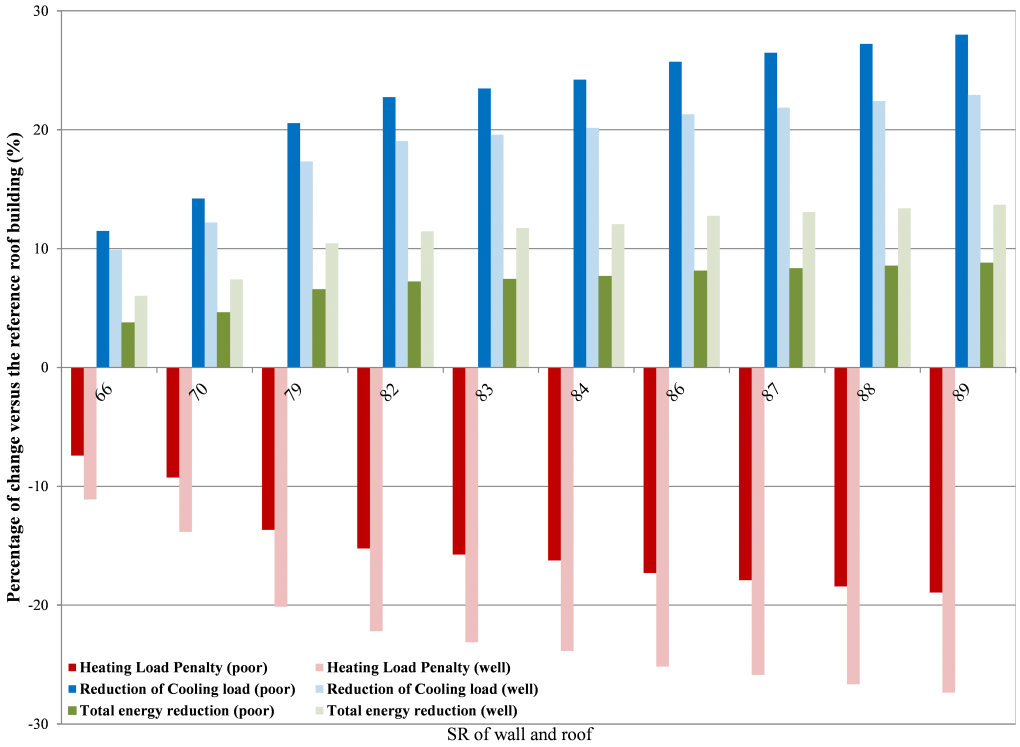

Figure 6.4 Comparison of the energy reduction on well versus poor insulated building.

Table 6.3 Comparison of peak power on well and poor insulated building.

	Low Insulated		Well insulated	
SR	Heating peak power increase (%)	Cooling peak power reduction (%)	Heating peak power increase (%)	Cooling peak power reduction (%)
66	0.73	8.94	1.80	5.92
67	1.09	9.35	1.80	6.58
70	1.09	10.57	2.70	7.24
79	1.45	14.63	3.60	10.53
82	1.82	15.85	3.60	11.84
83	1.82	16.26	3.60	11.84
84	1.82	16.67	4.50	12.50
86	1.82	17.48	4.50	13.16
87	1.82	17.89	4.50	13.16
88	1.82	18.29	4.50	13.82
89	1.82	18.70	5.41	13.82

Another major benefit of the use of developed cool coatings is the reduction of the peak load of the building. A reduction of almost 20% and 15% can be achieved in low insulation and well insulation buildings, respectively(Table 6.3). This reduction has multiple benefits for both the local electricity grid and building owner. The stress to the electricity grid is reduced and so the need upgrading the power grid capacity. The majority of electricity distribution companies charge extra the peak energy demand. The owner of the building in this case benefits firstly by the reduction of the base energy usage and secondly by the reduction of the peak power demand. Tabulated in Table 6.4 is the maximum roof temperature on well and poor insulated building. For low insulation model the maximum temperature is slightly increased by an average of 0.4K from the well insulated model, indicating that not only the SR of the surface coating but the insulation, solar and internal gains play a role on the surface. A significant reduction up to 33% is achieved in the maximum roof temperature if the developed coatings are used instead the reference coating.

Table 6.4 Comparison of maximum roof temperature on well and poor insulated building.

SR	Low Insulated		Well insulated	
	Maximum roof temperature (°C)	Reduction in maximum roof temperature (%)	Maximum roof temperature (°C)	Reduction in maximum roof temperature (%)
66	45.31	14.02	45.08	14.43
67	44.87	14.86	44.63	15.28
70	43.55	17.36	43.27	17.86
79	39.56	24.93	39.17	25.65
82	38.22	27.48	37.79	28.26
83	37.77	28.33	37.33	29.14
84	37.32	29.18	36.87	30.01
86	36.45	30.83	35.95	31.76
87	36.01	31.67	35.49	32.63
88	35.58	32.49	35.15	33.28
89	35.14	33.32	34.87	33.81

6.3 Contribution of cool coatings on the energy efficiency of buildings coupled with microclimatic simulation

The significant shifts in climate variables projected for the 21st century, coupled with the observed impacts of on-going extreme weather and climate events, ensure that climate change is set to remain a pressing issue for urban areas over the coming decades [126, 127]. Urban thermal deterioration is the combined result of the urban heat island developed mainly in cities with a positive thermal balance and of the global warming which affects the urban climate as well. Significant effort is being put by various researchers on the impact of the urban microclimate to the buildings' energy consumption. Nowadays it is evident that the increase of urban temperatures has a serious impact on the energy demand of buildings by increasing significantly the energy consumption for cooling, while decreasing to some extent the energy consumption for heating. Overall, the urban landscape creates a climate which affects, human comfort, air quality and energy consumption [12, 128]. The tools that support the quantification of the microclimatic impact on the energy consumption of buildings are the BES combined with microclimatic models. BES is an absolutely necessary tool in integrated building design and operation [129]. This importance can be illustrated by a large variety of BES software that are in use today [130]. The available BES combine many empirical and first-principle models to describe relevant energy transfer processes in buildings [131]. The modelling of urban thermal conditions is performed in different scales, namely mesoscale or microscale, depending on the area under investigation. For example, the climate of street canyons is primarily controlled by the micro-meteorological effects of urban geometry rather than the mesoscale forces. There are strong microscale variations of surface temperature that arise due to changes in radiant load with surface slope and aspect, shading, and variations in surface thermal and radiative properties [132]. Although there are no clear-cut distinctions between different categories, models might be classified into groups according to their physical or mathematical principles (e.g. reduced-scale, box, Gaussian, Computational Fluid Dynamics) and their level of complexity (e.g. screening, semi-empirical, numerical) [133]. In order to accurately estimate the impact of urban microclimate on the energy consumption, BES tools should be effectively interconnected to allow more sophisticated and, at the same time, more efficient calculations that take into account the impact of the microclimatic conditions on the energy demand for buildings. Various researchers have performed similar efforts. A simulation tool for the prediction of the effect of outdoor thermal environment on building thermal performance (heating/cooling loads, indoor temperature) in an urban block consisting of several buildings, trees, and other structures is proposed by [134]. External surface temperature and mean radiant temperature are used to estimate the impact of the outdoor environment. As underlined by [135]. the evaluation of policy measures in district level requires the effective combination of the building geometry with possible canyon formation, along

with local weather conditions and energy load prediction, in order to effectively manage the available resources. To this end, the aim of the present research is to combine the building simulation tools with microclimatic models targeting to improve the accuracy of the energy requirements' calculations.

6.3.1 Building energy - microclimatic simulation coupling methodology

A coupling procedure is developed between BES and microclimatic conditions in order to effectively evaluate the impact of outdoor conditions in the buildings' energy consumption. The key parameter for the coupling procedure is considered to be the Convective Heat Transfer Coefficient (CHTC) between the exterior building surfaces and the external environment since it can be 3 to 4 times higher than the radiative heat exchange [136, 137].

The CHTC is influenced by several factors, such as the orientation of the building envelope, the geometry of the building, building's surroundings, the building surface's characteristics, wind speed and wind direction, patterns of the local airflow around the building and surface to air temperature differences [138]. The geometry and position of nearby buildings in urban areas change the airflow patterns around the dwellings under study [139, 140], which powerfully influence their CHTC.

There are three main methods of obtaining the values for CHTC: a) analytical, b) numerical and c) experimental. Analytical methods are only valid for specific flow patterns and simple geometries, e.g. flat plates and cylinders [141]. Numerical methods, namely [142, 143]. Experimental methods, both in reduced-scale and full-scale tests, are currently still the main source of CHTC data [144–147].

The procedure developed is depicted in Figure 6.5 and is described below:

1. A building thermal model is developed using ESP-r [123]. The specific tool is selected for the specific study as it uses airflow networks which enable the calculation of the movement of air masses inside or outside buildings, etc.
2. A microclimatic model of the area surrounding the case study is developed using ENVI-met. More details can be found in Section 6.3.4.
3. A modified ESP-r weather file is created by the outputs of ENVI-met.
4. A set of CHTC values is calculated for each surface of the building envelope (see different surface types in Figure 6.6). The calculation methods are described in Section 6.3.5.
5. A set of simulation results is then extracted including:
   (a) The power and energy requirements extracted by ESP-r using the weather file generated by Meteonorm [148].

(b) The power and energy requirements extracted by ESP-r using the weather file created in step 3.

(c) The power and energy requirements by weather file created in step 3 combined with the CHTC values created in step 4.

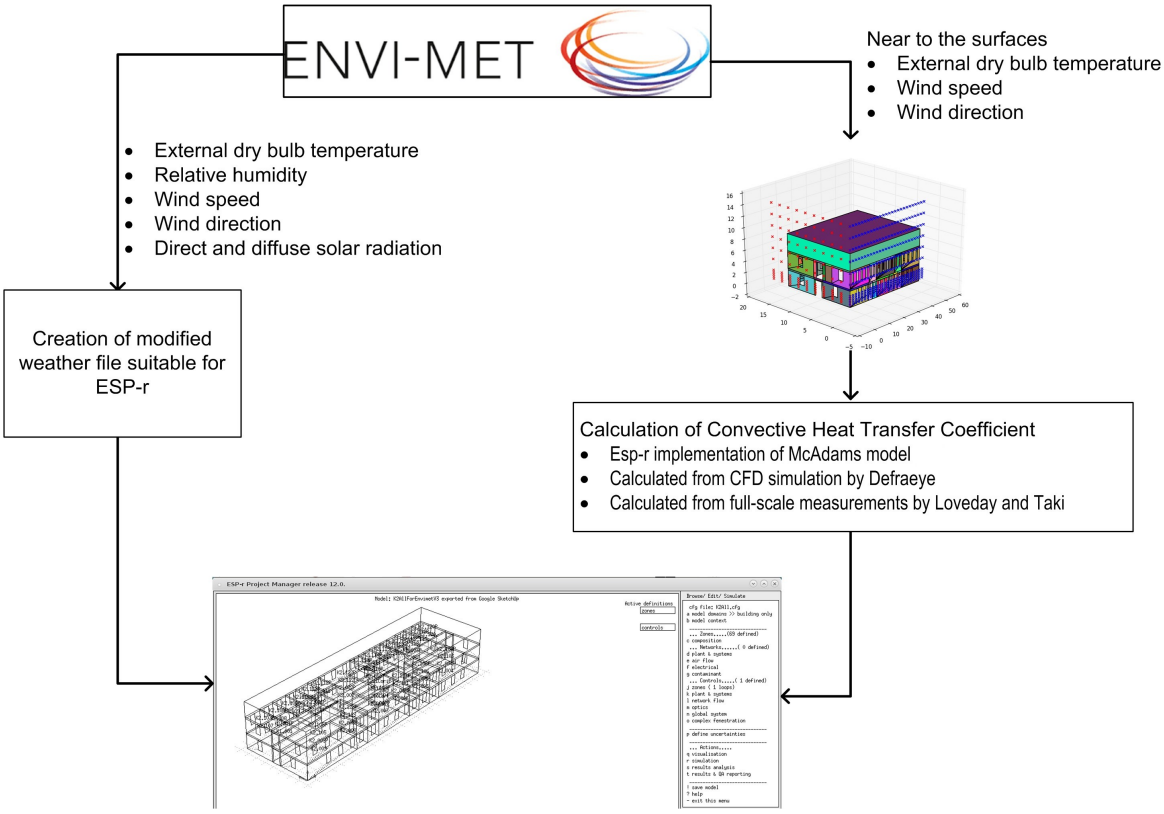

Figure 6.5 The coupling methodology.

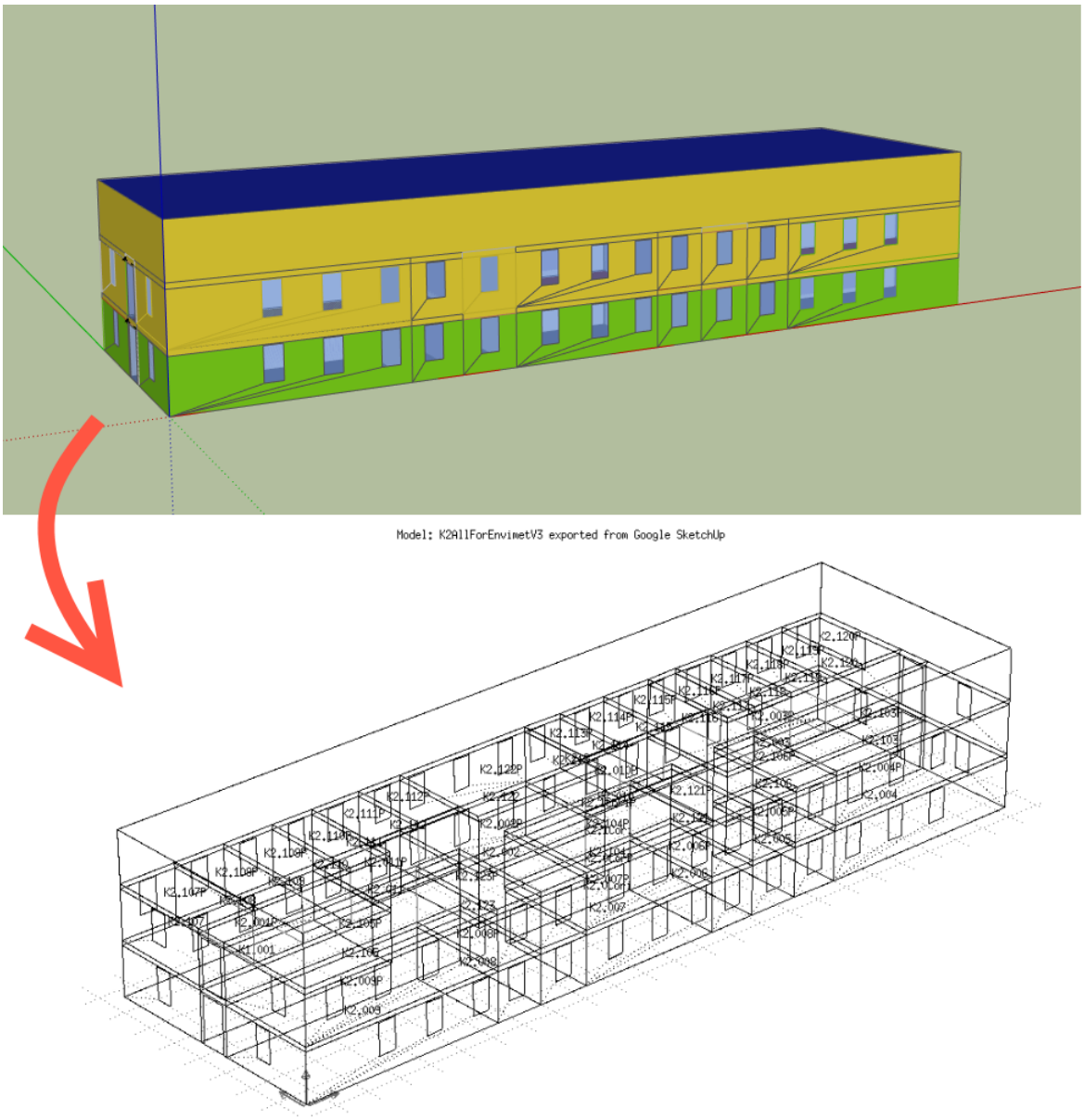

Figure 6.6 Building Model using ESP-r.

6.3.2 Description of the case study

The case study area is situated on the Campus of the Technical University of Crete [149], in Akrotiri, Crete. The region is characterized by a mild Mediterranean climate with low wind speeds (2014-2016 average:2.18 m/s). The Campus of the Technical University of Crete hosts five University departments, two libraries, administrative buildings and student dormitories. The Campus is one of the major energy consumers in the electricity grid of Crete with a peak power demand of 1.2-1.5 MW. It should

be noted here that Crete is supported by an autonomous energy system, not interconnected with Greece's mainland power network [150].

Figure 6.7 depicts the building under study, the exterior spaces around them and the topography of the area. The building K2 is located at the northern end of the campus with its main façade facing north-west. The distance between K1 and K2 is approximately 16.20m, with K2 sited to the south of K1. Each floor of K2 is divided in two wings, connected through an atrium. The main characteristics of the selected building, as well as their structural material, are tabulated in Table 6.5. The building is divided into 68 thermal zones: 32 offices/laboratories, 2 corridors, 34 plenums spaces above the offices and corridors and one storage/mechanical room. The majority of the heating ventilation and air conditioning (HVAC) equipment is located outside of the building. The solar gains are dynamically calculated by the simulation software. For the present study, ideal loads are considered to calculate the heating and cooling needs of the building. The ideal load is operating from 8:00 to 16:00 with 20°C and 26°C set point for heating and cooling respectively.

Table 6.5 Main characteristics of the selected building.

Characteristics of Building	
Location	Chania, Crete, Greece
General Dimensions (m)	(Length/ Width/ Height): 48.00 / 15.20 / 11.00
Number of Floors	3
Facilities on Ground floor	5 computer rooms, 1 printer room, 3 office, 1 mechanical room, elevators, stairs, WC
Facilities on 1st floor	3 laboratories, 14 offices, elevators, stairs, WC
Facilities on 2nd floor	Mechanical rooms
Characteristics of Exterior spaces	
Exterior spaces	Soil, marble, stone, tiles (cotto), plants, trees
Structural materials of Building	
Exterior walls	Ground and first floors ceilings
a) Double plasterboard (width:18mm each)	a) Uncoated concrete: 2cm
b) Insulation: 5cm rockwool, d=80kg/ m^3	b) Insulation: 5cm rockwool, d=80kg/ m^3
c) Cement board: 10mm	c) Ceramic tiles: 10mm
Second floor ceilings	Windows (68 windows)
a) Uncoated concrete: 2cm	a) Double pane windows
b) Insulation: 10cm	b) Aluminum frames
c) Asphalt membrane: 10mm	c) Exterior lamellas
Floor top coating	
a) Ceramic tiles: 10mm (in all spaces)	
b) Industrial flooring: 20mm (Chemistry lab)	
Building services	
Heating system	Ideal load 5 kW (set point: 20.0 °C) from 8:00 to 16:00
Cooling system	Ideal load 3 kW (set point: 26.0 °C) from 8:00 to 16:00
Internal casual gain	
0:00–8:00	0 + 0 W (Sensible + Latent)
8:00–12:00	250 + 50 W (Sensible + Latent)
12:00–14:00	150 + 30 W (Sensible + Latent)

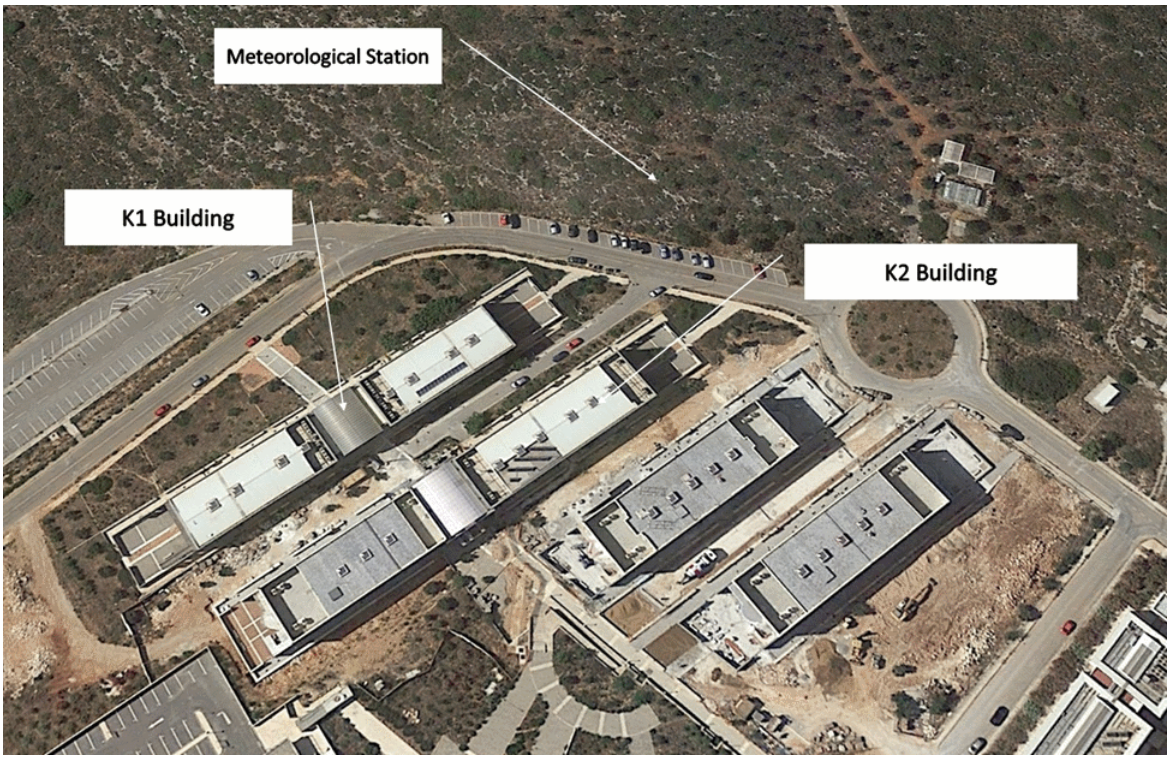

Figure 6.7 Aerial photo of campus buildings K1 and K2.

6.3.3 Development of the thermal model of the Case Study Building

ESP-r is used for the development of the thermal model of the building. A feature not supported by ESP-r is the import of 3D building models. Especially for buildings with complicated shapes and forms, the modelling procedure is time consuming and requires a good knowledge of the software. For that reason, a specific plugin is developed to simplify the process. The plugin, developed in the programing language Ruby [151], allows the export of any SketchUp geometry to ESP-r (Appendix C). Along with the creation of the geometry in ESP-r, the plugin also interconnects all the surfaces of the building model. Moreover, the plugin has the ability to transform a 2D diagram of the floor plan into thermal zones. With this functionality, the time for the development of the model is drastically reduced. The plugin also stores data of the coordinates, edges, surfaces and construction names for every different thermal zone of ESP-r in separate text file with the extension ".geo".

6.3.4 Modeling of microclimatic conditions

For the simulations of the conditions in the exterior area between the buildings of the Technical University of Crete, the three-dimensional microclimate model ENVI-met is used [152, 82]. ENVI-met

uses the Finite Difference method to solve the multitude of partial differential equations and other aspects in the model. An orthogonal Arakawa C-grid is used for the representation of the environment [153]. ENVI-met though allows only straight and rectangular structures. ENVI-met requires the following input data that are collected from a local weather station daily average air temperature, daily average relative humidity, average wind speed, direction for the specific location and simulation day. The parameters extracted by ENVI-met and their use are depicted in Figure 6.5.

The data input for the ENVI-met were designed using the integrated 3-D modeling software called SPACE where buildings, trees/vegetation and surfaces are placed. Those materials are represented as cell inside the grid. The resolution of the grid is depending on the cell size. The smaller the cell size, tje greater is the resolution of the digitalization is. For the current digitalization, the cell size is set at 2mx2m and the grid size (x y z) at 170x140x20 cells. The final digitalization of area under investigation is shown at Figure 6.8 and Figure 6.9. The buildings are constructed entire by Portland cement (represented with grey colour Figure 6.8) of the following characteristics:

- Reflectance:0.30
- Emmissivity:0.90
- Specific heat:840 $\frac{J}{kgK}$
- Thermal Conductivity:0.86 $\frac{W}{mK}$
- Density:2000 $\frac{kg}{m}$

In Table 6.6 and Table 6.7 are the surface materials (Figure 6.8) and plants (Figure 6.9) used for representing the under investigation area.

Table 6.6 TUC campus surface material.

Surface	Reflectance	Emissivity	Representation
Asphalt	0.2	0.90	
Concrete pavement	0.4	0.9	
Loam soil	0	0.98	
Red brick road	0.3	0.90	
Unseald Soil	0.20	0.65	

Table 6.7 TUC campus plant species.

Plant	Reflectance	Plant height (cm)	Representation
Grass I	0.2	63	
Grass II	0.2	10	
Olive tree	0.5	400	

Figure 6.8 Building and trees/vegetation representation of the TUC campus.

Figure 6.9 Surfaces of the TUC campus.

A typical summer day is selected to simulate the microclimatic conditions around the buildings. The results of the simulation at 12:00 are depicted in Figure 6.10, Figure 6.11 and Figure 6.12. The modelled surface temperature is as expected quite high, i.e. between 38-41°C in the area between the K1 and K2 building as well as in all areas covered with asphalt. The areas covered with soil and grass have a surface temperature of around 35°C and 29°C respectively.

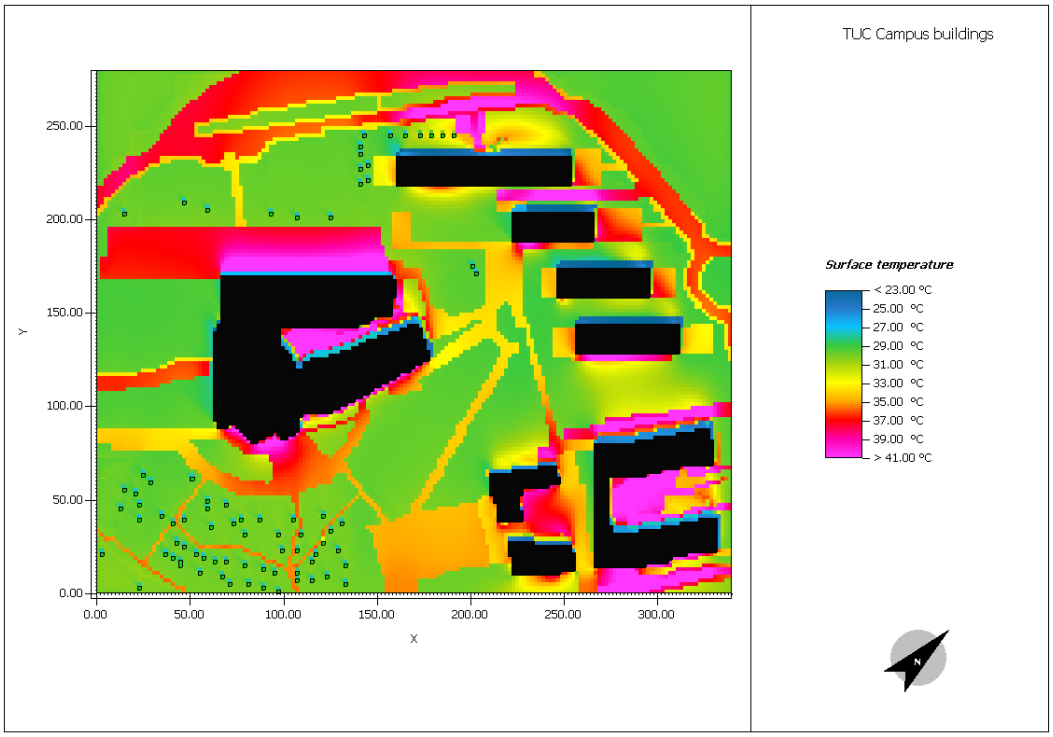

Figure 6.10 The surface temperature of the TUC Campus for summer period at 12:00.

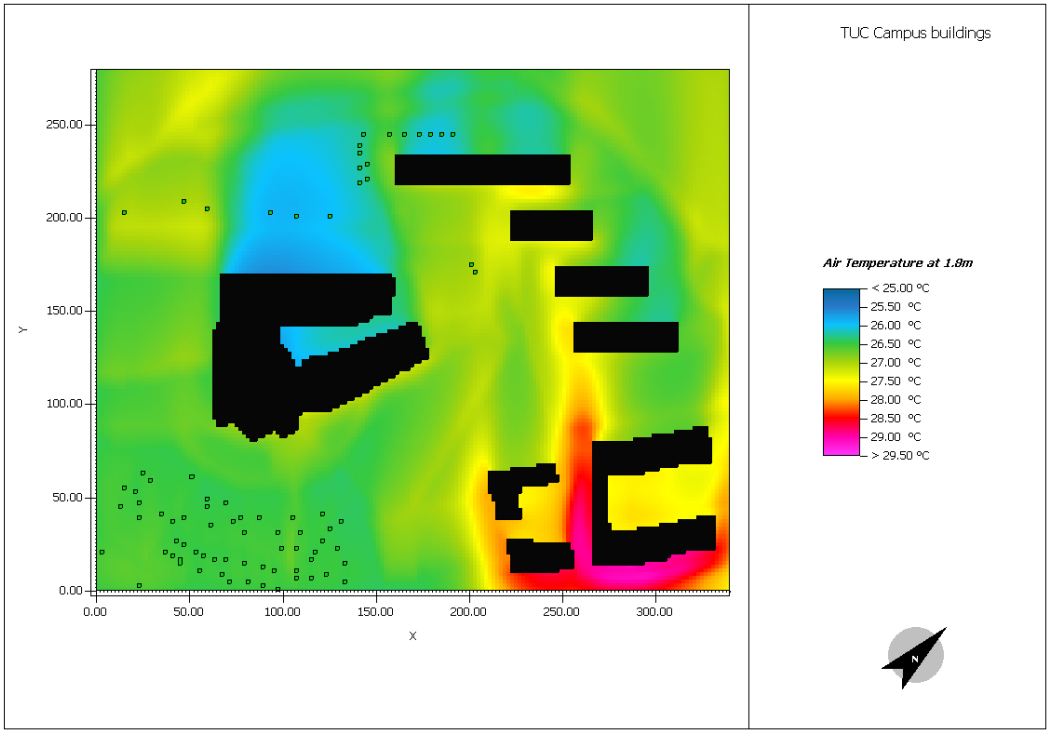

Figure 6.11 The air temperature around the TUC Campus Buildings for summer period at 12:00.

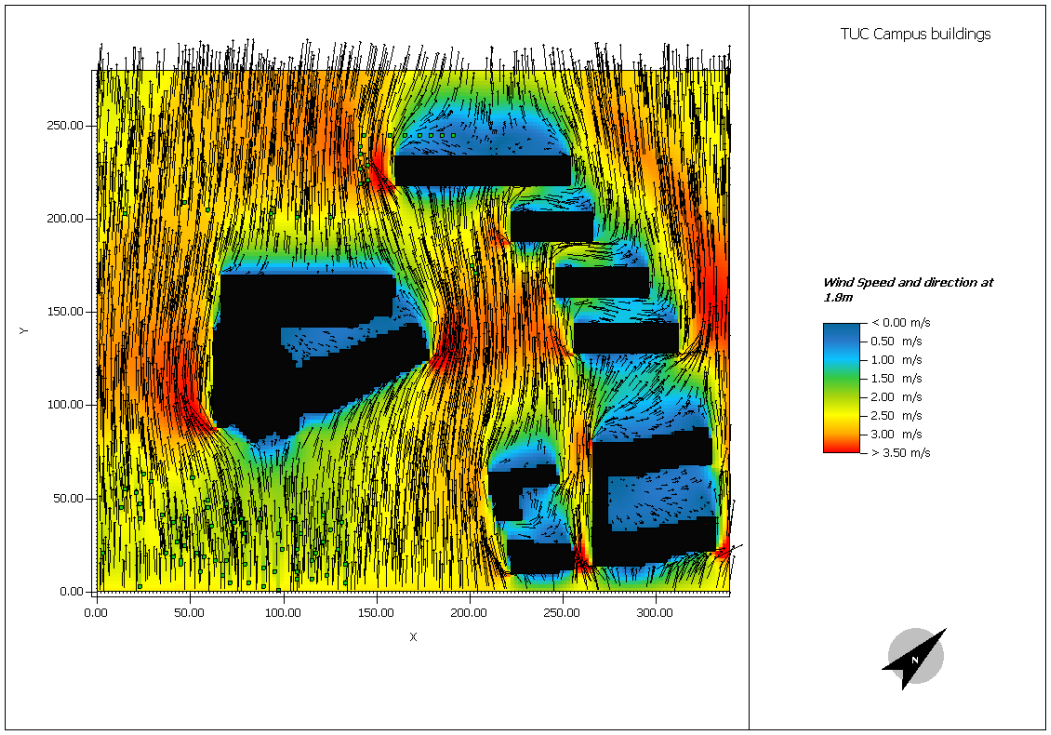

Figure 6.12 The wind speed and direction around the TUC Campus Buildings for summer period at 12:00.

6.3.5 Convective Heat Transfer Coefficient Calculations

The CHTC for an external building surface ($h_{c,ext}$) is defined as:

$$h_{c,ext} = \frac{q_c}{T_s - T_a} \left(\frac{W}{m^2 K} \right) \tag{6.1}$$

Where:

- q_c (W/m^2), convective heat flux at any exterior building surface
- T_s (^oC) the surface temperature and the
- T_a (^oC) the air temperature

There are three main methods of obtaining the values for CHTC:

- Analytical (Section 6.3.5)
- Numerical (Section 6.3.5.2)
- Experimental (Section 6.3.5.3)

6.3.5.1 CHTC Calculations in Building Energy Simulation tools

The calculation of CHTC is based on Equation (6.2) reported by McAdams [154] based on the wind tunnel experiments obtained using a vertical square copper plate (0.5 m x 0.5 m) in a uniform air flow parallel to the plate.

$$h_{c,ext} = 5.678 \left[m + n \left(\frac{V_f}{0.3048} \right)^p \right] \tag{6.2}$$

where: m, n, p are the roughness parameters for smooth and rough surface and V_f is the free stream wind speed. A linear expression is used by ESP-r as a more simplified approach for the implementation of the McAdams model (see Equation (6.3)) [155]:

$$h_{c,ext} = 3V_{loc} + 2.8 \tag{6.3}$$

where V_{loc} is the local wind speed measured at a constant distance d from the building facade and at a contain height H from the ground and is calculated using Equations (6.4) to (6.7):

In these equations, ϕ is the vertical angle between the ground plane and the surface plane and θ is the horizontal wind attack angle, i.e. the angle between the surface normal vector and the wind direction. If the horizontal surface and surface with slope angle (ϕ) is in the range: $0^o \leq \phi \leq 45^o$ or $135^o \leq \phi \leq 180_0$ then $V_{loc} = V_{10}$. If the slope angle in between $45^o \leq \phi \leq 135^o$ Equation (6.5) is used: If $0° \leq \phi \leq 45°$ or $135° \leq \phi \leq 180°$ then:

$$V_{loc} \cong V_{10} \tag{6.4}$$

If $45° \leq \phi \leq 135°$ then if windward surfaces with $0° \leq \theta < 10°$ then:

$$V_{loc} \cong \begin{cases} 0.5V_{10} \quad for\ V_{10} \leq 1m/s \\ 0.5\frac{m}{s} \quad for\ 1 < V_{10} \leq 2m/s \\ 0.5V_{10} \quad for\ V_{10} > 2m/s \end{cases} \tag{6.5}$$

If windward surfaces with $10° \leq \theta < 90°$ then:

$$V_{loc} = V_{10} \sin\theta \tag{6.6}$$

If leeward surface $90° \leq \theta < 180°$

$$V_{loc} = 0.25\ V_{10} \sin\theta \tag{6.7}$$

Where:

- V_{10} is the wind speed measured at 10m above the ground level.
- ϕ is the vertical angle between the ground plane and the surface plane.
- θ is the horizontal wind attack angle, i.e. the angle between the surface normal vector and the wind direction.

6.3.5.2 CHTC calculations using Computational Fluid Dynamics

CHTC has been calculated in the past using wind-tunnel experiments on flat plates and bluff bodies, full scale experiments on building and numerical Computational Fluid Dynamics (CFD) simulation. An overview of this calculations can be found in [142], along with a short description about the experimental procedure and setup used. Defraeye *et al.* [142],validate their simulation using data from [156]. In this experiment a channel of 50mm height and 600mm depth is used along with a cube of 15 mm height. Several Reynolds numbers ranging from 2.8 x 10^3 to 5.1 x 10^3 are utilized. Then, the following correlations of the surface average are produced:

$$h_{c,ext}=\begin{cases} 5.01\ V_{10}^{0.85} & for\ \ 270^o\leq\theta\leq90^o \\ 2.27\ V_{10}^{0.83} & for\ 90^o>\theta>270^o \end{cases} \tag{6.8}$$

6.3.5.3 CHTC calculations from full-scale measurements

The need for more accurate estimation of CHTC in the building's outer surface led to an extensive amount of field measurements for building façades [145, 146] and roofs [144, 146]. Loveday and Taki used a rectangular building with L-shaped ground floor (21m x 9m x 28m) at the campus of Loughborough University of Technology. The experimental setup included a heated test panel (482mm x 530mm x 65mm), an ultrasonic anemometer and wind vane. A total of 43,200 data points are recorded and analysed. The following correlations are found:

$$h_{c,ext}=\begin{cases} 16.15U_{loc}^{0.397} & for\ \ 270^o\leq\theta\leq90^o \\ 16.25U_{loc}^{0.503} & for\ 90^o>\theta>270^o \end{cases} \tag{6.9}$$

$$Where: U_{loc}=\begin{cases} 0.2V_R-0.1\ for-90^o<\phi<-70^o\ or\ 70^o<\phi<90^o \\ 0.68V_R-0.5\ for-70^o<\phi<70^o \end{cases} \tag{6.10}$$

for windward ($270^o\leq\theta\leq90^o$) and $U_{loc}=\ 0.157V_R-0.027$ for leeward ($90^o>\theta>270^o$) facades. V_R is the wind speed measured at the roof top of the building.

In Figure 6.13, the value of the CHTC are calculated for leeward wind for the above 3 cases [157].

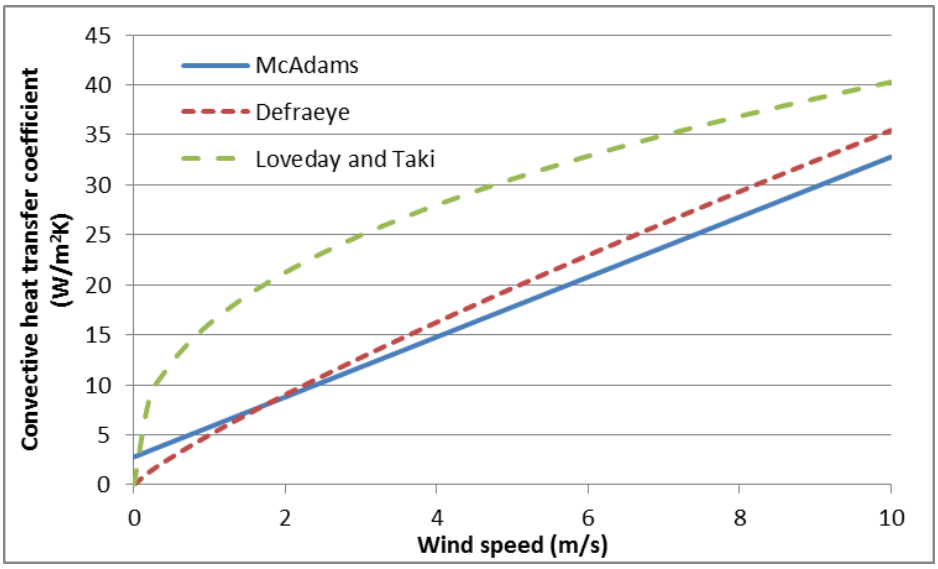

Figure 6.13 Comparison between the 3 difference methods calculating CHTC.

6.3.6 Coupling of indoor-outdoor models

The current BESs cannot take into account the microclimatic conditions of the buildings' surrounding area while usually they use weather files that contain statistically processed meteorological data. The use of real weather data requires meteorological station installed in the surrounding area of the building, which is not always available. Moreover, the wind velocity is considered stable at all points of the building and its surroundings and possible variations due to the fact that the geometry of the neighbourhood buildings and other obstacles are not taken into account.

The coupling procedure of BESs with ENVI-met is based on the following steps:

1. A library is created in the programing language Python [158] in order to extract information from the ENVI-met domain and ESP-r geometry of the building.

2. The two models, i.e. the ENVI-met model and ESP-r geometry representation of the buildings are deeply examined in order to avoid inconsistencies and support the interexchange of information.

3. A 3D representation of the building external surfaces is performed in Python programming language based on ESP-r model.

4. Then the ENVI-met grid is integrated in the 3D representation using Python. The results of the ESP-r and ENVI-met grid interconnection is depicted in Figure 6.14. Blue and red crosses correspond to the X and Y coordinates of the ENVI-met grid respectively. Each external surface of the ESP-r model is represented using different colour.

5. The air temperature, wind speed and direction on each outer surface of the building are extracted from ENVI-met domain for each ESP-r surface.

6. The CHTC on each outer surface of the model is calculated on hourly basis using Equation (6.3), Equation (6.8), Equation (6.9) using the data extracted by step 5. On the other hand ESP-r cannot accept changes of CHTC on hourly basis but only for seven time periods per day. For that reason, the 24-hours are split in seven slots:

   (a) 0:00 – 8:00

   (b) 8:00 – 10:00

   (c) 10:00 -12:00

   (d) 12:00 – 13:00

   (e) 13:00 – 15:00

   (f) 15:00 - 17:00

   (g) 17:00 – 24:00

   following the occupancy schedule. For each time slot the CHTC is calculated for every external surface and every hour, averaged over the time slot and is then fed into ESP-r. All other interactions between the building model and the environment are dynamically calculated by ESP-r, like long wave radiation heat transfer.

7. The weather files of ESP-r are updated with the outputs from ENVI-met, i.e. air temperature, wind velocity, wind direction, relative humidity and solar radiation.

For step 4, due to different surface area of ESP-r surfaces and ENVI-met cell surface the following procedure is followed. All cells that are in contact with the specific ESP-r surfaces are found and the percentage of contact area is calculated. The outside air temperature and wind of the specific ESP-r was calculated by the sum of the percentage times the values of all ENVI-met cells in contact. The wind direction for the specific ESP-r surface is the wind direction of the ENVI-met cell with the highest percentage of contact.

During the development of the above procedure, a bug was found and reported to the development team of ENVI-met [159, 160]. The software did not export the data located on the down right corner of the grid. Thankfully this did not affect the functionality of the procedure.

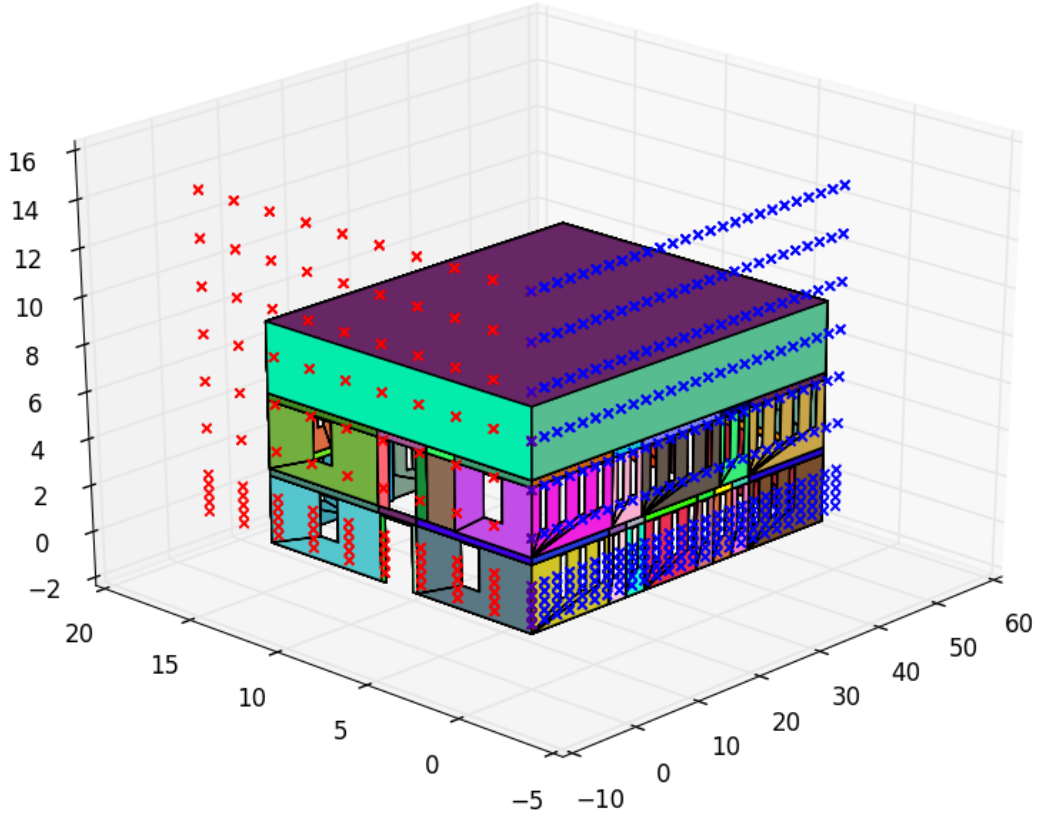

Figure 6.14 3D representation of building and outdoor environment using Python.

6.3.7 Validation of the coupling methodology

A no-working day is selected to compare the measured internal temperature for 2 rooms of the building with the result of the ESP-r model for 4 different cases as described below. Equipment to monitor the indoor environmental conditions of the building was installed in the framework of the CAMP-IT project [149]. Two rooms are selected, one (K2.001) located on the ground floor of the building facing south-east (SE) and another (K2.120) located on the first floor facing the opposite direction. The internal temperatures of the rooms are compared with the simulation result of the ESP-r model for the following conditions:

1. Weather file of the region generated by Meteonorm.
2. Weather file generated by ENVI-met and combined with the external CHTC calculated for the following 3 cases for all external surfaces:
   (a) ESP-r implementation of McAdams model using the Equation (6.3).

(b) Calculated from CFD by Defraeye using Equation (6.8).

(c) Calculated from full-scale measurements by Loveday and Taki using Equation (6.9).

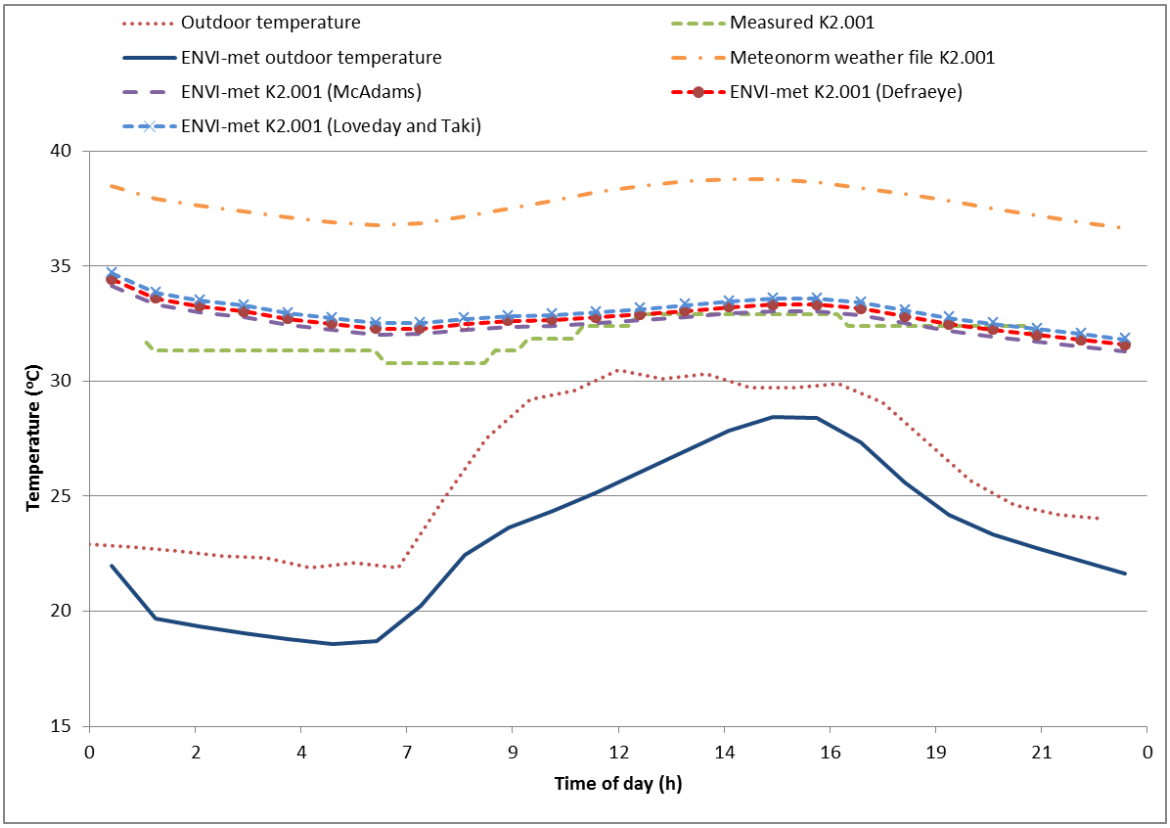

Figure 6.15 Comparison of the room temperature for room K2.001.

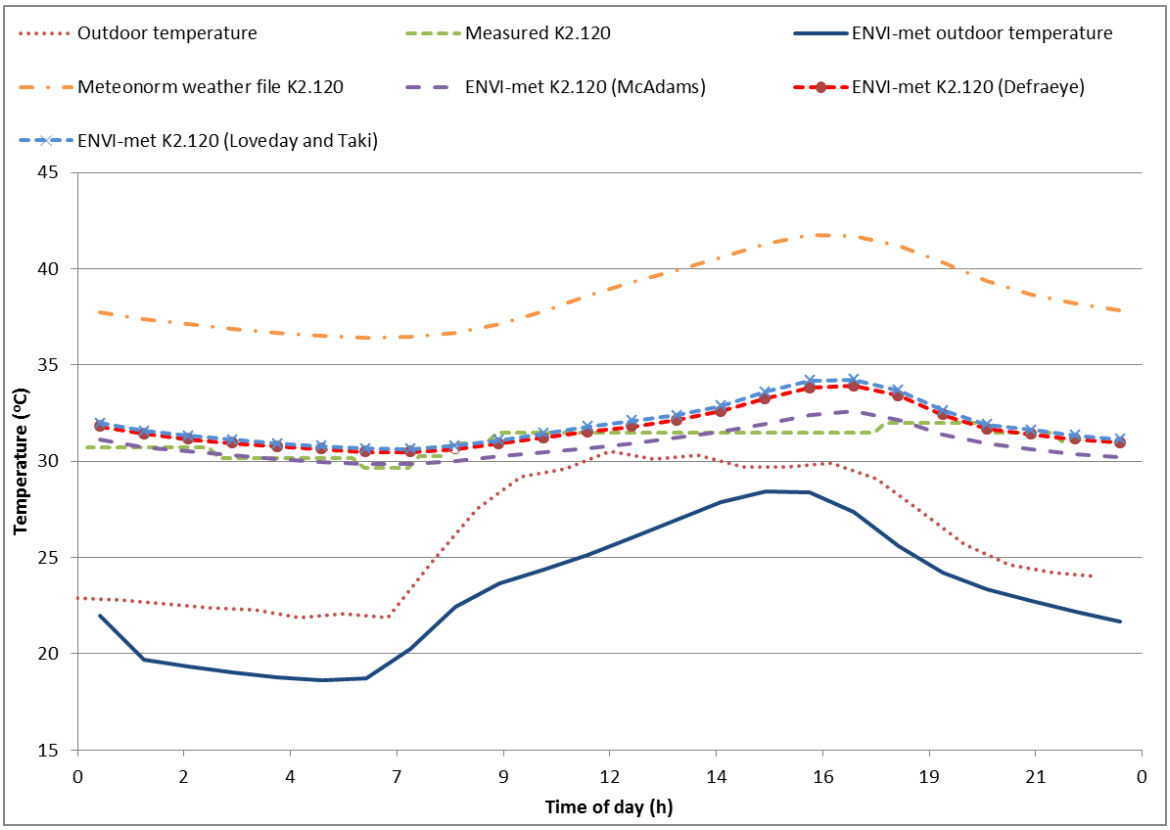

Figure 6.16 Comparison of the room temperature for room K2.120.

Figure 6.15 and Figure 6.16 demonstrate the comparison between the measured room temperature against a) simulated room temperature using the ESP-r weather file generated by Meteonorm and b) simulated room temperature using the weather file generated by ENVI-met combined with the external CHTC calculation for the a, b and c cases of external calculated CHTC. Additionally the outdoor temperature measured at the weather station near the building is presented as well the outdoor temperature from the ENVI-met simulation. As we can see on Figure 6.15 and Figure 6.16 the proposed coupling, simulated more accurately the room temperature than the ESP-r weather file without coupling for both cases. The differences in the room temperature for the 3 examined cases of external calculated CHTC are minimal with an average measured value of room temperature for room K2.001 of 31.82°C and a) 32.77°C, b) 33.00°C, c) 32.50°C for the weather file generated by ENVI-met and combined with the external CHTC calculated by the a) ESP-r implementation of McAdams model, b) calculated for CFD by Defraeye and c) calculated from full-scale measurements by Loveday and Taki. The average room temperature for room K2.120 is 30.84°C and a) 31.68°C, b) 31.91°C, c) 30.83°C respectively. A window is found to be opened during the night of the measurements for room K2.001, which explains the difference during the night. Moreover, we can observe that ENVI-met

simulates the microclimatic conditions of the region and consequently around areas the buildings quite accurately.

6.3.7.1 Simulation in four seasons

Spurred by the above accurate simulation of the rooms temperature additional three typical days are selected, to examine the proposed coupling for different seasons of the year. The selections are based on the meteorological data obtained by the meteorological station in the University campus. In Table 6.8 are the initial meteorological conditions for the four different seasons obtained by the meteorological station. The 24hour simulations are initiated at 00:00.

Table 6.8 Initial meteorological condition for ENVI-met simulations.

Period	Winter	Spring	Summer	Autumn
Air temperature (°C)	12.1	18.1	23.4	19.0
Relative Humidity (%)	80	72	60	80
Wind speed (m/s)	3.7	1.4	4.4	3.8
Wind direction (°)	135	112	135	255

The local microclimatic conditions are used to calculate the difference in the energy consumption of the building. Table 6.9 contains the outdoor temperature provided by the ESP-r weather file and the outdoor temperature calculated by the ENVI-met model as a difference from the outdoor temperature provided by the typical ESP-r weather file along with the heating/cooling rate needed for the two cases. By using the ESP-r weather file an overestimation of 2.5% for the heating requirements during the winter period is found. Moreover, an overestimation of 7.45% and 9.34% for summer and autumn cooling rate respectively is calculated. An underestimation of 8.61% for the cooling power needed for the spring period is calculated. Next a series of simulation are performed by using the external CHTC calculated for the above three cases on all external surfaces.

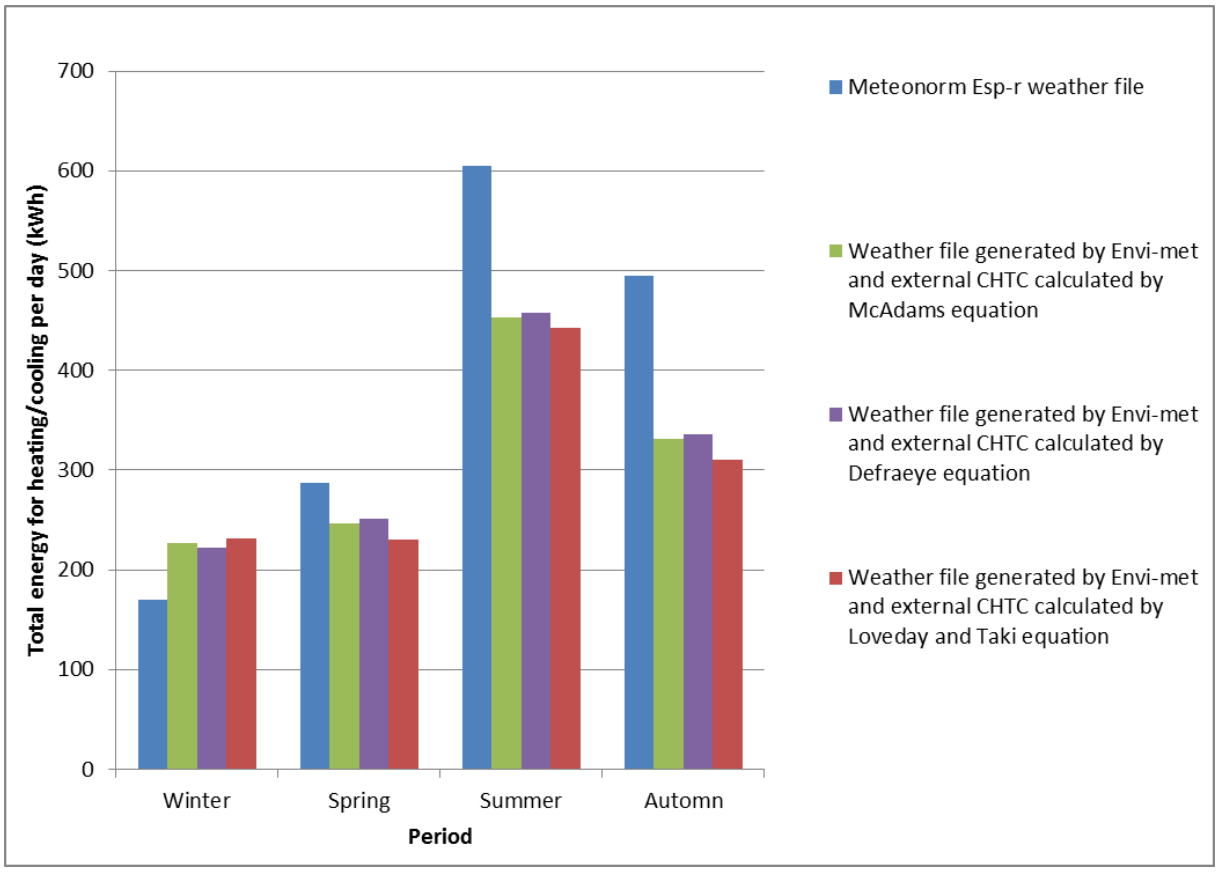

Figure 6.17 Total energy needed for heating/cooling for all period.

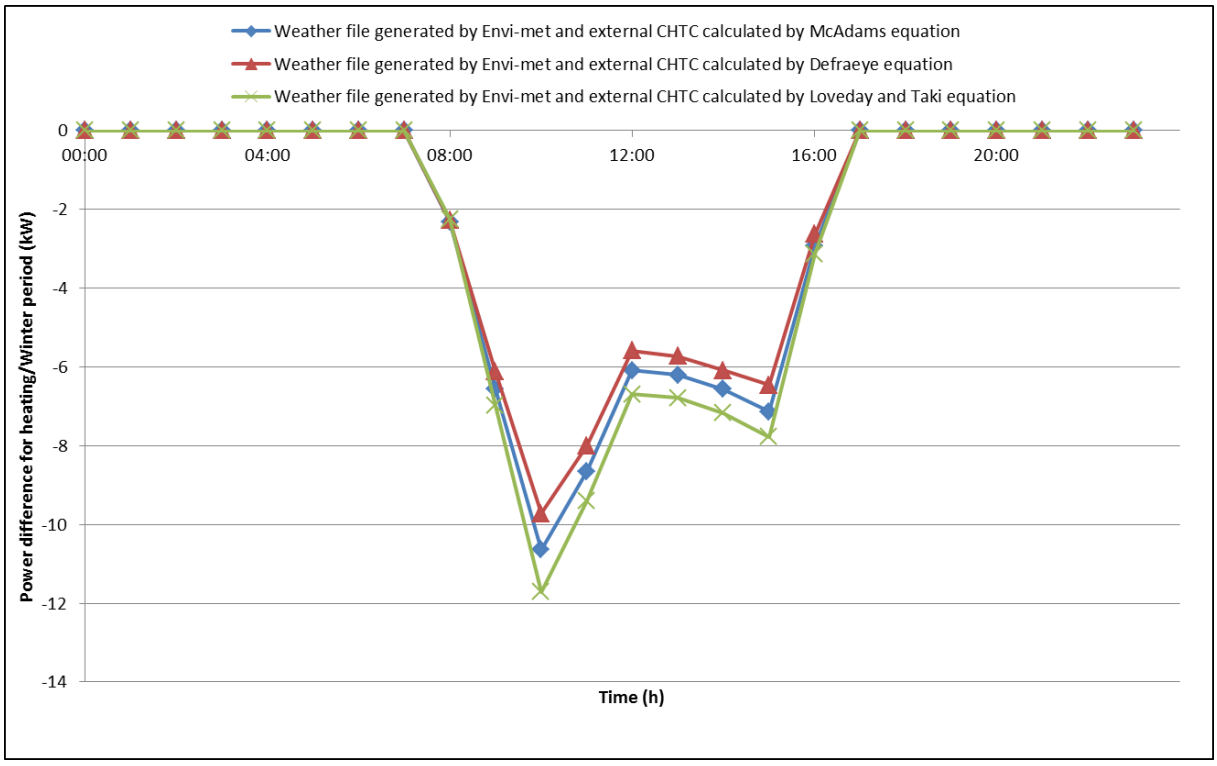

Figure 6.18 Difference in power needed for heating for difference external CHTC for winter period.

Table 6.9 Comparison of outdoor temperature and power for heating/cooling.

Period	Winter				Spring				Summer				Autumn			
Time	ESP-r T_{out} (°C)	Power for Heating (kW)	ΔT (°C)	δ(Power for Heating) (kW)	ESP-r T_{out} (°C)	Power for Cooling (kW)	ΔT (°C)	δ(Power for Cooling) (kW)	ESP-r T_{out} (°C)	Power for Cooling (kW)	ΔT (°C)	δ(Power for Cooling) (kW)	ESP-r T_{out} (°C)	Power for Cooling (kW)	ΔT (°C)	δ(Power for Cooling) (kW)
0:00	10.6	0	-1.5	0	14.2	0	-1.9	0	28.05	0	3.95	0	21.05	0	1.3	0
1:00	10.6	0	-2.8	0	13.9	0	-3.7	0	27.55	0	7.85	0	20.55	0	2.5	0
2:00	10.5	0	-2.3	0	13.8	0	-3.6	0	27.15	0	7.8	0	20.05	0	2.3	0
3:00	10.5	0	-2	0	13.6	0	-3.5	0	26.8	0	7.75	0	19.7	0	2.2	0
4:00	10.4	0	-1.7	0	13.5	0	-3.5	0	26.5	0	7.7	0	19.45	0	2.1	0
5:00	10.4	0	-1.5	0	13.4	0	-3.4	0	26.35	0	7.75	0	19.2	0	2	0
6:00	10.4	0	-1.2	0	13.6	0	-3	0	26.65	0	7.95	0	19.1	0	2.1	0
7:00	10.5	0	-1	0	14.2	0	-2.3	0	27.6	0	7.35	0	19.6	0	2.4	0
8:00	11	14.28	-0.7	0.85	14.8	13.91	-1.8	-0.65	28.85	32.84	6.4	1.77	20.75	24.42	2.8	0.77
9:00	12.2	25.93	-0.6	1.16	15.4	31.8	-1.8	-1.15	30.2	68.59	6.55	4.18	22.05	51.29	3.1	2.03
10:00	13.4	26.36	-0.4	0.8	16	34.65	-2.1	-1.67	31.5	77.78	7.15	6.66	23.25	58.23	3.6	4.96
11:00	14.5	22.84	0.2	0.49	16.5	35.5	-2.3	-2.25	32.65	77.42	7.5	6.37	24.25	62.93	4.1	8.27
12:00	15.4	20.01	0.8	0.01	16.9	34.53	-2.4	-2.56	33.6	77.19	7.55	6.35	25.05	65.01	4.3	8.91
13:00	15.8	19.09	0.9	0.06	17.3	34.68	-2.4	-3.17	34.3	77.39	7.35	6.27	25.65	65.87	4.6	7.19
14:00	16	18.18	1	0.15	17.5	38.48	-2.3	-4.79	34.8	78.37	6.95	6.02	25.95	66.97	4.8	5.81
15:00	16.1	17.01	1.4	0.41	17.5	41.53	-2.2	-5.78	35	78.94	6.55	5.72	25.9	67.3	4.9	5.61
16:00	15.7	6.04	1.7	0.31	17.4	21.94	-1.8	-2.68	34.85	36.17	6.45	1.72	25.5	32.78	5.1	2.67
17:00	15	0	1.9	0	17.1	0	-1.4	0	34.3	0	6.95	0	24.7	0	5	0
18:00	14.5	0	2.1	0	16.7	0	-1.3	0	33.4	0	7.8	0	23.95	0	4.9	0
19:00	14.2	0	2.2	0	16.1	0	-1.6	0	32.4	0	8.2	0	23.4	0	4.6	0
20:00	13.8	0	2.2	0	15.9	0	-1.6	0	31.35	0	8	0	22.8	0	4.3	0
21:00	13.5	0	2.1	0	16	0	-1.3	0	30.25	0	7.5	0	22.25	0	4	0
22:00	13.2	0	2	0	15.9	0	-1.2	0	29.2	0	7	0	21.7	0	3.6	0
23:00	12.8	0	1.8	0	15.9	0	-1.1	0	28.15	0	6.5	0	21.1	0	3.2	0

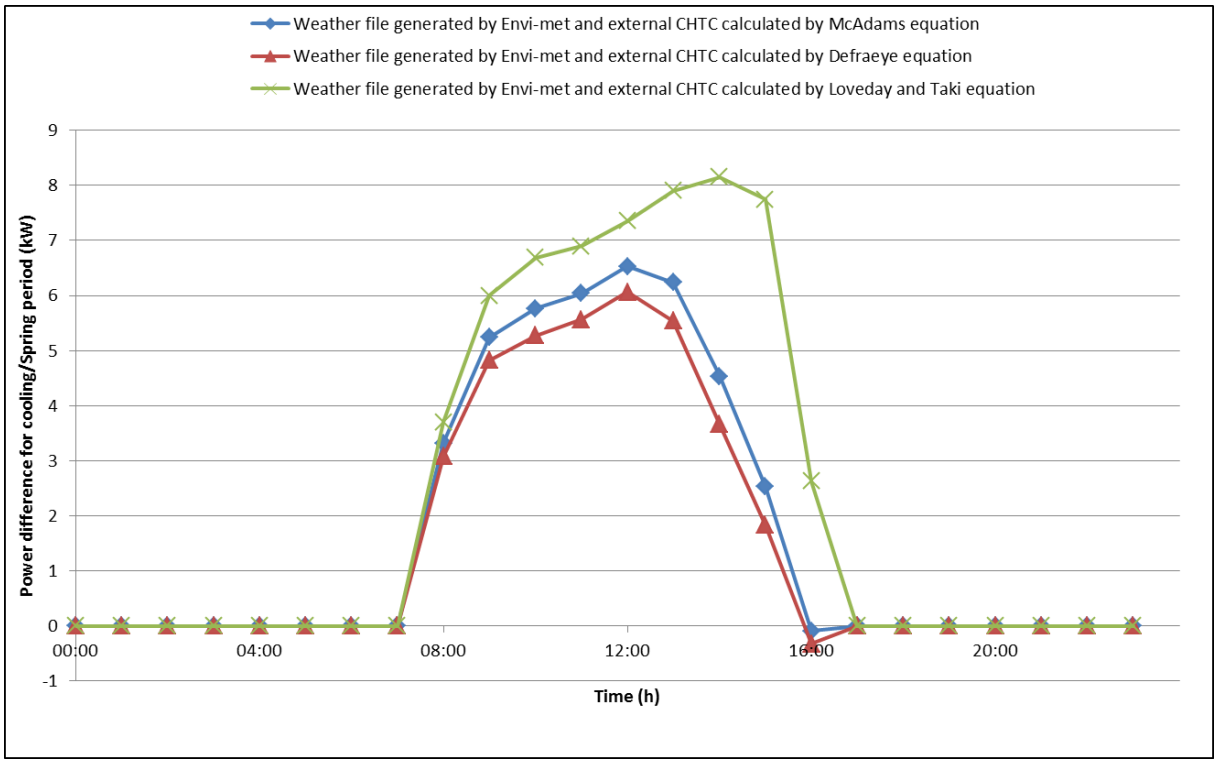

Figure 6.19 Difference in power needed for cooling for difference external CHTC for spring period.

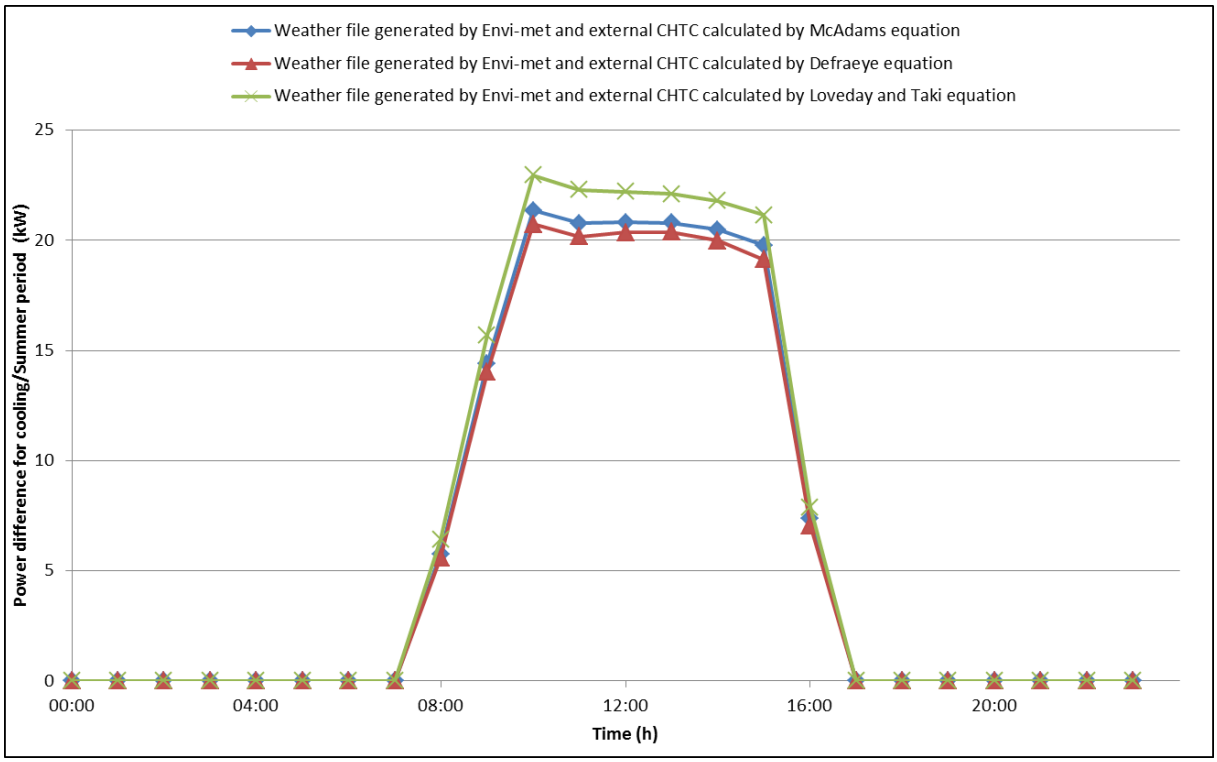

Figure 6.20 Difference in power needed for cooling for difference external CHTC for summer period.

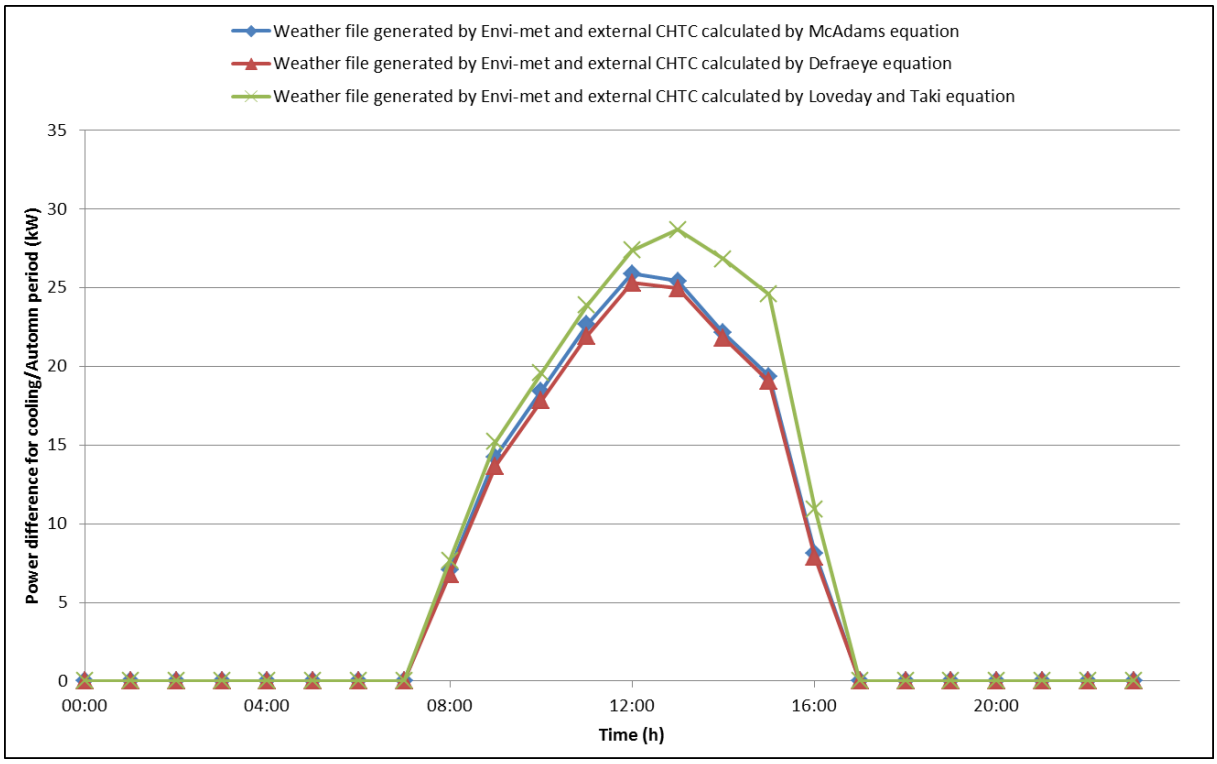

Figure 6.21 Difference in power needed for cooling for difference external CHTC for autumn period.

Figure 6.17 shows the total energy needed for heating/cooling for the four different periods. For three of the four cases spring/summer/autumn the typical ESP-r implementation overestimates the cooling energy. For the winter period the typical ESP-r implementation underestimates the heating energy needed by the building. Figures 6.18 to 6.21 present the difference in power required for heating/cooling for the four investigated cases and in the four seasons. The difference is calculated by subtracting the required power when simulation is performed using the ESP-r weather file generated by Meteonorm and internally calculated external CHTC for all external surfaces by the weather file as well as external CHTC generated by ENVI-met data.

Table 6.10 Comparison of difference in power needed for heating/cooling.

Period	Winter		Spring	
	Difference in energy needed for heating (kWh)	Percentage of change (%)	Difference in energy needed for cooling (kWh)	Percentage of change (%)
McAdams	-57.13	33.66	40.10	13.97
Defraeye	-52.64	31.01	35.50	12.37
Loveday and Taki	-61.93	36.49	57.05	19.88

Period	Summer		Autumn	
	Difference in energy needed for cooling (kWh)	Percentage of change (%)	Difference in energy needed for cooling (kWh)	Percentage of change (%)
McAdams	151.55	25.06	163.31	33.01
Defraeye	147.46	24.39	159.17	32.17
Loveday and Taki	162.51	26.87	184.66	37.32

Tabulated in Table 6.10 is the difference in energy needed for heating/cooling. An underestimation of 31-36% is calculated by the ESP-r for heating energy needed during winter. An overestimation of 12–19%, 24-26% and 32–37% is calculated for the cooling energy needed in spring, summer and autumn periods respectively. Especially for the spring period, despite the underestimation of 8.61% for the cooling energy if only the ENVI-met weather file is used, an overestimation of 12 – 19 % is calculated when the external calculated CHTC is included in the model. In all of the cases, greater difference is observed by using the Loveday and Taki equations followed by McAdmas and Defraey. These results also agree with the calculated CHTC values for the 3 methods as shown in Figure 6.13 and for low wind speeds that exist in the case study area as seen in Table 6.8. The influence of the combination of weather file generated by ENVI-met and external calculated CHTC is 2 to 4 times greater than running the BES simulation only with the weather file generated by ENVI-met.

6.3.8 Integration of developed cool coatings to the case study

The next step in the investigation is to introduce to the coupling methodology the developed coatings from Chapter 3. The cool coating will replace the outer layer of the buildings external walls for both ESP-r and ENVI-met domains. The large number of different (22 values) SR values that are developed in Chapter 3 and long computation time for ENVI-met simulation ($\tilde{6}$0 hours of actual running time with a Intel i7-3770 per 24 hours of simulation) resulted to the reduction of different SR values to three. The biggest, smallest and an intermediate SR values are chosen.

Firstly, the ENVI-met simulation is performed. A total of 16 simulations are performed (4 different SR values * 4 seasons) for the following SR values:

- 0.90 (WCM-DMP-GB)
- 0.79 (NHL–DMP, NHL-DMP-GB)
- 0.66 (NHL-QUA)
- 0.30 (Portland Cement, ENVI-met default value)

The impact of the use of the developed cool coatings is investigated below. The difference in average air temperature (at 1.8 m hight) from the reference SR value is calculated. As shown in Figure 6.22 around the K2 building 20 points are used to calculate the average air temperature. Tabulated on Table 6.11 is calculated the deference between the average air temperature of the different SR values and the IE.

Table 6.11 Difference in average air temperature around the K2 buildings (°C).

Periode	Solar Reflectance		
	0.9	0.79	0.66
Winter	0.010	0.008	0.006
Spring	0.047	0.038	0.027
Summer	0.028	0.023	0.017
Autumn	0.006	0.007	0.005

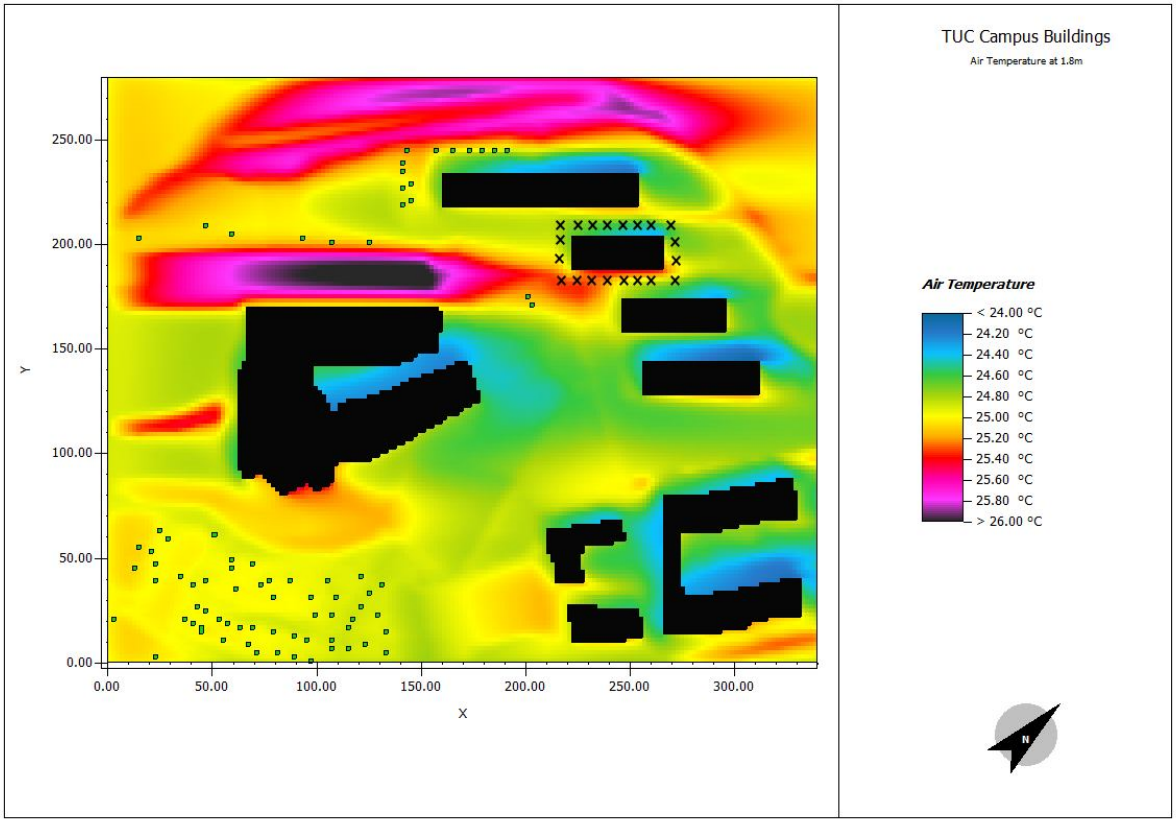

Figure 6.22 Point for calculating the temperature change around the building.

The methodology described in Section 6.3.6 is used to couple the two domains, ESP-r and ENVI-met for the four different SR values. Two different cases for each one of the four different SR values and three CHTC calculation methods are developed for the ESP-r domain. For the first case, only the SR value of the outer layer of the external envelope (both vertical wall and roof) of the K2 building is changed. For the second case, the SR value of the outer layer of the external surface is changed, a updated weather file is used generated from the ENVI-met simulation (Item 7) and one of the three different CHTC calculation methods with the use of ENVI-met data is used to generate the CHTC values (both vertical wall and roof) for all external surfaces are included. A total of 64 ESP-r simulations (4 different SR values * 4 seasons + 4 different SR values * 4 seasons * 3 different CHTC calculation methods) are conducted.

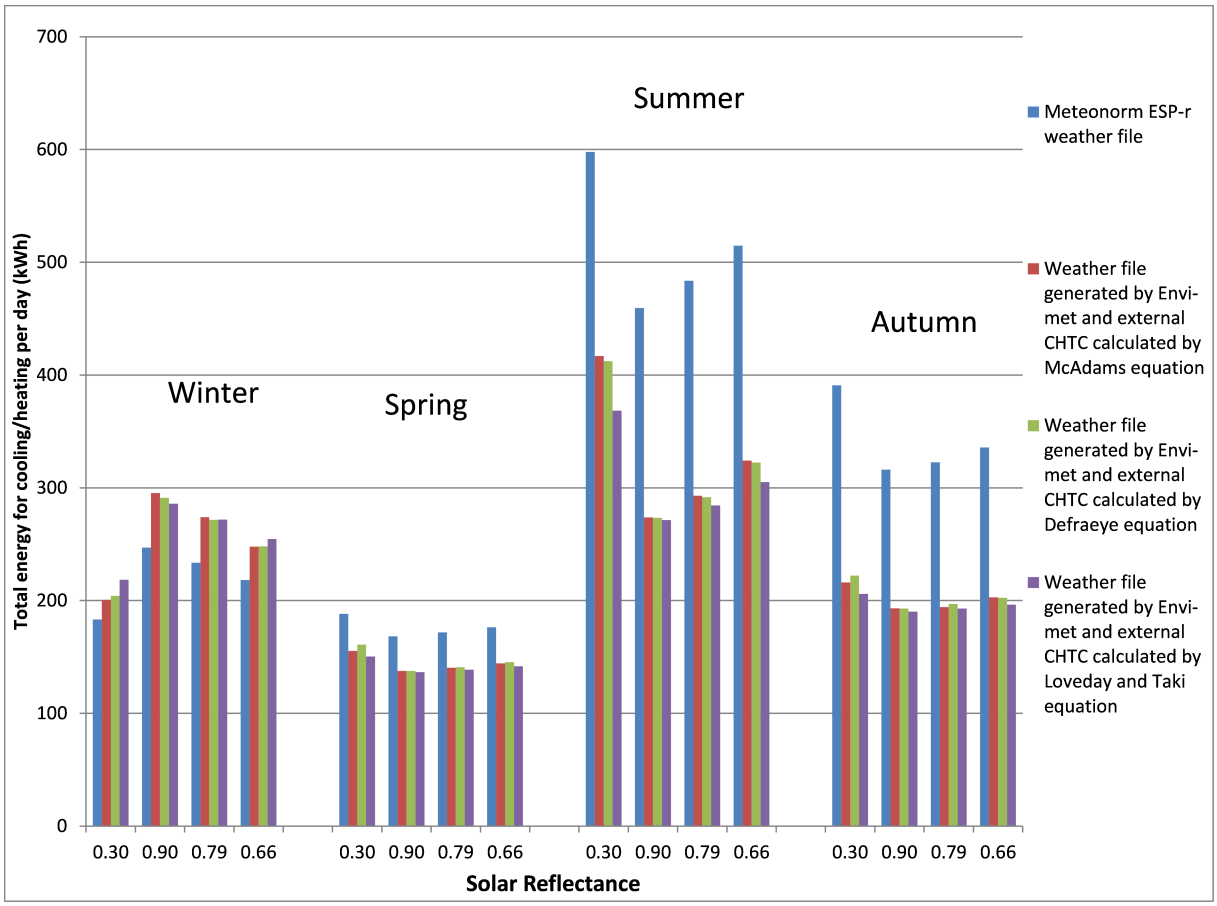

Figure 6.23 Total energy needed for heating/cooling different SR values and all seasons.

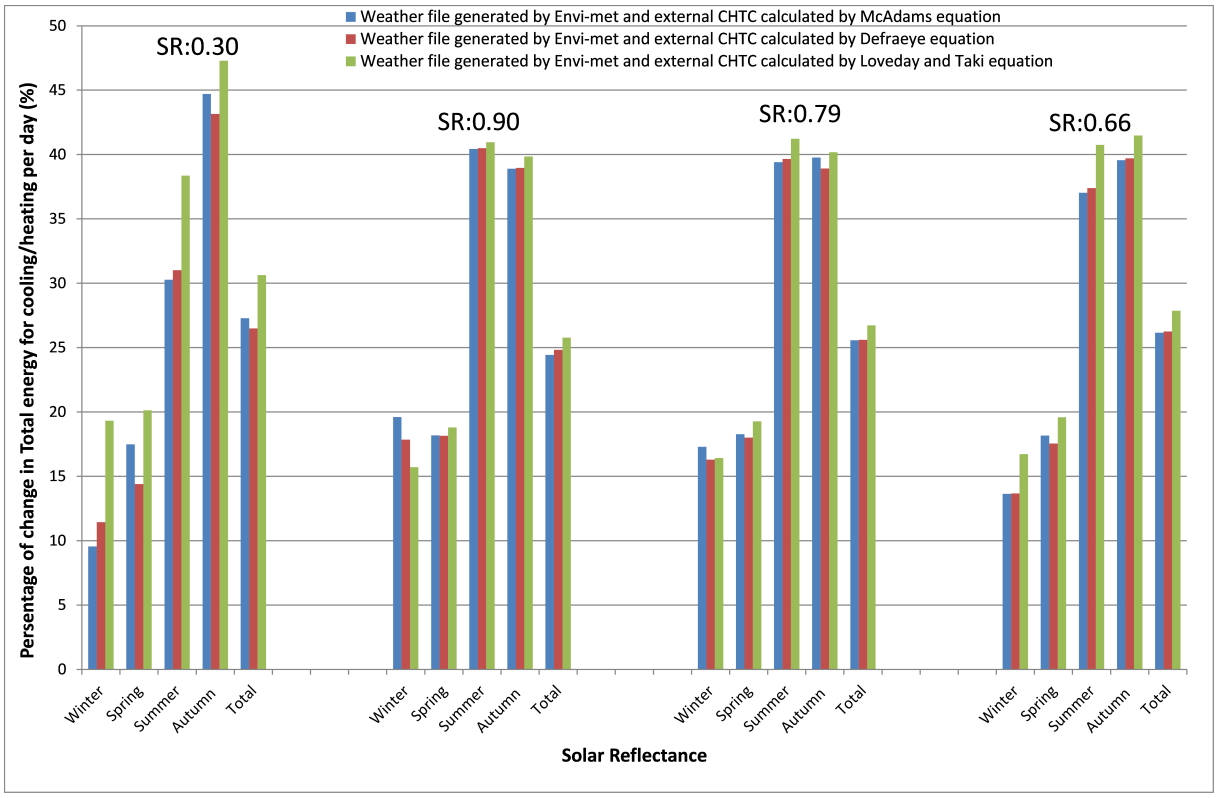

Figure 6.24 Percentage of change in total energy needed for heating/cooling for different SR values and all seasons.

Figure 6.23 shows the total energy needed for heating/cooling for the four different SR values and four seasons. The results confirm the initial conclusions for all four different SR values where three of the four seasons spring/summer/autumn the typical ESP-r weather file overestimates the cooling energy.

Figure 6.24 presents the percentage of change in total energy needed for heating/cooling for different SR values and periods. The difference is calculated by subtracting the required energy when the simulation is performed by ESP-r weather file generated by Meteonorm and internally calculated external CHTC for all external surfaces by the weather file as well as external CHTC generated by ENVI-met data. In Table 6.12 is the difference in peak power needed for heating /cooling and the percentage of change. The percentage difference in total energy for heating by the three methods of external calculating the CHTC depends on the SR value. The column labelled 'Total' is determined by aggregate the heating/cooling energy for the four seasons.

For the winter season and SR=0.30 the maximum difference is calculated by using Loveday and Taki equation while for SR= 0.90 by McAdams equation the lower difference. An underestimation of 10 - 20% for the heating energy is calculated. For the spring season for all SR values the smaller difference is calculated by using the Defreaye equation, followed by McAdams and Loveday and Taki. For the summer period the smaller difference is calculated by using the McAdams equations, followed by Defreaye and Loveday and Taki. For the autumn season and SR=0.30, 0.78 the minimum difference is calculated using the Defreaye equation while for SR=0.66, 0.90 by using the McAdams equation. An underestimation of 14 - 20%, 30 - 41 % and 39 - 47% for the cooling energy is calculated for spring, summer and autumn period

respectively. In most cases the biggest difference in total energy is calculated by using the Loveday and Taki equation. The SR values effects the calculation of the total energy needed for heating/cooling using external calculated CHTC in a no predictive manner although with no substantial difference between the three methods of external calculated CHTC.

Table 6.12 Comparison of difference in power needed for heating/cooling by different SR values and seasons.

Peroid	Winter						Spring					
	Difference in power needed for heating (kW)			Percentage of change (%)			Difference in power needed for cooling (kW)			Percentage of change (%)		
SR	McAdams	Defraeye	Loveday and Taki	McAdams	Defraeye	Loveday and Taki	McAdams	Defraeye	Loveday and Taki	McAdams	Defraeye	Loveday and Taki
0.30	-17.49	-20.96	-35.39	9.55	11.44	19.32	32.90	27.09	37.86	17.49	14.40	20.12
0.90	-48.44	-44.07	-38.81	19.61	17.84	15.71	30.58	30.52	31.62	18.18	18.15	18.80
0.79	-40.39	-38.05	-38.35	17.30	16.30	16.42	31.41	30.93	33.11	18.29	18.01	19.27
0.66	-29.76	-29.81	-36.48	13.64	13.66	16.72	32.03	30.96	34.55	18.16	17.55	19.59
Peroid	Summer						Autumn					
	Difference in power needed for cooling (kW)			Percentage of change (%)			Difference in power needed for cooling (kW)			Percentage of change (%)		
SR	McAdams	Defraeye	Loveday and Taki	McAdams	Defraeye	Loveday and Taki	McAdams	Defraeye	Loveday and Taki	McAdams	Defraeye	Loveday and Taki
0.30	180.95	185.45	229.36	30.27	31.02	38.37	174.73	168.65	184.81	44.71	43.16	47.29
0.90	185.82	186.10	188.16	40.44	40.50	40.95	122.95	123.18	125.96	38.90	38.97	39.85
0.79	190.58	191.81	199.34	39.41	39.66	41.22	128.30	125.52	129.62	39.77	38.91	40.19
0.66	190.61	192.48	209.74	37.03	37.39	40.74	132.85	133.29	139.26	39.57	39.70	41.48
Peroid	Total											
	Difference in power needed for cooling (kW)			Percentage of change (%)								
SR	McAdams	Defraeye	Loveday and Taki	McAdams	Defraeye	Loveday and Taki						
0.30	371.09	360.24	416.64	27.29	26.49	30.64						
0.90	290.91	295.73	306.94	24.43	24.83	25.78						
0.79	309.90	310.21	323.73	25.58	25.61	26.72						
0.66	325.73	326.92	347.05	26.16	26.26	27.87						

Chapter 7

Conclusions and further research

In the present thesis a series of cool and thermochromic coatings are developed and tested.

Concerning the inorganic cool coatings, their thermal and optical properties, as well as their contribution to energy conservation is examined. The main results demonstrate that the higher the solar reflectance, the higher the surface temperature reduction during the day. This surface temperature reduction can be almost 7K compared to conventional samples. More specifically, the coatings that are composed by either dolomite or limestone marble powder with the addition of glass beads can reduce significantly the surface temperature of the samples when exposed to the outdoor conditions. The use of hydraulic lime enhances the infrared emittance of the coatings contributing to a considerable reduction of the surface temperature of samples with lower solar reflectance. All coatings contribute to the energy efficiency of both well and poor insulated buildings by 5-14% on annual basis.

As far as the thermochromic coatings is concerned, all developed coatings demonstrate higher solar reflectance, higher infrared emittance and lower surface temperatures compared to conventional samples. The surface temperature of the thermochromic samples can be up to 5.5K lower than the conventional samples with the same colour. Solar reflectance and infrared emittance are coatings' properties that may change over time as a result of ageing, soil and dust deposition. The testing of the cool inorganic coatings developed in the present thesis showed a limited reduction of solar reflectance and infrared emittance. The same applies for the cool inorganic thermochromic coatings. The only coating that aged solar reflectance is more than 10% lower than the initial one, is the one where glass beads are included. Overall the samples with white Portland cement reported higher decrease in solar reflectance than the samples with natural hydraulic lime with pozzolanic additives as a binder. On the other hand all organic thermochromic coatings demonstrate severe ageing when exposed to solar radiation. Moreover, the coverage of the inorganic thermochromic samples with the polyurethane varnish reduced the ageing effect by 50% compared with the samples with no protecting coverage.

Finally the indoor – outdoor environment coupling mechanism presented in Chapter 6 showed the importance of the inclusion of microclimatic conditions in the buildings' energy simulations. A difference of ±10% in power for heating/cooling needs are pinpointed when the weather file typically used in building

simulations is replaced by the local microclimatic conditions' file. In addition if Convective Heat Transfer is calculated based on the microclimatic conditions, the difference in heating/cooling demands extracted can be as high as ±40%.

Finally, further future research effort should be put in:

- Examine the structural properties of the developed coating, mechanical compressive strength and tensile strength.
- Develop colour mineral based cool coatings with the addition on inorganic colour dyes.
- Use spectrally selective filters and design thermochromic coatings' filters.
- Test the coupling mechanism for different climate conditions, buildings topologies and locations (inside high populated city, rural area).

Bibliography

[1] Philippe Bocquier. World urbanization prospects: An alternative to the UN model of projection compatible with the mobility transition theory. *Demographic Research*, 12:197–236, 2005.

[2] Karel Neels and David De Wachter. Postponement and recuperation of Belgian fertility: How are they related to rising female educational attainment? *Vienna Yearbook of Population Research*, 27(1):77–106, 2010.

[3] Qihao Weng, Dengsheng Lu, and Jacquelyn Schubring. Estimation of land surface temperature-vegetation abundance relationship for urban heat island studies. *Remote Sensing of Environment*, 89(4):467–483, February 2004.

[4] M. Santamouris. Heat island research in Europe: The state of the art. *Advances in Building Energy Research*, 1(1):123–150, 2007.

[5] D. Kolokotsa, A. Psomas, and E. Karapidakis. Urban heat island in southern Europe: The case study of Hania, Crete. *Solar Energy*, 83(10):1871–1883, oct 2009.

[6] M. Santamouris, N. Papanikolaou, I. Livada, I. Koronakis, C. Georgakis, A. Argiriou, and D. N. Assimakopoulos. On the impact of urban climate on the energy consuption of building. *Solar Energy*, 70(3):201–216, 2001.

[7] Soushi Kato and Yasushi Yamaguchi. Analysis of urban heat-island effect using ASTER and ETM+ Data: Separation of anthropogenic heat discharge and natural heat radiation from sensible heat flux. *Remote Sensing of Environment*, 99(1-2):44–54, 2005.

[8] Haider Taha. Urban climates and heat islands: albedo, evapotranspiration, and anthropogenic heat. *Energy and Buildings*, 25(2):99–103, 1997.

[9] V. Ramanathan and Y. Feng. Air pollution, greenhouse gases and climate change: Global and regional perspectives. *Atmospheric Environment*, 43(1):37–50, 2009.

[10] S. A. Montzka, E. J. Dlugokencky, and J. H. Butler. Non-CO 2 greenhouse gases and climate change. *Nature*, 476(7358):43–50, 2011.

[11] T. R. Oke. The energetic basis of the urban heat island. *Quarterly Journal of the Royal Meteorological Society*, 108(455):1–24, 1982.

[12] A Mavrogianni, M Davies, P Wilkinson, and A Pathan. LONDON HOUSING AND CLIMATE CHANGE: Impact on Comfort and Health - Preliminary Results of a Summer Overheating Study, 2010.

[13] Umberto Berardi. Building Energy Consumption in US, EU, and BRIC Countries. In *Procedia Engineering*, volume 118, pages 128–136, 2015.

[14] Hashem Akbari, Susan Davis, Sofia Dorsano, Joe Huang, and Steven Winnett. Cooling our communities. a guidebook on tree planting and light-colored surfacing. Technical report, EPA, January 1992.

[15] M. Santamouris, A. Synnefa, and T. Karlessi. Using advanced cool materials in the urban built environment to mitigate heat islands and improve thermal comfort conditions. *Solar Energy*, 85(12):3085 – 3102, 2011. Progress in Solar Energy 2.

[16] A. Synnefa, T. Karlessi, N. Gaitani, M. Santamouris, D. N. Assimakopoulos, and C. Papakatsikas. Experimental testing of cool colored thin layer asphalt and estimation of its potential to improve the urban microclimate. *Building and Environment*, 46(1):38–44, 2011.

[17] A. Synnefa, M. Santamouris, and K. Apostolakis. On the development, optical properties and thermal performance of cool colored coatings for the urban environment. *Solar Energy*, 81(4):488–497, 2007.

[18] A. Synnefa, M. Santamouris, and H. Akbari. Estimating the effect of using cool coatings on energy loads and thermal comfort in residential buildings in various climatic conditions. *Energy and Buildings*, 39(11):1167–1174, 2007.

[19] Edward Ng, Liang Chen, Yingna Wang, and Chao Yuan. A study on the cooling effects of greening in a high-density city: An experience from Hong Kong. *Building and Environment*, 47(1):256–271, 2012.

[20] I. Zoulia, M. Santamouris, and A. Dimoudi. Monitoring the effect of urban green areas on the heat island in Athens. *Environmental Monitoring and Assessment*, 156(1-4):275–292, 2009.

[21] S.E Gill, J.F Handley, A.R Ennos, and S Pauleit. Adapting Cities for Climate Change: The Role of the Green Infrastructure. *Built Environment*, 33(1):115–133, 2007.

[22] Mattheos Santamouris and Dionysia Kolokotsa. Passive cooling dissipation techniques for buildings and other structures: The state of the art. *Energy and Buildings*, 57:74 – 94, 2013.

[23] G. Mihalakakou, M. Santamouris, and D. Asimakopoulos. Use of the ground for heat dissipation. *Energy*, 19(1):17–25, 1994.

[24] Yuan Ma, Zhilong He, Xueyuan Peng, and Ziwen Xing. Experimental investigation of the discharge valve dynamics in a reciprocating compressor for trans-critical CO2refrigeration cycle. *Applied Thermal Engineering*, 32(1):13–21, 2012.

[25] Jan F. Kreider, Peter. Curtiss, and Ari. Rabl. *Heating and cooling of buildings : design for efficiency.* Mechanical and Aerospace Engineering Series. CRC Press, 2010.

[26] Sarah E. Bretz and Hashem Akbari. Long-term performance of high-albedo roof coatings. *Energy and Buildings*, 25(2):159–167, jan 1997.

[27] A. Synnefa, M. Santamouris, and I. Livada. A study of the thermal performance of reflective coatings for the urban environment. *Solar Energy*, 80(8):968–981, 2006.

[28] Martyn S. Ray. Thermal Radiation Heat Transfer, 3rd edn, by R. Siegel and J.R. Howell, Hemisphere Publishing Corporation, USA (1992). 1072 pages. ISBN 0-89116-271-2. *Developments in Chemical Engineering and Mineral Processing*, 2(2-3):190–190, 2008.

[29] A. Synnefa, M. Saliari, and M. Santamouris. Experimental and numerical assessment of the impact of increased roof reflectance on a school building in Athens. *Energy and Buildings*, 55(0):7–15, 2012.

[30] ASTM E1980 - 11. Standard practice for calculating solar reflectance index of horizontal and low-sloped opaque surfaces, 2011.

[31] Linshuang Long, Hong Ye, Haitao Zhang, and Yanfeng Gao. Performance demonstration and simulation of thermochromic double glazing in building applications. *Solar Energy*, 120:55–64, oct 2015.

[32] Jian Lei Wang, Yuan Qing Li, Young Ji Byon, Shi Gang Mei, and Guang Lei Zhang. Synthesis and characterization of NiTiO3yellow nano pigment with high solar radiation reflection efficiency. *Powder Technology*, 235:303–306, 2013.

[33] Aijun Han, Mingquan Ye, Lili Liu, Wei Feng, and Minchun Zhao. Estimating thermal performance of cool coatings colored with high near-infrared reflective inorganic pigments: Iron doped La2Mo2O7compounds. *Energy and Buildings*, 84:698–703, 2014.

[34] Kai L. Uemoto, Neide M.N. Sato, and Vanderley M. John. Estimating thermal performance of cool colored paints. *Energy and Buildings*, 42(1):17–22, 2010.

[35] A. L. Pisello, V. L. Castaldo, G. Pignatta, F. Cotana, and M. Santamouris. Experimental in-lab and in-field analysis of waterproof membranes for cool roof application and urban heat island mitigation. *Energy and Buildings*, 114:180–190, 2016.

[36] Gian Marco Revel, Milena Martarelli, Marco Emiliani, Luca Celotti, Riccardo Nadalini, Antonio De Ferrari, Sacha Hermanns, and Erwin Beckers. Cool products for building envelope - Part II: Experimental and numerical evaluation of thermal performances. *Solar Energy*, 105:780–791, 2014.

[37] P. Ramamurthy, T. Sun, K. Rule, and E. Bou-Zeid. The joint influence of albedo and insulation on roof performance: A modeling study. *Energy and Buildings*, 102:317–327, 2015.

[38] C. Ferrari, A. Muscio, C. Siligardi, and T. Manfredini. Design of a cool color glaze for solar reflective tile application. *Ceramics International*, 41(9):11106–11116, 2015.

[39] M. Marangoni, B. Nait-Ali, D. S. Smith, M. Binhussain, P. Colombo, and E. Bernardo. White sintered glass-ceramic tiles with improved thermal insulation properties for building applications. *Journal of the European Ceramic Society*, 37(3):1117–1125, 2017.

[40] Ronnen Levinson, Hashem Akbari, Paul Berdahl, Kurt Wood, Wayne Skilton, and Jerry Petersheim. A novel technique for the production of cool colored roofing materials. *Asphalt*, 94(6):0–2, 2010.

[41] Anna Laura Pisello, Veronica Lucia Castaldo, Cristina Piselli, Gloria Pignatta, and Franco Cotana. Combined thermal effect of cool roof and cool façade on a prototype building. In *Energy Procedia*, volume 78, pages 1556–1561, 2015.

[42] Ronnen Levinson, Sharon Chen, Paul Berdahl, Pablo Rosado, and Louis A. Medina. Reflectometer measurement of roofing aggregate albedo. *Solar Energy*, 100:159–171, 2014.

[43] V. L. Castaldo, V. Coccia, F. Cotana, G. Pignatta, A. L. Pisello, and F. Rossi. Thermal-energy analysis of natural "cool" stone aggregates as passive cooling and global warming mitigation technique. *Urban Climate*, 14:301–314, dec 2015.

[44] Federica Rosso, Anna Laura Pisello, Franco Cotana, and Marco Ferrero. On the thermal and visual pedestrians' perception about cool natural stones for urban paving: A field survey in summer conditions. *Building and Environment*, 107:198–214, 2016.

[45] Anna Laura Pisello, Gloria Pignatta, Veronica Lucia Castaldo, and Franco Cotana. Experimental analysis of natural gravel covering as cool roofing and cool pavement. *Sustainability (Switzerland)*, 6(8):4706–4722, 2014.

[46] Federica Rosso, Anna Laura Pisello, Weihua Jin, Masoud Ghandehari, Franco Cotana, and Marco Ferrero. Cool marble building envelopes: The effect of aging on energy performance and aesthetics. *Sustainability (Switzerland)*, 8(8), 2016.

[47] Anna Laura Pisello, Federico Rossi, and Franco Cotana. Summer and winter effect of innovative cool roof tiles on the dynamic thermal behavior of buildings. *Energies*, 7(4):2343–2361, 2014.

[48] T. Karlessi, M. Santamouris, K. Apostolakis, A. Synnefa, and I. Livada. Development and testing of thermochromic coatings for buildings and urban structures. *Solar Energy*, 83(4):538–551, 2009.

[49] Yiping Ma and Beirong Zhu. Research on the preparation of reversibly thermochromic cement based materials at normal temperature. *Cement and Concrete Research*, 39(2):90–94, 2009.

[50] Arno Seeboth, Ralf Ruhmann, and Olaf Mühling. Thermotropic and thermochromic polymer based materials for adaptive solar control. *Materials*, 3(12):5143–5168, 2010.

[51] M. Santamouris, A. Synnefa, D. Kolokotsa, V. Dimitriou, and K. Apostolakis. Passive cooling of the built environment - Use of innovative reflective materials to fight heat islands and decrease cooling needs. *International Journal of Low Carbon Technologies*, 3(2):71–82, 2008.

[52] Paul Berdahl, Hashem Akbari, Ronnen Levinson, and William A. Miller. Weathering of roofing materials – an overview. *Construction and Building Materials*, 22(4):423 – 433, 2008.

[53] Paul Berdahl, Hashem Akbari, and Leanna S Rose. Aging of reflective roofs: soot deposition. *Applied optics*, 41(12):2355–60, 2002.

[54] Riccardo Paolini, Michele Zinzi, Tiziana Poli, Emiliano Carnielo, and Andrea Giovanni Mainini. Effect of ageing on solar spectral reflectance of roofing membranes: Natural exposure in Roma and Milano and the impact on the energy needs of commercial buildings. *Energy and Buildings*, 84:333–343, 2014.

[55] Mohamad Sleiman, George Ban-Weiss, Haley E. Gilbert, David François, Paul Berdahl, Thomas W. Kirchstetter, Hugo Destaillats, and Ronnen Levinson. Soiling of building envelope surfaces and its effect on solar reflectance - Part I: Analysis of roofing product databases. *Solar Energy Materials and Solar Cells*, 95(12):3385–3399, 2011.

[56] Mohamad Sleiman, Thomas W. Kirchstetter, Paul Berdahl, Haley E. Gilbert, Sarah Quelen, Lea Marlot, Chelsea V. Preble, Sharon Chen, Amandine Montalbano, Olivier Rosseler, Hashem Akbari, Ronnen Levinson, and Hugo Destaillats. Soiling of building envelope surfaces and its effect on solar reflectance - Part II: Development of an accelerated aging method for roofing materials. *Solar Energy Materials and Solar Cells*, 122:271–281, 2014.

[57] Mohamad Sleiman, Sharon Chen, Haley E. Gilbert, Thomas W. Kirchstetter, Paul Berdahl, Erica Bibian, Laura S. Bruckman, Dominic Cremona, Roger H. French, Devin A. Gordon, Marco Emiliani, Justin Kable, Liyan Ma, Milena Martarelli, Riccardo Paolini, Matthew Prestia, John Renowden, Gian Marco Revel, Olivier Rosseler, Ming Shiao, Giancarlo Terraneo, Tammy Yang, Lingtao Yu, Michele Zinzi, Hashem Akbari, Ronnen Levinson, and Hugo Destaillats. Soiling of building envelope surfaces and its effect on solar reflectance - Part III: Interlaboratory study of an accelerated aging method for roofing materials. *Solar Energy Materials and Solar Cells*, 143:581–590, 2015.

[58] Cool Roof Rating Council. Cool Roof Rating Council, 2018.

[59] B. Givoni, M. E. Hoffman, Makhon tekhnologi le-Yisrael. Tekhniyon, and Tahanah le-heker ha beniyah. *Effect of building materials on internal temperatures*. Haifa, Israel, 1968.

[60] E. Bozonnet, M. Doya, and F. Allard. Cool roofs impact on building thermal response: A French case study. *Energy and Buildings*, 43(11):3006–3012, 2011.

[61] C. Romeo and M. Zinzi. Impact of a cool roof application on the energy and comfort performance in an existing non-residential building. A Sicilian case study. *Energy and Buildings*, 67:647–657, 2013.

[62] M. Kolokotroni, B. L. Gowreesunker, and R. Giridharan. Cool roof technology in London: An experimental and modelling study. *Energy and Buildings*, 67:658–667, 2013.

[63] Anna Laura Pisello and Franco Cotana. The thermal effect of an innovative cool roof on residential buildings in Italy: Results from two years of continuous monitoring. *Energy and Buildings*, 69:154–164, 2014.

[64] Pablo J. Rosado, David Faulkner, Douglas P. Sullivan, and Ronnen Levinson. Measured temperature reductions and energy savings from a cool tile roof on a central California home. *Energy and Buildings*, 80:57–71, 2014.

[65] G. M. Stavrakakis, A. V. Androutsopoulos, and J. Vyörykkä. Experimental and numerical assessment of cool-roof impact on thermal and energy performance of a school building in Greece. *Energy and Buildings*, 130:64–84, 2016.

[66] Ronnen Levinson, Paul Berdahl, and Hashem Akbari. Solar spectral optical properties of pigments - Part II: Survey of common colorants. *Solar Energy Materials and Solar Cells*, 89(4):351–389, 2005.

[67] Wendy Miller, Glenn Crompton, and John Bell. Analysis of cool roof coatings for residential demand side management in tropical Australia. *Energies*, 8(6):5303–5318, 2015.

[68] Hashem Akbari, Sarah Bretz, Dan M. Kurn, and James Hanford. Peak power and cooling energy savings of high-albedo roofs. *Energy and Buildings*, 25(2):117–126, 1997.

[69] Yinghong Qin. A review on the development of cool pavements to mitigate urban heat island effect. *Renewable and Sustainable Energy Reviews*, 52:445–459, 2015.

[70] Valentina Dessì. Urban materials for comfortable open spaces. In *Proceedings of the World Renewable Energy Congress – Sweden, 8–13 May, 2011, Linköping, Sweden*, pages 3300–3307. Linköping University Electronic Press, 11 2011.

[71] Pablo Campra, Monica Garcia, Yolanda Canton, and Alicia Palacios-Orueta. Surface temperature cooling trends and negative radiative forcing due to land use change toward greenhouse farming in southeastern Spain. *Journal of Geophysical Research Atmospheres*, 113(18):D18109, sep 2008.

[72] Cynthial Rosenzweig, William Solecki, and Richard Slosberg. Mitigating New York City's heat island with urban forestry, living roofs, and light surfaces. *86th AMS Annual Meeting*, page 5, 2006.

[73] Dev Millstein and Surabi Menon. Regional climate consequences of large-scale cool roof and photovoltaic array deployment. *Environmental Research Letters*, 6(3):034001, jul 2011.

[74] L. S. Kalkstein David J. Sailor and E. Wong. The potential of urban heat island mitigation to alleviate heat related mortality: methodological overview and preliminary modeling results for philadelphia. In *Fourth Symposium on the Urban Environment*, 2002.

[75] National Center for Atmospheric Research (NCAR). MM5 Community Model, 2015.

[76] Melissa Goering and Glen Sampson. Weather Research and Forecasting Model, 2004.

[77] M. Santamouris. Cooling the cities - A review of reflective and green roof mitigation technologies to fight heat island and improve comfort in urban environments. *Solar Energy*, 103:682–703, 2014.

[78] N. Gaitani, A. Spanou, M. Saliari, A. Synnefa, K. Vassilakopoulou, K. Papadopoulou, K. Pavlou, M. Santamouris, M. Papaioannou, and A. Lagoudaki. Improving the microclimate in urban areas: A case study in the centre of Athens. *Building Services Engineering Research and Technology*, 32(1):53–71, 2011.

[79] Emiliano Carnielo and Michele Zinzi. Optical and thermal characterisation of cool asphalts to mitigate urban temperatures and building cooling demand. *Building and Environment*, 60:56–65, 2013.

[80] A. Dimoudi, S. Zoras, A. Kantzioura, X. Stogiannou, P. Kosmopoulos, and C. Pallas. Use of cool materials and other bioclimatic interventions in outdoor places in order to mitigate the urban heat island in a medium size city in Greece. *Sustainable Cities and Society*, 13:89–96, 2014.

[81] N. Fintikakis, N. Gaitani, M. Santamouris, M. Assimakopoulos, D. N. Assimakopoulos, M. Fintikaki, G. Albanis, K. Papadimitriou, E. Chryssochoides, K. Katopodi, and P. Doumas. Bioclimatic design of open public spaces in the historic centre of Tirana, Albania. *Sustainable Cities and Society*, 1(1):54–62, 2011.

[82] Xiaoshan Yang, Lihua Zhao, Michael Bruse, and Qinglin Meng. Evaluation of a microclimate model for predicting the thermal behavior of different ground surfaces. *Building and Environment*, 60:93–104, 2013.

[83] Wikipedia. X-ray Crystallography, 2005.

[84] H. M. Rietveld. A profile refinement method for nuclear and magnetic structures. *Journal of Applied Crystallography*, 2(2):65–71, jun 1969.

[85] Foil A. Miller and Charles H. Wilkins. Infrared Spectra and Characteristic Frequencies of Inorganic Ions. *Analytical Chemistry*, 24(8):1253–1294, 1952.

[86] Douglas A. Skoog, F. James. Holler, and Stanley R. Crouch. *Principles of instrumental analysis*. Brooks/Cole : Thomson Learning, Australia, 2007.

[87] Jesús J. Ojeda and Maria Dittrich. Fourier transform infrared spectroscopy for molecular analysis of microbial cells. In Ali Navid, editor, *Methods in Molecular Biology*, volume 881, pages 187–211. Humana Press, Totowa, NJ, 2012.

[88] Bestech. Thermogravimetric Analysis (TGA) & Thermogravimetry (TG) | Bestech.

[89] ASTM-E11-17. Standard Specification for Woven Wire Test Sieve Cloth and Test Sieves, 2013.

[90] Devices and Services. Technical note 10-2 emissometer model ae1 – slide method for high emittance materials with low thermal conductivity. Technical report, Devices and Services, 2010.

[91] Devices and Services Company. TN 04-1 Emissometer Model AE - Slide Method for AE Measurements. Technical report, Devices and Services Company, Dallas, 2010.

[92] G. T. Georgiev and J. J Butler. Long-term calibration monitoring of Spectralon diffusers BRDF in the air-ultraviolet. *Appl. Opt.*, 46(32):7892–7899, 2007.

[93] Hashem Akbari and Ronnen Levinson. Evolution of cool-roof standards in the US. *Advances in Building Energy Research*, 2(1):1–32, 2008.

[94] EUROPEAN COOL ROOFS COUNCIL. European cool roofs council, 2000.

[95] ECRC Technical Committee. Product Rating Manual. Technical report, European Cool Roof Council, 2014.

[96] Cool Roof Rating Council. CRRC-1 Product Rating Program Manual PRODUCT RATING PROGRAM MANUAL CRRC-1. Technical report, Cool Roof Rating Council, 2017.

[97] Environmental Protection Agency. Energy Star, 2015.

[98] EPA. ENERGY STAR® Program Requirements Product Specification for Roof Products. Technical report, EPA, 2008.

[99] Measuring Performance, Near Infrared Spectrophotom, Air Mass, Zero Solar, Irradiance Tables, Sheet Materials, and Using Sunlight. Standard Test Method for Solar Absorptance , Reflectance , and Transmittance of Materials Using Integrating Spheres 1, 1996.

[100] ASTM. ASTM E891 - 87(1992) Tables for Terrestrial Direct Normal Solar Spectral Irradiance Tables for Air Mass 1.5 (Withdrawn 1999).

[101] ASTM C1549 - 09. Standard test method for determination of solar reflectance near ambient temperature using a portable solar reflectometer, 2014.

[102] Standard Test Method. Standard Test Method for Determination of Emittance of Materials Near Room Temperature Using Portable Emissometers 1, 2011.

[103] Ioanna Papayianni and Maria Stefanidou. Durability aspects of ancient mortars of the archeological site of Olynthos. *Journal of Cultural Heritage*, 8(2):193–196, 2007.

[104] P. Maravelaki-Kalaitzaki, A. Bakolas, and A. Moropoulou. Physico-chemical study of Cretan ancient mortars. *Cement and Concrete Research*, 33(5):651–661, 2003.

[105] C. Genestar, C. Pons, and A. Más. Analytical characterisation of ancient mortars from the archaeological Roman city of Pollentia (Balearic Islands, Spain). In *Analytica Chimica Acta*, volume 557, pages 373–379, 2006.

[106] D. Kolokotsa, P. Maravelaki-Kalaitzaki, S. Papantoniou, E. Vangeloglou, M. Saliari, T. Karlessi, and M. Santamouris. Development and analysis of mineral based coatings for buildings and urban structures. *Solar Energy*, 86(5):1648–1659, 2012.

[107] B/516/11. Building lime. definitions, specifications and conformity criteria. Technical report, British Standards Institution, 2015.

[108] A. Arizzi, H. Viles, and G. Cultrone. Experimental testing of the durability of lime-based mortars used for rendering historic buildings. *Construction and Building Materials*, 28(1):807–818, 2012.

[109] M. Abdel-Mooty, S. Khedr, and T. Mahfouz. Evaluation of lime mortars for the repair of historic buildings. In *WIT Transactions on the Built Environment*, volume 109, pages 209–220, 2009.

[110] ASTM. References Solar Spectral Irradiance at Air Mass 1.5: Direct Normal and Hemispherical for a 37° Tilted Surface 1, 2004.

[111] Leandros Simeonidis. Weather station of chania. http://penteli.meteo.gr/stations/chania/, 2018.

[112] Davisnet. Wireless Vantage Pro2™ with 24-Hour Fan Aspirated Radiation Shield | Davis Instruments.

[113] Yiping Ma, Beirong Zhu, and Keru Wu. Preparation and solar reflectance spectra of chameleon-type building coatings. *Solar Energy*, 70(5):417–422, 2001.

[114] Sunhee Choi and James A. Larrabee. Thermochromic tetrachlorocuprate(II): An advanced integrated laboratory experiment. *Journal of Chemical Education*, 66(9):774, 1989.

[115] S. R. Hall, F. H. Allen, and I. D. Brown. The crystallographic information file (CIF): a new standard archive file for crystallography. *Acta Crystallographica Section A*, 47(6):655–685, 1991.

[116] Yiping Ma, Beirong Zhu, and Keru Wu. Preparation of reversible thermochromic building coatings and their properties. *Journal of Coatings Technology*, 72(911):67–71, 2000.

[117] Rosita M. Kantola, Hemmo Kurunmäki, Pekka K. Vallittu, and Lippo V J Lassila. Use of thermochromic pigment in maxillofacial silicone elastomer. *Journal of Prosthetic Dentistry*, 110(4):320–325, 2013.

[118] Theoni Karlessi and Mat Santamouris. Improving the performance of thermochromic coatings with the use of UV and optical filters tested under accelerated aging conditions. *International Journal of Low-Carbon Technologies*, 10(1):45–61, 2015.

[119] Fluke. FLIR Tools Software for PC and Mac, 2015.

[120] R.M. Akbahi H. Behre A. Levinson R. Graveline S. Foley K. Delgado A.H. and Paroli. Identification and lactic acid production of bacteria isolated from soils and tree barks. *Malaysian Journal of Microbiology*, 13(2):100–108, 2017.

[121] J. Pospíšil and S. Nešpurek. Photostabilization of coatings. Mechanisms and performance. *Progress in Polymer Science (Oxford)*, 25(9):1261–1335, 2000.

[122] European Energy Agency. Final energy consumption by sector and fuel. *Indicator Assessment | Data and maps*, page 20, 2015.

[123] Paul Strachan. ESP-r Summary of Validation Studies. *Analysis*, pages 0–8, 2000.

[124] Young Jeong and Fariborz Haghighat. Modelling of a Hybrid-Ventilated Building – Using ESP-r. *International Journal of Ventilation*, 1(2):127–139, 2002.

[125] Jon William Hand. *Strategies for Deploying Virtual Representations of the Built Environment. TheESP-r Cookbook.*, volume December. University of Strathclyde, 2015.

[126] Nicole Müller, Wilhelm Kuttler, and Andreas-Bent Barlag. Counteracting urban climate change: adaptation measures and their effect on thermal comfort. *Theoretical and Applied Climatology*, 115(1-2):243–257, apr 2013.

[127] A Prutsch, T Grothmann, I Schauser, S Otto, S McCallum, et al. Guiding principles for adaptation to climate change in europe. *Guiding principles for adaptation to climate change in Europe.*, 2010.

[128] M. Santamouris, C. Cartalis, A. Synnefa, and D. Kolokotsa. On the impact of urban heat island and global warming on the power demand and electricity consumption of buildings - A review. *Energy and Buildings*, 98(0):119–124, 2015.

[129] Christoph Morbitzer, Paul Strachan, Jim Webster, Brian Spires, and David Cafferty. Integration of Building Simulation Into the Design Process of an Architecture. In *Seventh International IBPSA Conference*, pages 697–704, 2001.

[130] Joana Sousa. Energy Simulation Software for Buildings: Review and Comparison. *Information Technology for Energy Applications 2012*, pages 6–7, 2012.

[131] Joe A. Clarke. *Energy Simulation in Building Design*. Butterworth-Heinemann, 2001.

[132] J. a. Voogt and T. R. Oke. Complete Urban Surface Temperatures. *Journal of Applied Meteorology*, 36(9):1117–1132, 1997.

[133] Sotiris Vardoulakis, Bernard E.A. Fisher, Koulis Pericleous, and Norbert Gonzalez-Flesca. Modelling air quality in street canyons: A review. *Atmospheric Environment*, 37(2):155–182, 2003.

[134] Jiang He, Akira Hoyano, and Takashi Asawa. A numerical simulation tool for predicting the impact of outdoor thermal environment on building energy performance. *Applied Energy*, 86(9):1596–1605, 2009.

[135] Neda Yaghoobian and Jan Kleissl. An indoor-outdoor building energy simulator to study urban modification effects on building energy use - Model description and validation. *Energy and Buildings*, 54:407–417, nov 2012.

[136] J.A. Palyvos. A survey of wind convection coefficient correlations for building envelope energy systems' modeling. *Applied Thermal Engineering*, 28(8):801 – 808, 2008.

[137] P. I. Cooper. The effect of inclination on the heat loss from flat-plate solar collectors. *Solar Energy*, 27(5):413–420, 1981.

[138] B. Blocken, T. Defraeye, D. Derome, and J. Carmeliet. High-resolution CFD simulations for forced convective heat transfer coefficients at the facade of a low-rise building. *Building and Environment*, 44(12):2396–2412, 2009.

[139] Theodore Stathopoulos and Hanqing Wu. Generic models for pedestrian-level winds in built-up regions. *Journal of Wind Engineering and Industrial Aerodynamics*, 54-55(C):515–525, 1995.

[140] R. Yoshie, A. Mochida, Y. Tominaga, H. Kataoka, K. Harimoto, T. Nozu, and T. Shirasawa. Cooperative project for CFD prediction of pedestrian wind environment in the Architectural Institute of Japan. *Journal of Wind Engineering and Industrial Aerodynamics*, 95(9-11):1551–1578, 2007.

[141] Ruixian Cai and Na Zhang. Explicit analytical solutions of 2-D laminar natural convection. *International Journal of Heat and Mass Transfer*, 46(5):931–934, 2003.

[142] Thijs Defraeye, Bert Blocken, and Jan Carmeliet. Convective heat transfer coefficients for exterior building surfaces: Existing correlations and CFD modelling. *Energy Conversion and Management*, 52(1):512–522, 2011.

[143] Thijs Defraeye, Bert Blocken, and Jan Carmeliet. Convective heat transfer coefficients for exterior building surfaces: Existing correlations and CFD modelling. In *Energy Conversion and Management*, volume 52, pages 512–522, 2011.

[144] Jiantao Shao, Jing Liu, Jianing Zhao, Wenwu Zhang, Dexing Sun, and Zhipeng Fu. A novel method for full-scale measurement of the external convective heat transfer coefficient for building horizontal roof. *Energy and Buildings*, 41(8):840–847, 2009.

[145] N Ito, K Kimura, and J Oka. A field experiment study on the convective heat transfer coefficient on exterior surface of a building. *ASHRAE Transactions*, 78(1):184–191, 1972.

[146] Aya Hagishima and Jun Tanimoto. Field measurements for estimating the convective heat transfer coefficient at building surfaces. *Building and Environment*, 38(7):873–881, 2003.

[147] D. L. Loveday and A. H. Taki. Convective heat transfer coefficients at a plane surface on a full-scale building facade. *International Journal of Heat and Mass Transfer*, 39(8):1729–1742, 1996.

[148] Meteonorm. Meteonorm - Global meteorological database, 2012.

[149] Dionysia Kolokotsa, Kostas Gobakis, S. Papantoniou, C. Georgatou, N. Kampelis, Kostas Kalaitzakis, K. Vasilakopoulou, and Mat Santamouris. Development of a web based energy management system for University Campuses: The CAMP-IT platform. *Energy and Buildings*, 123:119–135, 2016.

[150] Georgios P. Giatrakos, Theocharis D. Tsoutsos, and Nikos Zografakis. Sustainable power planning for the island of Crete. *Energy Policy*, 37(4):1222–1238, 2009.

[151] Carlos Serrano-Cinca, Yolanda Fuertes-Callén, and Cecilio Mar-Molinero. *Measuring DEA efficiency in Internet companies*, volume 38 of *Cookbooks (O'Reilly)*. O'Reilly Media, 2005.

[152] Vasiliki Tsilini, Sotiris Papantoniou, Dionysia Denia Kolokotsa, and Efpraxia Aithra Maria. Urban gardens as a solution to energy poverty and urban heat island. *Sustainable Cities and Society*, 14(1):323–333, 2015.

[153] R. J. Purser and L. M. Leslie. A Semi-Implicit, Semi-Lagrangian Finite-Difference Scheme Using Hligh-Order Spatial Differencing on a Nonstaggered Grid. *Monthly Weather Review*, 116(10):2069–2080, 1988.

[154] Williams H McAdams. Heat transmission. Technical report, 1954.

[155] Energy Systems Research Unit. Espr-r source code, 2015.

[156] E. R. Meinders, K. Hanjalic, and R. J. Martinuzzi. Experimental study of the local convection heat transfer from a wall-mounted cube in turbulent channel flow. *J. Heat Trans. - T. ASME*, 121(March):564–573, 1999.

[157] Marcelo G. Emmel, Marc O. Abadie, and Nathan Mendes. New external convective heat transfer coefficient correlations for isolated low-rise buildings. *Energy and Buildings*, 39(3):335–342, 2007.

[158] David Beazley and Brian K. Jones. *Python Cookbook*. O'Reilly Media, Inc., 2013.

[159] Konstantinos Gobakis. Data extraction in V4 - ENVI-met Board.

[160] ENVI-met. ENVI_met. A holistic microclimate model, 2013.

Appendix A

Spectral reflectance of mineral based cool coating

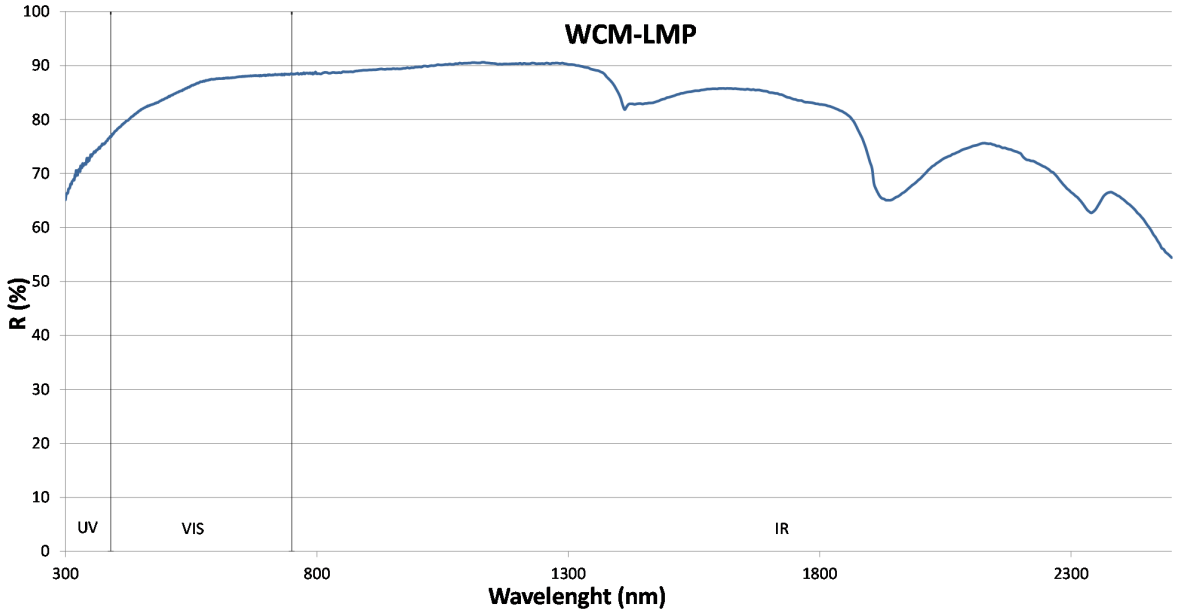

Figure A.1 Spectral reflectance of sample: WCM-LMP.

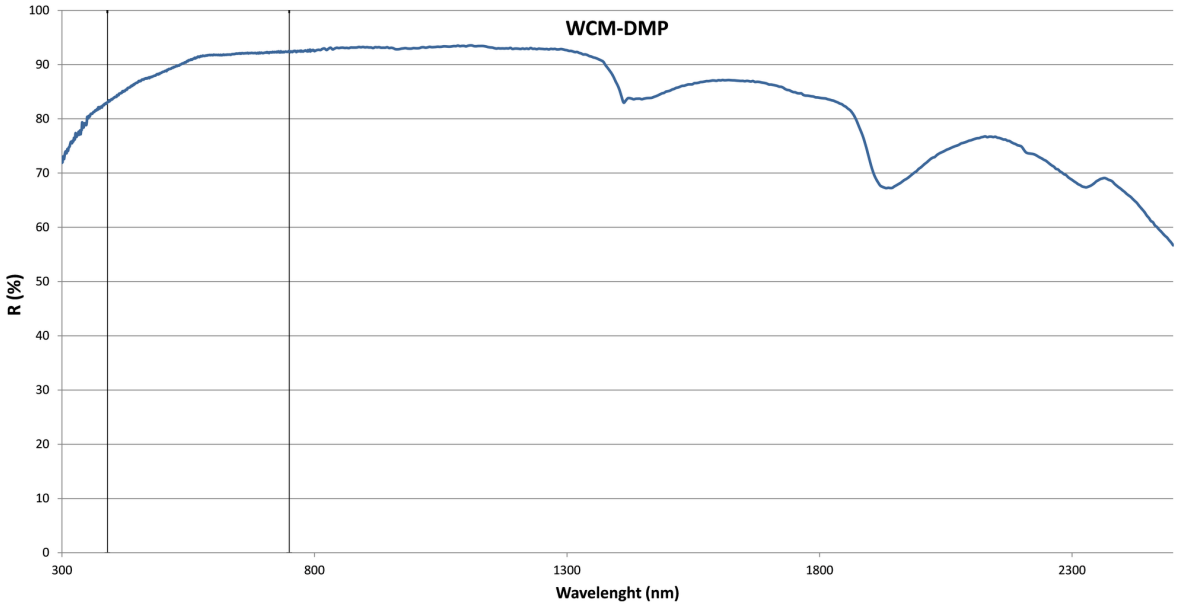

Figure A.2 Spectral reflectance of sample: WCM-DMP.

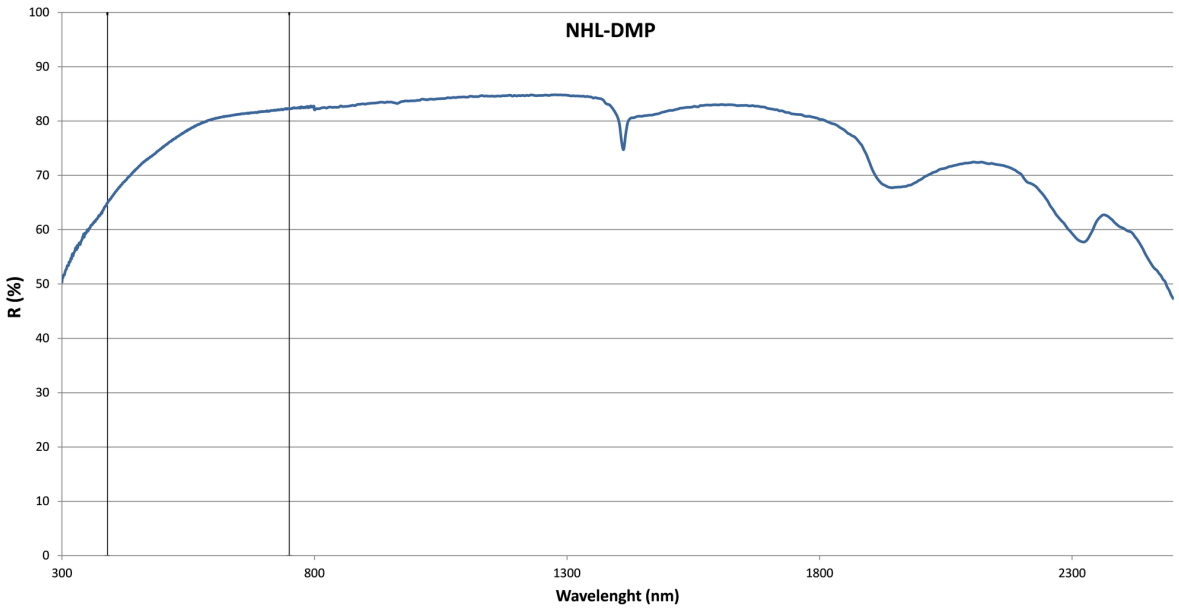

Figure A.3 Spectral reflectance of sample: NHL-DMP.

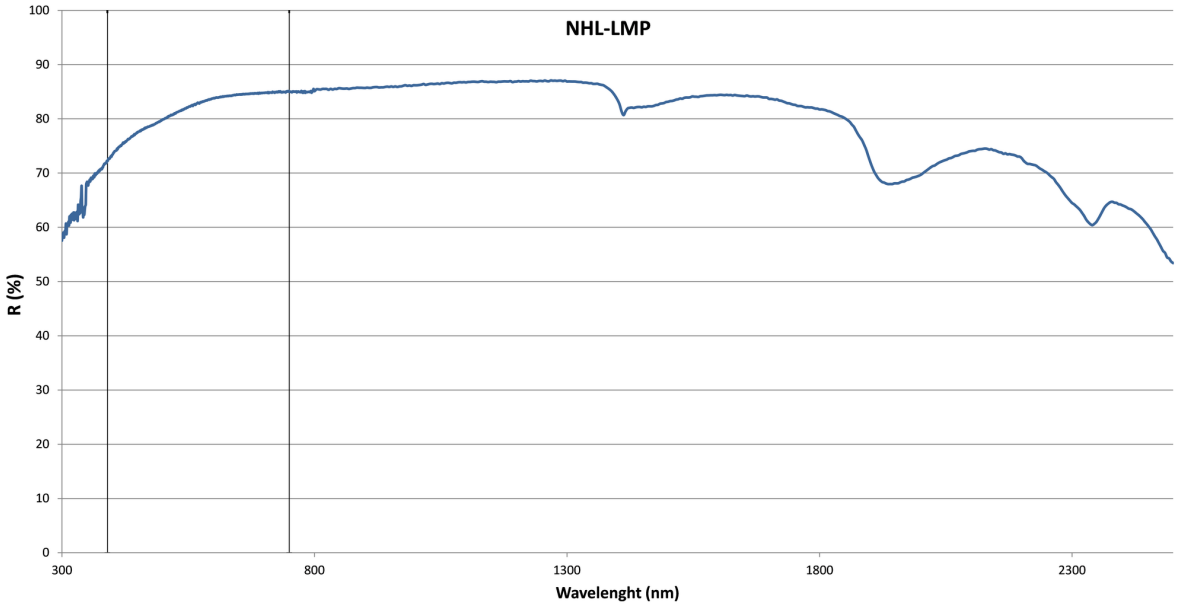

Figure A.4 Spectral reflectance of sample: NHL-LMP.

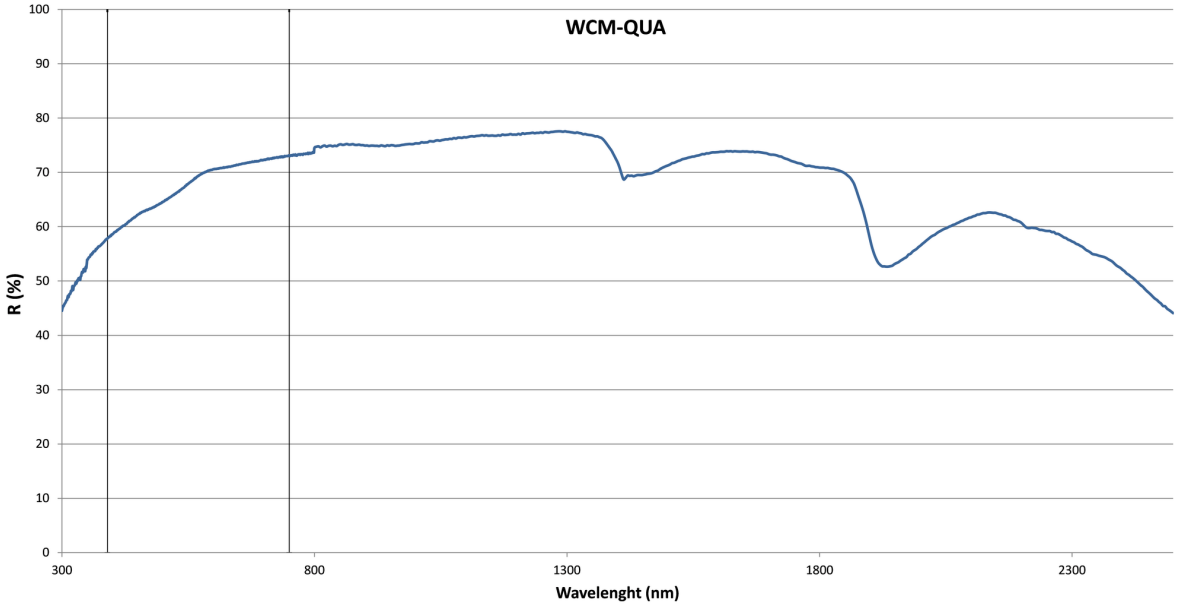

Figure A.5 Spectral reflectance of sample: WCM-QUA.

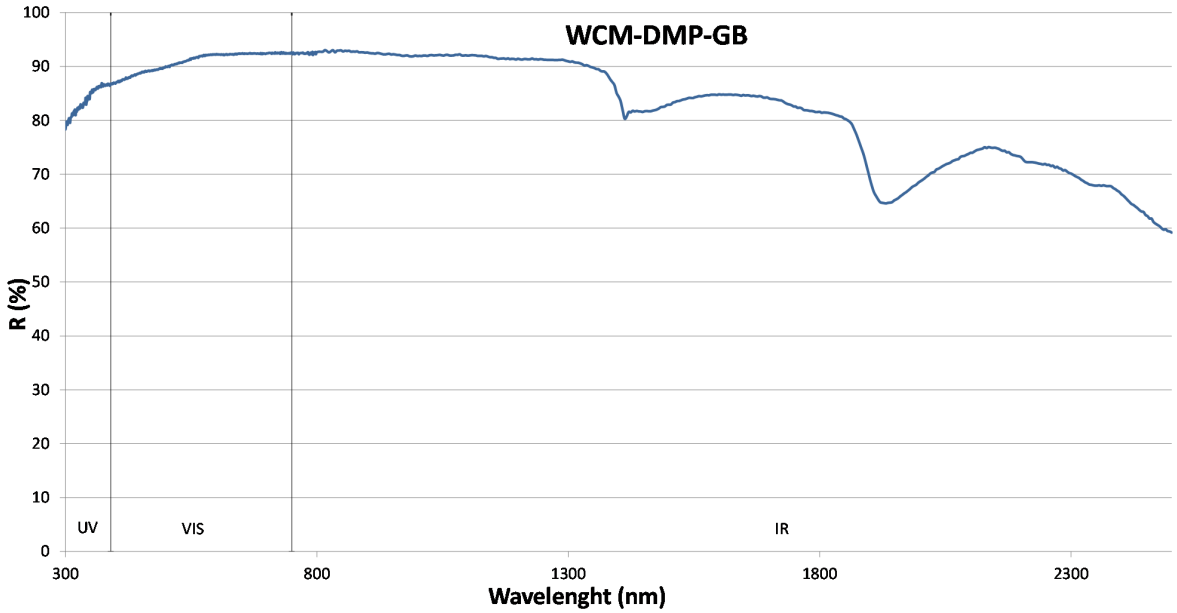

Figure A.6 Spectral reflectance of sample: WCM-DMP-GB.

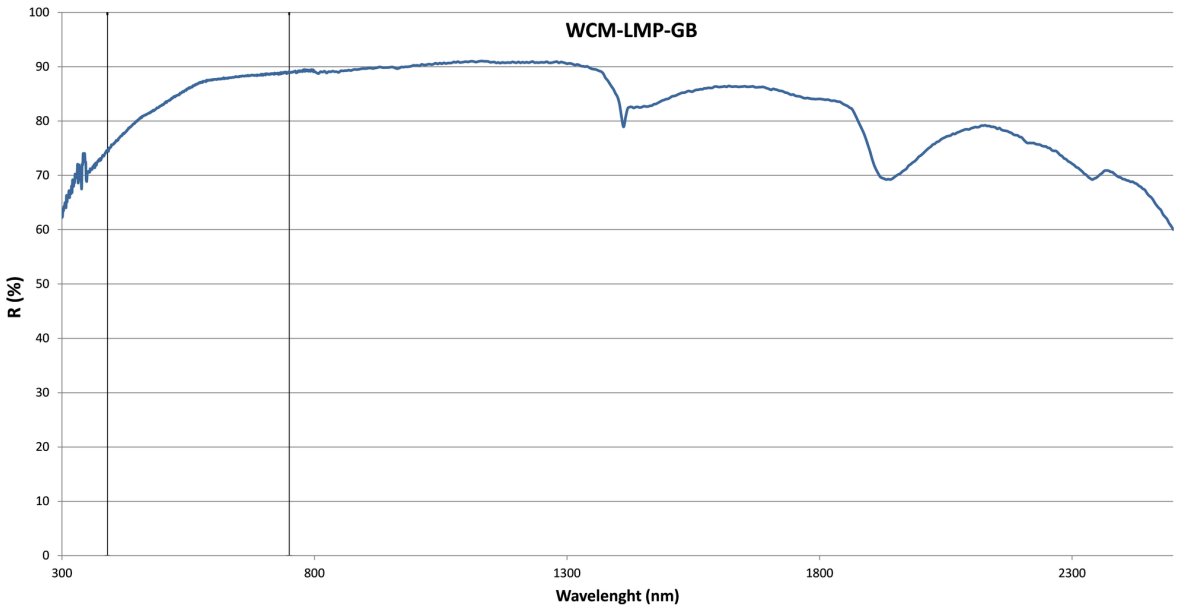

Figure A.7 Spectral reflectance of sample: WCM-LMP-GB.

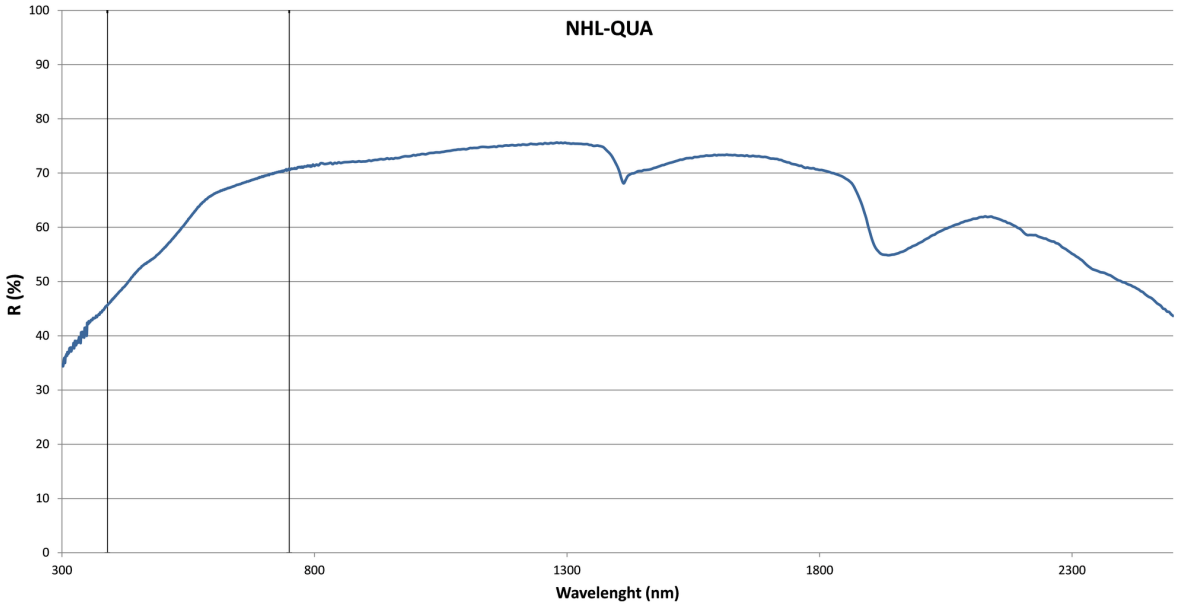

Figure A.8 Spectral reflectance of sample: NHL-QUA.

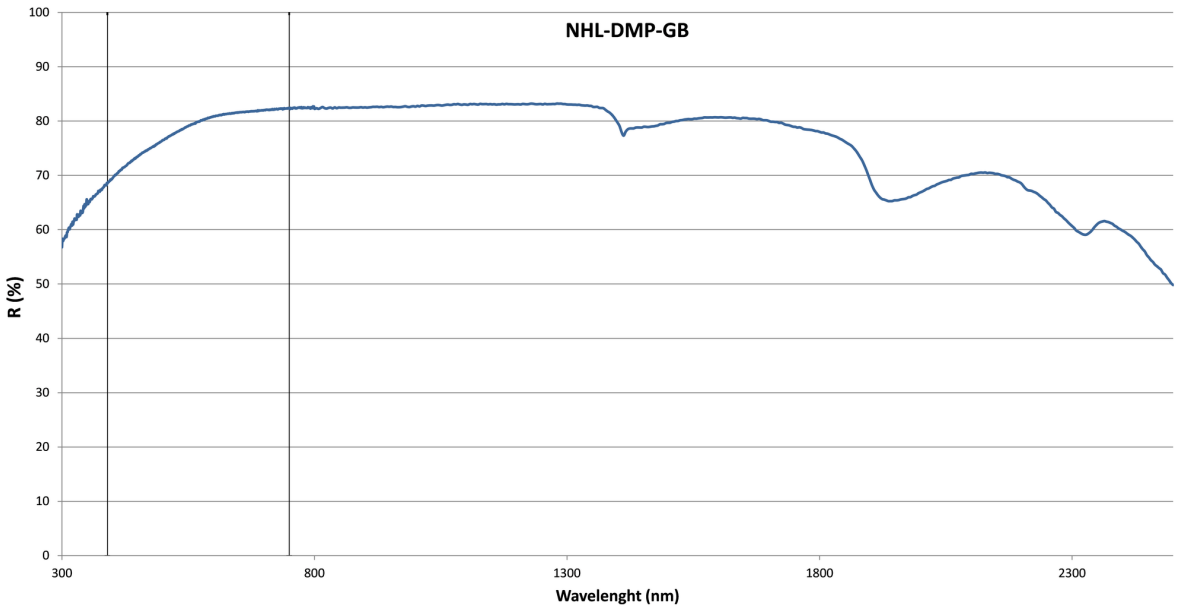

Figure A.9 Spectral reflectance of sample: NHL-DMP-GB.

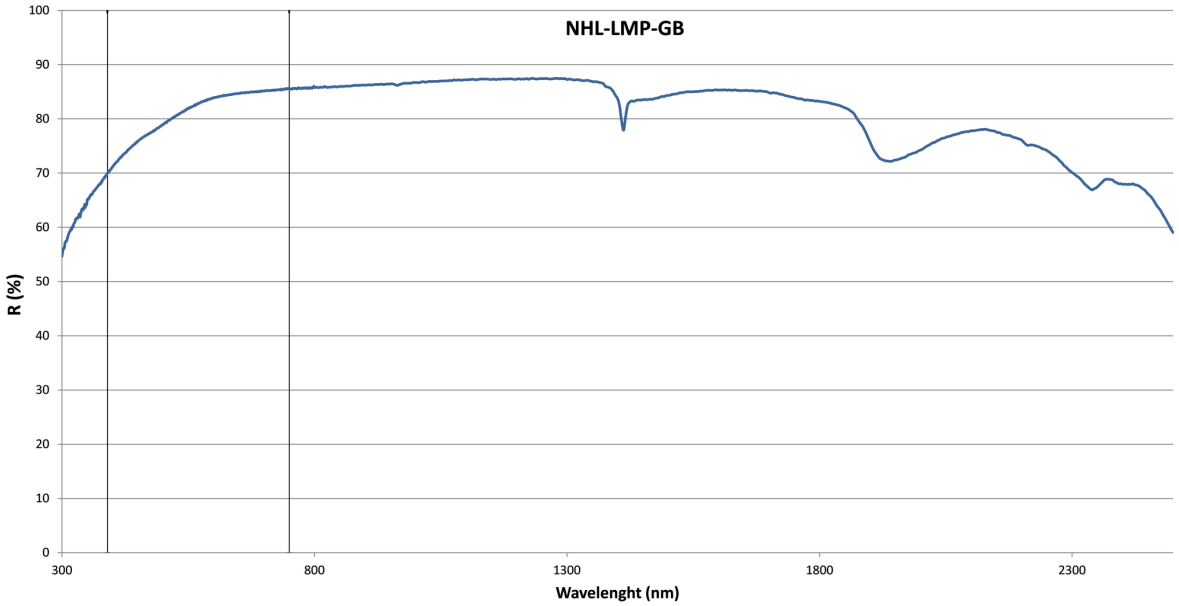

Figure A.10 Spectral reflectance of sample: NHL-LMP-GB.

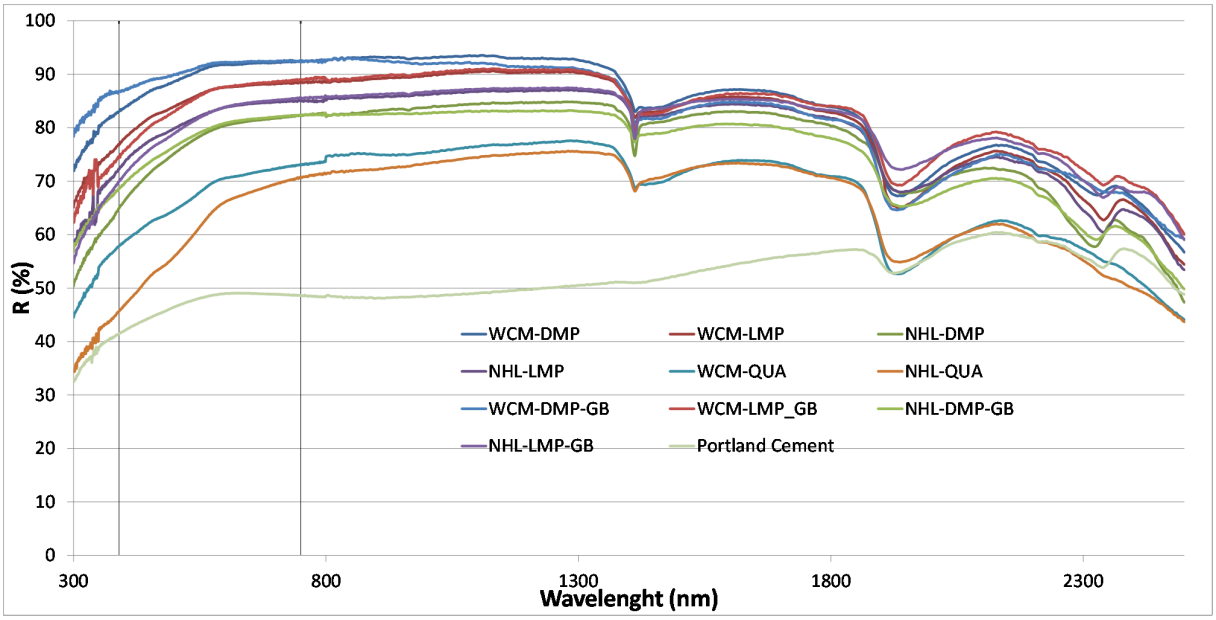

Figure A.11 Spectral reflectance of first phase samples.

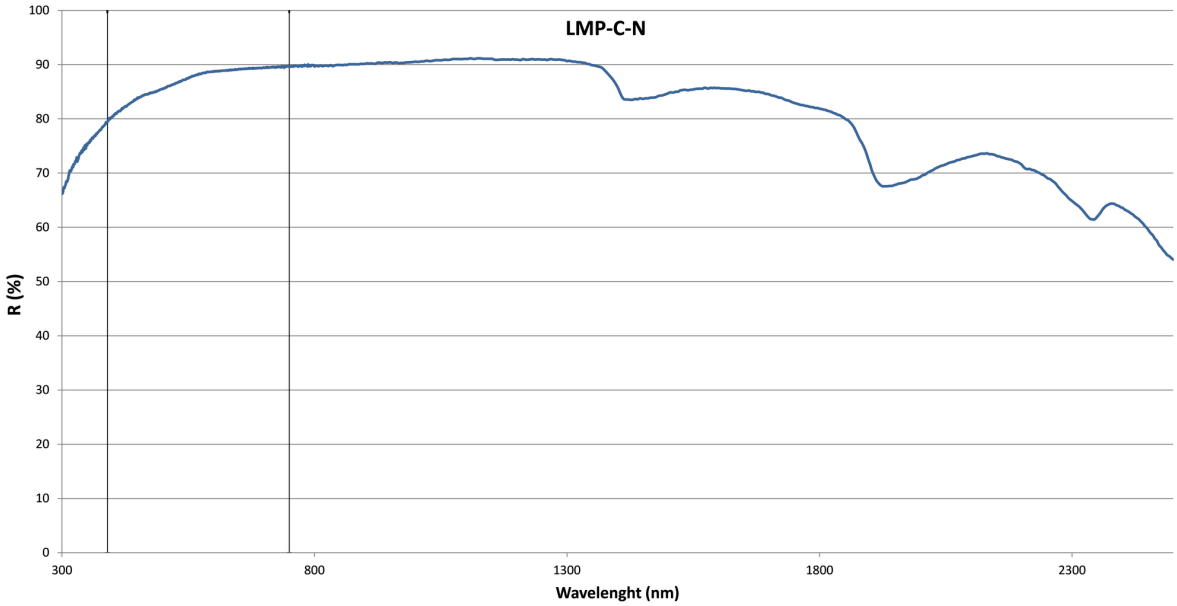

Figure A.12 Spectral reflectance of sample: LMP-C-N.

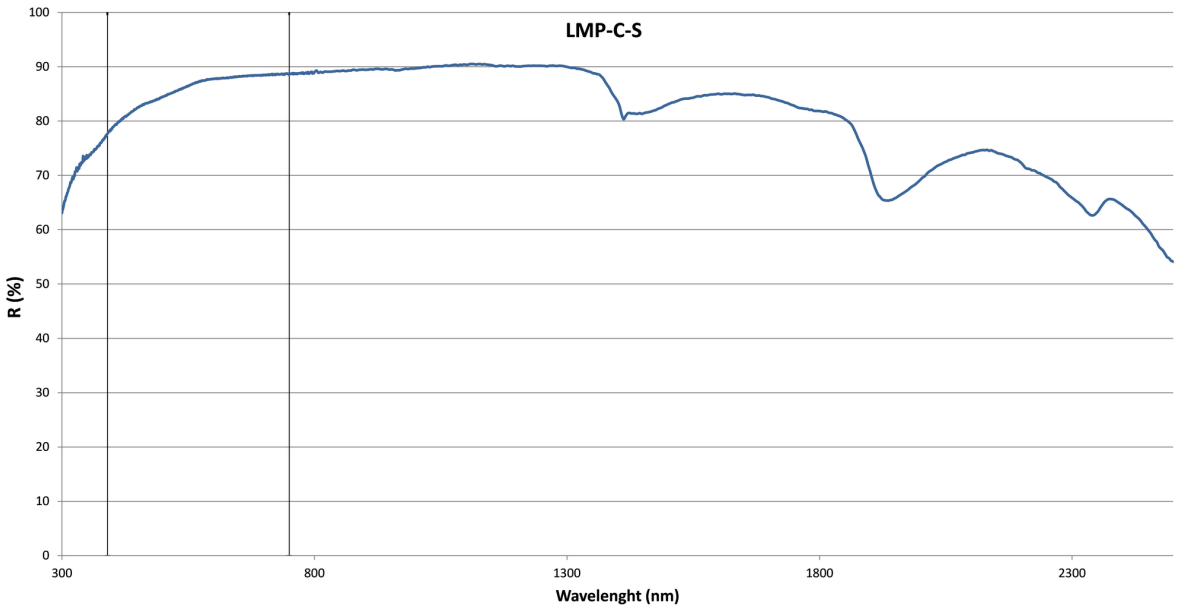

Figure A.13 Spectral reflectance of sample: LMP-C-S.

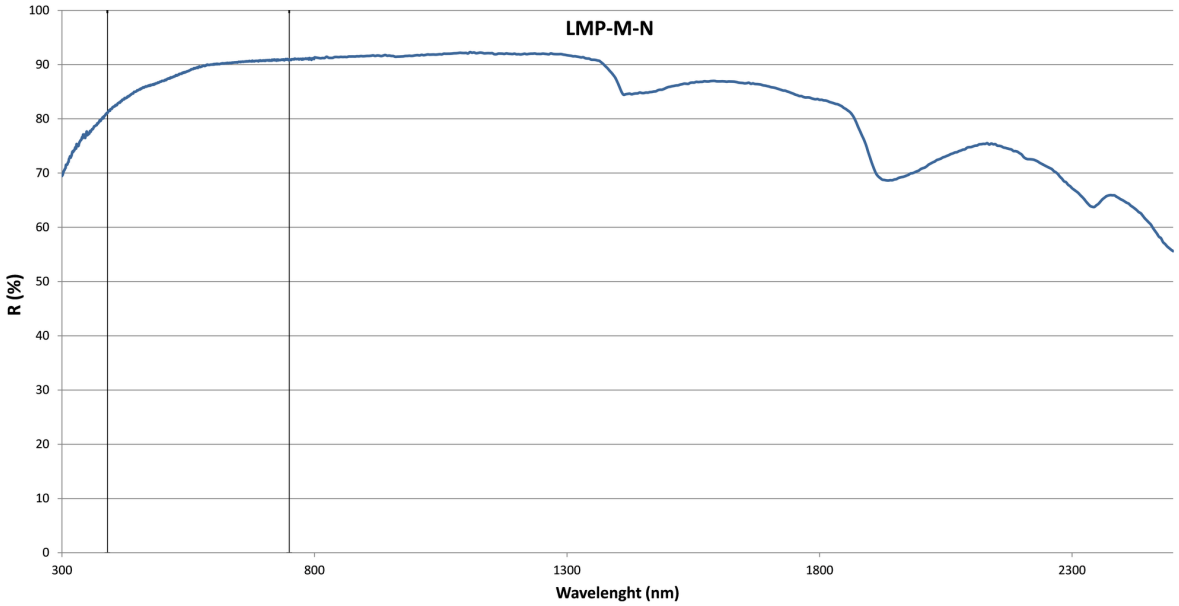

Figure A.14 Spectral reflectance of sample: LMP-M-N.

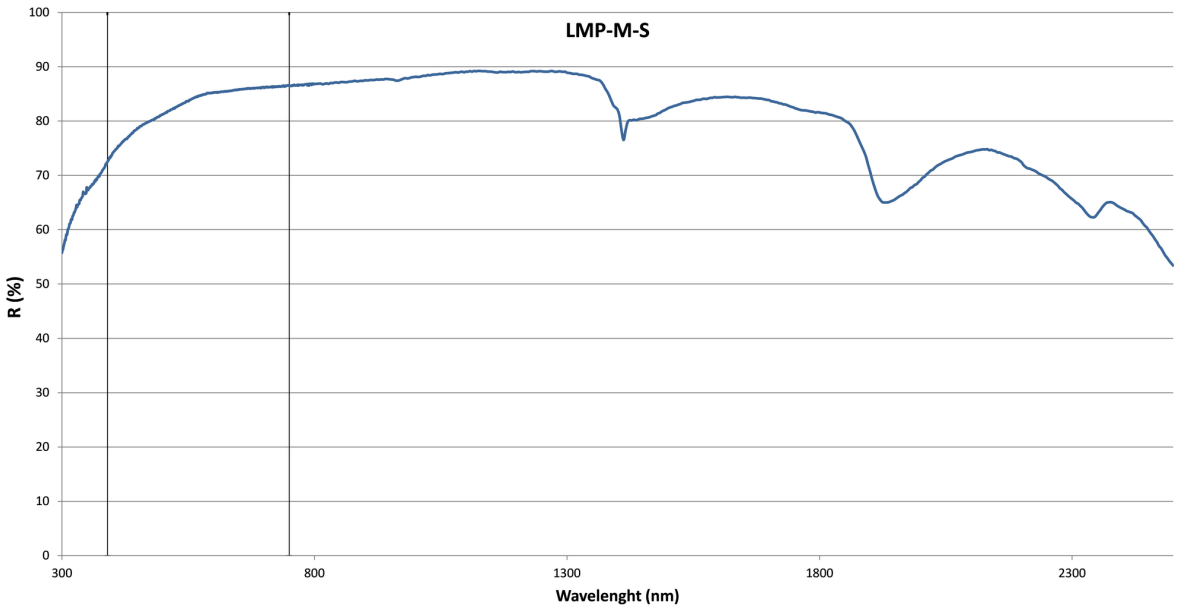

Figure A.15 Spectral reflectance of sample: LMP-M-S.

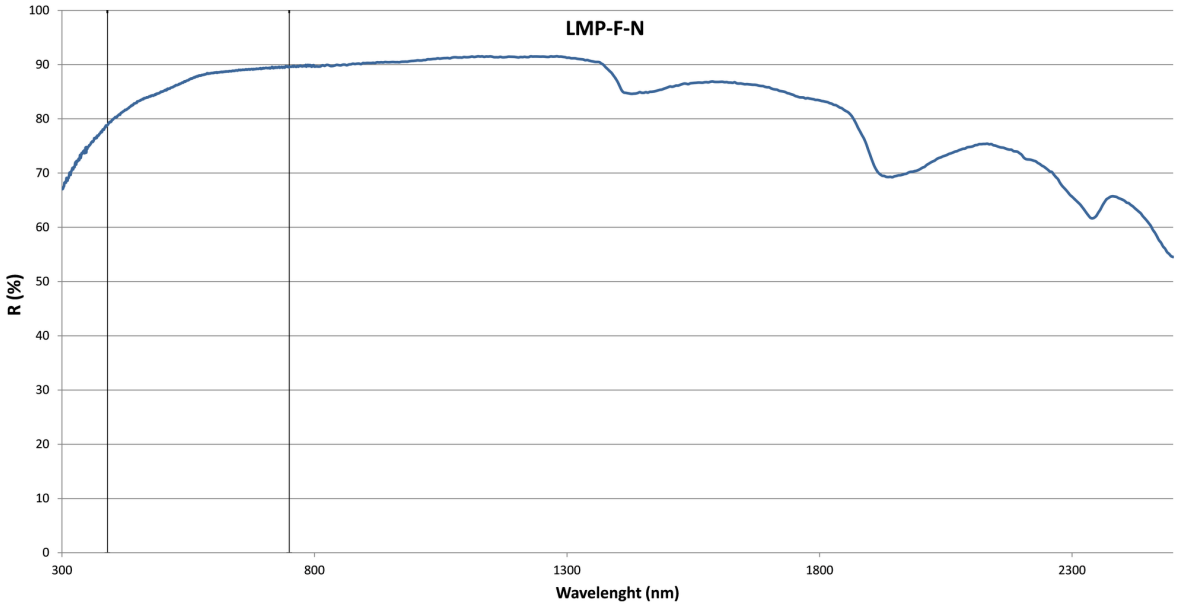

Figure A.16 Spectral reflectance of sample: LMP-F-N.

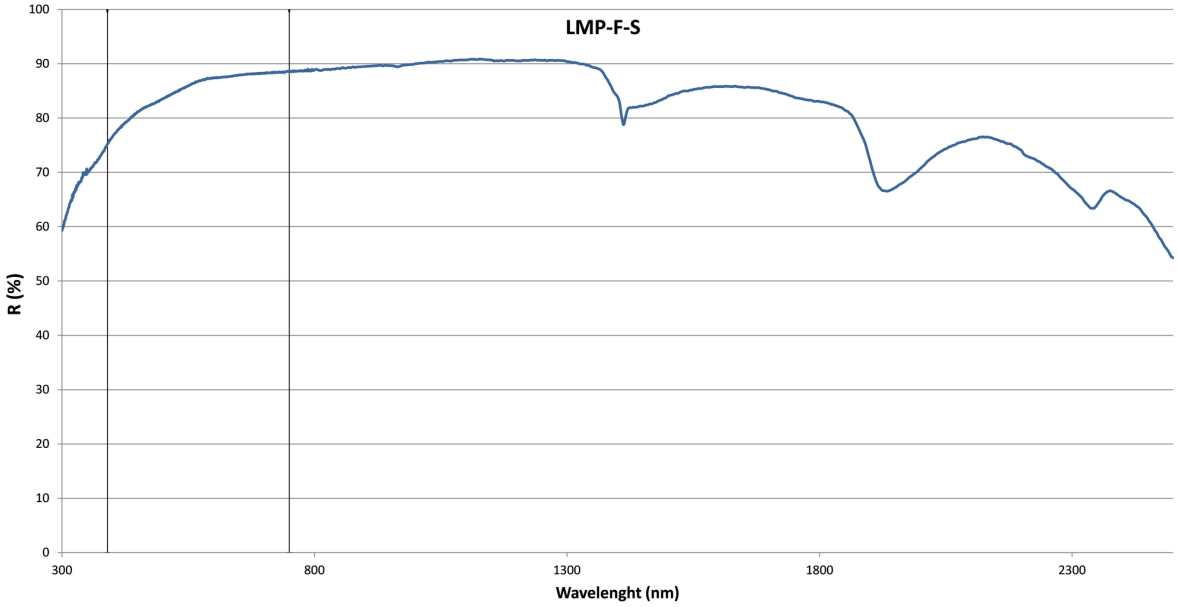

Figure A.17 Spectral reflectance of sample: LMP-F-S.

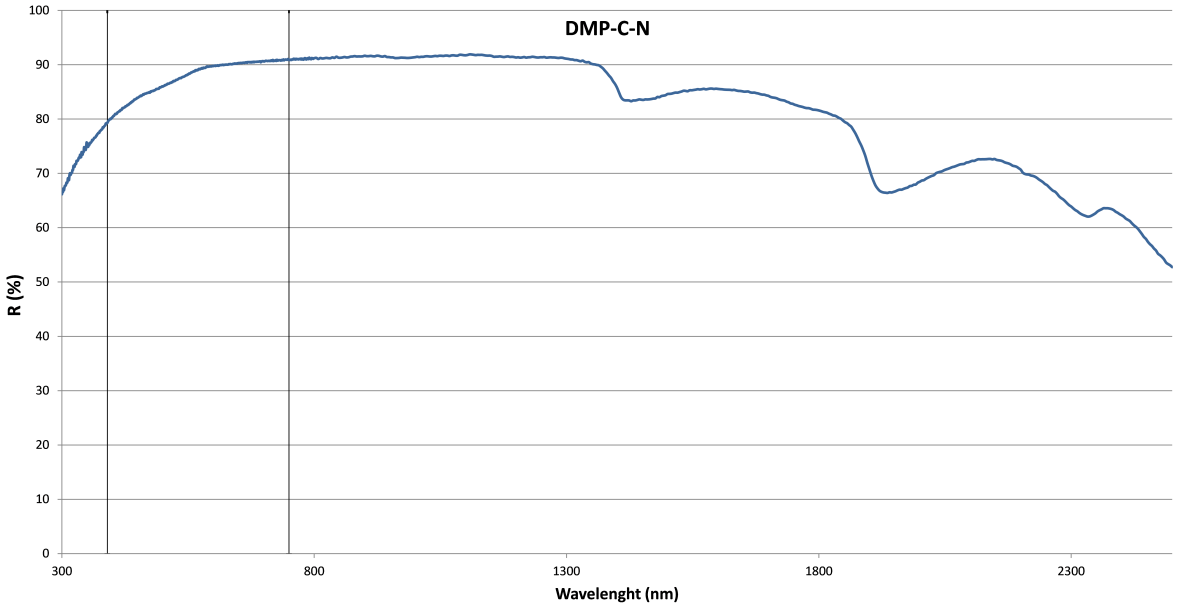

Figure A.18 Spectral reflectance of sample: DMP-C-N.

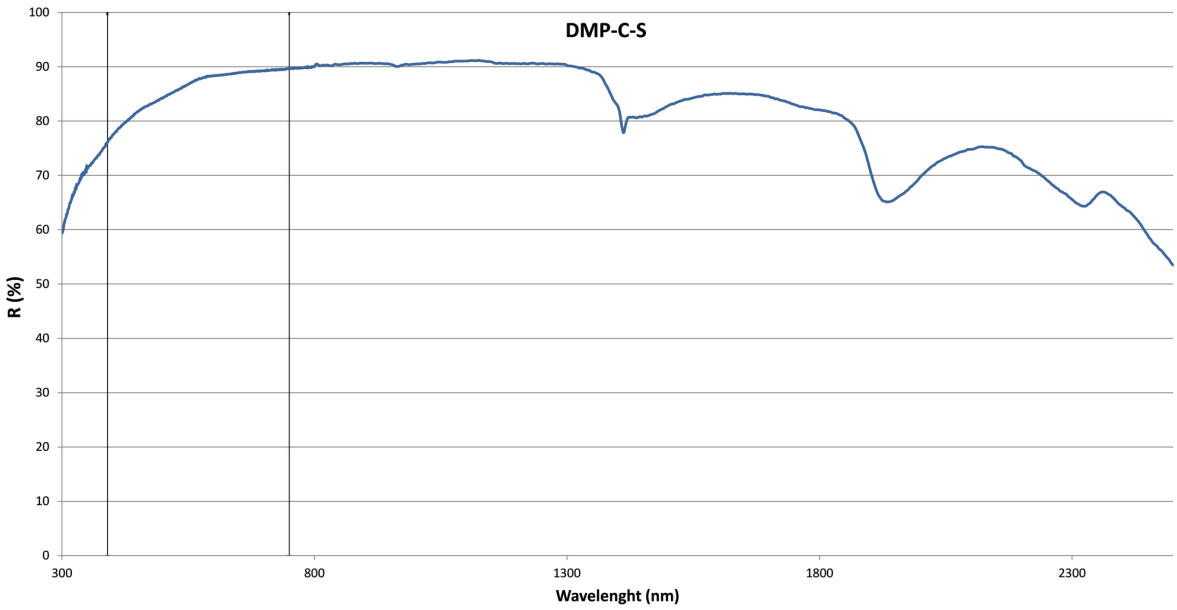

Figure A.19 Spectral reflectance of sample: DMP-C-S.

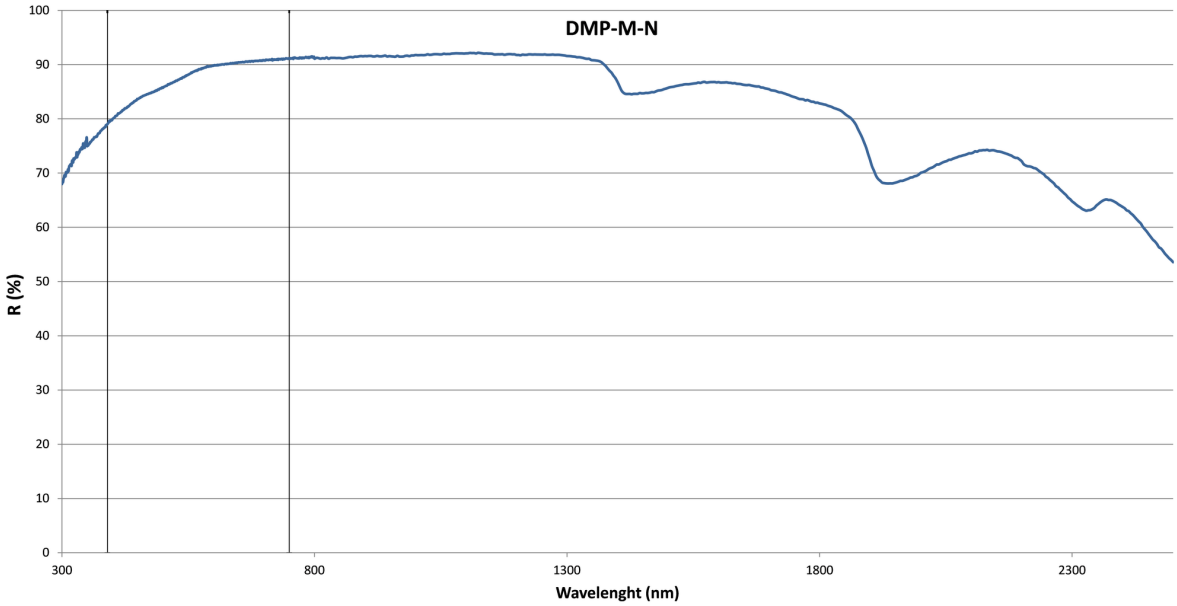

Figure A.20 Spectral reflectance of sample: DMP-M-N.

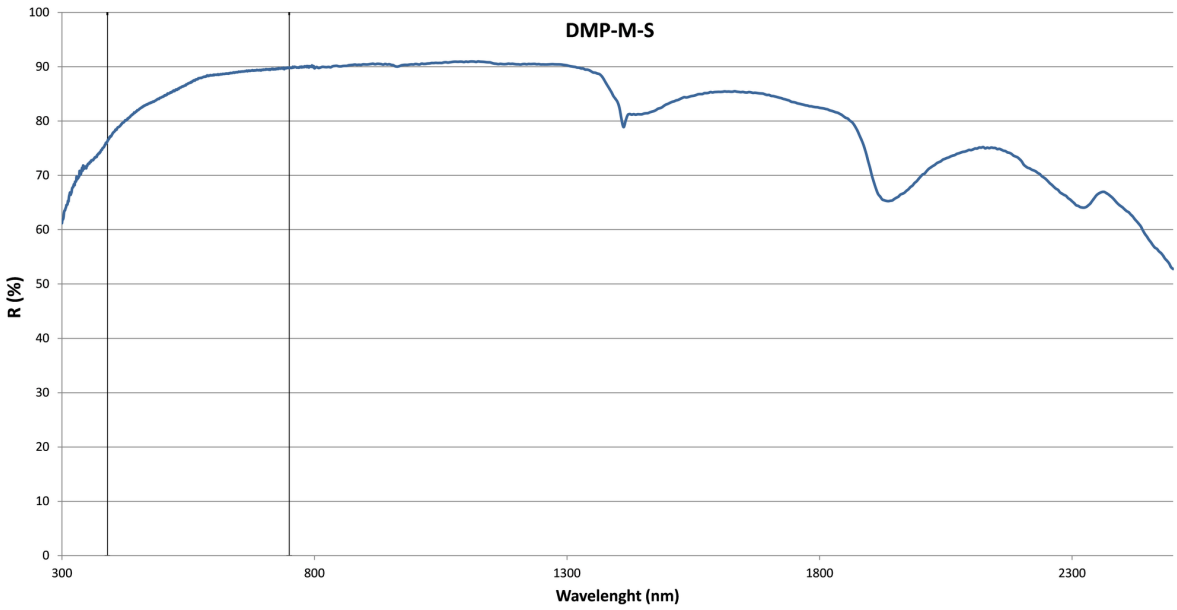

Figure A.21 Spectral reflectance of sample: DMP-M-S.

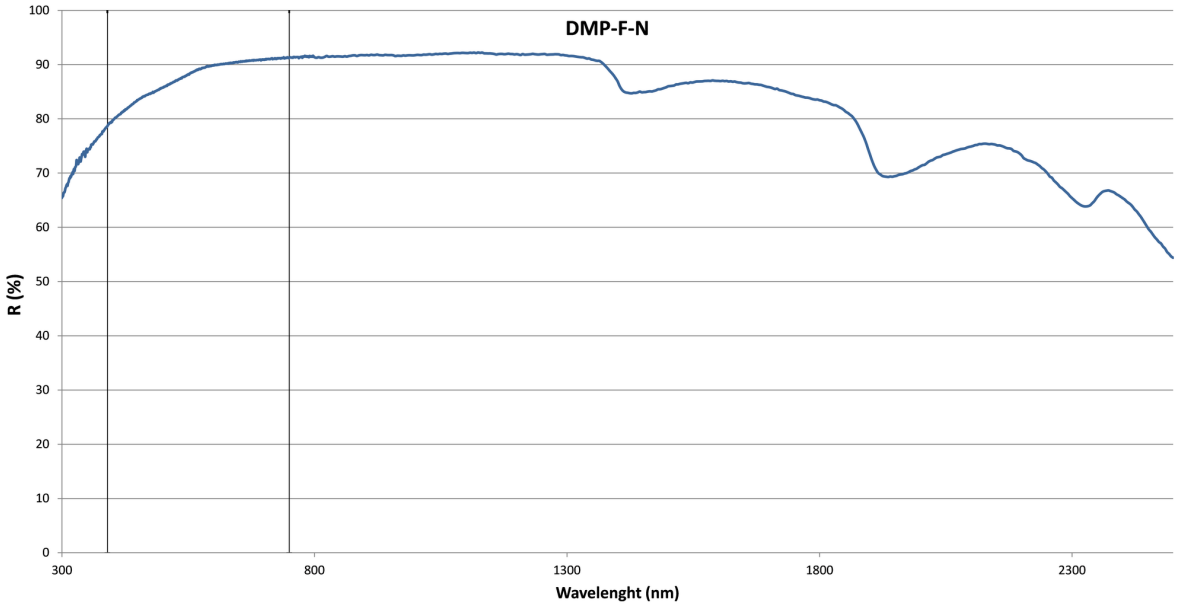

Figure A.22 Spectral reflectance of sample: DMP-F-N.

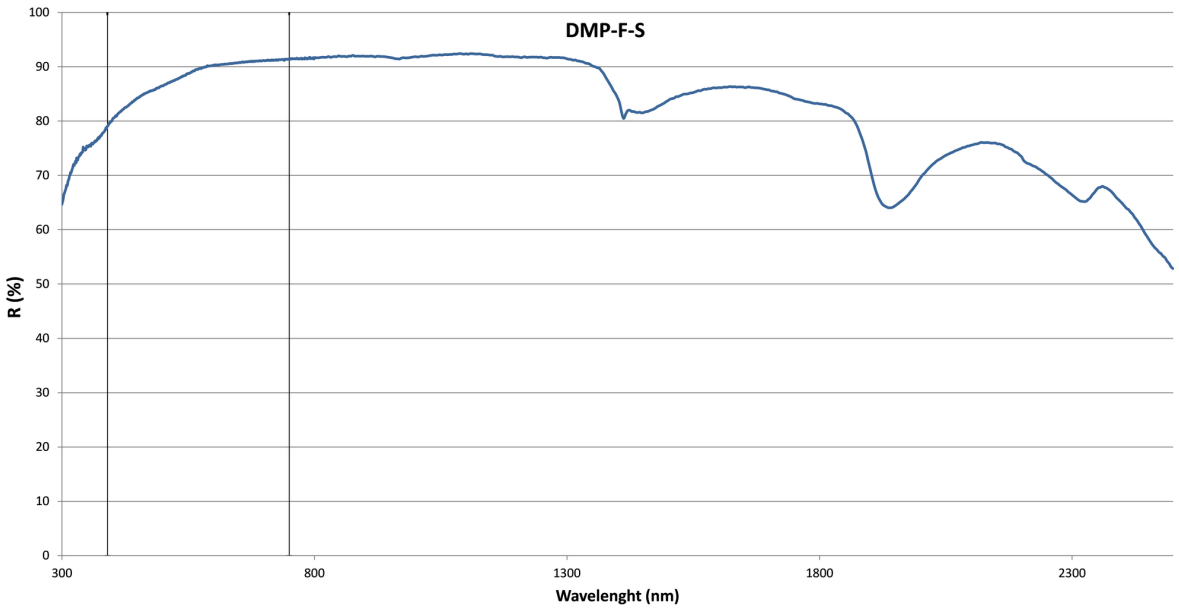

Figure A.23 Spectral reflectance of sample: DMP-F-S.

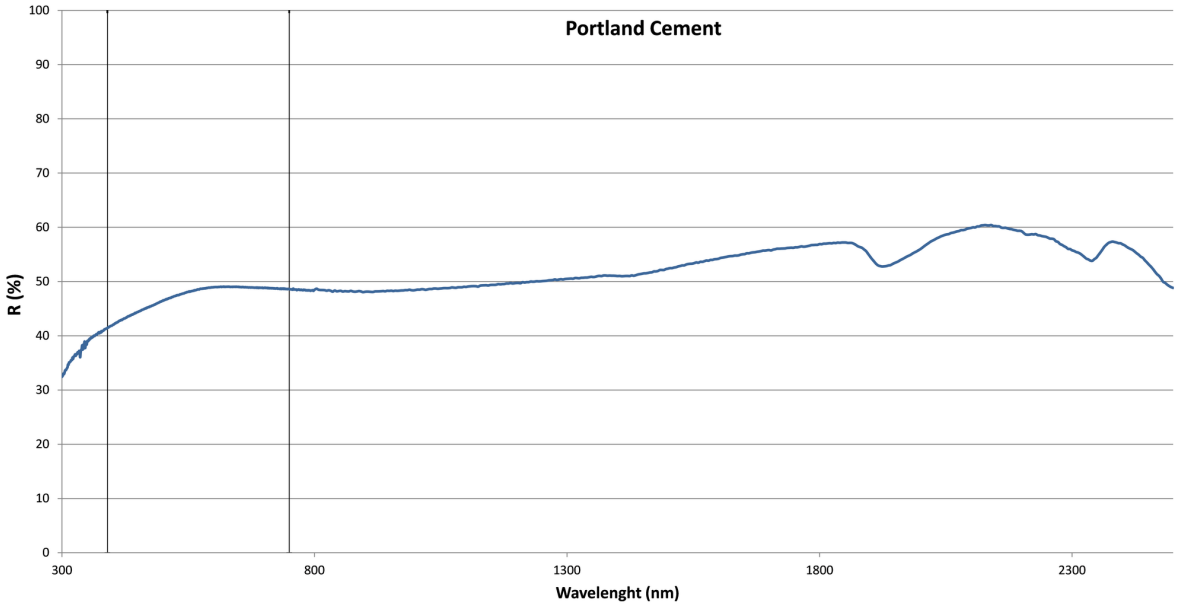

Figure A.24 Spectral reflectance of sample: Portland Cement.

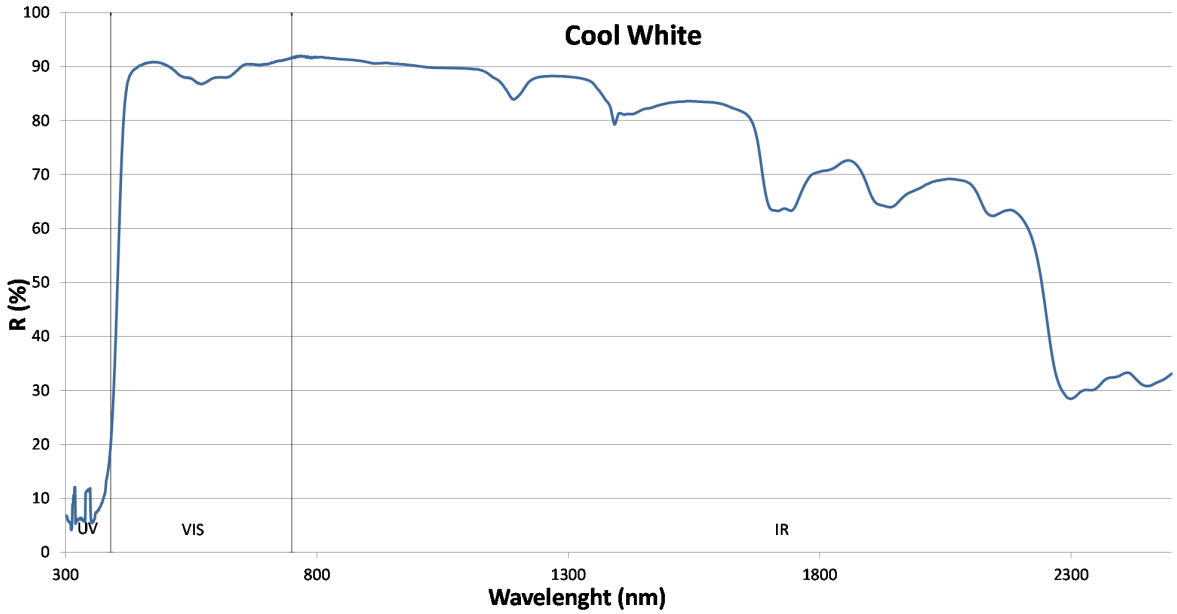

Figure A.25 Spectral reflectance of sample: Cool White.

Appendix B

Aging process of thermochromic samples

Table B.1 Blue thermochromic (BTC) side by conventional sample during the measuring period.

	Hour of Day								
	09:00			15:00			19:00		
	Surface Temperature (°C)			Surface Temperature (°C)			Surface Temperature (°C)		
Day	Thermochromic		Conventional	Thermochromic		Conventional	Thermochromic		Conventional
1				33.78	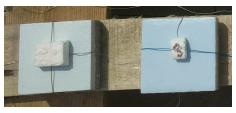	33.8	25.69	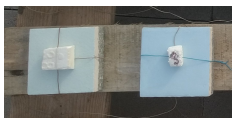	25.73
2	24.75		24.52	33.09	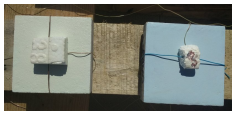	33.2	26.77		27.58
3	23.95		23.05	33.83	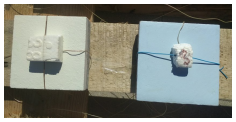	34.1	27.22		27.94
4	25.3	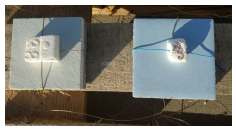	24.56	36.69	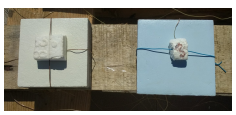	36.7	29.79	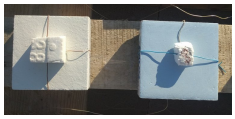	30.56
6	26.12		24.92	42.68	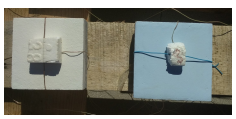	43	27.93		28.47
7	25.78	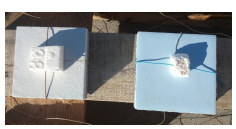	25.47	37.6		38	26.2		26.59
8	24.64	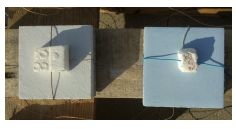	24.39						

Table B.2 Blue thermochromic tile covered with polyurethane varnish (BTC_V) side by conventional sample during the measuring period.

	Hour of Day								
	09:00			15:00			19:00		
	Surface Temperature (°C)			Surface Temperature (°C)			Surface Temperature (°C)		
Day	Thermochromic		Conventional	Thermochromic		Conventional	Thermochromic		Conventional
1				32.31		33.9	24.82		25.4
2	24.82	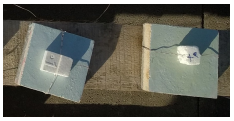	24.335	32.05		33.3	25.02		27.31
3	25.86		23.97	32.13		34.1	25.51		27.38
4	27.17		25.69	34.87		36.6	27.92		30.51
6	26.96	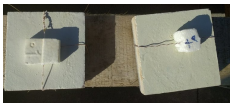	25.67	39.39		41.2	26.56		27.95
7	26.4	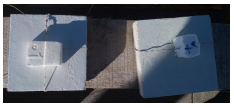	25.7	36.03		37.8	25.17	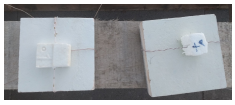	25.955
8	24.41		24.26						
9	24.64		24.09						
10	25.62		24.33	39.62		41.8			
13	28.5		28.11	32.56		34.4	21.18		21.745
14	30.89		30.585						

Table B.3 Blue thermochromic tile covered with UV stabiliser (BTC_S) side by conventional sample during the measuring period.

	Hour of Day								
	09:00			15:00			19:00		
	Surface Temperature (°C)			Surface Temperature (°C)			Surface Temperature (°C)		
Day	Thermochromic		Conventional	Thermochromic		Conventional	Thermochromic		Conventional
1				32.9	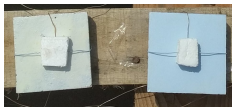	34	25.14	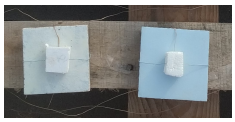	25.07
2	24.32	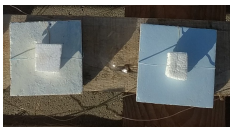	24.15	32.12		33.5	25.95		27.04
3	24.41		24.89	32.57		34.1	26.69		26.82
4	26.3		26.82	35.37		36.6	29.04		30.46
6	26.34		26.42	39.04		39.4	27.61		27.43
7	25.17		25.93	36.52		37.7	25.83		25.32
8	24		24.13						
9	23.69		24.31						
10	24.38		25.18	38.84	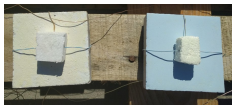	40.2			
13	27.62		28.16	33.36		34.1	21.64		21.65
14	29.84		31.04						

Table B.4 Brown thermochromic (BrTC) side by conventional sample during the measuring period.

	Hour of Day								
	09:00			15:00			19:00		
	Surface Temperature (°C)			Surface Temperature (°C)			Surface Temperature (°C)		
Day	Thermochromic		Conventional	Thermochromic		Conventional	Thermochromic		Conventional
1				34.81	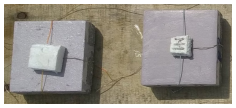	37.4	25.8	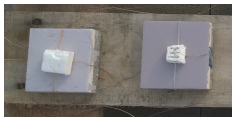	25.57
2	24.96		25.83	34.01	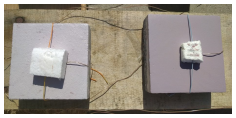	37.4	26.1		25.24
3	24.83	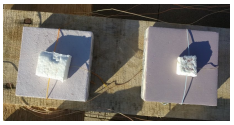	26.56	34.89	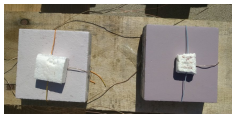	37.5	27.01	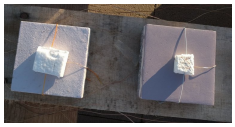	25.04
4	26.64	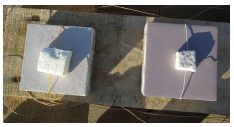	28.08	37.79	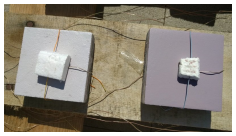	41.3	29.65		27.77
6	26.69		27.64	42.56	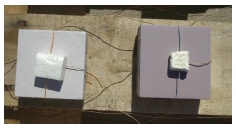	43.5	27.4	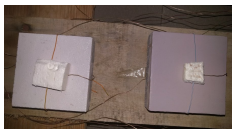	26.84
7	25.91		27.03	38.67		42.8	25.74	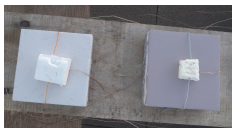	24.63
8	24.73		24.87						
9	24.25	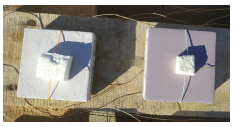	25.23						
10	24.84		26.27	42.61	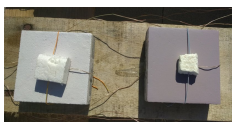	41.1			
13	28.73		31.21	34.79	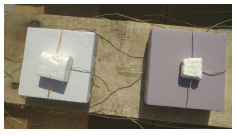	37.3	21.45	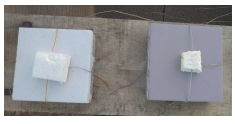	22.07
14	30.82		34.53						

Table B.5 Brown thermochromic tile covered with polyurethane varnish (BrTC_V) side by conventional sample during the measuring period.

	Hour of Day								
	09:00			15:00			19:00		
	Surface Temperature (°C)			Surface Temperature (°C)			Surface Temperature (°C)		
Day	Thermochromic		Conventional	Thermochromic		Conventional	Thermochromic		Conventional
1				34.34	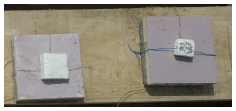	37.3	24.74	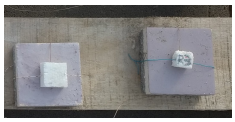	25.46
2	24	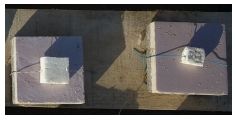	25.53	33.49	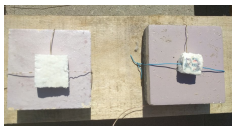	36.9	24.97	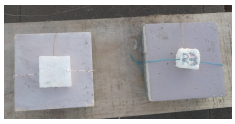	26.91
3	24.78	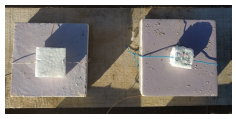	26.09	33.87	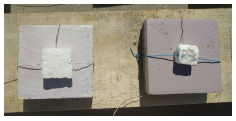	38.1	25.28	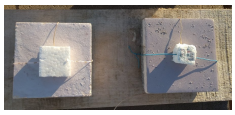	27.28
4	26.5	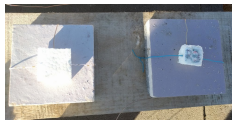	27.64	36.91	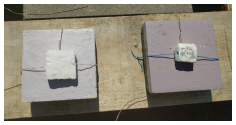	40.9	27.91	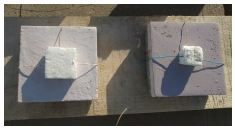	30.1
6	26.33		27.33	38.41	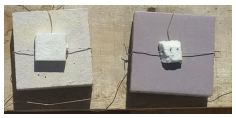	42.8	25.89	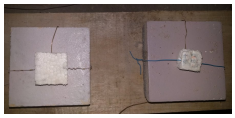	27.85
7	25.73	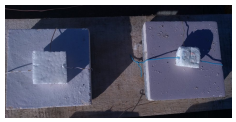	26.83	38.52	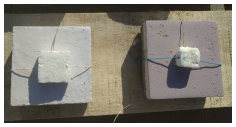	42.6	24.24	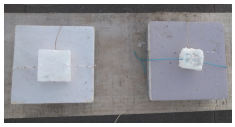	25.7
8	23.97	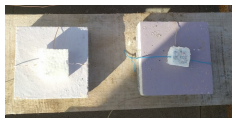	24.82						
9	24.12	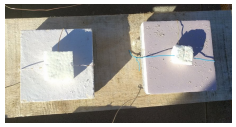	25.05						
10	24.93	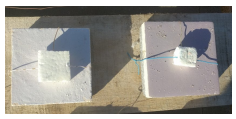	26.13	40.22	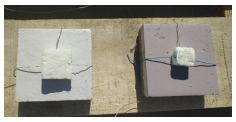	43.7			
13	28.26	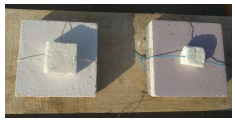	30.65	34.23	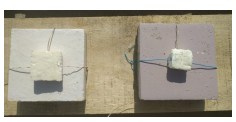	37.7	20.66	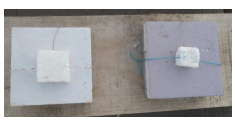	21.53
14	31.28	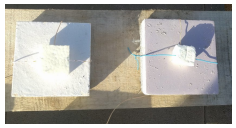	33.79						

Table B.6 Brown thermochromic tile covered with UV stabiliser (BrTC_S) side by conventional sample during the measuring period.

	Hour of Day								
	09:00			15:00			19:00		
	Surface Temperature (°C)			Surface Temperature (°C)			Surface Temperature (°C)		
Day	Thermochromic		Conventional	Thermochromic		Conventional	Thermochromic		Conventional
1				35.53	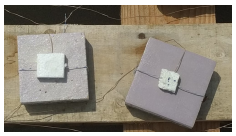	37.6	25.12	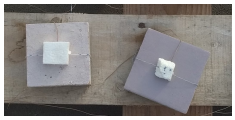	25.42
2	24.62		24.32	34.5	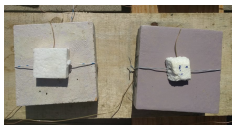	37.1	24.07	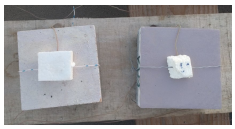	26.55
3	24.48		24.68	35.27		39.9	24.45		26.95
4	26.51		26.94	38.28	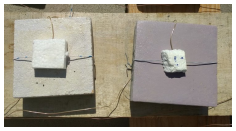	43	27		29.77
6	26.45	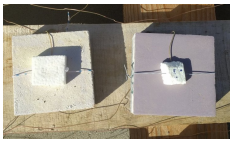	26.98	39.3		43.7	26	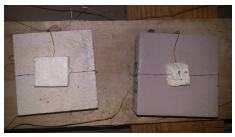	27.78
7	25.16		25.62	39.07		44.3	24.25	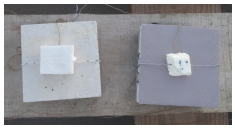	25.45
8	24.08	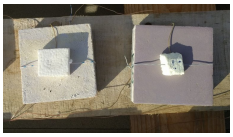	24.41						
9	23.66		24.02						
10	24.25		24.62	40.09		44.9			
13	28.62		30.21	35.11	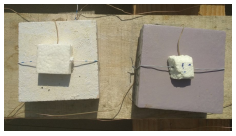	39.2	20.88	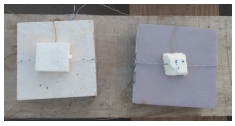	21.48
14	31.11	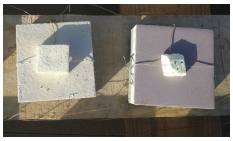	32.89						

Appendix C

Source code of Sketchup-ESP-r plug-in

```
#Sketchup To ESP-r Geometry Exporter
#
# >>>.rb
# Copyright 2014 Kostas Gompakis
#
# kgobakis at isc.tuc.gr
#
# This program is free software: you can redistribute it and/or modify
# it under the terms of the GNU General Public License as published by
# the Free Software Foundation, either version 3 of the License, or
# (at your option) any later version.
#
# This program is distributed in the hope that it will be useful,
# but WITHOUT ANY WARRANTY; without even the implied warranty of
# MERCHANTABILITY or FITNESS FOR A PARTICULAR PURPOSE.  See the
# GNU General Public License for more details.
#
# You should have received a copy of the GNU General Public License
# along with this program.  If not, see <http://www.gnu.org/licenses/>.
#
# All units into Ruby API is in inch
#
#
# copy the 2 generated folder cfg,zones to the a previous generated Esp-r project folder
```

```
# The .skp and the esp-r model must have the same name. Delete the last line of
#the cfg/projectname.cfg
#  "sed -i '$d' filenane", append at the end of the .cfg the cfg1
#"cat projectname.cfg1 >> projectname.cfg"
#   Open the projectname.cfg and change the *indx 0 to *indx 1.
#Run dos2unix * command on the zones and cfg directory
#
#
#
#
#
#

require 'sketchup.rb'


# Access the main View menu
view_menu = UI.menu "Plugins"
# Add a separator and a submenu
sub_menu = view_menu.add_submenu("Esp-rV2")
# Add two menu items to the submenu
it1 = sub_menu.add_item("2d to 3d") {
        resultado=d2tod3
        UI.messagebox(resultado)
}
it2 = sub_menu.add_item("3d to geo") {
        resultado=sku2espr
        UI.messagebox(resultado)
}
# Class definitions

class Zone
def initialize()
@id=0
@name=''
@faces=[]
@pntlist=[]  #holds all the vertex of the zone
@group=''
end
```

```
attr_accessor :id,:name, :faces, :pntlist, :group
end

class Surface
def initialize()
@id=0
@type=''
@name=''
@normal=[]
@area=0.0
@points=[]
@material=[]
@parent='-'
@facing='UNKNOWN'
@facingzoneid=00
@facingzonename=''
@facingsurfaceid=00
@facingsurfacename=''
end

attr_accessor :id, :type,:name, :area, :normal, :points, :material, :parent,
:facing, :facingzoneid, :facingzonename, :facingsurfaceid, :facingsurfacename
end

class Node
def initialize()
@id=0
@x=0.0
@y=0.0
@z=0.0
end

attr_accessor :id,:x,:y,:z
end

class Material_loc
def initialize()
@name=''
```

```
@alpha=''
end

attr_accessor :name, :alpha
end

class String
def just_latin?
!!self.match(/^[a-zA-Z_\-+]+$/)
end
end



# Function that exports geometry defined within Sketchup into ESP-r .geo format
def sku2espr
puts("HERE")
materialsInModel=[]

model=Sketchup.active_model
entities=model.entities
#       facesNamePoints=File.new('facesNamePoints.txt','w')
# checking adding all groups to an array

groupError=[]
for group in entities
if group.is_a?Sketchup::Group
groupError.push(group)
puts(group,group.name)
end
end

# check if all zones have name otherwise exit
# saves all the selected items and then clears them.
# If a zone has not name the pluin selects it
# so it is easy for the user to identify it.
sel=model.selection
sel.clear
for group in groupError
```

```
if group.name==''
sel.add group.group
end
end

if sel.length>0
return 'One or more zones have not names \n The zones with no name are selected'
end
# check if all the group names are English Characters
#
#   TO be fixed
#
sel.clear
for group in groupError
if (group.name.just_latin?)
sel.add group.group
end
end

if sel.length>0
return 'One or more zones have not English charecters \n
      The zones with no English charecters are selected'
end

# check if all the zone have possitive volume
sel.clear
for group in groupError
if (group.volume<=0.1)
sel.add group
#                       puts(group,group.volume)
end
end

#       if sel.length>0
#               return 'One or more zones have small volume'
#       end


# check if 2 zones have the same name
```

```
duplicatedgroups=[]
sel.clear
for group in groupError
count=0
for group2 in groupError
if(group.name==group2.name)
count=count+1
if(count>1)
duplicatedgroups.push(group.name)
sel.add group
sel.add group2
end
end
end

end

if duplicatedgroups.length>0
errormessage=''
for duplgroup in duplicatedgroups
errormessage=errormessage+" "+duplgroup
end
return 'Duplicate zones :' + errormessage+". Duplicate zones are selected"
end

#get the file name in order to name the .cnn and .cfg files
modelPath = Sketchup.active_model.path
filename = File.basename(modelPath, '.*')
zones=[]
warning=""
zone_id=1
for group in entities
if group.is_a?Sketchup::Group

pnt_id=1
sfc_id=1

#to check if 2 zones have the same or no name to give an error to user
zone=Zone.new()
```

```
zone.id=zone_id
zone_id=zone_id+1
zone.name=group.name
points=[]
for sk_face in group.entities
if sk_face.is_a?Sketchup::Face
face=Surface.new()
face.area=sk_face.area*0.0254*0.0254     #Converts area into square meters
face.normal=sk_face.normal
face.type=set_type(face.normal)
face.id=sfc_id

sfc_id=sfc_id+1

# Assigns a material to the face within Sketchup in case it has not been
# previously defined
if sk_face.material==nil
sk_face.material='red'
warning="\nRed surfaces have been assigned a material"
end

face.material=Material_loc.new()
face.material.name=sk_face.material.name
materialsInModel.push(sk_face.material.name.to_s)
# Defines the material transparency according to the material's alpha value
if sk_face.material.alpha!=1
face.material.alpha='TRAN'
else
face.material.alpha='OPAQUE'
end

for i in sk_face.vertices
exists=0
point=i.position

# Transformation to global coordinates
x_loc=point.x
y_loc=point.y
z_loc=point.z
```

```
xaxe=group.transformation.xaxis
yaxe=group.transformation.yaxis
zaxe=group.transformation.zaxis

point.x=group.transformation.origin.x+x_loc*xaxe.x+y_loc*yaxe.x+z_loc*zaxe.x
point.y=group.transformation.origin.y+x_loc*xaxe.y+y_loc*yaxe.y+z_loc*zaxe.y
point.z=group.transformation.origin.z+x_loc*xaxe.z+y_loc*yaxe.z+z_loc*zaxe.z
#

for j in 0...zone.pntlist.length
if point.x==zone.pntlist[j][1] and point.y==zone.pntlist[j][2] and point.z==zone.pntlist
exists=1
id2=zone.pntlist[j][0]
end
end

if exists==0
zone.pntlist.push([pnt_id,point.x,point.y,point.z])
id2=pnt_id
pnt_id=pnt_id+1
end

pnt=Node.new()
pnt.id=id2
pnt.x=point.x
pnt.y=point.y
pnt.z=point.z

face.points.push(pnt)
end
# Seting the name of the serface. the name conversion is zone name
#followed by the serface number. If no name is given to a zone => surface_+surfacenumber
if zone.name.to_s==''
face.name='surface_'+sfc_id.to_s
else
if face.normal[2]==1
face.name=zone.name+sfc_id.to_s+'CEIL'
elsif face.normal[2]==-1
```

```
face.name=zone.name+sfc_id.to_s+'FLOR'
else
face.name=zone.name+sfc_id.to_s
end
#hold only the last 12 characters of the face.name
if face.name.size>12
face.name=face.name[(face.name.size-12),face.name.size]
end
end
# show face name and how many points
#facesNamePoints.printf("%10s  %1f \n",face.name,face.points.length)

zone.faces.push(face)
end
end
zone.group=group
zones.push(zone)
end

end
#facesNamePoints.close()


# to make the connections
for zone in zones
check_facing(zone,zones)
end

if (!File.directory?('zones'))
Dir.mkdir("zones")
end

for zone in zones
write_geo(zone)
end

if (!File.directory?('cfg'))
Dir.mkdir("cfg")
end
```

```
#writes connection file
write_cnn(zones,filename)
#writes configuration file !!!! needs to be placed at the end of the original file of Es
write_cfg(zones,filename)
# wites material file
write_materials(materialsInModel,filename)
# Return message
if zones.length==0
return "There are no valid zones to be exported"
elsif zones.length==1
return "1 zone exported"+warning
else
return zones.length.to_s+" zones exported"+warning
end
end

# Function to write all the different construction on the file

def write_materials(materialsInModel,filename)
# remove all duplicates
materialsInModel.uniq
matFile=File.new('zones/'+filename.to_s+'.mat','w+')

for material in materialsInModel
matFile.puts(material.to_s)
end
matFile.close()

end


# Function that writes .geo files

def write_geo(zone)
#       puts(zone.name)
#       if(File.exist?('zones/'+zone.name+'.geo'))
#               puts('Error'+zone.name)
#       end
```

```
geofile=File.new('zones/'+zone.name+'.geo','w')

geofile.puts('*Geometry 1.1,GEN,'+zone.name+' # tag version, format, zone name')
geofile.puts('*date '+setDate()+' # latest file modification')
geofile.puts('Zone description')

write_vertex(geofile,zone.pntlist)

write_edges(geofile,zone.faces)

write_surfaces(geofile,zone.faces)

write_insolation(geofile)

write_baselist(geofile,zone.faces)

geofile.close()


end

# Write vertices' coordinates
def write_vertex(outfile,pnts)
outfile.puts('# tag, X co-ord, Y co-ord, Z co-ord')
for i in pnts # zone.pntlist[1]->x coordinate,zone.pntlist[2]->y coordinate,zone.pntlist
outfile.printf("*vertex,%.5f,%.5f,%.5f # %1d\n",i[1].to_m,i[2].to_m,i[3].to_m,i[0]) #
.to_m a value in meters if successful
#               outfile.printf("*vertex,%.5f,%.5f,%.5f # %1d\n",i[1],i[2],i[3],i[0])
end
outfile.puts('#')
end

# Write zone's edges
def write_edges(outfile,faces)
outfile.puts('# tag, number of vertices followed by list of associated vert')
for i in 0...faces.length
nv=faces[i].points.length
str=''
for j in faces[i].points
```

```
str=str+','+j.id.to_s
end
outfile.puts('*edges,'+nv.to_s+str+'  #  '+(i+1).to_s)
end
outfile.puts('#')
end

# Write zone's surfaces
def write_surfaces(outfile,faces)
outfile.puts('# surf attibutes:')
outfile.puts('# surf name, surf position VERT/CEIL/FLOR/SLOP/UNKN')
outfile.puts('# child of (surface name), useage (pair of tags)')
outfile.puts('# construction name, optical name')
outfile.puts('# boundary condition tag followed by two data items')

for i in 0...faces.length
check_parent(i,faces)
#                outfile.puts('*surf,'+faces[i].name+','+faces[i].type+','+faces[i].paren
#'+(i+1).to_s)
#outfile.puts('*surf,'+faces[i].name+','+faces[i].type+','+faces[i].parent+',-,-,'+faces
#'+(i+1).to_s)
outfile.print('*surf,'+faces[i].name+','+faces[i].type+','+faces[i].parent+',-,-,'+faces
outfile.printf("%02d,%02d, #%d", faces[i].facingzoneid,faces[i].facingsurfaceid, (i+1))
if faces[i].facing=='ANOTHER'
outfile.print(" ||< "+faces[i].facingsurfacename+':'+faces[i].facingzonename)
outfile.printf("\n")
elsif faces[i].facing=='EXTERIOR'
outfile.print(" ||< external\n")
else
outfile.printf("\n")
end
end
outfile.puts('#')
end

# Write data related to the insolation calculation
def write_insolation(outfile)
outfile.puts('*insol,3,0,0,0,0 # default insolation distribution')
outfile.puts("#\n# shading directives")
```

```
outfile.puts('*shad_calc,none # no temporal shading requested')
outfile.puts("#\n*insol_calc,none # no insolation requested\n#")
end

# Write base_list line
def write_baselist(outfile,faces)
area=0.0
list=''
num=0
for i in faces
if i.type=="FLOR"
num=num+1
list=list+i.id.to_s+','
area=area+i.area
end
end

if num==1
outfile.puts('*base_list,0,'+area.to_s+',1')
else
outfile.puts('*base_list,'+num.to_s+','+list+area.to_s+' 0')
end
end

# Set type of surface
def set_type(normal)
if normal[2]==1
type='CEIL'
elsif normal[2]==-1
type='FLOR'
elsif normal[2]<=0.001 and normal[2]>=-0.001
type='VERT'
else
type='SLOP'
end
return type
end

# Checks whether or not the surface has a parent
```

```
def check_parent(i,faces)
for j in 0...faces.length
if j!=i and faces[i].normal==faces[j].normal and faces[i].points.length<faces[j].points.
count=0

for pnt1 in faces[i].points
for pnt2 in faces[j].points
if pnt1.id==pnt2.id
count=count+1
end
end
end

if count<faces[j].points.length and count>=faces[i].points.length
faces[i].parent=faces[j].name
end

end
end
end



# Checks where the surface facing
def check_facing(zone,zones)
tolerance=0.5
cZoneName=zone.name
#search all the zones in order to find if there are surfaces that are adjation
for cZoneSurface in zone.faces
for allOhterZones in zones
# do not continue if the zone selected from zones is the zone under investigation
if allOhterZones.name!=cZoneName
for allOtherZoneSurface in allOhterZones.faces
# first check the 2 surfaces have the same number of point-vertices and the face under i
countAdjationVertices=0
if cZoneSurface.points.length==allOtherZoneSurface.points.length #and allOtherZoneSurfac
#checking all the points in the surface under investigation
for i in cZoneSurface.points
for j in allOtherZoneSurface.points
# the 2 points are very close <tolerance if all points of the 2 surfaces are very close
```

```
if (i.x-j.x).abs<tolerance and (i.y-j.y).abs<tolerance and (i.z-j.z).abs<tolerance # a v
countAdjationVertices=countAdjationVertices+1
end

end
end

# the 2 surfaces have are side by side
if countAdjationVertices==cZoneSurface.points.length
# set the nessasey arguments for this surface
cZoneSurface.facing='ANOTHER'
cZoneSurface.facingzoneid=allOhterZones.id
cZoneSurface.facingzonename=allOhterZones.name
cZoneSurface.facingsurfaceid=allOtherZoneSurface.id
cZoneSurface.facingsurfacename=allOtherZoneSurface.name
# set the nessasey arguments for other surface
allOtherZoneSurface.facing='ANOTHER'
allOtherZoneSurface.facingzoneid=zone.id
allOtherZoneSurface.facingzonename=zone.name
allOtherZoneSurface.facingsurfaceid=cZoneSurface.id
allOtherZoneSurface.facingsurfacename=cZoneSurface.name
end
end
end
end
end
end
# set all surfaces that they are not side by side as EXTERIOR
# SOS the ground surfaces needs to be altered inside Esp-r
if cZoneSurface.facing=='UNKNOWN'
cZoneSurface.facing='EXTERIOR'
cZoneSurface.facingsurfacename='External'
end
end
end



# Function that writes .cnn file
def write_cnn(zones,filename)
cnnFile=File.new('cfg/'+filename.to_s+'.cnn','w+')
```

```
cnnFile.puts('*connections for '+filename.to_s)
cnnFile.puts('*Date '+setDate()+' # latest file modification')
# count the number of serfaces inside the model
countNumberofSurfaces=0
for zone in zones
countNumberofSurfaces=countNumberofSurfaces+zone.faces.size()
end
cnnFile.puts(countNumberofSurfaces.to_s+' # number of connections')
countNumberofSurfaces=1
for zone in zones
for surface in zone.faces
#see ??? documentation for explanation
cnnFile.print('  '+zone.id.to_s+'  '+surface.id.to_s+'  ')
if surface.facing=='ANOTHER'
cnnFile.print('3')
elsif surface.facing=='EXTERIOR'
cnnFile.print('0')
else
cnnFile.print('-1')
end
cnnFile.print('  '+surface.facingzoneid.to_s+'  '+surface.facingsurfaceid.to_s+'
# ')
cnnFile.printf('%4d ',countNumberofSurfaces.to_s)

if surface.facing=='ANOTHER'
cnnFile.print(surface.name.to_s+' in zone >|< '+surface.facingsurfacename.to_s+' in '+su
elsif surface.facing=='EXTERIOR'
cnnFile.print(surface.name.to_s+' in zone is External')
else
cnnFile.print(surface.name.to_s+' in zone not yet define')
end
cnnFile.puts('')
countNumberofSurfaces=countNumberofSurfaces+1

end

end
cnnFile.close()
end
```

```
# Function that writes .cnn file
# needs to be placed at the end of the cfg file of the project
def write_cfg(zones,filename)
cfgFile=File.new('cfg/'+filename.to_s+'.cfg1','w+')
# count the number of serfaces inside the model
cfgFile.puts('* Building')
cfgFile.puts(filename+' exported from Google SketchUp')
i=0
for zone in zones
i=i+1
end
cfgFile.puts(i.to_s+' # no of zones')
countNumberofSurfaces=1
for zone in zones
cfgFile.puts('*zon  '+zone.id.to_s+'  # IE for '+zone.name.to_s)
cfgFile.puts('*opr ../zones/'+zone.name.to_s+'.opr # schedules') #cfgFile.puts('*opr UNK
# schedules')
cfgFile.puts('*geo ../zones/'+zone.name.to_s+'.geo # geometry')
cfgFile.puts('*con ../zones/'+zone.name.to_s+'.con # construction') #cfgFile.puts('*con
# construction')
if(checkZoneIfHasTransparenr(zone))
cfgFile.puts('*tmc ../zones/'+zone.name.to_s+'.tmc # transparent')
end
#               cfgFile.puts('*ihc ../zones/'+zone.name.to_s+'.htc # convective hc coef'
cfgFile.puts('*zend')
end
cfgFile.puts('*cnn '+filename.to_s+'.cnn  # connections')
cfgFile.puts('0  # no fuild flow network')
cfgFile.close()
end


def checkZoneIfHasTransparenr(zone)
for face in zone.faces
if(face.material.alpha=='TRAN')
return TRUE
```

```
else
puts(face)
return FALSE
end
end
end


def setDate()
t = Time.now
return t.strftime("%a %b %H:%M:%S %Y").to_s
end

# creates any 2d surfaces into a 3d- not extrude it
def d2tod3

allvertices=[]
allfaces=[]
model = Sketchup.active_model
entities = model.entities
materials=model.materials
faces = []

entities.each do |e|
if e.is_a?( Sketchup::Face )
faces << e
elsif e.is_a?( Sketchup::Group )
return "There is one/more group/s inside model.\n Explode the groups in order to prossed
end
end

for face in faces
for i in 0..face.vertices.size-1
if face.vertices[i].position.z>0.1
return "Error one/more surfaces have high"
end
end
end
```

```
# making the dialogue
inputdata= inputbox ["Hight of the rooms","External Walls","Internal walls","Floor","Ce
zonehigh= inputdata[0].to_l
ext_material=inputdata[1]
int_material=inputdata[2]
floor_material=inputdata[3]
ceiling_material=inputdata[4]

# flags for checking if in the .skp are all the materials
flag_ext=0
flag_int=0
flag_flo=0
flag_cel=0

#  checking if the materials are already exists
for material in materials
#       puts(material.name.to_s)
if material.name.to_s == ext_material.to_s
flag_ext=1
end
if material.name.to_s == int_material.to_s
flag_int=1
end
if material.name.to_s == floor_material.to_s
flag_flo=1
end
if material.name == ceiling_material.to_s
flag_cel=1
end
end

# error messages for missing material
erroroutput=""
if flag_ext==0
erroroutput="External wall material"
end
if flag_int==0
erroroutput=erroroutput+" ,internal wall material"
end
```

```
if flag_flo==0
erroroutput=erroroutput+" ,floor material"
end
if flag_cel==0
erroroutput=erroroutput+" ,celing material"
end
if erroroutput !=""
return erroroutput + " does not exist !!!! \n Right click on material Add to model"
end

#       file=File.open('test2.out','a')
# you need 4 vertices to make a surface (p1,p2,p3,p4) so we take all the vertices of the
# in order to make the walls of the room.
# p1 (ppriv) the privious vertice
# p2 (p) the current vertice
# p3 (p) p2+zonehigh
# p3 (ppriv) p1+zonehigh
for face in faces
allfaces=[] # store the all the surfaces in order to create a group at the end
allfaces.push(face)
face.material=floor_material.to_s
for i in 0..face.vertices.size
# the first vertices of the surface we cannot make a wall
if i==0
p=face.vertices[i].position
allvertices.push(Geom::Point3d.new(p.x, p.y, p.z+zonehigh))
next
elsif i>0 and i<face.vertices.size
p=face.vertices[i].position
allvertices.push(Geom::Point3d.new(p.x, p.y, p.z+zonehigh))
ppriv=face.vertices[i-1].position
elsif   i==face.vertices.size # we run out of vertices we need to take the first and the
#initial point of the surface
p=face.vertices[i-1].position
ppriv=face.vertices[0].position
end

sizeallvertices=allvertices.size
p1=Geom::Point3d.new(ppriv.x, ppriv.y, ppriv.z)
```

```
p2=Geom::Point3d.new(p.x, p.y, p.z)
if i!=face.vertices.size
p3=allvertices[sizeallvertices-1]
p4=allvertices[sizeallvertices-2]
else    # for the last vertice of the button surface we need to close it so we take the
p4=allvertices[sizeallvertices-i]
p3=allvertices[sizeallvertices-1]
end
cface=entities.add_face p1,p2,p3,p4
allfaces.push(cface)
if i==face.vertices.size #time to add the top-ceiling of the room
cface=entities.add_face allvertices[sizeallvertices-i...sizeallvertices]
allfaces.push(cface)
end
end
#creates a group of the current room
entities.add_group allfaces
end
setmaterialToAllFace(ext_material,int_material,floor_material,ceiling_material)#,file
#       file.close
return "OK"

end




#set the material to the face
def setmaterialToAllFace(ext_material,int_material,floor_material,ceiling_material)

tolerance=0.1
model = Sketchup.active_model
entities = model.entities
# get again all surfaces in order to give them material
faces=[]
faces2=[] #in order to iterate all the faces
groups=[] # store the group in order to make the correct transformation
entities.each do |e|
if e.is_a?( Sketchup::Group)
```

```
groupEntities=e.entities
for ee in groupEntities # if a group is created on Google Sketchup all the faces are liv
if ee.is_a?( Sketchup::Face)
faces.push(ee)
faces2.push(ee)
groups.push(e)
end
end
end
end

countercFace=0
for cface in faces
#               file.puts('face '+cface.to_s+' '+faces.size.to_s)
counterFace=0
for face in faces2
#                       file.puts('cface '+face.to_s)
if face!=cface
# first check the 2 surfaces have the same number of point-vertice
if cface.vertices.length==face.vertices.length
#checking all the points in the surface under investigation
countAdjationVertices=0
for i in cface.vertices
# Every group in GS has its own cordinates system so it needs a transformation in order
for j in face.vertices
#making the transformation
cfaceVertice=transformationToOrigin(groups[countercFace],i)
faceVertice=transformationToOrigin(groups[counterFace],j)
disX=(cfaceVertice[0]-faceVertice[0]).abs
disY=(cfaceVertice[1]-faceVertice[1]).abs
disZ=(cfaceVertice[2]-faceVertice[2]).abs

# the 2 points are very close <tolerance if all points of the 2 surfaces are very close
if disX<tolerance and disY<tolerance and disZ<tolerance
countAdjationVertices=countAdjationVertices+1
#                                                       file.puts('countAdjationVertices
break
end
end
```

```
end

# the 2 surfaces have are side by side so they are inside surfaces
if countAdjationVertices==cface.vertices.length
cface.material=int_material.to_s
face.material=int_material.to_s
#                                                    file.puts('OK')
break
else  #ceiling
if cface.normal[2]==1 #z cordinate
cface.material=ceiling_material.to_s
elsif cface.normal[2]==-1 #flor
cface.material=floor_material.to_s
else    #all other surface
cface.material=ext_material.to_s
end
end
end
end
counterFace=counterFace+1
end
countercFace=countercFace+1
end

end




# Give a Point3d and return global into an array
def transformationToOrigin(group,point)

x_loc=point.position[0]
y_loc=point.position[1]
z_loc=point.position[2]

xaxe=group.transformation.xaxis
yaxe=group.transformation.yaxis
```

```
zaxe=group.transformation.zaxis

x=group.transformation.origin.x+x_loc*xaxe.x+y_loc*yaxe.x+z_loc*zaxe.x
y=group.transformation.origin.y+x_loc*xaxe.y+y_loc*yaxe.y+z_loc*zaxe.y
z=group.transformation.origin.z+x_loc*xaxe.z+y_loc*yaxe.z+z_loc*zaxe.z

return [x,y,z]

end
```